Faculty of Mathematics and Physics
Charles University Prague

SYNOPTIC INTERPRETATION OF NUMERICAL PROGNOSTIC MODELS OUTPUTS

DOCTORAL THESIS

Michal Žák

Prague, 2006

Tato práce by jen těžko vznikla bez podpory mnoha lidí, kteří mi věnovali svůj čas, znalosti a také trpělivost. Zvláštní poděkování patří zejména mému školiteli prof. RNDr. Janu Bednářovi, CSc. a RNDr. Radmile Brožkové, CSc. za výraznou pomoc při výpočtech. Chtěl bych i poděkovat RNDr. Martinu Janouškovi, Mgr. Aleně Trojákové a Mgr. Martině Lacinové.

V neposlední řadě patří mé poděkování i mým kolegům a spolupracovníkům, zejména za zázemí včetně materiálního a technického, které mi bylo poskytnuto v ČHMÚ v Praze-Komořanech.

Hereby I confirm that I worked out this doctoral thesis by myself and I used only references listed here. I agree with lending of this thesis.

Michal Žák

Content

Introduction **2**

Chapter 1: Brief description and summary of the historical overview of synoptic meteorology knowledge in the 20th century **5**
1.1 The Norwegian school and its cyclone model 5
1.2 Classical versus modern storm track analysis 5
1.3 Quasi-geostrophic theory and self-development 7
1.4 Three-dimensional structure of cyclones and anticyclones 8
1.5 The isentropic view and air mass exchange concept 11
1.6 Observed cyclogenesis studies 12
1.7 The potential vorticity perspective 24
Invertibility 26
1.8 Some remarks about conceptual models of cyclone life cycles 28

Chapter 2: Applications of the satellites in the field of NWP **31**
2.1 Introduction 31
2.2 Relationship between satellite data and dynamical parameters computed by NWP models 31
2.3 Model-to-satellite approach and utilizing of satellite radiation measurements for model evaluation 40

Chapter 3: ARPEGE model and computation of brightness temperatures **45**
3.1 Introduction 45
3.2 Description of the ARPEGE model and of the scheme for brightness temperature computation 46

Chapter 4: Case studies and results **51**
4.1 October 2002 51
4.2 November 2004 61
4.3 August 2002 71
4.4 December 2004 84
4.5 April 2005 95
4.6 May 2005 107

Chapter 5: Conclusions and discussions **121**

References **123**

Introduction

Utilizing of Meteosat satellite data for „model to satellite" approach for synoptic interpretation of numerical weather prediction model outputs and for studying of upper troposphere and tropopause dynamics and comparison of these data with results of the numerical weather prediction (NWP) models are the main ideas of this work. The global model ARPEGE is used for this purpose. Simulation of the measured channels (in our case measured by Meteosat) by the NWP model with their predicted variables is realized in the form of forecasted brightness temperatures fields. These fields are constructed for comparison between the results of simulated and measured channels. This comparison is made for various prognostic times of model integrations (6, 12, ..., 72 or 96 hours). This can give us information about possible phase shift between model prediction and reality. This could then lead to the correction of the model forecast. The content of this work is oriented on the synoptic scale structures, such as tropopause anomalies, frontal sytems and large cloud clusters/systems and their connection with intensive cyclogenesis.

The first part, chapter 1, of this work brings together some historical review of synoptic meteorology and observed cyclone life cycle from the Norwegian Meteorological School times to the end of the 20th century. Very complex overview of this knowledge is given in *Bosart (1994)*, that's why great part of his work is reproduced here with some small corrections. Then a part about potential vorticity follows that has been developed during the second half of the 20th century.The respect is devoted to possible applications in this thesis and also to prepare a theoretical base for better understanding of this doctoral thesis.

In chapter 2, the application of modern knowledge about cyclogenesis and cyclones with utilizing of satellite measurements is presented. Some applications in this field are described as the recherché from references available in this field.

In chapter 3, the description of the computation scheme for the computations of brightness temperatures from the model ARPEGE outputs is presented.

In chapter 4 several case studies can be found. Here, the synoptic features for these case studies are presented, described and discussed with respect to their representation in the fields of brightness temperatures of NWP model outputs.

Finally, chapter 5 summarizes the results and discussed them, including the possibility of the following development and utilizing of our outputs.

Forecasting of extratropical cyclogenesis and of the associated weather patterns remains one of the most challenging aspects of operational meteorology, even though the past decade has witnessed some significant advances in our observation and understanding of these events. This is especially true for locations over eastern ocean basins and western continents where the accuracy of analyses and numerical guidance is limited by regions of conventional data sparsity upstream. On a routine basis, space-based remote sensors are the only feasible method to acquire information that can improve the forecast problem over these regions.

Since the first meteorological satellites were launched in the seventies, the number and efficiency of instruments carried on board increased dramatically. As for geostationary, so for polar-orbiting satellites their observations complement and partially substitute the observations based on classical methods (aerological and ground measurements). Mainly to their unique potential to provide global observations also over traditionally data sparse regions (oceans and weakly populated areas) a great success in satellite data utilizing for numerical weather prediction (NWP) models has been reached.

Qualitative satellite information, such as visible, infrared, and water vapour imagery, has already proven its value in this regard. More significantly, there is also a large reservoir of quantitative information that can be obtained from satellite measurements. Traditionally,

quantitative satellite information has been available in the form of high horizontal, but low vertical resolution, TIROS (Television Infrared Observation Satellite) Operational Vertical Sounding (TOVS) temperature soundings. These soundings are retrieved from satellite radiance data and knowledge of the vertical weighting function characteristics of the spectral frequencies measured by the onboard sensor is the problem. Unfortunately, observing system sensitivity experiments with modern data assimilation systems suggest that these "retrieved" satellite soundings do not produce great improvement in forecast skill and in some cases actually result in decreased skill (e.g. *Flobert et al., 1991*). One reason for these not satisfactory results, besides the inherent limitations of data quality and low vertical resolution, consists in the errors that are introduced by ill-posed inversion process from observed radiance values to temperature profiles. Furthermore, tropospheric temperature soundings cannot be confidently retrieved in areas of precipitation that are common in the vicinity of cyclones. In the light of current problems with converting satellite measurements into pseudoradiosonde soundings, techniques were being sought to more directly utilize the information provided by satellite sensors.

Concerning NWP it is now standard practice to use the radiances themselves and to assimilate them directly into a weather-forecast by the model fields adjusting to minimize the difference between the observed radiances and the results simulated by the model *(Chevalier, 2002; Velden, 1997)*. This requires an accurate forward NWP model to provide the simulated radiances, as well as the knowledge of the error characteristics both for the method and for the data to optimize the assimilation process by variational methods. The advantage of radiances used as representation of high-level products of NWP model for comparison with observed satellite data is that this way preserves the information content of the data with the minimum of processing and enables a wide variety of data types to be assimilated, provided that a forward model can be used.

In routine meteorological analyses the satellite measurements are used for wide variety of purposes. They can be utilized for large scale atmospheric phenomena location such as frontal zones or circulation centres at ground as well as at high levels *(Joly, 1997)*. They are also very important for identifying of much smaller scale features such as instability lines and strong convection regions, frontal waves and so on, that are only rarely detected by ground observations. Additionally, using a single images movement following the features movement make it possible to get a first guess of movement of mentioned features in the near future (*Fourrie, 2003*).

There exist well known connections between such weather systems like lows and their clouds or humidity signatures on satellite pictures. For example, during cyclogenesis there should exist strong correlations between location of the driest air that flows in the rear part of the developing cyclone and the potential vorticity (PV) maximum in the high levels or, alternatively, minimum of the 2-PVU surface height (PVU – potential vorticity unit, 1 PVU = 1×10^{-6} kg^{-1} m^2 s^{-1}) – see *Ringer (2002)*. It is a deformation of the tropopause that leads to an intrusion of a thin wedge of stratospheric air through upper-level fronts into the mid- and lower troposphere. A low tropopause level is generally characterized by stratospheric air intrusion associated with high potential vorticity values (*Mannsfield, 1996*). These upper-level PV anomalies are typical for tropopause breaks that correspond to the step between the high tropopause level south of the upper-level jet streak and the low tropopause level north of this streak. These upper-level PV anomalies represent upper-level components of the baroclinic interaction scheme. This scheme is involved in the surface lows deepening larger than 9-10 hPa per 24 h (*Ayrault and Joly, 2000*) and consists in the interaction between two PV anomalies, the first of them is located at the tropopause level and the second near the surface. There is a difference between these two anomalies that often indicates error in the development or analysis in NWP model. Because analysis errors often lead to the errors in the

forecast, these differences warn the forecaster and they identify the areas where adjustation in numerical model prediction should be made.

Morcrette (1991) compared as one of the first investigators model-simulated brightness temperatures with those obtained from Meteosat satellite and he demonstrated the potential of what he termed the "model-to-satellite" approach for evaluating model-generated cloudiness. His procedure is used for studying of synoptic features in this work.

There is a problem that these simulated radiances doesn't represent prognostic values and they must be computed during diagnostics. But the diagnostic time is very expensive. Another similar scheme for brightness temperature computing have been developed relatively recently, it is RTTOV - Radiative Transfer model based on TOVs (TOVS = TIROS Operational Vertical Sounder, equipment of NOAA's TIROS series of polar orbiting satellites), see e.g. *Saunders (1999)* for more details. It has been developed for fast satellite radiances simulation reasons and it is faster but with less complexity in comparison with Morcrette's scheme. But we study here synoptic scale features for several case situations and so the question of time consumption is not so important for us now. But, of course, for operational purposes in meteorological forecasting the problem with getting outputs in real time would be exist.

Chapter 1: Brief description and summary of the historical overview of synoptic meteorology knowledge in the 20th century

1.1 The Norwegian school and its cyclone model

From the historical point of view it seems evident that the study of synoptic meteorology was stimulated and energized by the widespread installation of the telegraph in the middle of the 19th century. This new technology made it possible to watch the evolution and movement of the complex surface weather systems on large scale (continental scale or oceanic scale) for the first time and provided possibility for the first comprehensive ideas of the structure of the cyclones. Of course, the first pioneers in observational meteorology emphasized the study of surface cyclones and anticyclones with special emphasis on documenting the evolution of temperature, wind and pressure fields associated with the movement of the individual cyclone and anticyclone centres. The most successful and most effective studies of their structures were made in Norway, Bergen, where T. Bergeron, J. Bjerknes and H. Solberg (see *Bjerknes and Solberg, 1922* and *Bergeron, 1959*) and their colleagues assembled numerous synoptic observations of surface fields of cyclones tracking northern part of Atlantic Ocean and north-western part of Europe. Due to this collection of observations and studies, they deduced not only the existence of warm and cold fronts but also they synthesized a complete cyclone life cycle, including the evolution of clouds and precipitation along these frontal zones (so called idealized Norwegian Meteorological School). One another innovative aspect of this school was the incorporation of air mass concept ("air mass thinking") that explained the time-dependent behaviour of warm and cold air currents that became involved in the developing cyclonic circulation. The important consequence of this concept was the necessity to view the cyclone as a fully three dimensional entity.

The early aerological studies in the 1920's and 1930's (e.g. *Bjerknes and Palmen, 1937*), that made use of temperature observations from balloon borne instruments, provided the first confirmatory evidence that the highly idealized conceptual models of cyclone life cycles of the Bergen School had a basis in fact. The improvement of the radiosondes during late 1930's and 1940's and its widespread operational deployment around the world in the late 1940's and 1950's intensified a range of synoptic studies on cyclone and anticyclone behaviour and their life cycles (*Palmén, 1951*). Of course, this rapid progress in observational capability stimulated theoretical advances in dynamic meteorology, as well. As an important example one can mention the paper by *Bjerknes (1937)* where he laid the theoretical groundwork for understanding of the generation and importance of ascending and descending currents in cyclones on the basis of upper and lower level horizontal divergence patterns deduced from variation in the gradient wind along the flow direction. Similarly, these observational and theoretical advances played a very important role in stimulating Rossby's pioneering theoretical work on planetary wave dynamics (*Rossby 1940*) and the equally significant theoretical work by *Charney (1947)* and *Eady (1949)* ("normal mode thinking") to explain mid-latitude cyclone evolution out of which came an appreciation of the crucial role played by the Earth's surface and the "quasi-rigid" tropopause in the process.

1.2 Classical versus modern storm track analysis

After observations became widespread over time and over the Earth, the resulting hemispheric dataset has been used by a number of authors to construct a series of

climatological analysis and charts. For example, *Petterssen (1956)* constructed maps of cyclone and anticyclone frequencies, cyclogenesis and cyclolysis in rectangles of 100 000 km^2 for the winter and summer seasons. From his figures arises, that the main cyclogenetic regions are situated: (1) over the western Pacific and Atlantic ocean basins and the very eastern parts of North America and Asia, (2) immediately downstream of major mountain ridges such as the Rocky mountains and Alps, and (3) over smaller water bodies such as west and eastern Mediterranean Sea and the NW part of Gulf of Mexico. Similar patterns can be seen in the summer with the appropriate poleward shift. The cyclone frequency maps show especially pronounced maxima downstream of the major mountain barriers caused by terrain-induced disturbances in the lee of these barriers. General, the regions of maximum cyclone frequency tend to lie downstream and somewhat poleward of the regions of maximum occurrence of cyclogenesis over the western Pacific and Atlantic Ocean basins. It means that mobile cyclones develop downstream of their genesis regions. Exceptions to this pattern are noted over the Mediterranean Sea and over some other selected regions, where vicinity of the Alps is the more likely reason to the orographic trapping of cyclones that have been once formed.

The corresponding anticyclone frequency and frequency of anticyclogenesis maps clearly reveal the preference for anticyclone centres to be found over the subtropical oceans in all seasons and over higher latitude regions of the continents in winter season. Given that the anticyclonic vorticity is destroyed by sensible heating in the boundary layer, it is no accident that anticyclone centres tend to avoid warm inland water bodies and bays in winter with the reverse situation in summer. Subsequent investigations of Northern Hemisphere cyclone and anticyclone frequencies and the occurrence of cyclogenesis and anticyclogenesis (e.g. *Chen et al., 1991*) have confirmed and expanded upon the earlier findings of Petterssen.

There are fewer studies in the Southern Hemisphere due to the lack of the observations, especially with regard to the observed behaviour of fronts. Although orographic cyclogenetic signatures are found downstream of the Andes over eastern coastal South America and the Southern Alps in New Zealand, overall cyclone frequencies tend to be more zonally homogeneous with less variation between summer and winter in comparison to the Northern Hemisphere.

The classical definition of storm tracks as used by *Klein (1958)* refers to the focus of paths followed by individual sea-level cyclones with no regard to the tracks of the flanking sea-level anticyclones or the mobile short wave troughs and ridges aloft. *Blackmon (1976)* proposed an alternative definition of the storm track based upon the location of variance maxima in the fields of geopotential height in the middle and upper troposphere arising from transient disturbances with the period less than about one week. The advantage of this definition is that storm tracks are readily interpretable as variance maxima of both cyclonic and anticyclonic geopotential height perturbations and his results reveal that prominent storm tracks in the Northern Hemisphere extend from the east coasts of North America and Asia eastward across the ocean basins. The region of maximum sea level pressure variance lies equatorward (poleward) of the geopotential height variance maxima aloft in the storm track entrance (exit) regions, indicative that developing cyclones typically form equatorward of the principal polar jet stream and move to the poleward side of the jet stream as they mature and die. This behaviour of cyclones is entirely consistent with the expectations from quasi-geostrophic theory (see later) in that deepening cyclones must be accompanied by ascent (driven largely by the upward increase of cyclonic vorticity advection, see e.g. *Holton, 1992*), low-level convergence and resultant cyclonic vorticity generation and adiabatic cooling in the lower half of the troposphere over the cyclone centre.

Typically, sea-level pressure variance maxima over the oceans lies somewhat poleward of the classical storm track position given that geopotential height falls and rises

aloft are more prominent north of the jet stream axis and north of the surface cyclone and anticyclone positions. Despite the widespread acceptance of *Blackmon's (1976)* modernized definition of the storm track it is important to remember that the classical storm track definition is still of considerable use to climatologists and weather forecasters because areas of clouds and precipitation are most likely to be concentrated downshear of cyclones and upshear of anticyclones.

Comparable studies of closed cyclones and anticyclones in the middle troposphere, although not as abundant as the studies of the surface systems as mentioned above, have been conducted for the Northern Hemisphere by *Parker et al. (1989)* and *Bell and Bossart (1989)*. Closed cyclones frequently occur in the storm track entrance regions of eastern North America and eastern Asia poleward of the main baroclinic zone and over south-western North America and southern Europe equatorward of the main baroclinic zone. In these latter regions lysis and genesis maxima nearly coincide, suggestive that life cycles of the closed cyclones are strongly influenced by topography. Individual case composite studies (e.g. *Bell and Bossart, 1993 and 1994*) suggest that closed cyclone formation equatorward of the polar jet is strongly associated with the upstream anticyclogenesis and a shortening of the distance between the upstream ridge and the downstream trough in the north-westerly flow whereas closed cyclone formation poleward of the polar jet is related to vigorous planetary-scale downstream ridge amplification. The same results were obtained for cases of explosive cyclogenesis and rapid anticyclogenesis (*Colucci and Davenport, 1987*).

It is also interesting that both regions of closed cyclone frequency maxima equatorward of the polar jet occur downstream of regions of large 500 hPa geopotential height variability and in area where the baroclinic waveguide tend to shift equatorward. This shift is particularly robust in the case of the southern Europe. A similar shift would probably occur overt south-western North America at 300 hPa and 200 hPa, given that the subtropical jet entrance region is frequently in this location during the cooler half of the year. It is hypothesized that "seams" in the baroclinic waveguides downstreams of geopotential height variance maxima are particularly well conducive to closed cyclone formation as ridge development occurs poleward and immediately upstream of equatorward cyclone development in a region of large scale flow deformation coincident with the waveguide seams.

1.3 Quasi-geostrophic theory and self-development

Sutcliffe and his collaborators designed to understand the dynamical basis of the characteristically observed vertical structure and associated cloud and precipitation patterns in cyclones. A cornerstone of this approach was the use of the concept of thermal vorticity and the advection of vorticity by the thermal wind (*Sutcliffe and Forsdyke, 1950*) to deduce atmospheric thermal or thickness structures and to diagnose the development (defined as the difference between the upper level and lower level divergence) of cyclones and anticyclones. Their model indicates that the ascent (descent) is favoured in the equatorward (poleward) confluent entrance and the poleward (equatorward) diffluent exit regions of the thickness jet. This work, in which the presence of the synoptic scale ascending and descending vertical motion is linked to the advection of vorticity by thermal wind, might be called the invention of the quasi-geostrophic theory that was formalized by *Phillips (1963)*. It also anticipates a similar description of four-cell vertical motion patterns in a straight jet model as put forth by *Beeby and Bates (1955)* in study of the release of convective instability and used subsequently by many authors to help understand the dynamical importance of jet stream configurations to the evolution of vertical circulations associated with cyclones and anticyclones and

convective weather disturbances. It should also be noted that Sutcliffe's advance was motivated by the practical necessity of providing improved short term (one to two day) weather forecasts in support of military operations during World War II. In this regard he was one of the truly outstanding early pioneers because of his insightful recognition of the importance of linking the needs of the operational community to progress in understanding the dynamical basis of observed cyclone structures and cyclone life cycles.

The work by Sutcliffe and colleagues stimulated Petterssen and his colleagues (e.g. *Petterssen et al., 1962*) to expand and quantify the "self-development"-concept (cyclone development at sea level begins wherever and whenever an area of cyclonic vorticity advection aloft overspread a surface baroclinic zone) to a range of continental and oceanic cyclone investigations that include the application of the quasi geostrophic omega equation to diagnose vertical motion field. They introduced also the concept of dual cyclone development paths which they called type "A" and type "B" disturbances. The type A category was assigned to amplifying frontal wave disturbances in which atmospheric development appeared to originate from the bottom upward with little, if any, evidence for a predecessor disturbance aloft. Type B disturbances were characterized by a well defined predecessor vorticity maximum aloft that triggered subsequent surface cyclogenesis as it crossed an old low-level baroclinic zone. The problem with this categorization scheme is that the evidence for type A cyclone development has been tenuous at best as there almost always appears to be some incipient disturbance aloft that can be related to the surface development (see e.g. *Sanders, 1986*). As evidence for this statement note that the example used by *Petterssen and Smebye (1971)* as somewhat illustrative of a type A development, had a type B signature as well. Instead of attempting to distinguish between type A and type B cyclonic developments perhaps it would be more revealing to recognize that type B developments come in many "flavours" representing a full spectrum of predecessor disturbances.

Although quasigeostrophic theory (QG) has been used for decades in both theoretical and operational work, innovative ways of applying the theory have begun to come into vogue, most notably Q-vectors. With grid point data from numerical models available to forecasters, calculating Q-vectors and their divergence is a simple matter. A main use of the Q-vectors has been in the assessment of vertical motions. Using Q-vectors is superior to the traditional method of using vorticity and temperature advections. Although some may argue that the vertical velocities generated by primitive equation models are superior to those estimated by QG theory, but the poorly resolved terrain in the numerical models may be a leading cause for the less accurate primitive equation vertical velocities. Nonetheless, having a physical understanding of the causes of the vertical motions is an important aspect of the forecast process.

In addition to Q-vectors, deformation of the wind, geostrophic frontogenesis and frontolysis and their induced vertical motion fields (*Eliassen 1962*) are other parameters that have not enjoyed much operational popularity until recently. Applying these concepts via QG diagnostic models have proven to be excellent forecast tools.

1.4 Three-dimensional structure of cyclones and anticyclones

An important aspect of the radiosonde era that began in the late 1940's and continued into the 1960's was the proliferation of synoptic studies designed to elucidate the three dimensional structure of troughs and ridges in the middle and upper troposphere and their role in controlling the behaviour of mobile cyclones and anticyclones. Notable scientific contributions in this area were made by Palmén, Newton, Kleinschmidt and collaborators. Palmén's scientific papers resulted in advances in our knowledge and understanding of the

evolution of synoptic scale circulations in the middle latitudes. Particularly noteworthy was his documentation of the process whereby cut-off cyclones broke off from the main belt of westerlies and took up residence in lower latitudes with a similar behaviour demonstrated for cut-off anticyclones at higher altitudes. Research in this area was motivated by the desire to uncover the physical mechanisms responsible for satisfying this planetary heat budget.

For example, studies by *Palmén (1949)*, *Palmén and Newton (1951)* or *Krishnamurti (1968)* were central to uncovering the life cycles of cut-off cyclones and anticyclones and related features such as cold air outbreaks into lower latitudes associated with the formation of a cold cut-off cyclone. Formation of a cut-off cyclone is associated with a deepening diffluent trough in which the largest cyclonic vorticity (mostly in the form of shear) lies upstream of the trough axis in a strong jet stream. Accordingly, cyclonic vorticity accumulates in the trough axis and in association with cold air advection into the trough axis below 500 hPa the midtropospheric trough intensifies. A cross section through the cut-off cyclone also reveals the following cut-off signatures:

1) a locally depressed tropopause coincident with a dome of cold air (uplifted isentropic surfaces) in the troposphere

2) a relatively warm and depressed stratosphere above the tropospheric cold dome.

The resultant cyclonic circulation, strongest near to tropopause, follows immediately by hydrostatic considerations. Alternatively, the cut-off cyclone can be viewed as a positive potential vorticity anomaly that has broken off from the main PV reservoir farther poleward (see e.g. *Hoskins, 1985*) with the reverse situation being true for cut-off anticyclones. This observation, the essence of "PV thinking" as quantified by *Hoskins et al. (1985)* will be mentioned later.

Krishnamurti (1968) first employed a general balance equation model to diagnose a case of extratropical cyclogenesis of the type previously studied by Palmén and his colleagues. He chose a case of deepening diffluent trough in north-westerly flow over North America east of the Rockies for his case study. Cyclogenesis originated in a lee trough east of the Rockies beneath north-westerly flow aloft. As this intensifying trough crossed the Rockies the surface cyclone began to deepen substantially as it moved away from the mountains and became situated beneath the forward side (east of the trough axis) of the trough. Krishnamurti also showed how cross-flow sinking motion in the north-westerly flow at mid levels of the atmosphere was crucial to the generation of large values of cyclonic vorticity on the cyclogenetic side of the jet at upper levels. The vorticity thus generated was advected south-eastward into the base of the intensifying trough, eventually leading to the formation of a closed cyclone centre. An important result from his work was that much of the observed cross contour flow toward higher heights in the upper troposphere in association with the cyclogenesis could be attributed to the nondivergent wind.

In October 1954 Hurricane Hazel destroyed the Carolinas region of the USA. Subsequent to landfall the storm became situated beneath the forward side of a very strong large amplitude baroclinic trough approaching from the west. Hazel was transformed into an intense extratropical cyclone that moved poleward and westward and resulted in widespread damage from high winds and flooding over portions of the Appalachian Mountains and southern Canada. In a contribution from 1958 Palmén provided evidence that the transformation of Hazel into an extratropical storm was strongly related to the vertical circulations associated with the advancing synoptic scale trough and he speculated that the substantial amount of latent heat release in the tropical air that was swept into the larger scale circulation must have been crucial to the extraordinary intensity of the transformed cyclone. *Anthes (1990)* provided confirmation of Palmén's speculation in a numerical simulation of this historic storm. Without latent heat release the cyclone central pressure in the simulated storm was approximately 25 hPa higher than in the run incorporating latent heat release. The

air parcels trajectories showed that the implied moisture originated over the warm waters of the Gulf Stream and its ensuing north to north-westward path beneath the forward side of the impressively-deep large amplitude 300 hPa trough.

Palmén (1958) also provided the primary motivation for the author and one of his former graduate students, Geoffrey DiMego, to research the transformation of Hurricane Agnes into an extratropical storm over the eastern United States in June 1972. *DiMego and Bosart (1982 a ,b)* showed that the ambient cyclonic vorticity and deep moisture surrounding Agnes subsequent to landfall was crucial to the transformation and regeneration process when it was acted upon by strong low level convergence beneath the updraft region of an advancing unusually strong polar trough from the west. A comparable Southern Hemisphere investigation by *Sinclair (1993)* showed that ascent in the equatorward entrance region of a propagating subtropical jet helped to sustain the transformation of a tropical cyclone to an extratropical disturbance as tropical moisture was swept poleward beneath the updraft region.

Palmén (1958, 1959, 1961) also used the Hazel case to calculate kinetic energy and water vapour budgets from which he deduced that extratropical cyclones must play a very important role in the general circulation of the atmosphere. He was particularly intrigued by the generation of a very strong jet stream on the forward side of the aforementioned large amplitude trough in the 400-200 hPa layer. The existence of this jet stream was deduced from the comparatively few available radiosonde wind observations in the upper troposphere combined with geostrophic wind estimates inferred from numerous mass field observations. As noted *Palmén (1958)* "the kinetic energy produced by the sinking cold air and ascending warm air in the extratropical cyclone "Hazel" was to a very large extent available for export out of the source region. This export occurred ... between 400 and 200 hPa in the form of an upper jet stream leaving the active disturbance". *Palmén's (1958)* demonstration of the outward kinetic energy flux in the upper troposphere away from Hazel and its importance in the maintenance of the upper level westerlies in middle latitudes is also completely consistent with the recent theoretical interest in the phenomena of downstream development (see e.g. *Orlanski and Chang 1993*, *Chang 1993* or *Orlanski and Sheldon 1993*). Downstream development was also evident in the original work of *Hövmöller (1949)* in which he plotted longitude-time diagrams of 500 hPa height variations along key latitudes.

In another landmark scientific contribution, *Newton and Palmén (1963)* documented the kinematic structure of an intense large amplitude trough over eastern Northern America and an equally impressive large amplitude ridge over the central Atlantic Ocean. This real data example clearly illustrates the important differences between the geostrophic and gradient winds in the upper troposphere, particularly in the Atlantic ridge where the flow aloft was supergeostrophic but consistent with gradient wind balance limitations in a quasi-stationary large-amplitude ridge. Equally noteworthy was the presence of a geostrophic vorticity maxima in the base of the 500 hPa trough while observed vorticity maxima first appeared on the back side (west of the trough axis) of the trough and then shifted to the forward side of the trough as a transient disturbance rounded the base of the long wave trough. The *Newton and Palmén (1963)* case study was especially important in illustrating that jet streaks, consisting mostly of shear vorticity in the north-westerly flow behind the trough axis, typically reform on the forward side of the trough (in conjunction processes described by *Palmén, 1959*) as opposed to simple advection around the base of the long wave trough. Taken together the innovative aspects of the *Palmén (1958, 1959, 1961)*, *Newton and Palmén (1963)* and *Krishnamurti (1968)* papers lay in their emphasis on quantitatively diagnosing the three dimensional airflow through developing extratropical cyclones and the budgets of kinetic energy and water vapour (in Palmén's case) by a variety of suitable means. An important outcome from their (and other) investigations was the understanding that

cyclogenesis should be viewed as a process and not a thing and that the process consists of both dynamical and thermodynamical components.

1.5 The isentropic view and air mass exchange concept

The emphasis on examining the evolutions of cyclones in three dimensions as cited above was also the core of viewing development in isentropic coordinates as originally pioneered by *Rossby and Collaborators (1937 a, b)*, *Montgomery (1937)*, *Wexler and Namias (1938)* and *Namias (1938, 1939)* and discussed subsequently by (for example) *Browning and Harold (1969)*, *Carlson (1980)*, *Iskenderian (1988)* and *Browning (1990)*. A crucial assumption in most of these papers is that time-to-space conversion techniques can be used to "create" observations at intermediate times between radiosonde launches to facilitate the preparation of isentropic trajectories necessary for the Lagrangian perspective on storm development. A clear weakness of this approach, however, is that the evolution of highly time-dependent secondary circulations associated with rapidly developing (or weakening) weather systems may be masked by the required steady state assumption for atmospheric flow between the times of available radiosonde datasets. However, in the comparatively few case studies of nondeepening cyclones (*Iskenderian 1988*) in the literature the time-to-space conversion technique has been useful in understanding the mechanism of precipitation growth and concentration near the cyclone centre and along and ahead of the surface warm front. Ascending air parcels beneath the southerly flow overspread the warm front and bifurcate with the eastern branch turning anticyclonically and exiting the storm downstream and the western branch turning cyclonically around the cyclone centre before descending back toward the ground or ascending and turning anticyclonically farther west.

The use of isentropic analysis as a tool to uncover the time-dependent behaviour of air movement through middle latitude cyclones received an unexpectedly large boost in the 1960's by the United States Atomic Energy Commission. The Commission was motivated to provide research support to study the circulations in cyclonic storms because of widespread reports of radioactive debris from above-ground atomic tests in Nevada and the tropical Pacific being brought to the surface as wet and dry fallout during the passage of these storms over USA. *Briggs and Roach (1963)* and especially Danielsen and colleagues (*Danielsen 1964, 1966, Danielsen and Bleck 1967*; *Danielsen et al. 1987*), whose early research was supported by the Atomic Energy Commission and *Shapiro (1974, 1976, 1980)* pioneered the use of research aircraft observations and conventional datasets to study the structure of middle latitude cyclones and upper level fronts using quasi-conservative tracers such as PV, ozone and selected radioactive isotopes to map air movement on isentropic surfaces. These authors took advantage of earlier studies by *Reed and Sanders (1953)*, *Newton (1954)*, *Reed (1955)* and *Staley (1960)*, among others that had established the general validity and significance of using PV conservation as a diagnostic tool in synoptic-dynamic studies of upper-level frontogenesis.

To same extent *Danielsen's (1964, 1966)* scientific contribution to the understanding of airflow cyclonic disturbances was somewhat undervalued because he published many of his detailed findings in unrefereed scientific reports. Danielsen used his superb manual analysis skills to combine special radiosonde datasets with aircraft observations to prepare vertically consistent three dimensional analyses of meteorological fields in isentropic surfaces for selected cyclonic disturbances in the early 1960's. These analyses were then manually gridded and digitized for the purpose of diagnosing quantities such as PV. Isentropic trajectories were computed manually using the methodology described in *Danielsen (1961)*. The care in which the analyses were prepared enabled Danielsen to produce a reliable set of

isentropic trajectories at 6 or 12 h intervals over 36-48 h periods that were noteworthy for quasi-conservatism of PV (*Starr and Neiburger, 1940*), ozone and radioactive isotope concentration. Danielsen's trajectories provided convincing evidence that air parcels in the upper troposphere and lower stratosphere in the north-westerly flow behind the cyclone descended abruptly with time-averaged vertical motions of upwards of 10 cm/s such that stratospheric air was extruded deep into the lower and middle troposphere.

A careful inspection of the plotted maps and analyses in *Danielsen (1964, 1966)* also reveals that the quasi-PV conservation along the isentropic trajectories enabled him to deduce the existence of the "dry-slot" and the characteristic comma cloud shape in cyclonic storms of middle latitudes prior to the widespread availability of satellite imagery that showed such signatures to be commonplace. Furthermore, Danielsen's analyses established that the air parcels comprising the dry slot were very dry because of a previous history of subsidence, often from the lower stratosphere, and that individual air parcels near the tip of the dry slot were beginning to ascend again on the forward side of the trough. Danielsen noted how this dry air could contribute to the generation of deep conditional instability as it was swept downstream above the deep warm front cloud, raising the possibility that wet fallout could be triggered by areas of convection embedded in the warm frontal precipitation region. *Carr and Millard (1985)* in a composite study of the structure of comma clouds over the United States also showed that ascending air near the tip of the dry slot could be instrumental in helping to trigger the growth of new convection in the poleward segment of the dry slot in response to differential diabatic heating in the initially clear air.

Data at isentropic surfaces give forecasters the opportunity to take full advantage of the many benefits derived from viewing the atmosphere in isentropic coordinates. The ability to see "three dimensionally" in isentropic space is especially useful in applying conceptual models of cyclone circulation and moisture transport such as described by *Carlson (1980)* and in determining the structure of upper level jet/front systems.

1.6 Observed cyclogenesis studies

In search of synoptic/dynamic conceptualizations of the life cycles of fronts, jet streams and the tropopause the Bergen school investigators were continually formulating refinements and alternatives to their discoveries. Tor Bergeron sketched conceptual schematics for a variety of frontal occlusions, in addition to new interpretations such as cold and warm fronts aloft and their associated cloud systems, including the symbols to be used for their depiction in surface frontal analysis, some of which are routinely applied to this day. *Bjerkness (1930)* formally acknowledged that the existing frontal models did not always satisfy the complexities of daily weather events and presented case study analyses that differentiated between broad (such as 100 km) versus narrow (10 km or less) cold fronts with similarly distributed precipitation systems, in addition to examples of multiple cold fronts within the same cyclone. In this same study, cold and warm fronts with rearward sloping ascent and associated broad areas of cloud precipitation were interpreted as in earlier studies. However, cold fronts with clouds and precipitation focused at their leading edge were described as subsiding cold fronts. Subsequent refinements by *Bergeron (1934, 1937)* integrated surface observations, differential cloud motions, cloud types, precipitation, and inferred microphysical processes into the front-relative flow visualisations of ana (ascending) and kata (descending) cold fronts, and the warm anafront. These ideas were expanded upon by *Carlson (1980)* and *Browning (1986)* who combined relative isentropic-flow analysis and satellite cloud imagery to introduce the quasi-Lagrangian perspective of front-relative air stream referred to as the conveyor belt model of frontal cyclones. Besides, difficulties in

explaining of some observed features have also led to alternative conceptualizations such as split cold fronts (*Browning and Monk, 1982*), and cold fronts aloft (*Hobbs et al., 1990*).

The conveyor belt visualization is contrasted by the dynamical perspective of geostrophic momentum theory and it is *Sawyer (1956)-Eliassen (1962)* circulation equation that couples the geostrophic motions (primary circulation) to their companion ageostrophic vertical (secondary) circulations. A difficulty in conceptual reconciliation arises from the fact that the conveyor-belt models do not include a theoretical basis for their diagnosed air parcels displacements. Likewise, the Sawyer-Eliassen diagnosis does not address the relationship of clouds and precipitation to the geostrophic motions and their secondary circulations. Our attempt at unifying these two perspectives is based upon a qualitative application of the Sawyer-Eliassen equation, which deduces the geostrophic motions and their thermal deformations from secondary circulations consistent with front-relative air stream visualizations.

Difficulties in applying diagnostic frontal conceptualizations arise when (1) secondary circulation attribution (shear versus confluence) and frontogenesis partitioning (horizontal deformation versus differential vertical motion) vary significantly throughout that baroclinic life cycle, as was noted by *Bosart (1970)*, who presented three-hourly frontogenesis diagnostics revealing alternating dominance and sign reversals for deformation versus "tilting" for an upper-level front propagating trough a synoptic-scale wave; and (2) the temporal interval for an air parcel transect of a relative air stream is on the order of the period of the cyclone life cycle. When this is the case, the air streams are trajectories that do not easily couple to a specific jet/front or to instantaneous cloud and precipitation distributions in a manner that is valid trough much of a cyclone's life cycle. In either case, the difficulties are surmountable if the life cycles are partitioned into identifiable phases such as birth, growth, maturity and decay.

A mature extratropical cyclone shows usually the northward intrusion of warm air in advance of a surface cold front with the axis of the warm intrusion sloping eastward with the increasing height ahead of the cold front, and the low-level southerly jet beneath the axis. The earlier description of the warm air aloft in advance for cold fronts was by *Bjerknes and Palmén (1937)* in their analysis of the thermograph swarm ascents. This thermal feature and the associated low-level jet are also found within the mature idealized cyclones that develop in the numerical simulations of *Hoskins and West (1979)* and *Davies et al. (1991)*. *Hoskins and Heckley (1981)* suggest that a fundamental difference between cold and warm front is the forward tilt of the temperature wave for cold fronts and the backward tilt for warm fronts, noting that the vertical tilt of the thermal wave is necessary characteristic of amplifying baroclinic wave. The presence of the low-level jet enhances the cyclonic horizontal shear forcing at the leading edge of the cold front, with anticyclonic shear forcing to the anticyclonic side of the jet. The resulting secondary circulation contains two components: (1) the pure horizontal, shear, cold anafront circulation; and (2) the superimposed dipole circulation of the low-level jet that lies within the cold frontal zone, the combined frontal and jet forcing induces a cross-frontal circulation where the near-surface ageostrophic flow is directed toward the front from both the cold and warm sides (an enhancing mechanism for the frontal scale contraction) and the frontal ascent is directed vertically at the leading edge of the front. For situations in which the low-level jet is located in advance of the front, the jet-induced ascent of the secondary circulation precedes the cold front, and the associated cloud and precipitation systems are considered prefrontal.

A renewed interest in scientific issues related to the cyclogenesis process was sparked by the paper of *Sanders and Gyakum (1980)* on the synoptic-dynamic climatology of the "bomb" – explosively deepening cyclone. They have revealed that explosively deepening cyclones are primarily a cool season marine phenomenon, are generally confined to the

western portions of the Atlantic and Pacific Ocean basins, occur preferentially in the vicinity of the Gulf Stream and Kuroshio Current, and are highly baroclinic systems that are subject to potentially large amounts of diabatic heating. Confirmation and extension of the *Sanders and Gyakum (1980)* climatology have come in subsequent studies by e.g. *Roebber (1984)* or *Rogers and Bosart (1986)*. These studies showed that differences in cyclone deepening rates were most dramatic between continental and marine cyclones. Important scientific issues were raised by these and other investigations as to the degree of importance of oceanic sensible and latent heat fluxes, convection, and latent heat release in the marine cyclogenesis process. At issue was whether explosive marine cyclogenesis was a manifestation of an extraordinary response to ordinary baroclinic forcing or was a unique response to special physical processes characteristic of the marine environment.

The degree of modulation of cyclogenesis by latent heat release has been debated for years in the earlier literature. For example, *Palmén and Holopainen (1962)* stressed the importance of latent heat release in augmenting the intensity of vertical circulations accompanying cyclogenesis. *Danard (1964)* made a similar point and emphasized that the impact of latent heat release in augmenting dry adiabatic vertical motions was a function of the environmental static stability. *Tracton (1973)* hypothesized that one possible reason that early operational Norwegian Meteorological School models frequently failed to predict the timing and intensity of cyclogenesis when deep convection was present near the cyclone centre was that they were unable to replicate the bulk effects of cumulus convection. Tracton further hypothesized that latent heat release associated with deep convection near the cyclone centre acted to intensify the ridge aloft over and downstream of the cyclone centre. As a result he argued that cyclonic vorticity advection was augmented over the cyclone centre immediately ahead of the advancing upstream trough aloft, a view consistent with the original self development ideas of *Sutcliffe and Forsdyke (1950)*. Recent support for this idea was provided by *Jury and Laing (1990)* in a study of a South African cyclone but in this case it was the oceanic heat fluxes in excess of 200 W/m^2 over the Agulhas Current that helped sharpen the downstream ridge, rendering cyclonic vorticity advection over the cyclone centre more effective in development.

The publication of Sanders and Gyakum climatology (*1980*) also triggered an avalanche of explosive cyclogenesis studies that included such famous storms as the great New England bomb of March 1971 (*Boyle and Bossart 1986*), the Cleveland Superbomb (e.g. *Hakim et al., 1994*), the Queen Elisabeth II (QEII) storm of September 1978 (e.g. *Kuo et al., 1991a*), the President's Day storm of February 1979 (e.g. *Whittaker, 1988*), the eastern Pacific storm of November 1981 (e.g. *Kuo and Reed, 1988*), the Ocean Ranger storm of February 1982 (e.g. *Kuo et al., 1991b*) and various ERICA (Experiment on Rapidly Intensifying Cyclones over Atlantic) storms (e.g. *Reed et al. 1993a, b*). Points of scientific contention in these and other investigations included the issues raised previously as well as questions to what extent data limitations and uncertainties may have masked attempts to identify the physical processes responsible for the cyclogenesis.

As an example, *Petterssen et al. (1962)* computed oceanic sensible heat fluxes for a variety of Atlantic cyclone events. They observed that these fluxes maximized in the advancing cold air mass behind the cold front and the surface cyclone and that in general the fluxes acted to damp the lower tropospheric environmental thickness wave, a situation unfavourable for cyclogenesis. The opposite situation occurred in the President's Day storm as *Bossart (1981)* demonstrated that oceanic sensible heat fluxes maximize in the south-western quadrant of an arctic anticyclone. These fluxes were of critical importance in warming, moistening and destabilizing the coastal marine boundary layer, thereby leading to the development of an intense coastal front along which the initial cyclogenesis commenced with explosive development following as a potent trough aloft (PV anomaly) reached the

eastern coast of North America. In the view of *Bossart and Lin (1984)* the antecedent growth of baroclinity , low level vorticity, and reduction in atmospheric static stability in the lower troposphere "preconditioned" the atmosphere for future rapid cyclonic vorticity growth as the updraft region and attendant low level convergence field associated with the advancing upper level trough reached the coast.

Accordingly, the findings from which a scientific consensus may be emerging, include: (1) that the role of oceanic heat and moisture fluxes in the cyclogenesis is time, regional, and life cycle dependent for a wide spectrum of extratropical cyclones (including polar lows and baroclinic developments that transform into warm core tropical storms), (2) that numerical studies of explosive marine cyclogenesis suggest that the oceanic sensible and latent heat fluxes are most crucial early in the life cycle of the cyclone and that much of the controversy in the literature as to their potential importance could be traced to the choice of model initialization time with respect to the phase of the cyclone life cycle, (3) that latent heat release processes may dominate dry baroclinic dynamics processes in the most explosive marine cyclogenesis case, (4) that extratropical cyclogenesis need to be viewed as a nonlinear interaction between ordinary baroclinic dynamics and diabatic processes, and (5) that extratropical cyclones exhibit a rich spectrum of three dimensional structures that are tied to the configuration and evolution of the synoptic scale flow and are modified regionally and locally.

This interpretation of the potential importance of a pre-existing cyclonic vorticity maximum to explosive cyclogenesis is also consistent with the results from *DiMego and Bosart (1982a, b)* on the reintensification of Hurricane Agnes and its ultimate transformation into an extratropical cyclone and is in agreement with the original ideas on the subject expressed by *Palmén and Newton (1969)*. A similar conclusion was reached by *Gyakum (1991)* who showed that growth of a small scale cyclone along an intense low-level frontal zone provided the antecedent vorticity for later rapid vorticity growth in the QEII storm. More generally, *Gyakum et al. (1992)* in a study of 794 North Pacific cyclones over nine cold seasons showed that the "sample of cases with a history of existence prior to maximum deepening is characterized by significantly larger maximum deepening rates" , a clear indication of the importance of "preconditioning" as defined above. Similarly, *Roebber (1993)* argued that the long tail of explosively deepening cyclones in his earlier statistical studies (*Roebber 1984 and 1989*) "may be a statistical manifestation of the more robust preconditioning of the cyclone environment in oceanic regions".

As to the issue of the importance of upper level versus lower level dynamical and thermodynamical processes (including oceanic sensible and latent heat fluxes) on cyclogenesis, recent papers (in addition to those cited above) by, e.g. *Hirschberg and Fritsch (1991a,b)*, *Rogers and Bosart (1991)* or *Reed et al. (1992)* and *Lackmann et al. (1994)* on these and related topics have helped to both clarify and sharpen existing scientific controversies and to provide testable scientific hypotheses for reconciling differing viewpoints.

To address the disparities between theory and observations, the research has then focused on the examination of the physical mechanisms that may contribute to baroclinic development. Relatively recently, the significance of processes associated with phenomena such as tropopause folds and isentropic potential vorticity anomalies, which reside in the upper troposphere and lower stratosphere, have emerged as potentially significant aspects of the problem. For example, *Shapiro (1982)* and *Uccelini et al. (1985)* have demonstrated that upper-level fronts and tropopause folds can exist prior to the onset of surface cyclogenesis and suggest that they are significant components of the deepening process. *Sanders (1986)* provided evidence that explosive maritime cyclogenesis is basically a baroclinic phenomenon in which the low levels respond dramatically to pre-existing upper-level forcing. Pertaining to

larger-scale effects, *Hoskins et al. (1985)* have revitalized and formalized concepts introduced by *Kleinschmidt (1950a, 1950b)*, and discussed the hypothetical cyclogenesis that would result from the movement of a pre-existing lower-stratospheric mass of anomalously high potential vorticity over a pre-existing low-level baroclinic zone.

The hypothesis that processes occurring near the tropopause influence the development and evolution of extratropical cyclones and, more generally, the three-dimensional distribution of pressure changes is not altogether new, however. Before the advent of baroclinic instability theory, which professes the importance of lower-tropospheric baroclinity, there was significance attached to the role that the lower stratosphere and the tropopause region played during development. Based partly on the findings of *Dines (1911)*, a German-Austrian school of thought developed under *Ficker (1920)* whereby stratospheric advections were an integral cause of pressure change in the lower levels. Later, statistical studies and analyses based on various forms of pressure- and height-tendency equations (e.g. *Vederman 1949*) found that sea level pressure changes were often associated with large density changes in the lower stratosphere. These studies also showed that processes such as divergence and temperature advections occurring in the vicinity of tropopause were highly correlated with pressure changes near the surface of the earth. In particular, *Fleagle (1948)* found that maximum rates of temperature advection occurred in a layer just above the tropopause, and that lower-tropospheric pressure change was largely determined by the temperature changes associated with these advections in the lower stratosphere. These and other early empirical and theoretical studies led to a number of cyclogenetic conceptualizations that focused on the apparent causal relationship between upper-level temperature change and cyclogenesis (e.g. *Austin, 1952*).

Due to sparsity of data and lack of computational speed and accuracy, these studies did not present conclusive evidence that linked the upper-level processes to low-level pressure change in a mutually consistent manner. Moreover, these studies never showed how and why these upper-level processes were initiated and maintained. As a result of these shortcomings and the diversion of efforts into the exciting arena of baroclinic instability theory, the focus on the cyclogenetic role of the lower stratosphere became secondary.

Hirschberg and Fritsch (1991a, b) studied the role of the tropopause undulations in the development, evolution, and structure of extratropical cyclones. These undulations, which are necessarily associated with isentropic potential vorticity anomalies, are such that relatively warm and cold air resides above the low and high portions of the undulation, respectively. The baroclinic nature of the atmosphere (specifically increasing wind speed with height) potentates the possibility of (1) large lower-stratospheric temperature advection downstream of warm and cold anomalies, and (2) the superposition of these upper-level thermal features over favourable regions of low static stability and warm advection in the lower troposphere.

Tropopause undulations are commonly observed in cross section trough synoptic-scale baroclinic waves (see Fig. A for three stages of a cyclone development and of its associated tropopause fold on the following page). Characteristically, the tropopause is high and the lower stratosphere is relatively cold over relatively warm tropospheric air on the west and east sides of the upper-level trough. Conversely, the tropopause is low and the lower stratosphere is relatively warm over relatively cold tropospheric air over the centre of the trough. Between the trough and the upstream and downstream ridges the tropopause slopes upward. The vertically sloping portion of the undulation, particularly on the east side of the trough, intersects a rather thick (~ 7 km) layer of air between 150 and 350 hPa. Hence, relatively warm air exists alongside relatively cold air at high isobaric levels throughout a deep layer. For example, at 200 hPa, there is a pocket of greater than -45°C air over the low portion of the undulation and less than -60°C air to its east, just under the highest portion of the undulation.

Slightly above this point, on the highest part of the tropopause, the temperature is less than -70°C. The horizontal scale of the tropopause undulation is also noteworthy.

From the centre of the warm pool, over the low portion of the tropopause, eastward to the centre of the cold pool is approximately 2000 km. Comparing with the upper-level fronts and the tropopause folds which are also presents in the section indicates that undulation is a much larger-scale feature as also can be seen on other high-level analyses (e.g. PV analyses).

With a typical tropopause undulation some typical characteristics have been connected. At 200 hPa the strong temperature gradient between the warm and cold temperature anomalies reveals the position of the sloping portion of the tropopause. This temperature gradient is not simply an upper-frontal baroclinic zone or a much smaller-scale tropopause fold. Such a frontal zone or fold may, however, be embedded within the large-scale gradient. The temperature gradient is aligned almost perpendicular to the wind, so that strong warm advection exists between the warm and cold pools. Strong cold advection is present on the west side of the warm pool. Often, such strong upper-level temperature advections exist over a relatively deep layer. In addition to the upper-level warm and cold pool structures and large temperature advections, other common characteristics of tropopause undulations include large horizontal static stability and isentropic potential vorticity gradients. *Boyle and Bossart (1986)* proposed that the extraordinary deepening of an extratropical cyclone was due to a combination of factors including pronounced thermal advection in a layer extending from the midtroposphere to the lower stratosphere in association with a steeply sloped tropopause.

The implication of the relationship between high-level temperature change and low-level pressure and height change to the development and evolution of extratropical cyclones is immediate and obvious. Any mechanism that can induce high-level warming or cooling can conceivably have a large impact on the intensity and distribution of pressure and pressure change in the lower troposphere. The processes associated with the development and evolution of tropopause undulations in a baroclinic environment can produce substantial temperature changes in the lower stratosphere. Moreover, the temperature advections that accompany the warm and cold pools near the tropopause undulations can become large and occur over relatively deep layers.

On the basis of this evidence, it is hypothesized that tropopause undulations, especially their associated temperature changes, can act synergistically with lower-tropospheric processes to initiate, maintain, and enhance the development of the extratropical cyclones. Specifically, if hydrostatic balance is assumed and if an isobaric lid exists, then the juxtaposition of high-level warmth associated with a developing tropopause undulation and low-level warmth associated with tropopause baroclinic regions creates the potential for the production of relatively low pressure at the ground. Background baroclinity trough its increase in wind speed with height provides the mechanism by which high- and low-level warmth can become superposed. That is, the relatively strong wind speeds at tropopause levels, in addition to the large temperature gradients, not only create large high-level temperature advections but also the possibility that this warm advection can become superposed over favoured regions of low stability and warmth in the lower troposphere where air masses propagate much more slowly.

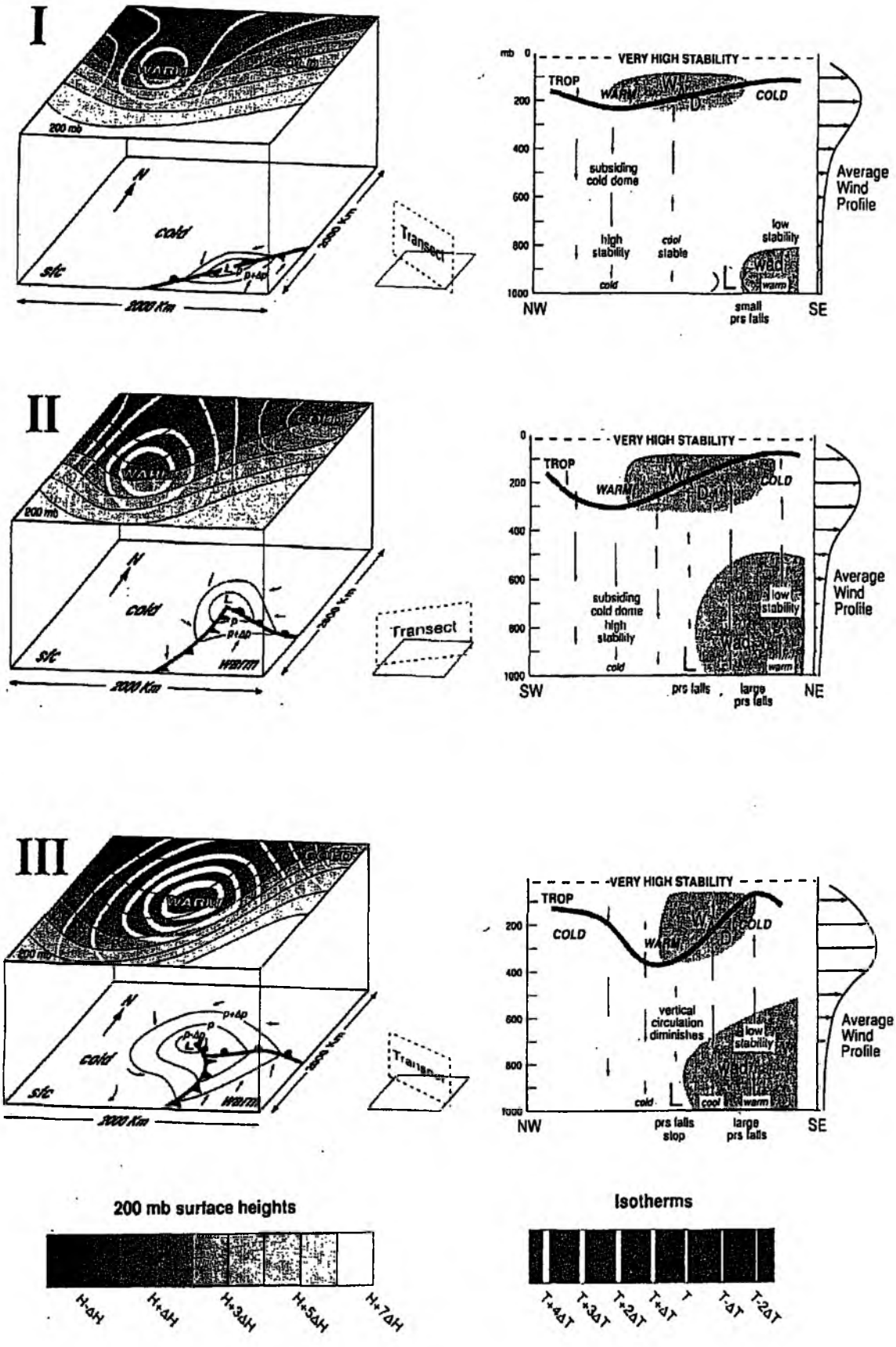

Fig. A: The development of tropopause undulation (from *Hirschberg and Fritsch, 1991 a, b)*

If a balance condition exists between the wind and the mass field, then the initiation and/or development of a surface cyclone is implicit with the formation of a low pressure centre. Subsequently, the upper-level temperature anomalies, the undulation, and the low-level cyclone can amplify simultaneously as a result of a self-development type of process, much like that envisioned by *Sutcliffe and Forsdyke (1950).*

Tropopause undulations are typically present prior to and during lower-tropospheric cyclone development. Since tropopause undulations exhibit large temperature anomalies in the upper troposphere and lower stratosphere as cyclone development ensues, the relationship of these temperature anomalies to lower tropospheric pressure and height changes was explored.

From a hydrostatic standpoint, a low pressure or low height centre must be associated with, in the vertical mean, a locally warm column of air above the low centre. Moreover, if the balance condition such as geostrophy is assumed, then cyclones must also be associated with a locally warm column of air. For intensification of a low centre or cyclone to occur, there must be a net warming of the air column above. Examination of the temporal derivative of the hypsometric equation shows that a given temperature change at low pressure (high altitude) will increase the mean temperature of a column and therefore the height and pressure falls in the lower portion of a column much more than would occur if the same temperature change occurred at a higher pressure (lower altitude). Therefore, temperature changes in the upper troposphere and lower stratosphere are potentially very important for lower-tropospheric development.

A case study of a rapidly developing cyclone showed that a region of warm lower-stratospheric air, associated with a developing tropopause undulation, significantly affected the location and intensity of the surface cyclone. The deepening low centre increasingly was located underneath relatively cooler tropospheric and warmer stratospheric temperatures. Similarly, the three-dimensional distribution of height and pressure change appears to have been very sensitive to the distribution of relative temperature changes and consequently on the development of the cyclone.

It was also found that there were large negative correlations between the observed high-level temperature changes and low-level height and vorticity changes. Lower-tropospheric height falls were associated with large lower-stratospheric warming, especially near 200 hPa, despite a deep layer of cooling in the tropopause. In general, the relationship between the spatial distributions of observed upper-level temperature and lower-level height change found in this study confirms many of the conclusions of previous pressure change studies. Moreover, the relationships are consistent with potential vorticity arguments and provide one explanation of how upper-level IPV anomalies can induce low-level vortices.
Based upon observations of many developing cyclones, *Hirschberg and Fritsch (1991 a, b)* have developed a conceptual model. It is based on certain hydrostatic and wind-field adjustments that occur between the upper and lower atmosphere when upper-level warm anomalies become superposed over low-level baroclinic zones. The adjustments are primarily due to imbalances caused by upper- and lower-level temperature and wind changes. Besides the obvious necessity for upper- and lower-level temperature gradients, the significance of baroclinicity to the overall process appears to be twofold. First, background baroclinicity is necessary for the maintenance of the large horizontal wind and phase speed at the tropopause level; and second, baroclinity implies that horizontal gradients of static stability exist.

This conceptual model is outlined by the following salient points about development (see also Fig. A for details):

I. Out-of-phase stage

1) Different vertical motion associated with a subsiding cold pool creates an undulation in the tropopause;
2) owing to the large ambient static stabilities, the subsidence-generated lower portion of the undulation is characterizes by large warming in the lower stratosphere while the downstream upper portion of the undulation is anomalously cold from the compensating ascent;
3) background tropospheric baroclinity coupled with the large temperature gradient above the sloping portion of the undulation produces strong high-level warm advection;
4) the high-level warm advection overwhelms cooling due to ascent and cold tropospheric advection;
5) net stratospheric warming produces height and pressure falls in the troposphere;
6) pressure falls enhance the horizontal winds, generate vorticity, and intensify the upper-level divergence and low-level convergence pattern, which strengthens the vertical circulation;
7) the intensified vertical circulation pattern enhances the tropopause undulation and the magnitude and vertical extent of the lower-stratospheric temperature anomalies;
8) the strengthening horizontal winds and tightening lower-stratospheric temperature gradient lead to larger lower-stratospheric temperature advections.

II. Developing stage

9) The superposition of the lower-stratospheric warm advections over favoured region of less stable air produces a state in which cooling by vertical motion and tropospheric advection is less able to compensate for the warming by lower-stratospheric advection;
10) in this state, height and pressure fall, vertical motions and stratospheric advections intensify rapidly;
11) eventually a surface cyclone arises or a shallow lower-tropospheric cyclone is encountered;
12) the lower-stratospheric warming deepens the low;
13) enhanced divergence and convergence in response to the deepening intensify the vertical motions and subsequently, the lower-stratospheric advections;
14) the enhanced vertical motions amplify the undulation which increases the stratospheric advections;
15) the largest height and pressure falls occurs where upper- and lower-level warm advections overlap;
16) the positive feedback process intensifies if less stable air is drawn into the circulation and/or condensation occurs;
17) the low migrates progressively closer to the base of the stratospheric warm pool as a consequence of the warming and deepening of the warm pool;
18) while the surface low is downstream from the high-level warm pool, i.e., while there is tilt, development can continue.

III. Occluded stage

19) Development of the primary low ends when it is directly under the warm pool;
20) height and pressure falls may continue downstream where upper- and lower-level warm advection overlap as long as lower stability air is available.

Although not mentioned specifically in the previous paragraph the configuration of the large scale flow also figures prominently in the evolution and characteristic cloud-shield signatures of extratropical cyclones and anticyclones. For example, *Namias and Clapp (1949)* and *Sawyer (1956)* demonstrated the frontogenetical nature of large scale confluent flow and the implied generation of cloud and precipitation by ascending motions on the equatorward side of the confluent jet entrance region. Large scale confluent flow in the entrance region of the great Asiatic jet stream plays and important role in focusing frontogenesis and small scale cyclogenesis along east-west oriented bands several thousand kilometres long in association with the Mei-Yu and Baiu rainy seasons in China and Japan, respectively in spring and early summer (e.g. *Wang et al., 1993*). During the cooler half of the year synoptic disturbances forming within the large scale confluent region over eastern Asia can become quite robust (e.g. *Chen and Dell'Osso, 1987*) in response to synoptic scale forcing mechanisms operating over a comparatively widespread regions (*Bullock and Gyakum, 1993*). These large scale confluent patterns are also a prominent feature of the baroclinic waveguides of *Wallace et al. (1988)*.

Sanders (1988) constructed a nine year climatology study of 500 hPa trough birth and death regions around the Northern Hemisphere. He found that on the average troughs are born (die) preferentially in north-westerly (south-westerly) flow regions downstream (upstream) of prominent mountainous regions. Although Sanders' results are open to challenge (he traced daily trough evolutions on the basis of the configuration/curvature of the 552 dam geopotential height contour as opposed to tracking individual vorticity centres) because his relatively simple analysis methodology may result in trough "loss" over mountain barriers and "rediscovery" downstream, his findings are in accord with synoptic experience. Frequently one finds large scale confluence in north-westerly flow in characteristic trough birth regions as noted by *Sanders et al. (1991)*. More generally, the results from *Sanders (1988)* clearly establish the long-lived nature of transient disturbances in the middle latitude westerlies and their importance in triggering surface cyclogenesis, especially in north-westerly flow situations downstream of prominent mountain barriers such as the Rockies (e.g. *Keishishian et al., 1994*) and Alps (e.g. *Tibaldi et al., 1990*).

In particular, the initial blocking of low level cold air by a mountain barrier such as the Alps can lead to a situation where a jet streak crossing the mountain barrier becomes unbalanced in that there is excess vertical wind shear for the weaker thermal gradient downwind of the barrier so that vigorous deep vertical circulations arise in response to the requirement for appreciable geostrophic adjustment. The mountains can also play an important role in the evolution of frontal structure associated with the developing lee cyclones, so much so that as the cyclone develops and eventually moves away from associated fronts through the occlusion stage may depart significantly from that envisioned in the idealized NCM. As noted in *Keshishian et al. (1994)* the degree of disagreement with the classical NCM is strongly a function of the synoptic scale flow and its orientation with respect to the mountains.

The theoretical and observational study of cyclogenesis has experienced a remarkable renewal of interest owing to the simultaneous emergence of new theoretical problems and new approaches to diagnose this phenomenon. The result is a significant change of perspective in cyclone conceptualization. It suggests, in turn, new approaches to observation and prediction of cyclones.

The new problems have arised from the studies of cyclogenesis on the 1000-km scale. This scale of motion is the only one explicitly mentioned in the founding paper on the life cycles of cyclones by *Bjerknes and Solberg (1922)*. This work related cyclones to previously existing fronts. The semigeostrophic theory of frontogenesis (*Sawyer, 1956; Eliassen, 1962*)

provides a simple but realistic description of atmospheric fronts. It may be worth recalling for reference that fronts combine rapid changes in temperature with vorticity maxima primarily localized near the vertical boundaries of the troposphere. Returning to 1000-km scale cyclogenesis, the first idea was to provide an instability theory of frontal cyclogenesis in the same spirit as *Charney (1947)* and *Eady (1949)* did for the larger-scale cyclogenesis in jet flows. The fronts offer greater organization of the wind field than the simple baroclinic zone. This can lead to a new set of conditions under which normal mode instability can occur along a front. For example, when remaining in the context of semigeostrophic theory, see *Joly and Thorpe (1990)*. This work provides a review of a number of other approaches in a variety of dynamical frameworks. *Malardel et al. (1993)*, however, pointed out that a frontal environment provides (downscale kinetic energy transfer due to the presence of wind shear) leads to active but short lived systems with very little pressure deepening, in contrast to "bombs".

The new theoretical approaches result from the long-lasting questioning of the relevance of the normal mode stability analysis as a theoretical explanation of cyclogenesis. This question, together with the alternative approach of the new development of already existing structures, had been voiced originally by *Sutcliffe (1947)*, *Kleinschmidt (1950a, b)*, and *Petterssen (1955)*; for historical review, see *Gronas a Shapiro (1997)*. *Farrell (1985, 1989)* provided the theoretical support to these views, applied originally to the explosive growth of large-scale waves in the context of quasigeostrophic dynamics. The general idea is that the same physical mechanisms present in the normal modes can be triggered much more efficiently by initial conditions involving organized precursors. The framework proposed by *Farrell (1988)* also addressed some of the difficulties noticed in the new work on frontal stability. For example, the timescale of frontogenesis is not different from that of frontal cyclogenesis, so the two mechanisms cannot be separated as neatly as the normal analysis requires. In the same spirit, it appears that time-dependent basic flows, not amenable to normal mode analysis in the strict sense, can lead to new mechanisms for the development-or the absence of development-of cyclonelike features.

The combination of these new problems and approaches has led to new theoretical interpretations of cyclogenesis. *Thorncroft and Hoskins (1990)* illustrated the nonlinear development of a cyclone along the cold front of a baroclinic wave initiated by an upper-level (tropopause) feature. This upper anomaly overcomes the stabilizing effect of frontogenesis shown by *Bishop and Thorpe (1994a, b)*. Bishop and Thorpe studied the effect of stretching deformation on moist frontal cyclogenesis. The effectiveness of the deformation to hinder cyclone formation is shown quantitatively. *Bishop (1993)* also explored the influence of deformation on the growth of a baroclinic wave. *Joly (1995)* generalized the results of *Malardel et al. (1993)* on the finite amplitude growth to a variety of initial conditions as well as to transient development: the baroclinic interaction appears to be the only mechanism that allows deepening greater than 10 hPa. This does not imply that the nonbaroclinic systems are weak during their short life cycle: just the reverse, it shows that looking only at the pressure field can be misleading. It appears that a whole new set of ideas and hypotheses are now available for testing against observations. The meteorological subjects of interest are not the explosive large-scale waves but a wider spectrum of more or less modest cyclones, which form along pre-existing fronts trailing behind large low pressure zones. These cyclones strongly depend on many properties of their environment: the baroclinity, the presence of low-level frontal jets and frontogenetic forcing, and the existence of transient, organized features, for example, potential vorticity features.

The ultimate objective, numerical forecast of these frontal or more generally, these "end-of-storm-track" cyclones, remains a serious practical problem, in spite of the continuous progress in numerical weather prediction. Although the general cyclone characteristics are

well predicted, an accurate forecast of precipitation in the concrete region varies with every new forecast, leading to little confidence in quantitative forecasts of these and other parameters. Clearly, however, the problem is not simply the ability of these models to represent cyclones properly, as some of the forecasts for a given event are excellent. This situation call for a different approach, something else than, for example, trying to improve parameterizations. This problem is indeed related to the sensitivity of these developments to initial conditions. Incidentally, the change of perspective advocated by Farrell in the theoretical understanding of cyclogenesis directly leads to expect such a problem with cyclone forecasting (*Farrell, 1990*). The richness of possible mechanism makes the difficulty even larger than with the pure baroclinic development problem.

Beside the need to evaluate the new theoretical ideas of cyclogenesis, there is also a demand for improved, validated, conceptual models of cyclogenesis, including improvements to physical process parameterizations, which can help the assessments of the real forecasts. There is a real need to explore technologies to provide, with a given model, a series of consistent successive forecasts in the range of 24-96 h, or at least to know whether this is conceivable. These requirements motivated the design of the FASTEX (*Jolly et al., 1997*).

The recent theoretical results presented above, supported by new case studies suggest the following hypotheses:

a) Dynamics of the frontal cyclones:

- The appearance or genesis of a cyclone at low levels (step 1) involves a variety of mechanisms, but its subsequent development (step 2), if it occurs involves only one mechanism, a baroclinic interaction with upper levels. These two stages may be separated by a few days of essentially nondevelopment behaviour.
- The genesis mechanisms include (1) the presence of a dynamically unstable quasi-steady low-level frontal environment or (2) triggering of the same energy conversion mechanism as in the instability theory by a precursor structure in an environment that then does not need to be unstable. Also (3), the active participation of the environmental flow is expected to play a crucial role through, for example, its induced deformation field.
- The development mechanism, the baroclinic interaction, results primarily from either upper-level pre-existing potential vorticity anomalies or from the upscale growth of the new, low-level cyclone generating its own upper-level component. A consequence is that a cyclone can go trough several stages of baroclinic development with transient upper-level coupling.

To address these issues, thermal and dynamical observations have to be collected when a low level cyclone forms, possibly prior to this occasion, as well as when it develops or reaches its mature stage. Also, not only the cyclone should be measured, but a fair portion of its environment as well.

b) Cyclone predictability:

Part of the problem of cyclone predictability is to obtain, as a result of the dynamical objectives, new theoretically and observationally validated conceptual models. These will identify the key properties of the flow that need to be observed and analyzed properly.
There is another approach, though, that is complementary to the previous one. Indeed, it may not be enough to get the generating mechanisms right to obtain a good forecast. It is also necessary to keep the error level in other parts of the flow as low as possible. As has been said above, cyclones may form in several different ways. This also means that small initial errors in the analysis have just as many different ways to grow, sometimes very rapidly, and wreck

the forecast. The predictability of cyclogenesis depends, therefore, on improved control of analysis and forecast error growth.

A possible practical solution is to concentrate measurements in the areas where small uncertainties may cause the greatest threat to the forecast quality. These areas, assumed to be few in numbers and relatively local in space, will obviously depend on the current flow. Hence the idea of an adaptive observing system has arised.

The basic concept is to concentrate measurements on areas that are dynamically critical for a proper prediction of cyclogenesis downstream of these zones in the next 24 to 36 h. Another key idea is that these areas should be objectively determined or predicted. At least part and perhaps all of, the answer can be provided by adjoint models.

Upper- and lower-troposphere coupling processes studied *Bouniol et al. (2002)* for the case of FASTEX IOP 16 cyclone (FASTEX - The Fronts and Atlantic Storm-Track Experiment, IOP - Intensive Observing Period). Authors investigated to identify processes involved in the deepening of frontal cyclones. They documented the ageostrophic circulation associated with the frontal cyclone observed during this FASTEX IOP. As the main goal was to investigate the environmental flow of the cyclone, the ECMWF analysis was used instead of the dedicated in situ and remote-sensing measurements that document the internal dynamics of the cyclone. It was observed that the cloud head develops in a region corresponding in the upper levels to the exit of a jet streak. Without curvature effects the expected circulation would be and indirect one and the variations in curvature suppress the ascending branch at 06 UTC while these vertical motions are amplified at 12 UTC. In the low levels, the dynamical flow that feeds the cloud head, commonly called the cold conveyor belt is associated with vertical motions that result from forcing (diabatic and adiabatic) processes. At 12 UTC, these ascending motions are the located below the ascending motions of the upper-level ageostrophic circulation. It was then found that the major process involved in the intensive cyclone development is the coupling process between the upper-level-jet and low-level-front ageostrophic circulation.

An investigation of the role of instability processes shows that the equivalent potential vorticity suggests that the tendency is to relax this instability in the coupling region leading then to a reinforcement of the vertical motions.

1.7 The potential vorticity perspective

First of all, let's focus on definition and characteristics of potential vorticity.
The potential vorticity (PV) is the absolute vorticity of an air parcel that is enclosed between two isentropic surfaces. If PV is displayed on a surface of constant potential temperature, then it is officially called isentropic potential vorticity (IPV). Of course, PV could also be displayed on another surface, for example on pressure surface. From the relation below we can deduce, that PV is simply the product of absolute vorticity on an isentropic surface and thermal stability. So PV consists, in contrast to vorticity on isobaric surfaces, of two factors, a dynamical element and a thermodynamical element:

$$PV = -g(\zeta_\theta + f)\frac{\partial \theta}{\partial p}$$

f Coriolis parameter,
g acceleration due to gravity,
p pressure,
PV potential vorticity,

Θ potential temperature,
ζ_Θ relative isentropic vorticity

Within the troposphere, the values of PV are usually low. However, the potential vorticity increases rapidly from the troposphere to the stratosphere due to the significant change of the static stability. Typical changes of the potential vorticity within the area of the tropopause are from 1 (tropospheric air) to 4 (stratospheric air) PV units (10^{-6} m^{-2} s^{-1} K kg^{-1}). Today in most of the literature the 2 PV units anomaly, which separates tropospheric air from stratospheric air, is referred as dynamical tropopause. The traditional way of the tropopause describing, is based on using of the potential temperature or thermal stability. But this is only a thermodynamical way of the tropopause characterising. The benefit of using PV is that the tropopause can be understood in both thermodynamic and dynamic terms. An abrupt folding or lowering of the dynamical tropopause can also be called as upper PV-anomaly. When this occurs, stratospheric air penetrates into the troposphere resulting in high values of PV with respect to the surroundings, creating a positive PV-anomaly. In the lower levels of the troposphere, strong baroclinic zones often occur which can be regarded as low level PV anomalies.

It must be stressed that this other way of looking at the dynamics of the atmosphere will not necessarily result in new conclusions. However, it may give new dimensions to things that in fact already have been known. The two main advantages of potential vorticity (with certain assumptions) are:

1) Conservation
2) Invertibility

Conservation

With the following assumptions PV is a conserved parameter:

- adiabatic stream (no diabatic heating or cooling),
- no friction in stream,
- homogenous stream,
- non-compressing sream.

A first mathematical consequence of the conservation can be derived from the definition of PV: A parcel will keep the same value of PV if it moves along an adiabat through the atmosphere. Thus the equation for PV can be written as:

$$-g(\zeta_\theta + f)\frac{\partial \theta}{\partial p} = const.$$

Due to the conservation of PV, there is a close relationship between absolute vorticity and thermal stability. The diagram (see Fig. B) below shows a cylinder with the top and bottom defined by the two isentropic surfaces. Difference in potential temperature between the top and bottom is the same for the two cylinders. If PV is conserved, and the cylinder is stretched as shown in (b), then thermal stability is decreasing and absolute vorticity must increase. Alternatively, if one goes from (b) to (a), then thermal stability is increasing and absolute vorticity must decrease.

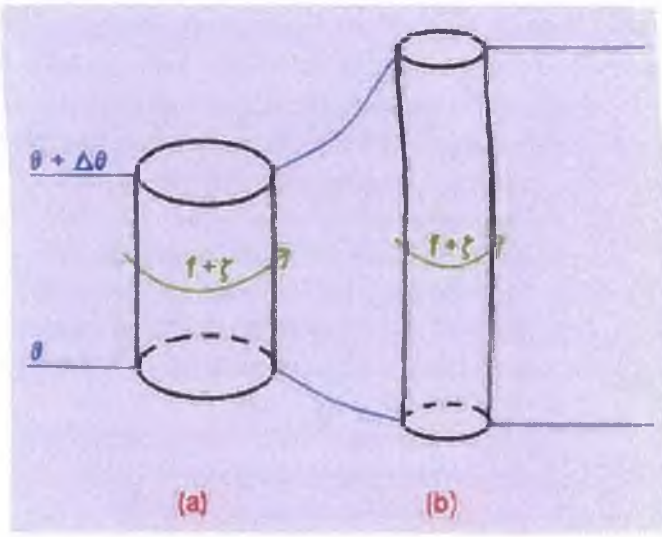

Fig. B: To the PV description

Due to the conservation of PV, significant features that are related to synoptic scale weather systems can be identified and followed in space as well as in time. This is a very powerful characteristic of this property. For instance, in the case of a lowering of the dynamical tropopause, the upper PV - anomaly can be followed in time and space rather easily. PV anomalies are well related to a lot of dynamical processes in the troposphere. A distinct example of this are cases of rapid cyclogenesis where PV - anomalies play an important role.

The sudden creation or destruction of PV means that diabatic processes are involved (release of latent heat, friction, radiation). This fact can be used as tool to identify or even to quantify the influence of these processes.

Invertibility

The second advantage of PV, invertibility, is a very important tool, because it allows one to obtain familiar meteorological fields, like the geopotential, wind, temperature and the static stability, when the distribution of the PV and the boundary conditions, potential temperature at the surface, are known. Further with the help of the invertibility it is possible to quantify the importance of PV-anomalies and the strength of their associated circulation and/or temperature pattern.

The pioneering using of PV as a quasi-conservative tracer of atmospheric motion on isentropic surfaces (quasi conservative in the sense that data limitations and uncertainities of analysis would preclude finding full PV conservation even under pure adiabatic and frictionless conditions) to diagnose life cycles of upper level fronts and cyclones is represented by the contributions of *Bleck (1990)* or *Reed et al. (1992)*. They were stimulated by *Hoskins et al. (1985)*. These authors conceptualized and quantified "PV thinking" as a base for dynamical studies of atmospheric motions on a wide variety of scales. They accomplished this task by demonstrating that knowledge of the PV distribution throughout the atmosphere combined with the specification of the boundary potential temperature could be used to deduce unambiguously three dimensional mass field in the atmosphere with point of view to the application of a balanced flow constraint. The publication of these seminal papers (see also the summary paper by *Hoskins (1990)*) has triggered a new avalanche of PV-based observational, numerical and theoretical studies.

An attraction of "PV thinking" is that synoptic development can be viewed as the interaction of a predecessor disturbance (PV anomaly) on the dynamical tropopause (defined

as a surface of constant PV) with a comparable disturbance near the ground (where a warm region can be viewed as equivalent to a positive PV anomaly on the bottom boundary) within the quasi-geostrophic framework. This dynamical interpretation of "PV thinking" is consistent with the original Sutcliffe-Petterssen self-development ideas described in subsection 1.3 and it is also in accord with quasi-geostrophic theory since the quasi-geostrophic height tendency equation is equivalent to the quasi-geostrophic potential vorticity equation. It also appeals to many theoreticians and modellers because, subject to a number of restrictions, the governing dynamics of atmospheric motions are "simplified" within the context of the *Eady (1949)* model in which atmospheric development is interpreted in terms of the mutual interaction of waves propagating along the tropopause and along the surface of a constant PV. *Frederick Sanders (1988)* has demonstrated convincingly what new ideas about cyclone development and cyclone life cycles have been learned from the PV approach. These ideas were unknown to Sutcliff-Petterssen self-development and traditional quasi-geostrophic theory authors.

Illustrative examples of the use of "PV thinking" to introduce diagnostic analysis of cyclone behaviour can be found, for example, in papers by *Hoskins et al. (1985)*, *Uccellini et al. (1987)* or *Davis and Emanuel (1991)* and *Davis (1993)*. Collectively these and other papers have pointed out that:

(1) predecessor disturbances (positive PV anomalies) are invariably present along the tropopause immediately upstream of the region where the lower level cyclonic disturbance will form,

(2) the shape, height and orientation of the tropopause with respect to the surface are of crucial importance to the overall evolution and intensity of cyclones and anticyclones.

Davis and Emanuel (1991), *Davis (1992)*, *Black and Dole (1993)* and *Davis (1993)*, among others, have attempted to quantify cyclogenesis on scales from 1000 to 10 000 km by attempting to isolate the dynamical contributions of upper- and lower-level PV anomalies using PV inversion methods. Use of this strategy, patterned after the *Eady (1949)* problem, enables them to quantitatively compare and contrast the contribution of transient individual tropopause and bottom boundary disturbances to individual cyclone life cycles.

Mannsfield (1996) utilized potential vorticity in cyclones forecasting. He have found out that operational aspects have presented a statistical analysis that was made to give an indication of the longevity of PV anomalies which establishes the reality of features in such highly differentiated fields and assesses their usefulness in tracing upper forcing patterns. A particular focus has been devoted to the correlation between 2 potential vorticity units (PVU) height charts and the water vapour image. The nature of this relationship between 2 PVU height and the water vapour channel radiance will be shown in the next section.

A mismatch between these two fields can indicate errors in either the model analysis or the forecast. An advantage of the use of PV in this way is that the nature of the error is clearly defined through the dynamical significance of the shape of the PV field. Furthermore, errors in the upper flow can be detected in cloud free regions and in principle a poor forecast of cyclogenesis could be adjusted before the development in apparent on infrared or visible imagery. Given suitable routines to invert the PV to the basic model variables, intervening in the analysis or data assimilation process to force the PV field to fit the water vapour image, is a potentially powerful technique for improving the model initial conditions, and hence the forecast.

However numerical models rarely fail to predict major cyclogenesis at short range (1-2 days) and in these cases the forcing mechanism is usually clear from other diagnostics such as upper height charts. Nevertheless PV charts can provide extra detail not readily apparent from height charts. This can suggest to the forecaster the forcing of less intense cyclones and small

synoptic scale or mesoscale features such as organized convective systems, which may not be well picked out on standard charts.

Ideally PV at more than one level would be used to fully diagnose the model behaviour but in the operational environment there is not enough time for the forecaster to assimilate a multitude of diagnostics and that's why it was felt a single preferred chart should be chosen. Upper forcing is clearly an important influence on the formation of troughs and small scale cyclones on the cold side of the polar front, whereas equatorward of the front high-level forcing is probably less important and initial developments dependent on low level thermal advection. Anomalies on the 2 PVU surface give a good representation of the forcing in the cold air, whereas a surface of potential temperature, chosen to intersect the tropopause near the polar front, will show only stratospheric anomalies in this region. Although not conserved, the geopotential height of the 2 PVU surface is surprisingly coherent temporally as well as being of dynamical significance, as it indicates the strength of any interaction between the tropopause and the surface (*Thorpe, 1994*). The lower the tropopause then, the more a tropopause anomaly can influence the surface development; in contrast, a large PV anomaly on an isentropic surface in the stratosphere may have only a weak influence at the surface due to its small vertical penetration. The height of the PV surface rather than its potential temperature is preferred as a diagnostic because it directly indicates the degree to which the anomaly is likely to influence the low level flow. As the tropopause (and therefore local PV anomaly) descends, say in the rear of a developing cyclone, this is shown by a decrease in the 2 PVU height, whereas the potential temperature remains constant giving no indication of the increasing potency of the lowering PV anomaly.

1.8 Some remarks about conceptual models of cyclone life cycles

Bergeron (1937) compared the surface temperature contrast between the air ahead of the warm front and the air behind the cold front to distinguish between warm and cold frontal occlusions as envisioned in the detailed Norweigan Meteorological School described in section 1.1. Although the idealized Norweigan Meteorological School has come under increasing criticism recently as being unrepresentative of the spectrum of observed cyclone, similar criticism already exists in the earlier literature. For example, *Palmén (1951)* states "there is no doubt that many occluded cyclones on surface maps have never gone through a real process of occlusion, although they show the same characteristic structure as really occluded polar-front perturbations". An illustrative example would be the formation of a lee trough downwind of the Rockies accompanying lee cyclogenesis. Typically, the lee trough is marked by a thermal ridge in the 1000-500 hPa thickness field. This thermal ridge differs little in appearance from a similar axis of warm air delineating a typical occluded front. *Schultz and Mass (1993)* examined 25 previously published case studies of occluding cyclones and found very little definitive evidence for the existence of a cold occlusion structure during the mature stage of the cyclone life cycle. Also, in their detailed numerical simulation (see also *Mass and Schultz, 1993*) of an intense North American cyclone they found evidence of a warm-type occlusion that differed significantly in structure and evolution from that envisioned by the idealized NCM.

The problem is the applicability of an idealized conceptual model of cyclone life cycles to real world cyclones that exhibit a rich spectrum of behaviour as a function of the mutual interaction of large scale and synoptic scale circulations that in turn are modulated regionally and locally by an additional spectrum of physiographic factors. *Rossby and Willett (1948)* suggested that the aspect ratio (zonal to meridional elongation) of individual transient cyclones was strongly dependent upon the amplitude of the large scale flow. More recently,

Black and Dole (1993) used PV inversion techniques to investigate the origin and maintenance of persistent cyclonic flow anomalies over the North Pacific in winter. They noted that "a few days prior to large-scale development, anomalies over the western North Pacific region, advect high PV air south-eastward from Asia into the western Pacific. As the PV maximum reaches the central Pacific, its associated circulation penetrates to the surface, resulting in a thermal advection pattern that produces a warm surface anomaly and associated surface cyclone development downshear of the upper-level centre. This is followed by strong baroclinic intensification. In several aspects this behaviour resembles a classical Petterssen Type B development (predecessor disturbance aloft) but occurs on a scale that is much larger than for typical synoptic scale cyclogenesis. The results indicate that the primary mechanism for the developments is a large-scale instability of (or initial value development upon) the three-dimensional time-mean flow, and suggest that nonmodal transient growth plays a significant role during development".

This process provides further evidence as to the rich variety of ways that cyclones can originate and evolve in response to circulation signatures that are modulated across a spectrum of length and time scales by physiographic features peculiar to specific regions of the planet. *Colucci (1985)* and *Bullock and Gyakum (1993)*, among others, have also demonstrated that the configuration of the large scale circulation impacts, and in turn is impacted by, synoptic scale flow evolution associated with cyclogenesis and anticyclogenesis. These often complex planetary scale and synoptic scale interactions come in a variety of "flavours" that can make it difficult to isolate and classify characteristic flow interaction signatures on the basis of a few idealized conceptual models alone.

Within the polar front theory no separation between wave development and rapid cyclogenesis can be found, and the distribution of the key parameters is very similar to, and even more distinct than, that for wave development. In addition to the wave model, the jet streak and surrounding sinking dry air play key roles. The emerging cloud head in the initial stage usually appears in the left exit region of a jet streak. The jet streak is parallel to the initial cloud band with dry stratospheric air approaching downstream into the cloud head. This can be seen as the typical black stripe in the WV imagery as well as the field of PV showing values higher than one PV units. While in the case of wave development stratospheric air (if present at all) does not reach down to levels lower than 300 hPa, in the case of rapid cyclogenesis stratospheric air is a key feature and protrudes much further downward (down to approximately 500 hPa or even lower).

The dry sinking stratospheric air has a significant impact upon the cloud configuration. As it dissolves the cloudiness between the front and the cloud head, a spiral structure as well as the typical V - pattern develops. This is closely connected with special characteristics of relative streams.

There are several conveyor belts involved belonging to the different cloud systems. The cloudiness of the main frontal zone is produced by a typical warm conveyor belt together with a humid relative stream from behind while the dry stream from behind appears behind the poleward edge of the frontal cloud band. This is the dry stream containing stratospheric air described above. The cloud head is formed within the lower and mid-levels of the troposphere by a rapidly ascending conveyor belt advecting warm and moist air from lower latitudes beneath the warm conveyor belt of the frontal zone. After crossing this cold front zone the conveyor belt often splits into a westward and an eastward flowing branch. This splitting of the relative flow leads to the convex-formed cloud edge at the pole ward side of the cloud head. This is comparable to the occlusion process in wave development.

As PV anomalies and baroclinic zones are involved, rapid cyclogenesis may be a good example of the Hoskins theory that an upper level PV anomaly, with its associated lowered

tropopause, overrunning a low level baroclinic zone induces a cyclonic circulation within the upper levels of the troposphere.

Comparing again wave development and rapid cyclogenesis, a main difference can be found in the orientation of the relative stream forming the cloud head, or cloud bulge. It is similar to a warm conveyor belt in the case of the wave turning to east/north-eastern direction, but quite opposite in the case of rapid cyclogenesis turning to west/south-western directions. There are some differences between the two models, which can lead to this different behaviour:

- in the case of rapid cyclogenesis, two frontal zones (or at least a very broad one) exist which cause the rising conveyor belt to reach the rear side of the surface low. This may result, together with the upper stream, in a south-westward split;
- in the case of a wave, the relative stream remains on the leading edge of the surface low, which may, together with the upper level stream, lead to a north-eastward split.

Chapter 2: Applications of the satellites in the field of NWP

2.1 Introduction

Since the first meteorological satellites were launched in the seventies, the number of instruments carried on board increased dramatically. As for geostationary, so for polar-orbiting satellites their observations complement and partially substitute the observations based on classical methods (aerological and ground measurements). Mainly to their unique potential to provide global observations also over traditionally data sparse regions (oceans and weakly populated areas) a great success in satellite data utilizing for numerical weather prediction (NWP) models has been reached.

Satellite data provide important information for assessing of the climate models performance and for studies of climate variability and trends, as well. For these applications, the calibrated radiances are usually processed to produce high-level products, such as cloud amounts, radiative fluxes, precipitation rates and so on. Such products are very convenient for evaluating models, because the corresponding fields are produced routinely during model simulations, so that relatively little additional processing of the model output is required (*Chaboreau, 2000*).

Concerning NWP it is now standard practice to use the radiances themselves and to assimilate them directly into a weather-forecast model by the model fields adjusting to minimize the differences between the observed radiances and the results simulated by the model. This requires an accurate forward NWP model to provide the simulated radiances, as well as knowledge of the error characteristics both for the method and for the data to optimize the assimilation by variational methods. The main advantage of radiances used as representation of high-level products of NWP model for comparison with observed satellite data consists in preservation of information content of the data with the minimal processing. It enables a wide variety of data types to be assimilated, by the help of a forward model.

In routine meteorological analysis the satellite measurements are used for wide variety of purposes. They can be used for location of large scale atmospheric phenomena such as frontal zones or circulation centres at ground as well as at high levels. Satellite measurements are also very important for identifying of much smaller scale features such as instability lines and convection regions, frontal waves and so on, that are only rarely detected by ground observations. Additionally, using of single images following the features movement make it possible to get a first guess of movement of these features in the near future (*Fourrie, 2003*).

2.2 Relationship between satellite data and dynamical parameters computed by NWP models

Upper troposphere and lower stratosphere region is a significant reservoir of the potential vorticity (PV), as already mentioned above. The structure of the upper-level PV field, specifically the structure of anomalous PV near the tropopause, plays a critical role in the dynamics of tropospheric weather systems (e.g. *Hoskins et al.*, 1985). That's why connection between PV-field and signatures in the satellite images are the subject of many studies.

There exist well known connections between such weather systems like lows and their clouds or humidity fields on satellite pictures. For example, during cyclogenesis there should exist strong correlation between location of the driest air that flows in the rear part of the developing cyclone and the potential vorticity maximum in the high levels or, alternatively,

minimum of the 2-PVU surface height (*Ringer, 2002*). It is a deformation of the tropopause that leads to an intrusion of a thin wedge of stratospheric air through upper-level fronts into the mid- and lower troposphere. A low tropopause level is generally characterized by a stratospheric air intrusion associated with high potential vorticity values (*Mannsfield, 1996*). These upper-level PV anomalies are typical for tropopause breaks that correspond to the step between the high tropopause level south of the upper-level jet streak and the low tropopause level north of this streak. These upper-level PV anomalies represent upper-level components of the baroclinic interaction scheme. This scheme is involved in the surface lows deepening larger than 9-10 hPa per 24 h (*Ayrault and Joly, 2000*) and consists in the interaction between two PV anomalies, the first of them located at the tropopause level and the second near the surface. There is a difference between these two anomalies that often indicates error in the development or analysis in NWP model. Because analysis errors often lead to the errors in the forecast, these differences warn the forecaster and they identify the areas where adjustation in numerical model prediction should be established.

Great attention has been paid to the possibility of utilizing of TOVS (TIROS Operational Vertical Sounder) observations for the identification of tropopause-level thermal anomalies. TOVS, which is carried on-board the National Oceanic and Atmospheric Administration (NOAA) satellites, consists in three passive vertical sounding instruments: HIRS-2 (High Infrared Resolution Spectrometer), radiometer with 19 channels in the infrared band and with one channel in the visible band; the MSU (Microwave Sounding Unit), a microwave sounder with four channels in the vicinity of 55 GHz; and the Stratospheric Sounding Unit (SSU), a pressure-modified infrared radiometer with three channels near 15 micrometers. The channels that are most sensitive to the temperature around the tropopause are HIRS-2 channels 2 and 3 and MSU channels 2, 3 and 4. The spatial resolution of HIRS-2 is about 17 km at nadir: the swath width is about 2400 km. There are two operational NOAA satellites. At low latitudes each satellite observes a point on the earth every 12 hours, but at high latitudes, overlap between swaths allows more frequent sampling.

As for MSU channels, *Velden (1992)* has demonstrated the applicability of utilizing 54.96-GHz channel (channel 3) of MSU brightness temperature imagery to infer the position, size orientation and relative strength of tropopause-level thermal anomalies. These warm and cold anomalies that lie over the low and under the high portions of tropopause undulations, respectively, are dynamically linked to PV anomalies and they are also directly related to the hydrostatic structure and development of baroclinic waves and cyclones, as described in chapter 1. Synoptic-scale tropospheric troughs and low pressure centres are hydrostatically induced underneath stratospheric warm (low density) pools and they are deepened by strong tropopause-level warm (negative density) advection. This *Velden (1992)* study have suggested that the channel 3 of MSU observations that are available every 6 h may be a valuable diagnostic tool that can be used to monitor the progression of upper-level features in numerical simulations of cyclone events over conventional data-sparse regions, especially when used in conjunction with other satellite-derived products. He founded several interesting conclusions:

1) A qualitative presentation is made of the large-scale and upper-level thermal pattern evolution. For this patter there is characteristic warm anomaly, which can be used to infer the position, size, orientation and relative strength of the descended portion of the associated tropopause undulation. Most important fact: the tendencies of these parameters can be followed by examination of the sequenced imagery that is nominally available in 6-h intervals.

2) In those cases of rapid cyclogenesis, the prolonged juxtaposition of the downstream portion of the MSU-depicted warm anomaly with the surface low appears related to the period of rapid deepening. Conversely, the superposition of the MSU warm-anomaly maximum with

the surface low centre indicates an occlusion stage has been reached, marking the cessation of the development phase.

3) In the three cases of explosive cyclogenesis that were examined by *Velden (1992)*, the MSU warm signature strengthened concurrently with the rapid deepening phase of the surface cyclogenesis, indicating these observations may be best used in a nowcasting framework. In one case, the warm anomaly increased in size and strength preceding the development of the surface low, suggesting trough amplification was occurring prior to the rapid surface cyclogenesis. In fact, a possible stratospheric extrusion feature was suggested in the imagery just prior to rapid development.

4) Forecaster confidence in operational model performance can be enhanced in real time by matching model-based forecasts of upper-level thermal fields with the verifying MSU imagery. This application can also extend to the research community, to help support conceptualizations and verify model-based evaluations of the relative importance of upper-level processes in rapid cyclogenesis events.

But the comparison illustrated that care should be taken in regard to single image interpretation. It is physically reasonable to observe surface lows of different intensities supported by warm anomalies (upper-level troughs) of equal strength. It is the proper juxtaposition and not just the absolute magnitude of the MSU warm anomaly that appears important to surface development. The four cases examined suggest that the optimum nowcasting utilization of the MSU observations might result from monitoring the evolution of the warm anomalies with respect to the surface low positions. The MSU signatures can be useful in analysis tools and may contribute to improved nowcasting of rapidly deepening oceanic events. From a research standpoint, numerous case studies and modelling simulations have suggested that upper-tropospheric processes can play a key role in rapid surface cyclone development which is especially prevalent over marine areas. However, it is uncertain whether the retrieval scheme makes optimum use of the MSU data in this application. Inherent errors in the inversion process of converting radiances to atmospheric profiles may dampen the full extent of the anomalies observed in the radiance data (imagery) alone.

Hirschberg et al. (1997) has made a comparison between the MSU channel 3 brightness temperature and conventional fields during many events. This statistically study was performed on a 6-month global dataset over Northern Hemisphere during cold season consisting of satellite-derived channel 3 MSU (MSU3) brightness temperature and various conventionally derived fields to quantify the potential usefulness of MSU3 analyses in the nowcasting and forecasting of baroclinic waves. In general, statistically significant correlations were found between the MSU3 brightness temperature and various conventional fields that have been shown to be dynamically linked to the upper-level temperature field and baroclinic wave development. The strongest positive correlations were found between the MSU3 brightness temperature and the 400-100 hPa thickness field. High positive correlations between these two fields were evident in both time and space and over all wavelengths and periods in global data. Thus, features in the 400-100 hPa thickness are readily observed by the MSU3 over majority of the global domain and can be used with a high degree of confidence for tracking these features. Hirschberg also pointed out the potential usefulness of the MSU3 to detect and track more specific thermal anomalies along the tropopause. These tropopause-level thermal anomalies are important features in cyclogenesis. The ability of the MSU3 to detect and track these features is evident in the high positive temporal correlations found between the whole spectrum of MUS3 brightness temperature and the 200 hPa temperature patterns over much of the domain. The MSU3-500 hPa and MSU3-50 hPa height correlation results have indicated scale dependence in the hydrostatic spreading of thickness anomalies in the vertical. Most significantly, relatively high negative MSU3-500 hPa height correlations for the short (less than or equal to synoptic scale) wavelength portion of the data suggest that

upper-level thermal anomalies are reflected downward and that MSU3 analyses can be used to track midlevel synoptic-scale baroclinic waves. This conclusion is also supported by relatively high negative MSU3-500 hPa vorticity and MSU-3 dynamic tropopause correlations along the climatological storm tracks.

Fourrié et al. (2000) have used TOVS (HIRS-2 and MSU) observations converted into atmospheric variables by the help of the 3I retrieval algorithm. The 3I method is a physical and statistical algorithm which determines temperature profiles from surface up to 10 hPa as well as other atmospheric variables (cloud occurrence, cloud amount and height, total water-vapour content and relative humidities in three tropospheric layers and other). All variables are retrieved for rain-free areas in boxes of 100x100 km^2, resulting from a compromise between HIRS-1 and MSU spatial resolution. The inversion of the radiative-transfer equation is split into two steps: first, the observed clear column or "de-clouded" radiances are used to retrieve the "best" initial guess solution. The procedure makes use of the previously defined TIGR (Thermodynamic Initial Guess Retrieval) dataset. In the second step, the deviations between the observation and the initial solution are minimized using a Bayesian-type direct estimation method. Authors have computed the so-called TLS ("Temperature of lower stratosphere"), which is supposed to represent the temperature around the tropopause and slightly above. TLS is obtained through a combination of brightness temperatures from five TOVS (HIRS-2 and MSU) channels weighted by a set of regression coefficients obtained from the TIGR dataset. In the first step, an increased horizontal-resolution determination of this variable was develop (30x30 km^2 instead of 100x100 km^2), in order to be able to detect small-scale features. Then, the contribution of each channel and the coefficients used in the determination were carefully analysed, so that the role of each channel was assessed. While, as expected, MSU3 plays the major role, the other channels are also significant. TLS variations were studied for three FASTEX IOPs, conducted over the northern Atlantic in January and February 1997. A case of cold-air cyclogenesis (IOP 18), a case of frontal cyclogenesis (IOP 17) and a second-generation wave (IOP 16) were investigated. For the three cases, TLS fields were carefully analysed and local maxima tracked. TLS fields show more variability than MSU3 due to better spatial and vertical resolutions. TLS anomalies generally appear earlier and are more intense than MSU3 anomalies. An important result is that TLS fields show closed anomalies, while MSU3 often displays only steep gradients. This comes from ancillary information provided by HIRS-2 channels and, to a certain extent, from TIGR through the regression coefficients. This peculiarity enables the amplitude of the TLS anomaly to be followed, which is important in itself, as illustrated by the comparative temporal evolution of the low surface pressure and the maximum in TLS. It shows in some cases: (i) before the triggering phase of the low, an increase in TLS values, and (ii) during the development phase, a good coincidence between the increase of TLS values and the deepening of the low in the case of surface/upper-level interactions.

In addition, global comparisons with synoptically based diagnostics (temperature at 2 PVU level - T-2pvu, wind and geopotential height) show that TLS fields allow the detection of other upper-level structures such as troughs, ridges and tropopause breaks along the cyclonic-shear side of an upper level jet. When looking at TLS anomaly centre positions, and T-2pvu core trajectories, a good agreement is generally found. The position of the anomaly maximum relative to the surface low is informative about the processes that govern its development. Quantitative comparisons of TLS and the temperature deduced from APREGE for different PVU surfaces, indicate that, quantitatively, TLS is a good indicator of the temperature between 4 and 8 PVU (i.e. in the layer 1-4.5 km above the tropopause).

The current practice of forecasting has transformed the forecaster into a decision-taker: he does not perform the forecast but he has to assess the reliability of numerical scenarios proposed to him. The comparison with information other than that obtained from numerical

suites is a critical step in this assessment. Parameters such as TLS are needed to make this part of the work as objective as possible. The Advanced Microwave Sounding Unit (AMSU), now on-board the NOAA satellites (replacement of MSU and SSU), significantly increases the remote-sensing capabilities for temperature retrievals both in terms of horizontal and vertical resolution: it consists of twenty channels with horizontal resolution of 45 km at nadir. A study conducted before the launch of AMSU showed that the accuracy of the TLS regression, using only a combination of AMSU channels, was significantly increased. This emphasizes the future capability of TLS for detection upper-level structures.

Recently, much progress has been made in the direct assimilation radiance measurements in numerical weather-prediction systems *(Harris and Kelly, 2001)*. E.g., in order to use radiances from the TIROS Operational Vertical Sounder, biases between the observed radiances and those simulated from the model first guess must be corrected. The original scheme for TOVS radiance-bias correction at the ECMWR utilized a global scan correction, and a linear air-mass correction, with the observed radiances from the MSU channels 2, 3 and 4 as predictors. The new scheme differs in two fundamentals ways. Analysis of radiance data shows a significant residual scan bias which depends strongly on latitude for some channels. The new scheme applies a latitudinally dependent scan correction to take this into account. The air-mass predictors are now computed from the background field, since the background field contains a more consistent representation of the air-mass and surface characteristics than the observed microwave radiances. Four new predictors are used, 1000-300 hPa thickness, 200-50 hPa thickness, model surface skin temperature and total precipitable water. In particular, the skin –temperature predictor is able to differentiate between ocean and sea-ice, performing much better than the old scheme in the winter hemisphere. The use of model predictors is a change in philosophy away from correction of the observations to correction of the computed forward radiances. This leads to a natural extension where the gradient of the bias correction can be taken into account in variational retrieval schemes.

Chevallier and Kelly (2002) have presented a monitoring of the ECMWF model with the Meteosat infrared window channel during December 2001. The Meteosat images are simulated every 3 h during the 31 days of the month from the model fields, at a resolution of 35 km. The study of both the spatial and the temporal variabilities of the model cloudiness have been based on forecasts, from 3 to 48 h, as well as on analyses. Despite a reduced cloud forcing in the model, the variations of the extratropical cyclones are shown to be well represented in the short-range (up to 1 day) forecasts. The intertropical convergence zone is well located but the representation of its temporal variations significantly differs from the observations, in particular over land. The variability of the Meteosat brightness temperature time series usually differs by more than 10 % from one model grid point to another, whereas the structures described by the model have scales of about three to four grid points at least. This work prepares the routine monitoring of the ECMWF analysis and forecast system with the raw images from Meteosat, now to be replaced by the Meteosat Second Generation imager/sounder, and is an important step toward the assimilation of cloud-affected satellite radiances.

Very "popular" in the studies there is utilizing of the water-vapour (WV) spectral channel images for validating and comparing the NWP outputs with the reality, since the WV images give us a lot of information about dynamics of the atmosphere.

One of the main features in WV images are rather narrow dark (in the usual way of white-black colouring where warmer colours are more dark) stripes lying along the cyclonic side of bright bands and fibres. Typically they occur on the cyclonic side of a jet axis, to the rear of cold fronts and occlusions, and along the leading edge of warm fronts. The dark stripe represents sinking dry air which could be of stratospheric origin. As such, the stripe can be

used as an indication of cloud dissipation from above and/or to indicate possible unstable development at the boundary between dry and moist air.

Dark stripes in WV images are especially useful if they are combined with relative streams where they can frequently be found associated with dry intrusions as well as with isentropic potential vorticity. Dark stripes in WV images are often accompanied by PV anomalies. The distribution of PV shows a long narrow elongated zone of high PV gradients within the dark stripe, often with separate maxima. Dark stripes in WV can also be used to detect discrepancies between numerical models and actual observations because of the tight relationship between PV and WV.

WV dark stripes are not only associated with PV but can also be used as indicators for the advection of PV. Because of the fact that dark stripes are narrow and elongated they are difficult to find in numerical model output. Therefore, advection of PV can be used for more detailed forecasts of the potential vorticity field.

Synoptic scale dry zones, detectable by radiance in WV channel are associated with areas of tropopause folding. The vertical distribution of potential vorticity depicts the folding of the tropopause. The tropopause folding is a very important feature and its evolution is closely related with the synoptic development, as documented above. Interpreting WV imagery in the view of PV concept enables to follow the tropopause folding, associated with PV anomalies, and provides with a set of powerful methods for synoptic scale analysis.

In addition to the tropopause folding and PV anomalies, the jet stream related patterns are the other important for the operational forecasting features, seen on WV imagery. Typically, on a WV image, there are many well defined boundary features, and only some of them are associated with jet stream axes. The constant surface of potential vorticity (PV) equal to 1.5 PVU or 2 PVU (*Santurette and Georgiev, 2005)* represents the tropopause from a dynamical point of view (see). The jet stream axes are present along the boundaries of different moisture regimes produced by significant tropopause foldings, indicated by strong gradient in geopotential of this dynamical tropopause surface. Generally, there is well defined jet stream axis nearly coincident with the moisture boundaries oriented southwest-northeast. The jet axis of the maximum wind speed is likely along the most contrast part of moisture boundary in the WV image.

The relationship between upper-tropospheric PV fields and water vapour images is very complex and has been explored by number of authors. It is as yet a qualitative rather than quantitative relationship, and is rather subjective in sense that its interpretation is highly dependent on the experience of the human interpreter. These are many features of it which can cause confusion and misinterpretation. The WV channel is not an atmospheric window, so the satellite sees only the WV radiation emitted from the upper moist part of the troposphere. This usually corresponds to a layer from the tropopause down to about 500 hPa.

But in a very simplified manner, the correlation between potential vorticity fields and water vapour images can be explained, as follows. The stratosphere consists of air of which the potential vorticity is much larger than in the troposphere. Therefore, a positive potential vorticity anomaly-at midlatitudes to be associated with a low pressure area-can be envisaged as a local lowering of the tropopause. In the so-called "topographic interpretation" of water vapour satellite imagery (*Weldon and Holmes, 1991*) the radiation/brightness temperature can be identified with the temperature of the upper boundary of tropospheric moist air, which boundary roughly coincides with the tropopause. So, since temperature decreases with height, a local lowering of the tropopause expresses itself in a higher value of radiation/brightness temperature. A higher radiation/brightness temperature is indicated by a darker shade of grey in a water vapour image. Therefore, positive potential vorticity anomalies correspond to dark regions in water vapour images. This relationship becomes problematic at lower latitudes, as discussed, among other difficulties, by *Swarbrick (1999). Mansfield (1996)*, as already

mentioned above, in particular demonstrated that valuable insights into the dynamics of cyclonic misforecasts can be obtained by comparing PV fields with WV images. *Appenzeller and Davies (1992)* have shown that potential vorticity fields and water vapour images are remarkably well correlated at midlatitudes.

However, there is no simple one-to-one correspondence between high PV and high radiance. Some of the more important complicating factors which must be taken into account when interpreting the PV-WV comparison air as follows:

- The PV-WV comparison is usually examined in a single isentropic level (typically 315-330 K) or isobaric level (typically 300-400 hPa), which intersects the tropopause at polar front latitudes. However, PV anomalies and dry intrusions both have vertical depth. It is necessary to examine them on a range of vertical levels in order to asses how the PV is to be adjusted on different levels. This is particularly pertinent when the image is affected by clouds (which is usually the case); for example, a dry intrusion will often pass beneath a layer of overlying cirrus and so be partly obscured from the satellite's view.
- As explained above, WV channel radiance depends on the humidity distribution in the atmospheric column. However, it also depends on the mean air temperature of the column. So, for example, a stratospheric dry intrusion which happened to occur at a location where the mean column temperature is relatively low would give rise to a lower radiance feature than would a similar intrusion at a location with higher mean column temperature.
- Stratospheric intrusions occur only in the vicinity of the polar front, so the PV-WV relationship is valid only in this vicinity, and to some extent on the poleward side of it. There is no meaningful PV-WV relationship on the equatorward side, but they are not associated with PV anomalies. They are rather a consequence of the higher atmospheric mean column temperature in air masses of tropical origin.
- The PV-WV relationship is meaningful only in connection with developing cyclonic systems. It is not meaningful, for example, in connection with decaying cyclones, since by that stage of development the moist air and dry air have become too mixed up with each other. Nor is it meaningful for anticyclonic systems, in general.

The water vapour image and the corresponding potential vorticity can be seen very well on the isentropic surfaces, typically between 310 and 320 K. These surfaces show the most pronounced gradients in potential vorticity and therefore indicate most clearly where the tropopause has large slopes. According to the interpretation discussed above, plots of potential vorticity on these surfaces are expected to correlate maximally with water vapour images.

Quantitative relationship between Meteosat WV data and positive potential vorticity anomalies for a case study (for Mediterranean region) has been studied by *Georgiev (1999)*, who has applied the concept of isentropic potential vorticity to help interpret and understand cyclone development. Potential vorticity on the 300 and 850 hPa isobaric surfaces as well as the 300 hPa relative vorticity have been used for systematic description of western Mediterranean cyclones. He has found that comparing some of fields such assuming PV on the isentropic surface 310 K and potential temperature on the 1.5 PVU with WV imagery has the potential to verify and validate numerical output. Other dynamical parameters that are closely corresponding to the WV brightness are the 300 hPa absolute vorticity and positive PV advection at 500 hPa. For this reason, as well as being associated with midtropospheric descent or ascent, they could be successfully used as complementary diagnostic and prognostic tools for studying both cyclogenesis initiation and cyclonic evolution over the Mediterranean. Georgiev presented here case study of 2 cyclones over Northern Africa and in

the Alpine region and studied the correlation between Meteosat WV data and positive anomalies of potential vorticity. The layer of contribution where the main part (about 80 percent) of the WV channel radiance is formed is on average 320 hPa thick. The level of maximum contribution lies between 380 and 500 hPa and moves downwards for dry air. The correlation analyses are performed at different isobaric surfaces in the middle and upper troposphere for two latitudinal belts (southern and northern). A significant correlation is obtained at 500 hPa (correlation coefficient range between 0.58 and 0.64). On the basis of results, the use of WV data as a tool for detection of errors in model-derived PV fields is discussed. It is concluded and suggested that, though some of the discrepancies between PV fields and WV images could be due to errors in the channel because of the changes in pressure over the commonly used PV fields, the comparison of the WV data with the field of positive PV anomalies at 500 hPa might be another approach to help solve the problem of verifying and validating numerical outputs. The relative lack of conventional upper-air data in the region of the Mediterranean-North African area tends to produce limitations for numerical modelling. This is the reason for stressing the use of WV data as an alternative and complementary way of using only numerical output.

Similar problem has solved *Swarbrick (2001)*. He has used the proposed relationship between model-generated upper-tropospheric PV fields and Meteosat WV images in forecast of initialization for a number of case studies involving model forecasts of North Atlantic cyclones. The objective of case studies was to reduce the errors in the forecast track and depth of cyclone by re-initialising the forecast via upper-level PV adjustment and PV inversion. The methodology has employed the PV-water vapour relationship to detect mismatches between PV fields and water vapour images, and has attempted to correct these mismatches by manual adjustment of the PV fields. These PV adjustments have been converted to wind and temperature increments by means of PV inversion and used to initialise the model fields in a way that preserves dynamical balance. Five case studies with small initialisation errors were carried out. The results of these case studies show some particular positive impacts on forecasts of cyclonic development, but overall the results do not demonstrate that the use of the PV-WV relation for forecast initialisation is a practical proposition for operational use. There is no doubt that PV-WV image comparison is very useful as a subjective diagnostic tool. However, case study work of this type is unlikely to yield useful results for the initialisation of NWP forecasts until a definitive quantitative relationship between upper-tropospheric PV and WV images is established.

Roca et al. (1997) have directly compared the WV channel with general circulation model results. Following a "model to satellite" approach authors have pointed out the ability of the general circulation model of the Laboratoire de Météorologie Dynamique to reproduce the observed relationship between tropical convection and subtropical moisture in the upper troposphere. Because the net effect of convection is to moisten the upper atmosphere, the relationship between convective cloudiness and water vapour is also one of the key issues for modelling the atmosphere. Authors have used observations from Meteosat 2 water vapour channel (5.7-7.1 micrometers) from July 1989 to July 1997. Under clear sky conditions, this channel is sensible to the atmospheric water vapour content above 500-600 hPa, whereas in cloudy atmosphere, the water vapour equivalent brightness temperature (WVEBT) is mainly influenced by the cloud top temperature, cloud optical properties and the water vapour above. Monthly means of WVEBT were constructed from the imagery available every 3 hours; the resolution has been averaged 3.7° in longitude x 2.5° in latitude net, which does no affect the smooth and large patterns of the WV monthly mean images. The study was restricted to the area: 45°N, 45°S, 45°E and 45°W.

The moist processes were simulated using threes schemes: a supersaturation scheme for non convective precipitation, a moist adiabatic adjustment scheme and Kuo scheme for

penetrative cumulus convection. The radiative transfer code was an improved formulation of the solar radiation algorithm of (*Fouquart and Bonnel, 1980*). The longwave radiation algorithm deals with clouds as grey bodies with a longwave emissivity depending on the cloud liquid water path. The radiances have then been converted into WVEBT using the filter function of the satellite.

The results have been compared from the climatological point of view for January, April, July and October. Generally, it can be said that the model results well represent the main observed features, although the upper level of the GCM tends to be too wet in the dry areas and too dry in the moist areas. But this seems to be characteristic of many climate and forecast models, may be due to an underprediction in the strength of the Hadley cell (*Soden and Bretherton, 1994*) or to a deficiency of the water vapour transport (*Schmetz and van de Berg, 1994*). Those results show the great potential of satellite water vapour observations for models validation.

Finally, *W.T.M. Verkley et al. (2005)* have developed a method that can be used to manually adjust a numerical weather analysis and they have studied the impact of the adjustment on the ensuing forecast. The research has been motivated by the fact that, at present, the highly automated numerical weather-forecasting system is not designed to allow for active invention by the operational forecaster. Indeed, the only instant at which intervention is supposed to take place is during the final stage of the forecasting procedure when the computer-generated weather maps are interpreted, possibly modified, and translated in terms understandable by the users. The On Screen Field Modification (OSFM) system developed by *Carroll (1997)* can, for example, be used to adjust the forecast afterwards by means of graphical interaction. There are, however, situations in which intervention is appropriate at an earlier stage. This is the case when it is noticed, e.g. by studying satellite images, that an analysis produced by the model is evidently wrong. The method described in this paper provides a possibility to intervene in such a situation.

This method is based on two important properties of PV, the invertibility principle (see chapter 1.8 for details), and that PV is (approximately) materially conserved which implies that its time evolution is mainly characterized by (horizontal) advection: changes in PV are mainly displacements and deformations. This is also a characteristic feature of tracers observed from satellite, like water vapour and ozone. The result is that fields of PV, water vapour and ozone develop the same kind of structures.

The model state to be modified is referred to as the analysis although in practice-as in the example to be discussed-it may also be a forecast. After the PV field of the analysis is adjusted, the adjustment needs to be translated in terms of pressure, wind and temperature. One way of doing this is to invert the modified PV field directly using some form of balance condition. In this case a three-dimensional variational data-assimilation technique is used (*Courtier et al. 1998*) in combination with nonlinear normal-mode initialization. The modified PV field is treated as information that is to be assimilated into the analysis. This is accomplished by replacing the observation term in the cost function of the three-dimensional variational data-assimilation system by a PV term. This term-in analogy with the observation term-measures the difference between the modified PV field and the PV field of the model state. By minimizing the cost function, a new model state is obtained that, after the nonlinear normal-mode initialization, approximates the modified PV field and respects the balance constraints of the model. The degree of resemblance between the modified PV before and after the data assimilation and initialization depends on the relative weights of the background term and the PV term in the cost function. The model is used to implement the technique is the HiRLAM of the Royal Netherlands Meteorological Institute and good results are obtained, at least for case studies described in this article.

In the last decade, greater attention has been paid not only to the WV channel but also to the infrared (IR, 11 micrometers) channel and its applications.

F. Chevallier and G. Kelly (2002) have compared model clouds with those seen from space. Because it has been emphasized in earlier studies that for validation as well as for assimilation derived products may be ambiguous because they are to be understood as radiative effective quantities, in the sense that they are pre-processed products with questionable errors associated with this processing. Therefore, an effort is made to develop the use of raw radiances. The high spatial resolution of the geostationary images makes it necessary to perform some averaging when comparing to model data. The resolution of global models has been dramatically increased in recent years so that synoptic scales features are taken into account more accurately.

IR images from the two Meteosat satellites operated by EUMETSAT have been compared to the simulated images from ECMWF system in this paper. The Meteosat images allow the investigation of both the spatial and the temporal variabilities of the cloudiness in the ECMWF analyses and forecasts. The resolution of Meteosat images has been degraded from 5 km to about 35 km in order to compare with the ECMWF model. This has been done by remapping the native satellite images to an equal-angle latitude-longitude grid. The Meteosat images have been simulated every 3 h by the model and the forecast is done to +48 hours.

Results have shown that the variability in the brightness temperature time series of the Meteosat data degraded to 35-km usually differs by more than 10% from one grid point to another, whereas the structures described by the model have scales about three to four grid points at least. Also, forecast quality when going from a 3-h range to a 24-h range has been very similar from the correlation point of view. The temporal variation of convection in the Tropics has been not well represented, in particular over land. The Intertropical zone of convergence has been well situated, but its time variances have differed significantly from observations. Otherwise, the model has reproduced the location of the midlatitude fronts very well, even over land.

2.3 Model-to-satellite approach and utilizing of satellite radiation measurements for model evaluation

In the context of numerical weather forecasting, the parameterizations responsible for producing the clouds and associate radiative fields were, for years, only questioned when meteorological parameters such as the temperature, within the atmosphere, or at the surface, were displaying a bias relative to the analyzed temperature profiles, or to the observations of the temperature at two metres. Precipitation was also produced independently from the clouds, trough the large scale condensation or convective processes, with almost no relation to the state of cloudiness. Profiles of cloud fraction and cloud water were than produced using diagnostic relationships (*Slingo, 1987*) linking those parameters to the relative humidity, with filters on vertical velocity and potential temperature gradient in an effort to represent boundary-layer clouds, or to the convective precipitation for representing the convective clouds and associated anvils. A study of the diurnal cycle of the model cloudiness as diagnosed from radiances simulated from the model fields (*Morcrette, 1991*) was one among other studies indicating the limited success of the model at representing the four-dimensional distribution of the cloudiness and cloud water at that time.

In 1995, the introduction of a cloud scheme (*Tiedtke, 1993*) with two prognostic equations for cloud amount and cloud water into the ECMWF model, shifted the emphasis, and more diagnostic studies have since been related to an evaluation of the quality of the clouds, particularly of the cloud cover and height (*Klein and Jakob, 1999*). However, in a

weather forecast context, the overall limited number of such studies, in the past, is mainly explained by the fact that, only the so-called cleared radiances are operationally used in the analyses, out of radiance data sets, measured either from polar-orbiting or geostationary satellites that originally include also cloudy radiances.

In the development of physical parameterizations, climatologies of clouds and radiation fields have been used over the years, but mainly for checking the long-term behaviour of the model, in seasonally-long simulations. However, in an operational environment such as ECMWF's, the time-scales over which such a validation should be conducted is quite large, from instantaneous snapshots to be compared to satellite imagery, to the 12-hours span of the first-guess forecasts used to create the background fields over which the analysis is performed, to the length of the operational forecasts, and to the several months encompassed by seasonal forecasts.

In the physical package of the ECMWF model, the Rapid Radiation Transfer Model, RRTM has been included. RRTM is a longwave radiation transfer scheme developed by *Mlawer et al. (1997)*, with accuracy equivalent to that of the line-by-line model from which it was developed. It replaced the longwave radiation scheme of Morcrette (*1991*).

J.J. Morcrette et al. (2001) have compared the outgoing longwave radiation (OLR) at top of the atmosphere produced by the ECMWF model derived from several HIRS/2 channel radiances from NOAA-14. He has concluded that the gross features of the OLR are properly represented by the ECMWF model, but a number of local deficiencies are also apparent, e.g. the too large OLR over equatorial Africa, north of South America or Papua New Guinea that indicates a lack of convective activity with clouds not penetrating high enough and/or with too little condensed water in their upper extent. In this respect, the revision of the evaporation of the falling precipitation has led to a decrease in the amount of cloud water, partly responsible for overestimation of the OLR. Over some of the desert areas of the globe, the model gives slightly smaller OLR, however part of the problem might be linked to the retrieval of LR from HIRS/2 observations and potential biases linked to the diurnal coverage of the satellite observations. At the other extreme of the range, the OLR over the Antarctica plateau is too high, certainly linked to too few or too transparent clouds.

As well as broadband fluxes, one can also diagnose (narrow) spectral radiances similar to the observations from the model vertical profiles of temperature, humidity and cloud cover and cloud condensed water using various radiation codes. The intercomparison procedure used in the above mentioned study is similar to the original approach by *Morcrette (1991)*. When attempting to validate the cloud distribution produced by a model with satellite-observed radiation fields, one can try to derive cloud physical parameters from these radiances and compare with the same model parameters (e.g., cloud condensates, cloud optical thickness, cloud effective radius, cloud top height or cloud fractional cover).

Most of the time, with the radiance data set there usually exist a large ensemble of differing cloud parameters likely to give very similar radiances at the top of the atmosphere. Another approach completely bypasses such retrieval and produces satellite-type radiances from the model temperature, humidity, and cloud fields, and the same cloud radiative parameters from the model temperature, humidity, and cloud fields, and the same cloud radiative parameters as used in the radiation scheme. This has the obvious advantage of minimizing the impact of modelling assumptions when transforming satellite-observed radiances into physical parameters (i.e., cloud fractional cover and cloud vertical overlap, cloud top height and/or temperature, condensed water content and cloud longwave emissivity). The modelling assumptions are basically only on the model side and the only difficulty is to make the model radiation scheme produce the satellite radiances within the same spectral channels and under the same geometry as the observations. Over the recent years, such an approach has recruited more and more adepts, not only within the operational

weather forecast community where the simulation of satellite radiances from model variables is at the core of variational assimilation methods (*Saunders et al., 1998; Rabier et al., 2000*), but also from the climate and mesoscale modelling community (*Roca et al., 1997; Chaboureau et al., 2000*). In this above mentioned study, RTTOV-6 (Radiative Transfer for TOVS) package is used (*Saunders et al., 1999*) first modified by *Rizzi (1994)* to include not the one-layer effective cloud of the original scheme, but the effect on the outgoing radiance of a vertical distribution of effective cloud layers also used in the ECMWF model radiation scheme. This package was recently further updated by *Chevallier et al. (2001)* to replace these effective cloud layers by a more proper treatment of the semi-transparent clouds using the true fractional cloud cover and layer emissivity following *Raisanen (1998)*. This so-called "cloudy" RTTOV-6 package has been used to simulate the radiances in various parts of the longwave spectrum. They have been compared to the corresponding radiances measured by different geostationary satellites.

By comparing model to satellite, it can be seen that model is reasonably successful in representation of the mid to high-level cloudiness that really impacts the top of the atmosphere brightness temperatures. Most of the main cloud systems are properly located. The only missing feature is the streak of the cirriform clouds across the Sahara.
Overall brightness temperature through these high clouds is usually overestimated by the model, with clouds either absent, not high or not optically thick enough. As for time evolution of the simulation and observed brightness temperatures in the Meteosat-7 longwave window it can be seen better results when comparing to the similar studies made by *Morcrette (1991)*. Mainly, a large fraction of the underestimation in the radiative effect of the high cloudiness linked to large-scale condensation, has now disappeared, compared to the 1990 model. Similarly the signature of the high cloudiness linked to convection, either as active towers or as optically thick anvil-type high clouds has somewhat improved relative to the 1990 model, but the high clouds do not still appear high, extended or optically thick enough and besides, the situation has not improved so drastically in areas of stratocumulus clouds off-cost Angola or trade-wind cumulus clouds in central mid-Atlantic. On the other hand one can see a too cold maximum surface temperature around local noon in Sahara area.

It has been shown how some satellite data are used to check and validate the clouds and radiation fields produced by ECMWF forecast model. In a weather forecast environment, stress is usually put on relatively short time and space scales for which the new generation of operational polar-orbiting (AMSU and forthcoming AIRS, IASI) and geostationary satellites (i.e., GOES-8, MSG) offer observations allowing to build more stringent test on the model representation of the cloud-radiative processes, particularly with respect to the life cycle of cloudiness, diurnal evolution of semi-tropical and tropical cloudiness. Observations from experiments on other research satellites (i.e., ADEOS-POLDER, but also CERES, MODIS) can also offer new avenues for verifying the model behaviour. The challenge is to find new and better ways of exploiting this information to first invalidate than improve the model.

J.J. Morcrette (1991) studied the diurnal cycle of the outgoing radiation at the top of the atmosphere. This offers a challenge to all large-scale numerical models of the atmosphere if a model is able to correctly reproduce the phase and amplitude of the response of the atmosphere to the diurnal cycle of insolation. That would be a strong proof of the validity of various parameterization schemes. Diurnal cycles of outgoing longwave radiation (OLR) produced by models been presented in the literature for the first time in the 1986 and 1987 (*Slingo et al. 1987*). They were, however, not compared to actual satellite observations.

One reason for scarcity may be that diurnal cycle is a relatively recent feature in most large-scale models. Moreover, comparisons between satellite-observed and model-generated diurnal cycles of OLR have been hindered by numerous obstacles. A meaningful comparison requires consistency in the space and time samples of the compared fields as well as in their

geometrical and radiometric characteristics. Up to now, comparisons of model output with observations (usually on a time-averaged basis) have used satellite measurements that were modified so as to obtain a quantity comparable to the model-generated quantity ("satellite-to-model approach"). That process introduces some uncertainties at best and some inconsistencies at worst. They are linked either to an insufficient sampling of the diurnal cycle (as with measurements from a single polar-orbiting satellite), or to the satellite viewing geometry (and the consequent necessity to account for limb darkening in the measurements), or to the conversion of the narrowband channel satellite measurement to broadband data.

The validation of the cloudiness forecast by a large-scale atmospheric model is difficult because of problems inherent in the retrieval of an "observed" cloudiness from satellite observations of radiances (*Slingo 1987*). Model cloudiness is characterized by cloud parameters such as fractional cover, cloud-top temperature, and cloud emissivity. These can be either diagnosed of prognosed via a cloud generation scheme. In the diagnostic approach, cloudiness is predicted through a statistical relationship from model variables. In general, relative humidity and at times other quantities are used (e.g., convective activity, atmospheric stability and vertical velocity in Slingo's scheme). In the prognostic approach, cloudiness is directly related to liquid water which is and additional model variable. Observational validation of these cloud parameters is highly dependent on the type of observations available (spatial and spectral resolution of the radiometer, time and space sampling of the data) and on the retrieval algorithm used. Important aspects include the definition of the background clear-sky radiance, the threshold values for threshold-type methods, the definition of the learning set for statistical methods, the role of the radiation scheme, and the optical characteristics assumed for the model clouds in the methods based on a radiative transfer analysis. *Rossow et al. (1985)* have given a detailed discussion of the methods and problems related to the extraction of the cloud cover from satellite-observed radiative measurements.

This paper adopts the "model-to-satellite approach" (*Morcrette et al., 1988*). It has used the temperature, humidity and cloudiness profiles produced by ECMWF operational forecast model to simulate as closely as possible measurements of the brightness temperatures in the longwave window (10.5 – 12.5 micrometers) channel of METEOSAT satellite. Comparisons of observed and simulated brightness temperatures are used to evaluate various aspect of the parameterization of the diurnal cycle of the surface-cloud-radiation interaction as seen from the top of the atmosphere. *Li and Le Treut (1989)* discussed comparisons between satellite data and model simulations using a simplified radiation transfer algorithm and neglecting the effects of the earth's sphericity. ,

In this paper the authors have justified the validity of their approach through comparisons of observed and simulated clear-sky longwave window brightness temperatures. In doing so, they have discussed some of expected differences between observed and simulated brightness temperatures. They have showed that comparison of the diurnal variability of the observed and model simulated brightness temperatures, as inferred from evolution histograms of brightness temperatures, sheds the valuable light on various deficiencies in the parameterization schemes.

The approach used in this paper has followed recommendations by ECMWF and proposals by *Slingo (1987)*, namely to produce model quantities directly comparable to satellite measurements. To do so, model outputs have been processed to reproduce the satellite measurements as closely as possible. Brightness temperatures in the longwave window channel of METEOSAT have been simulated from cloudiness, temperature and humidity fields produced by the forecast model and compared to the equivalent observations. The approach "model-to-satellite" minimizes the uncertainties due to potentially different assumptions (regarding for example cloud optical properties or surface emissivity) in the cloud retrieval scheme and the model radiation scheme. This is especially true if the same

radiation scheme is used both for simulating the diagnostic radiances and for computing the radiative heating rates required by the model's thermodynamic equation. Moreover, this approach makes provisions for a consistent use of radiance measurements from geostationary satellites on a real-time basis in as much as all necessary diagnostics are produced on the model side and do not rely on external satellite data processing the results of which might be available only in a delayed mode. Furthermore, this approach can be applied regardless of the horizontal resolution of the satellite measurements and the model outputs. Finally, the emphasis put on the evaluation of the radiative impact of the clouds more than of the clouds themselves is consistent with the cloud radiative forcing approach proposed by *Ramanathan (1987)* and with his work performed with ERBE (Earth Radiation Budget Experiment) measurements (*Ramanathan et al. 1989*).

Direct comparison of observed and model brightness temperatures illustrates the qualities and deficiencies of the diagnostic cloud scheme (*Slingo 1987*) operational in the ECMWF forecast model. For time and space scales considered in this study:

1) Frontal cloud systems are generally well represented.
2) Extended stratiform clouds associated with subsidence above cold oceanic currents along the subtropical western side of the African continent are underestimated and trade-wind cumuliform clouds are not represented at all.
3) Model brightness temperatures over high clouds are generally too warm, showing deficiencies in the diagnosed cloud cover and cloud liquid-water content.
4) The vertical extent of the convective cloudiness is rather well represented, but the deep clouds over land generally dissipate 6 h earlier than the observed ones.

Chaboureau et al (QJRMS 2000) has used a "model-to-satellite" approach to evaluate a simulation over the life-cycle of a cloud system during the FASTEX (Fronts and Atlantic Storm Track EXperiment), by comparing synthetic and Meteosat observed radiances. The usefulness of this approach, combining an explicit cloud scheme implemented in a mesoscale model with a detailed radiative-transfer code, has been shown. For a clear-sky evaluation of the radiative model, especially needed for the WV channel of METEOSAT, it has been shown that the operational calibrations warm the brightness temperatures by 3 K, a value relevant for climate studies. The precision in the brightness temperatures simulation is 4.5 K for the IR channel and 2 K for the WV respectively. In cloudy skies these values are found to be twice as large then in clear skies, when compared with TOVS-3I cloud parameters.

The occurrence of key patterns in the simulated infrared images has confirmed the good quality of the model simulation and the accuracy of the radiative code. On the other hand, discrepancies identified by the comparison have shown that the model overestimated the cloud-system extent, mostly at upper levels. As a suggestion, too much water might be detrained at upper levels by present meso-non-hydrostatic schemes, or the residence time of the cloud ice and water might be too long. Further investigations have been suggested to examine these possibilities, as well as to attempt higher-resolution simulations (in 10 km resolution range). Finally, significant improvement in the cloud-cover description and in the simulated BT maps has been found when the meso-non-hydrostatic cloud scheme was extended to include ice processes. These improvements have been noticed both in low level polar clouds over the Labrador Sea and at higher levels in frontal areas. However, this improvement hasn't corrected the overall cloud-cover overestimation in the model, particularly at upper levels.

Chapter 3: ARPEGE model and computation of brightness temperatures

3.1 Introduction

The synoptic interpretation of the NWP models outputs in this work is based on utilizing of the "model-to-satellite" approach. This approach consists in construction of satellite radiances for different observation channels for atmospheric profiles coming from numerical model outputs.

The overview of some articles and documents enables us to find/compare some similar studies in the field of this approach and techniques usable for users. The following list presents the interesting conclusions from references mentioned in chapter 2.3:

I) The idea is based on the application of the approach model versus observation that consists in the simulation of the observed fields with the forecasted values coming from the numerical model.
2) Some methods of the radiative transfer enable us to do this effective simulation, but they can generate some errors. These remaining faults are often neglected during the interpretations of the results.
3) The satellite observation is generally already available in the time and space term of the model output. For the final comparison the observation is averaged or sampled on the model grid and available for validation of the forecast.
4) The next statistics are computed for the observed and simulated variables: average, deviation, spatial and temporal correlation, the curvature frequency.
5) Some studies point out the techniques for image handling to explore the movement of the selected features on one image.
6) Based on the approach "model-to-satellite" for fine validation of the model, the interpretation of the model deviation must catch consideration of some probably errors sources:
    1. The insufficiently exact model description of the surface and atmosphere state (surface temperature, emissivity, temperature of the upper stratosphere levels, the profile of water vapour and so on).
    2. Inaccuracy of the collocation in time and space of the input data of the satellite and radiosondes.
    3. Problems with radiometers onboard of satellites.
    4. Limitations of the radiative transfer model.
    5. The limited representation of the surface emissivity.
    6. Insufficient description of the gases active radiative effect.
    7. And also the limitations coming from the radiation theory used in construction of the radiative transfer scheme.
7) The forecasted satellite images make it possible for perfect serve as the help tool for the operational forecast quality, but it has two problems: the time needed for computation and the difficulty for interpretation of the results due to some possible errors sources.
8) 3I technique (Improved Initialization Inversion) allows determine any thermodynamic fields to minimize the differences between simulation and observation. This technique is mostly applicable before the approach model versus satellite in points of these simulated thermodynamic fields approaching to that observed.

3.2 Description of the ARPEGE model and of the scheme for brightness temperature computation

Concerning model data, outputs from global model ARPEGE (ARPEGE=Action de Recherche Petite Echelle Grande Echelle) has been used. ARPEGE is used by the French Meteorological Service, and it is constructed with a variable step of grids (stretching) which enables to obtain higher resolution in the areas of interest. This concept can be utilized for numerical integration up to 4 or 5 days (according to the stretching coefficient) but the integration for longer period is carried out by ECMWF model (European Centre for Medium-Range Weather Forecasts) that uses the same code as ARPEGE model. The variable network is based on Schmidt's transformation which is a conform imaging (globe on globe). Two steps are used in operative practice, first one pole is rotated to the place of interest and, second, the resolution is increased poleward (and decreased in the vicinity of another pole). But the results in the network with stretching can not be reasonably studied and so interpolation to another network more suitable for visualisation must be established.

ARPEGE model can be integrated with various resolutions. Minimal configuration (Oper) for the case studies computed for this work has been about 25 km over France, about middle Europe about 30 km. Focussing here on synoptic features, resolution of NLON=240 (number of grid points on parallel) and NLAT=120 (number of grid points on meridian) is proved to be quite acceptable (i.e. the step of about 60km on the 50. parallel). Computations started on 00 UTC and maximal time integration interval was +96 hours (due to the stretching limitation-see above). Time step of integration was 15 minutes.

Finally, there must be remained that the brightness temperatures are diagnostic values. So their computation is based on the integration of prognostic model values and these integrations should be made at least two-times to minimize computational problems.

Data from geostationary satellite Meteosat 7, in infrared (IR) as well as in water vapour (WV) spectral band have been used and coloured according to the visualisation of the model brightness temperatures. For case studies presented in this work, hourly Meteosat data corresponding to forecast outputs were used. The horizontal resolution of Meteosat data in the central Europe is about 6-9 km. That's why we can observe more detailed structure in the observed images inclusive mesoscale structures. But this should be neglected due to focus on synoptic scale features as mentioned above.

The input data consist in observed and forecasted parameters used for global direct comparisons of model outputs with simulations of satellite measurements. The purpose is to simulate for model outputs those brightness temperatures that would be measured by satellites, if the observed atmosphere would be the same as the model atmosphere after process of integration. It means to make something like "synthetic" satellite images.

Comparison "model versus satellite" is based on creation of satellite images from parameters computed by ARPEGE model. These images represent simulated lota that can be directly compared with real observed images (for validation purposes).

Atmosphere is described by help of thermodynamic parameters and forecasted clouds are expressed in used scheme. Radiative transfer scheme by Morcrette computes spectral luminance as energy received by satellites in two forms: 1) cloudy-sky energy constructed by interactions of water droplets and ice particles radiation with Earth's radiation, 2) clear-sky energy caused by absorption and irradiation of Earth's long-wave radiation by various atmospheric components.

Therefore the brightness temperatures could be found as an inversion function to Planck's function. Computations are made for long-wave absorption bands, especially for infrared long-wave band (10.5-12.5 μm) and for the water vapour band (5.7-7.1 μm).

Morcrette's scheme of "model versus satellite code" has been used to compute brightness temperatures received from profiles constructed for predicted meteorological parameters of ARPEGE model. These brightness temperatures could be simulated in each grid point of ARPEGE model.

In the radiative transfer scheme various thermodynamic and physical variables are used, such as cloudiness, humidity, pressure etc., which have been computed by physical part of the ARPEGE model. Using of the function named SIMULRAD enables us to simulate spectral bands for both cases: cloudy as well as clear sky conditions. Function TBRIGHT enables to compute brightness temperatures for infrared and water vapour spectral band by Planck's function inversion. Then function of transitivity corresponding to the chosen satellite is called.

Both functions mentioned above are defined in frame of numerical process ALPAR added to ARPEGE's code and they are constructed with different schemes of physical parameterization. In the functions named MF_PHYS and CPG four new simulated temperatures corresponding to the brightness temperatures for clear and cloudy sky and for IR and WV bands are obtained. This scheme is shown on the Fig.1.

Finally, outputs of these four brightness temperatures are used in function CPG to compute function named CPXFU. For these integrated fields of brightness temperatures full-pos was done and the data were transformed to the GRIB format and drawn in Metview 3.4 software. The results can be then shown graphically in the form of numerical basis GRIB and compared with the real observed data. On Figs. 2-5 one example of these simulated images is presented for case of October 18th 2004, 00 UTC, for all four cases (e.g. always for situation with no cloudiness and with cloudiness in IR and WV channel).

This is the way how to get simulation of synthetic images by the model ARPEGE. These images can be then used for quantitative validation of the numerical model results and this procedure is utilized for each model pixel of the Earth for the numerical interpretation.

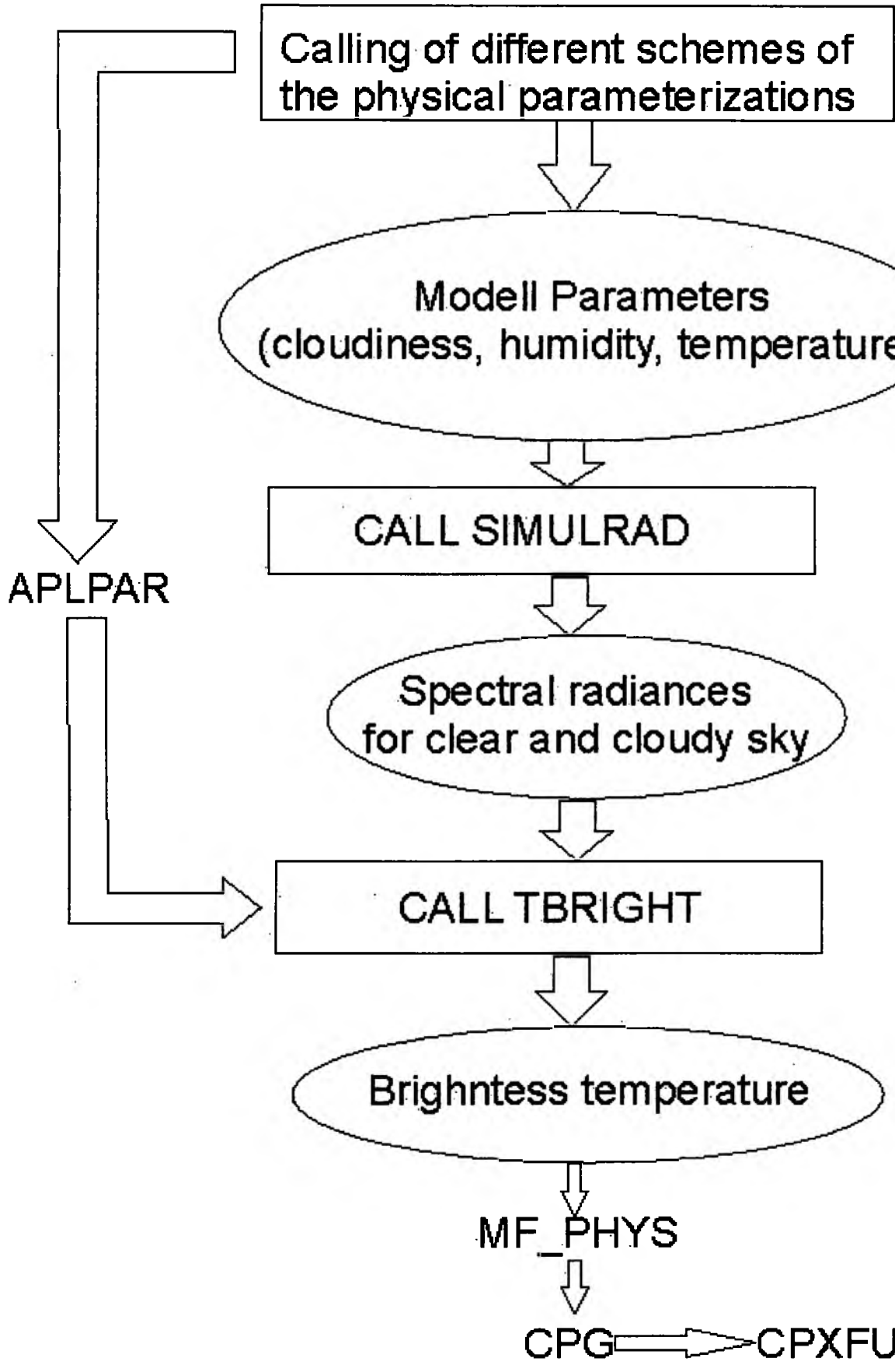

Fig. 1 Scheme for computing of brightness temperatures

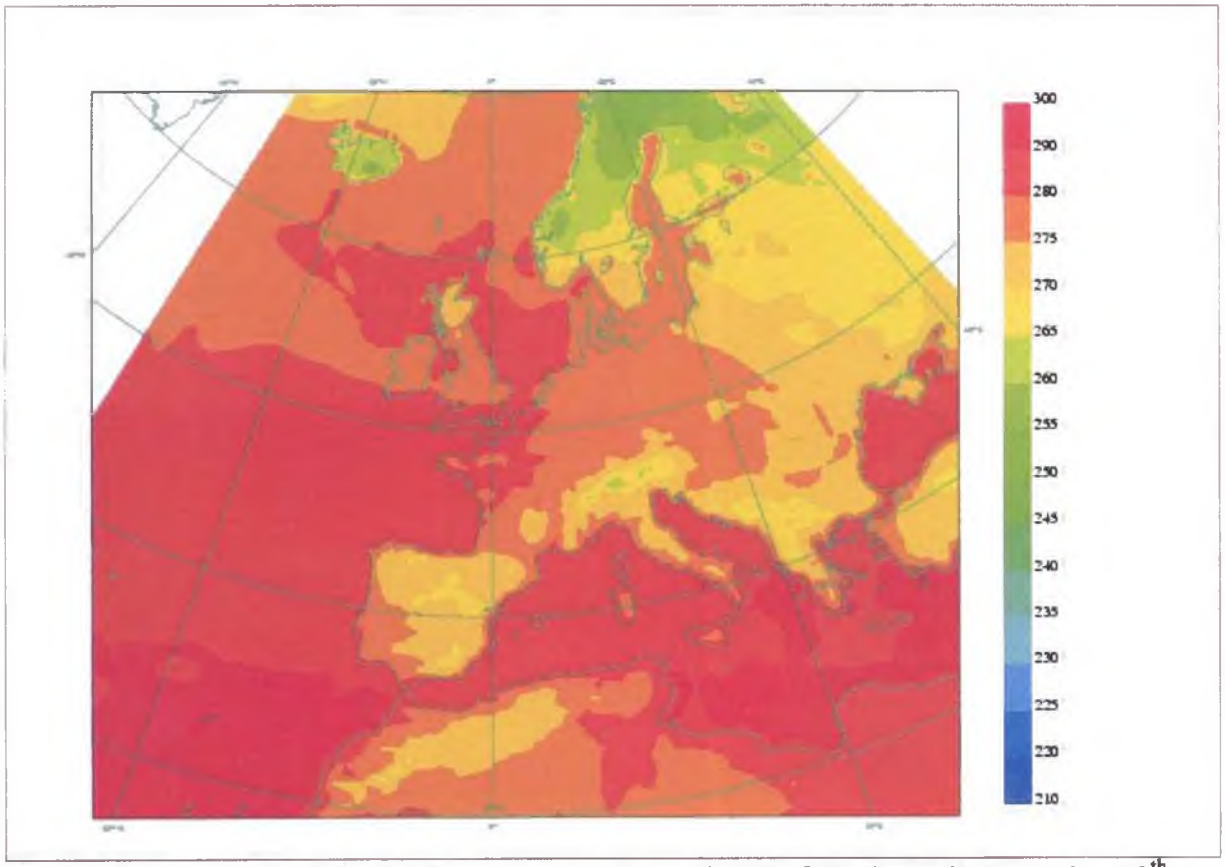

Fig. 2: Model analysis of the brightness temperatures (in K) of IR channel, November 18th 2004 00 UTC, simulation with no cloudiness

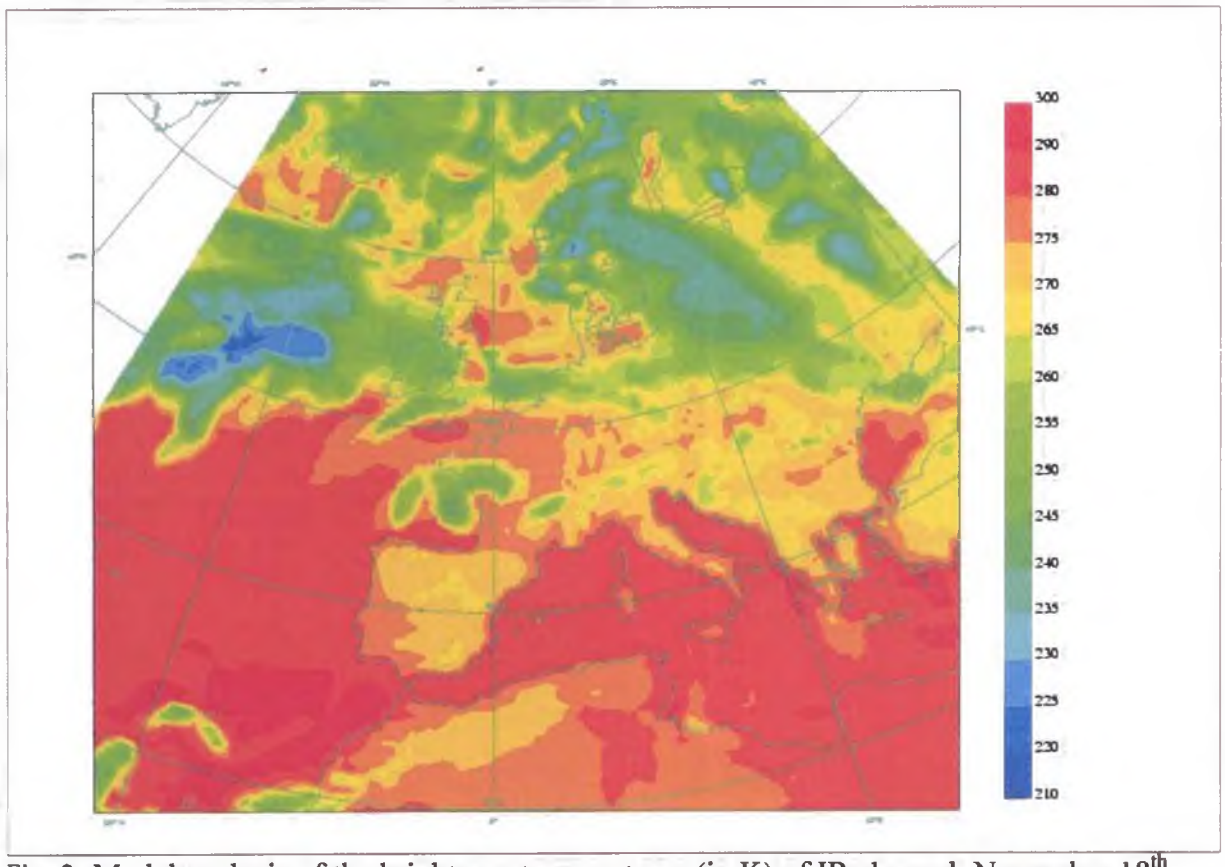

Fig. 3: Model analysis of the brightness temperatures (in K) of IR channel, November 18th 2004 00 UTC, simulation with cloudiness

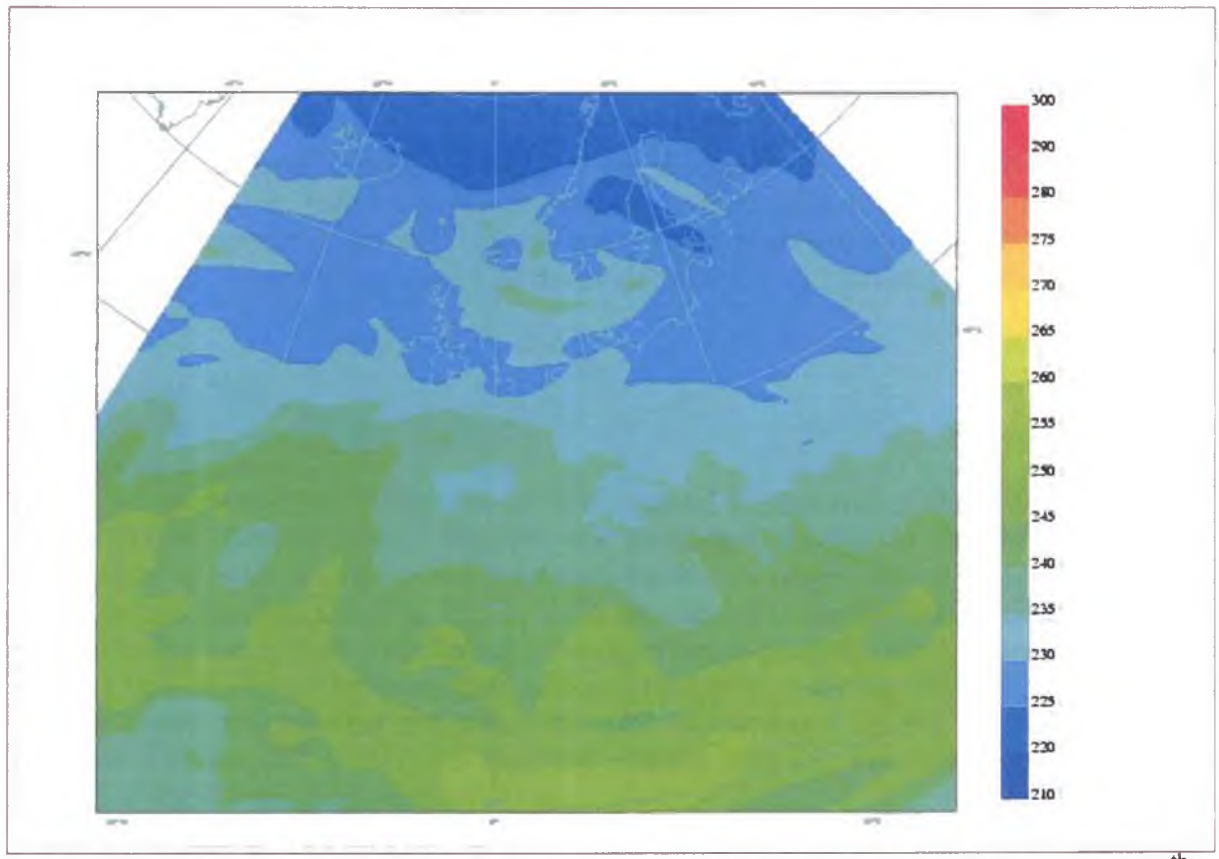

Fig. 4: Model analysis of the brightness temperatures (in K) of WV channel, November 18th 2004 00 UTC, simulation with no cloudiness

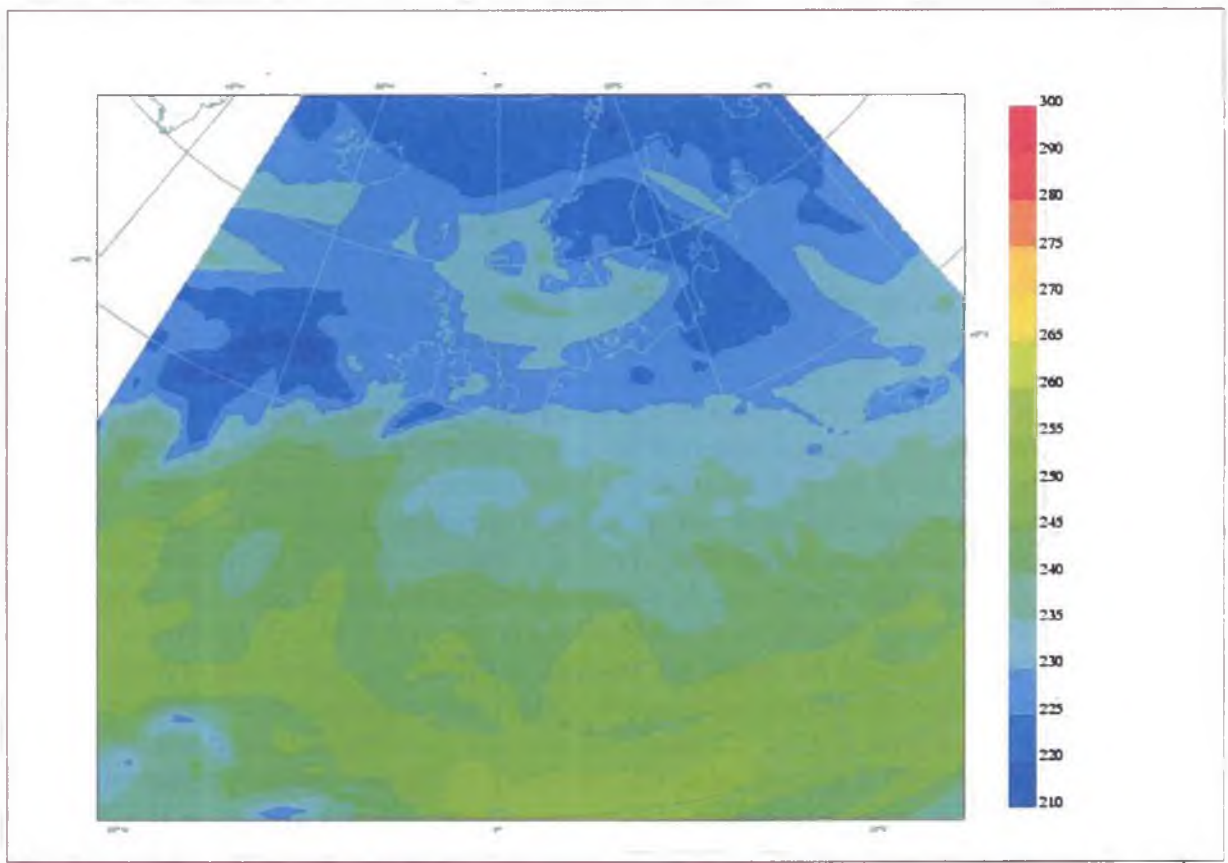

Fig. 5: Model analysis of the brightness temperatures (in K) of WV channel, November 18th 2004 00 UTC, simulation with cloudiness

Chapter 4: Case studies and results

In this chapter chosen case studies are discussed and described. For each case the synoptic description, both for in the sea surface level as well as for in the upper and middle levels of troposphere is given. Then the comparison model-to-observation is described and discussed with respect to the quality of the model analysis and forecast.

4.1 October 2002

Synoptic description

In the second half of October 2002, the central Europe was influenced by strong south-westerly flow. Besides others, one low was developed at night to October 26th 2002 over central part of Atlantic (Fig. 6) and it reached the British Islands during 24 hours with surface pressure less than 980 hPa (Fig. 7). Then this low moved to the east and northeast. Because of strengthening anticyclone over France a strong pressure gradient over northern half of central Europe was developed between these two pressure centres during October 27th and October 28th. It caused heavy storms and gales over northern Germany. On Fig. 8 the surface pressure field for October 28th 00 UTC is analysed. During next day the cyclone mentioned above moved to Byelorussia and begun to fill up.

Two main features existed at middle troposphere: well developed cyclone over Norwegian Sea and anticyclone over south-western Europe, as can be seen on Fig. 9 with analysis at 500 hPa for October 26th 00 UTC. This anticyclone intensified and moved somewhat eastward during next two days. As a consequence, a strong pressure gradient developed over central Europe in this level as well (see Fig. 10 for analysis on October 28th 00 UTC at 500 hPa level). The similar development could be detected at 200 hPa level, too (the situation for October 28th 00 UTC is presented on Fig. 11).

Comparison model-to-observation

On Figs. 12 and 13 the situation observed by satellite on October 28th 00 UTC is shown. Figs. 14 and 15 show corresponding analyses of the fields of brightness temperatures obtained by the model processing. The forecasts for October 28th 00 UTC from October 27th (+24h) are then presented on Figs. 16 and 17. For these forecasts a good agreement can be found between the dry air belt positions over Slovakia obtained by the model forecast and obtained one by satellite observation (these dry belts correspond to the highest temperature in 2 PVU level). The typical synoptic features in the field of brightness temperature can be observed, mainly in the WV channel, e.g. very good agreement between model analysis and forecast in the field of brightness temperatures in the cloud whirl near the cyclone centre could be noticed. On 48 h forecast synoptic features in brightness temperature field are still quite close to the reality but for 72 h forecast the centre of the mentioned low is simulated more westerly in comparison with reality. Some discrepancies between forecast and reality could be detected already during October 26th (also the 2 PVU level temperature field shows more intensive development of the first low). Situation for the 2 PVU level temperature field for +72h is shown on Fig. 18 and analysis of this field for October 28th 00 UTC is presented on Fig. 19 for brief illustration. Some discrepancies are detectable over Atlantic during October 26th in the brightness temperatures. These discrepancies could be important for the pressure field development mentioned above.

A more thorough assessment of the model can be obtained by accumulating statistics over extended period such as October 27-29th 2002. Histogram of observed and simulated brightness temperatures for IR channel is shown on Fig.20. In this channel model underestimates the number of grids with brightness temperatures less than 250 K corresponding to higher level clouds and overestimates number of warmer grids. In WV channel (Fig. 21) similar picture with underestimation of the coldest brightness temperatures below 220 K as well as the overestimation of warmest grids could be seen.

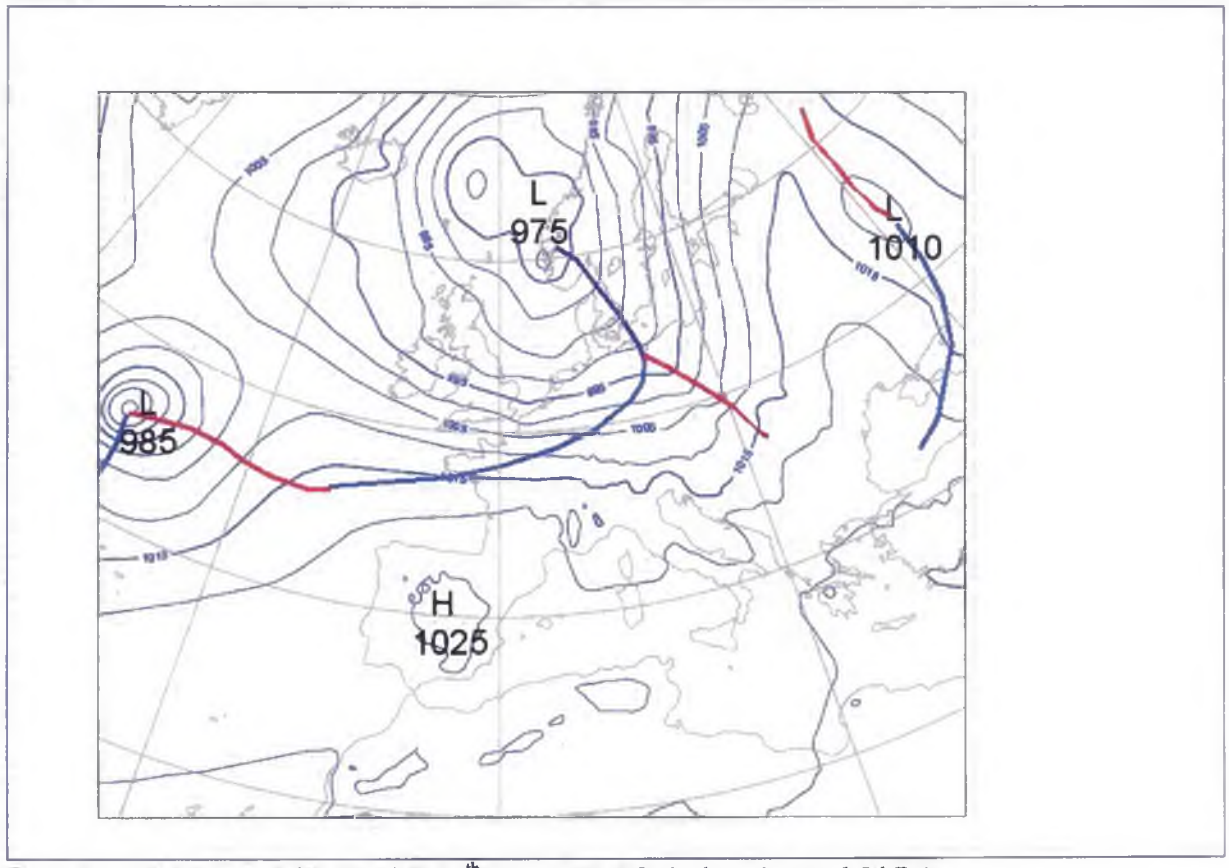

Fig. 6: Surface analysis for October 26th 2002 00 UTC (isobars interval 5 hPa)

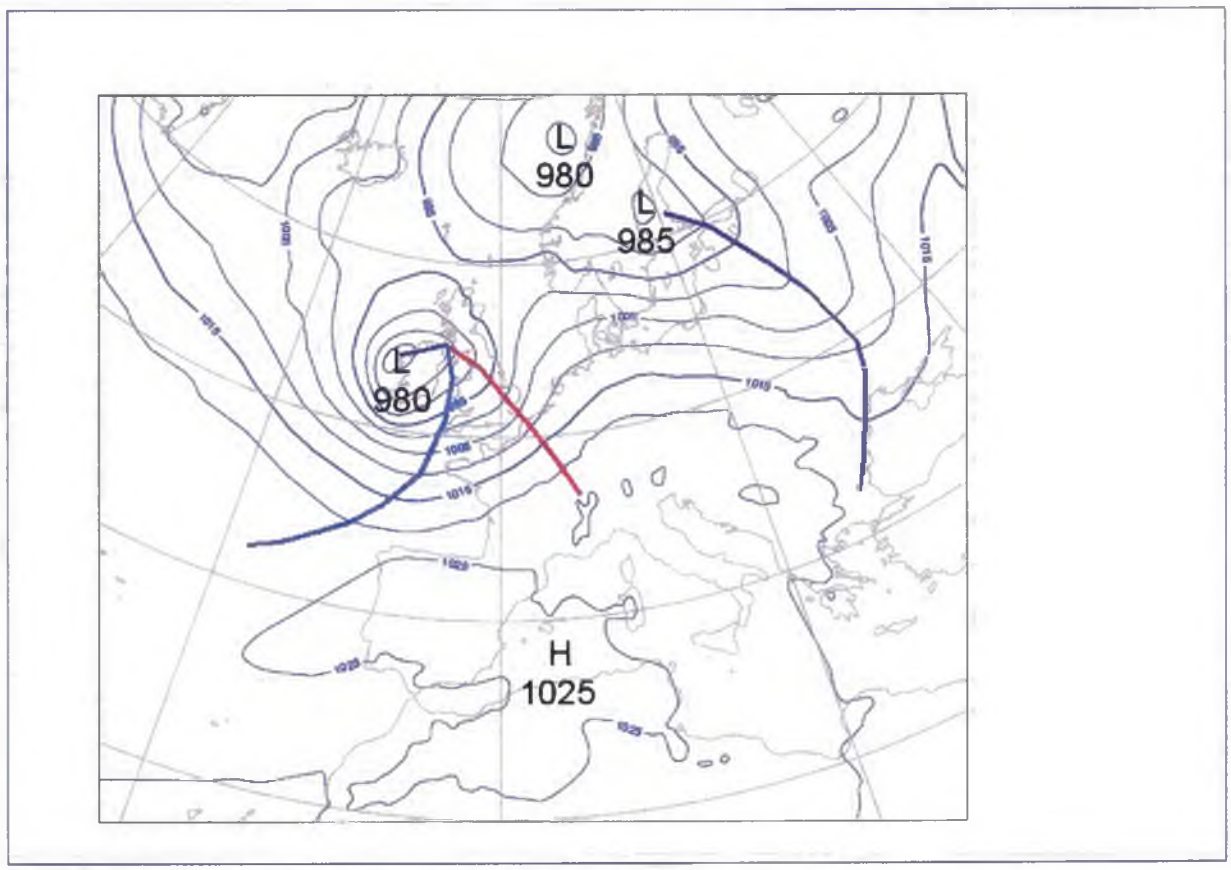

Fig. 7: Surface analysis for October 27th 2002 00 UTC (isobars interval 5 hPa)

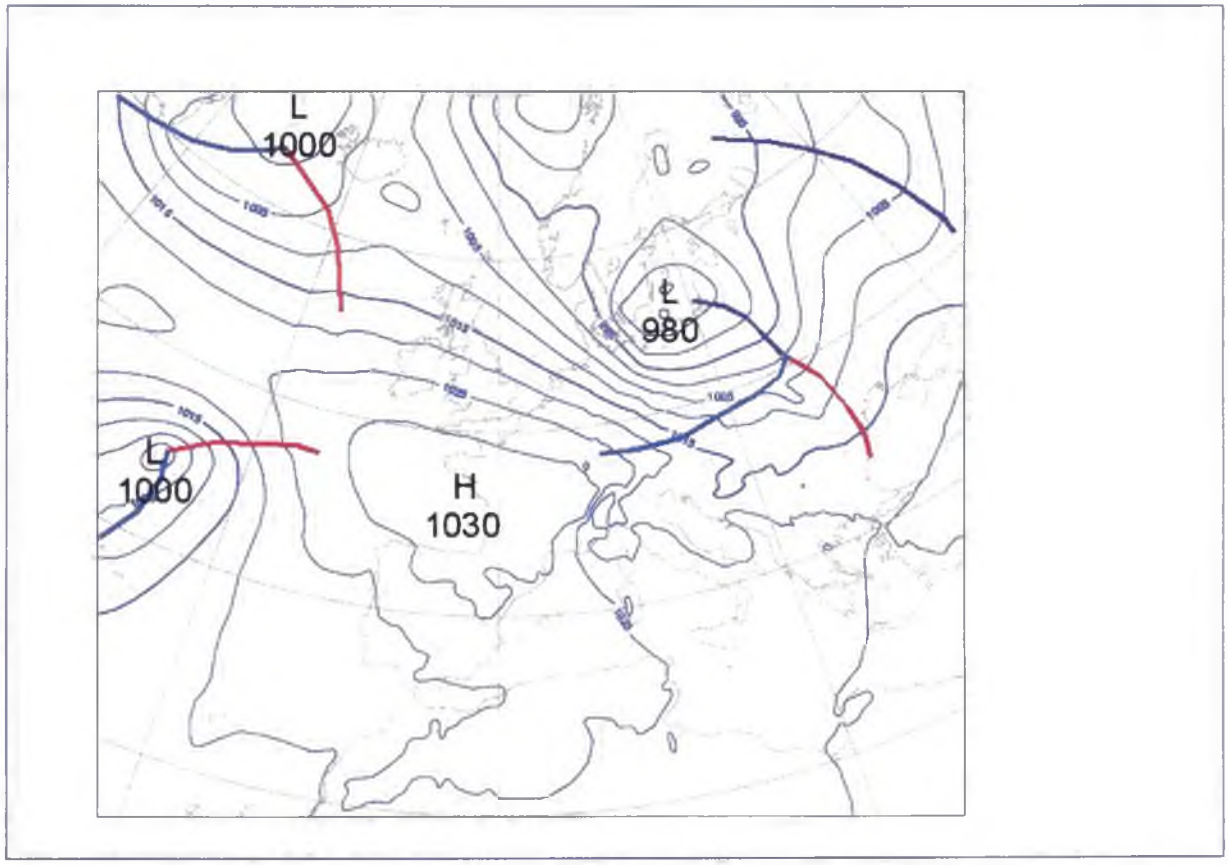

Fig. 8: Surface analysis for October 28th 2002 00 UTC (isobars interval 5 hPa)

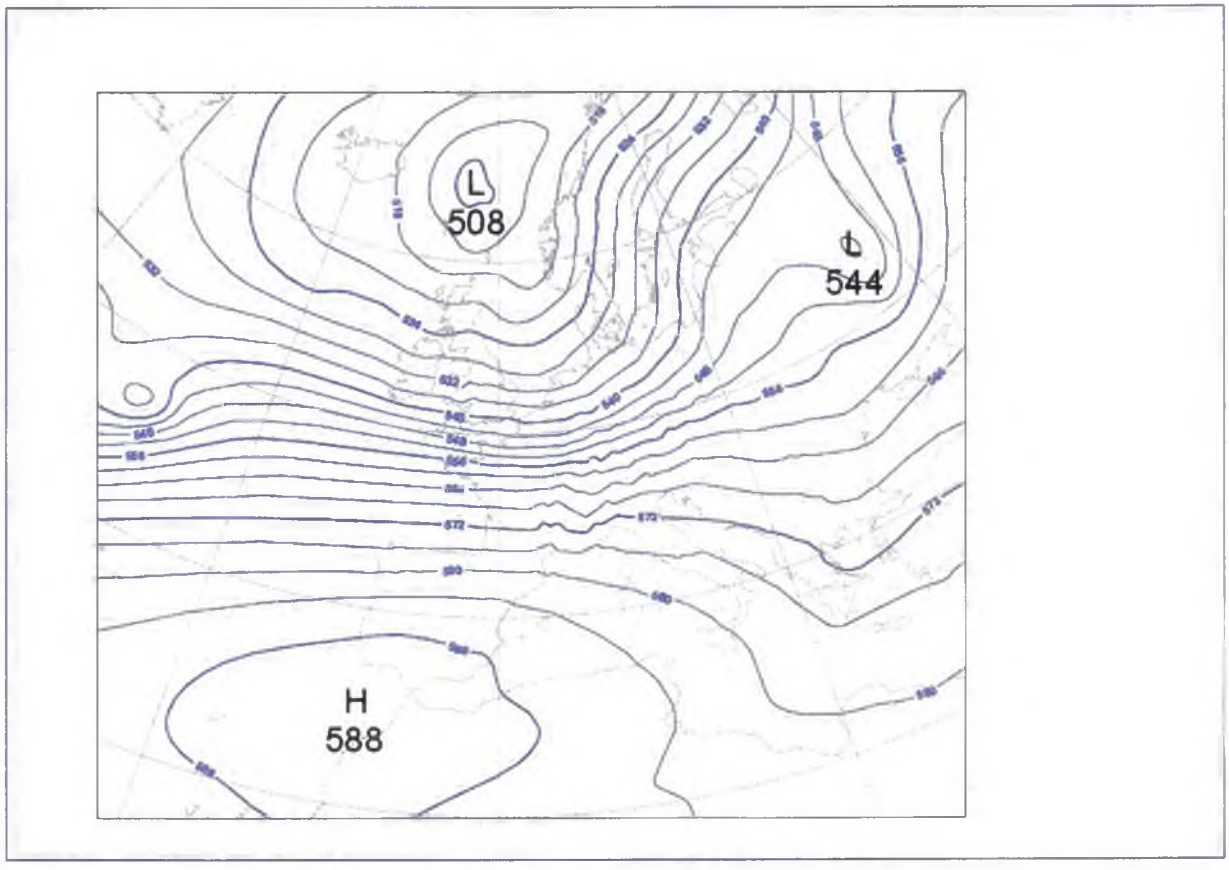

Fig. 9: Geopotential height of 500 hPa level (interval 4 decametres), analysis for October 26th 2002 00 UTC

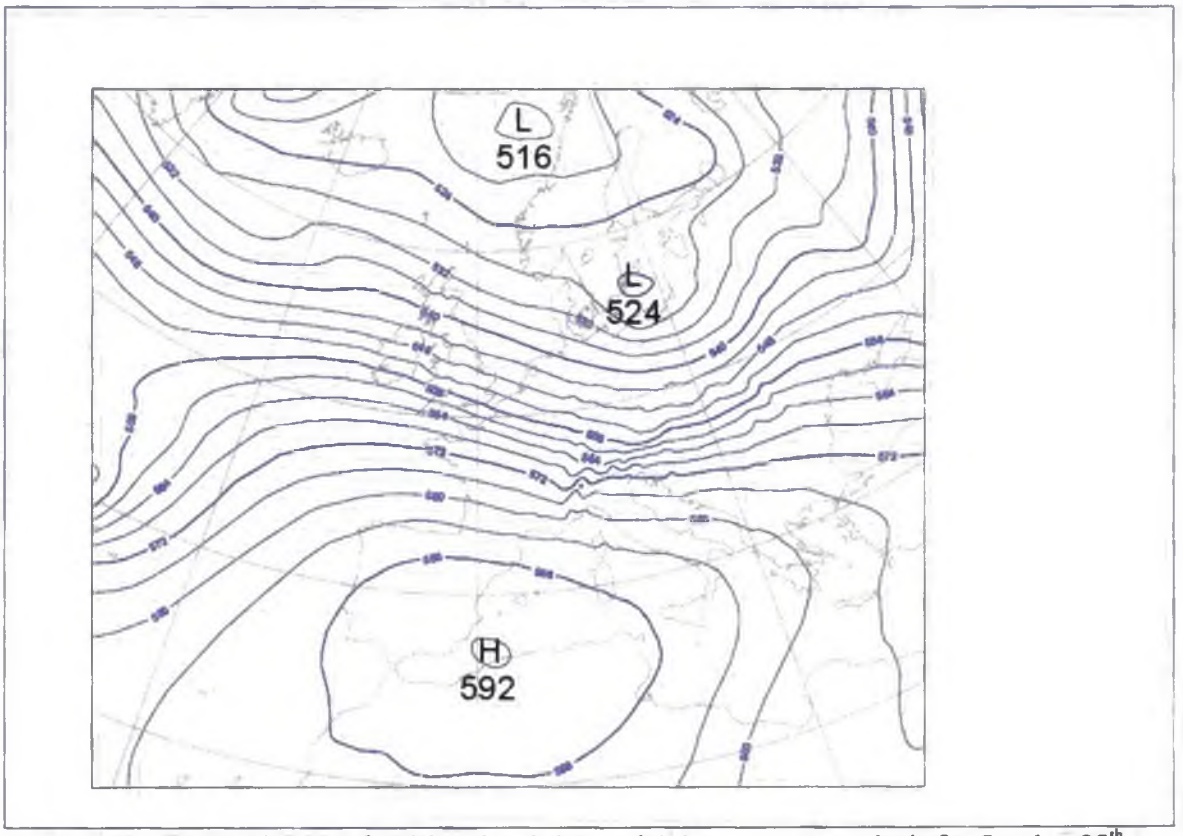

Fig. 10: Geopotential height of 500 hPa level (interval 4 decametres), analysis for October 28th 2002 00 UTC

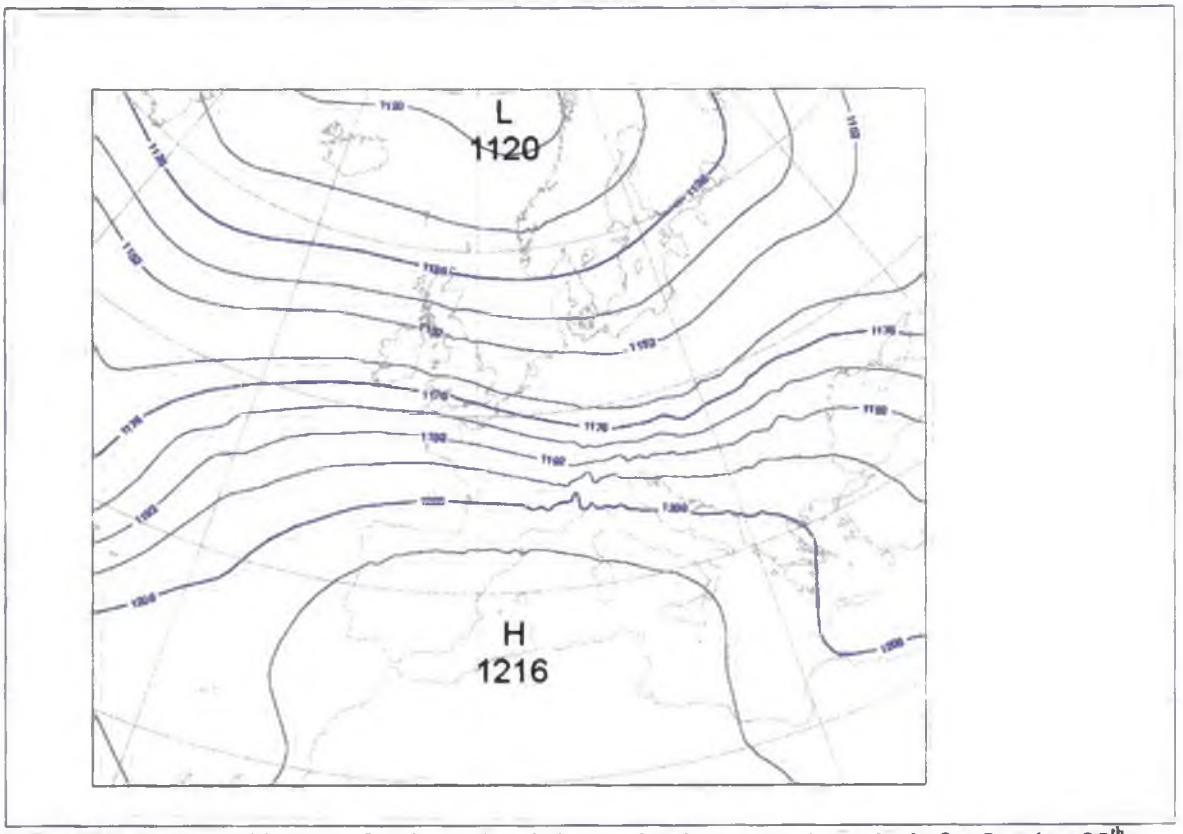

Fig. 11: Geopotential height of 200 hPa level (interval 8 decametres), analysis for October 28th 2002 00 UTC

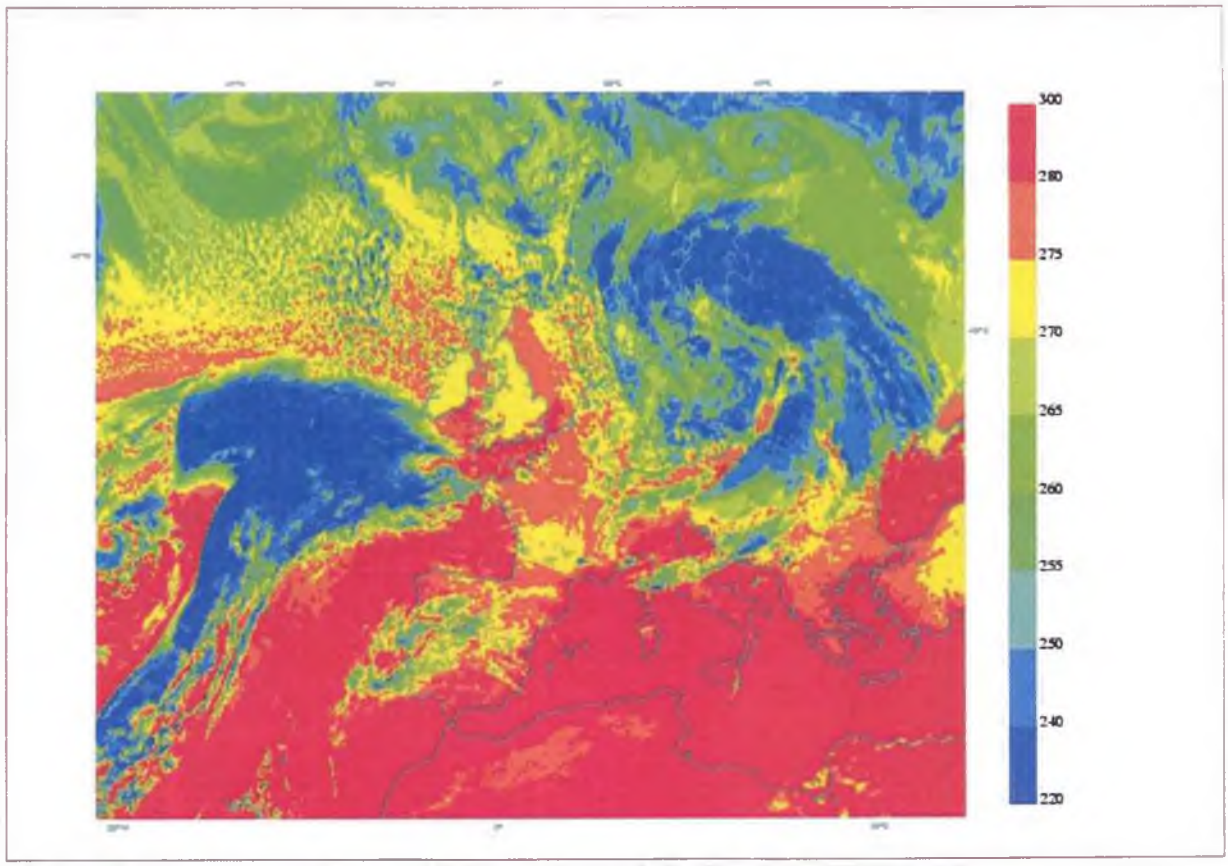

Fig. 12: IR channel image of METEOSAT-7 satellite, October 28th 2002 00 UTC

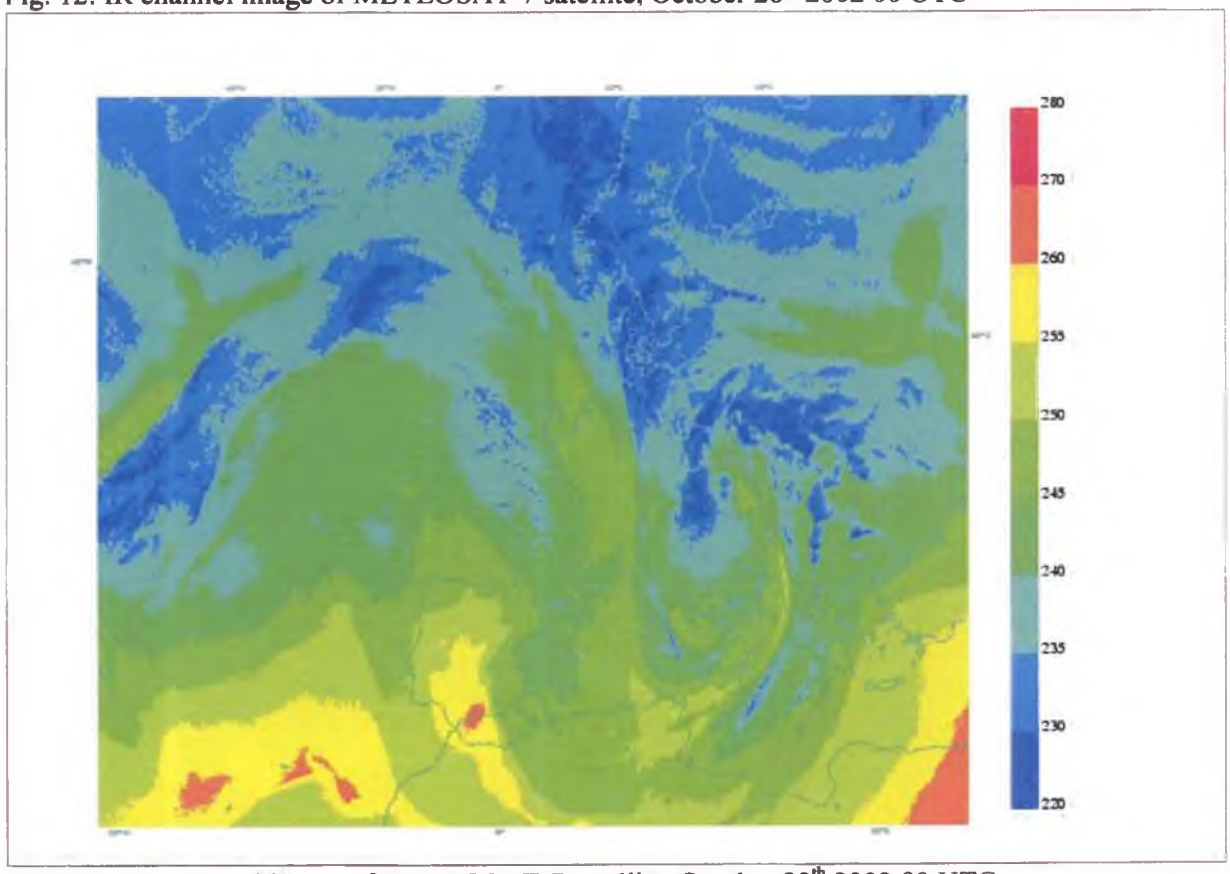

Fig. 13: WV channel image of METEOSAT-7 satellite, October 28th 2002 00 UTC

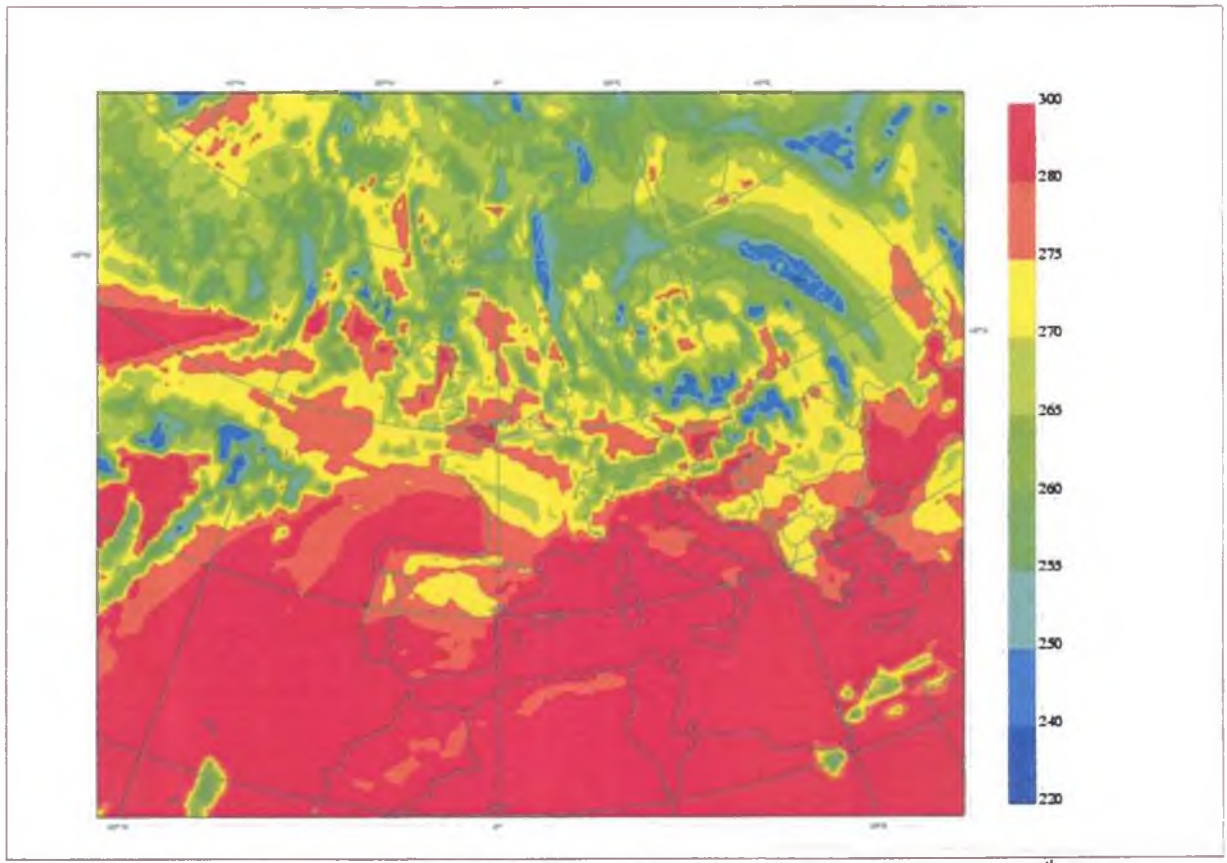

Fig. 14: Model analysis of the brightness temperatures (in K) of IR channel, October 28th 2002 00 UTC

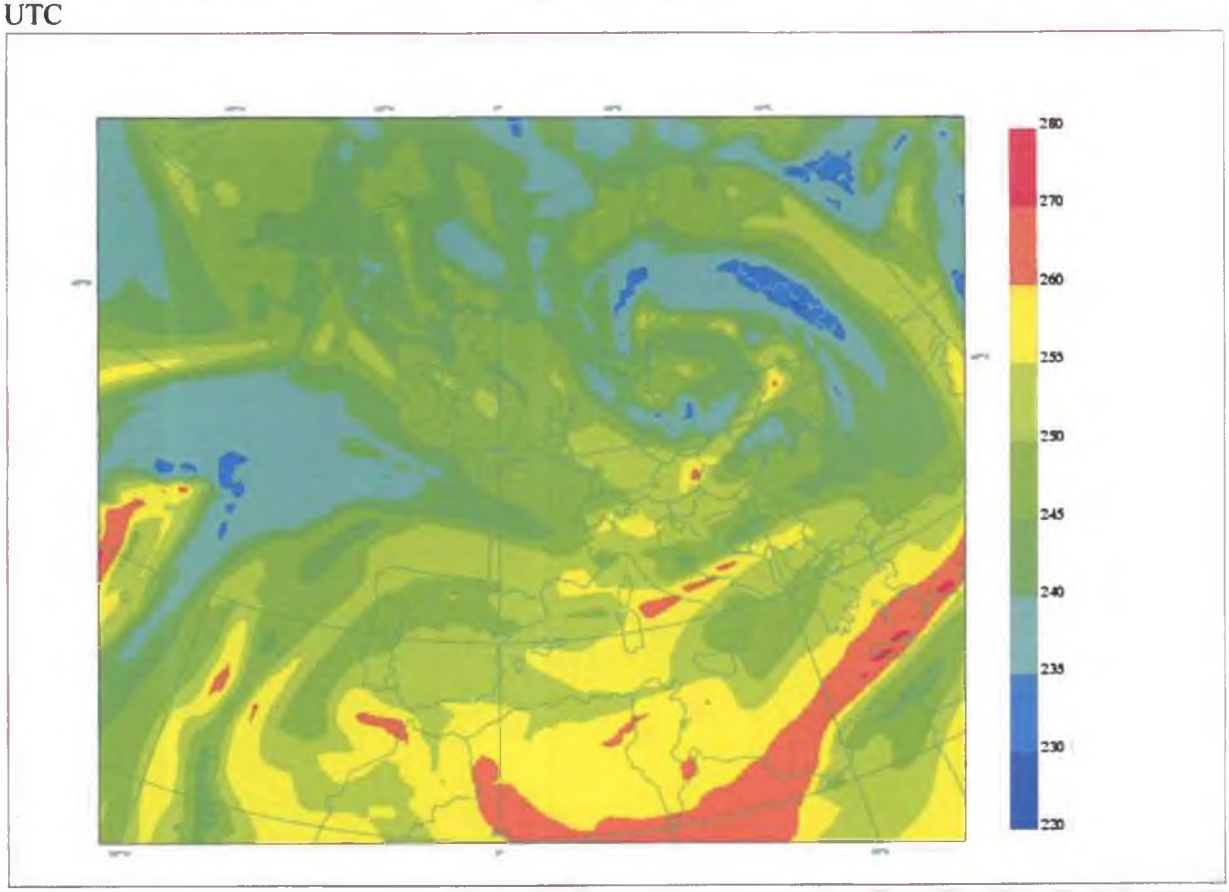

Fig. 15: Model analysis of the brightness temperatures (in K) of WV channel, October 28th 2002 00 UTC

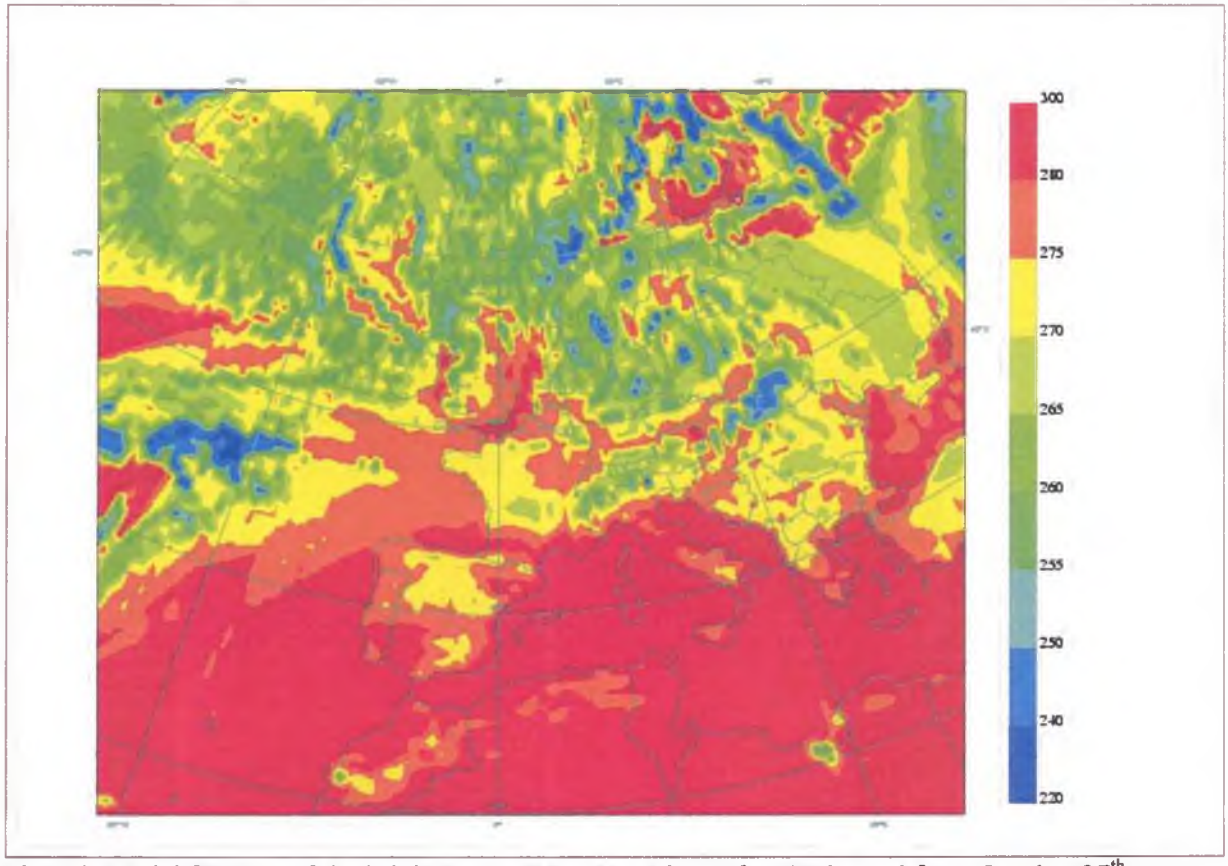

Fig. 16: Model forecast of the brightness temperatures (in K) for IR channel from October 27th 2002 00 UTC for October 28th 2002 00 UTC

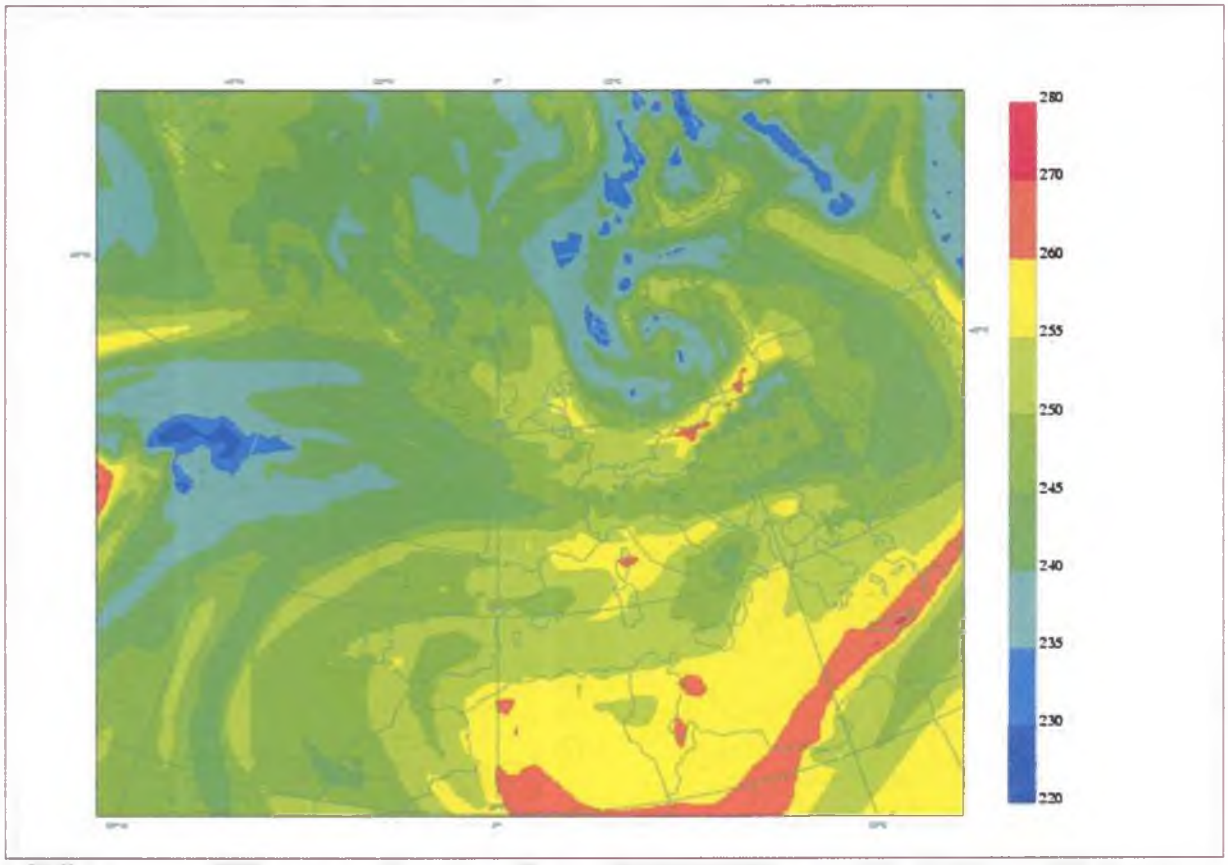

Fig. 17: Model forecast of the brightness temperatures (in K) for WV channel from October 27th 2002 00 UTC for October 28th 2002 00 UTC

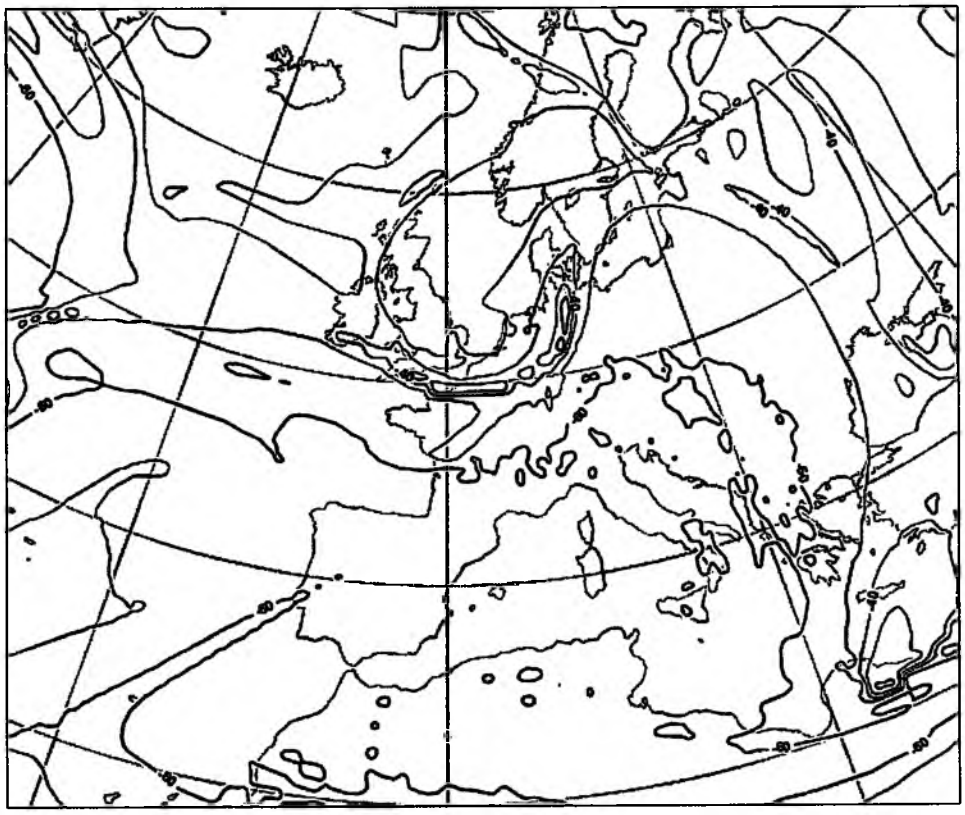

Fig. 18: Temperature at 2 PVU level (interval 10°C), forecast from October 25th 2002 00 UTC for October 28th 2002 00 UTC

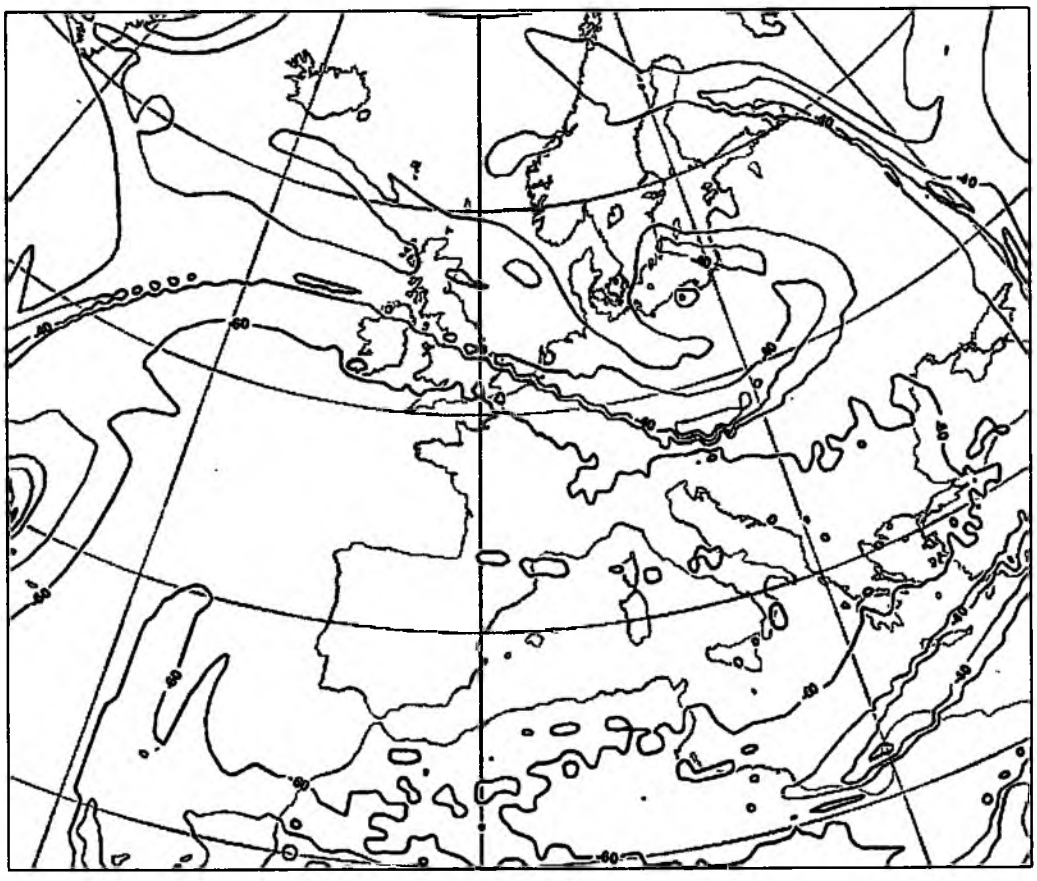

Fig. 19: Temperature at 2 PVU level (interval 10°C), analysis from October 28th 2002 00 UTC

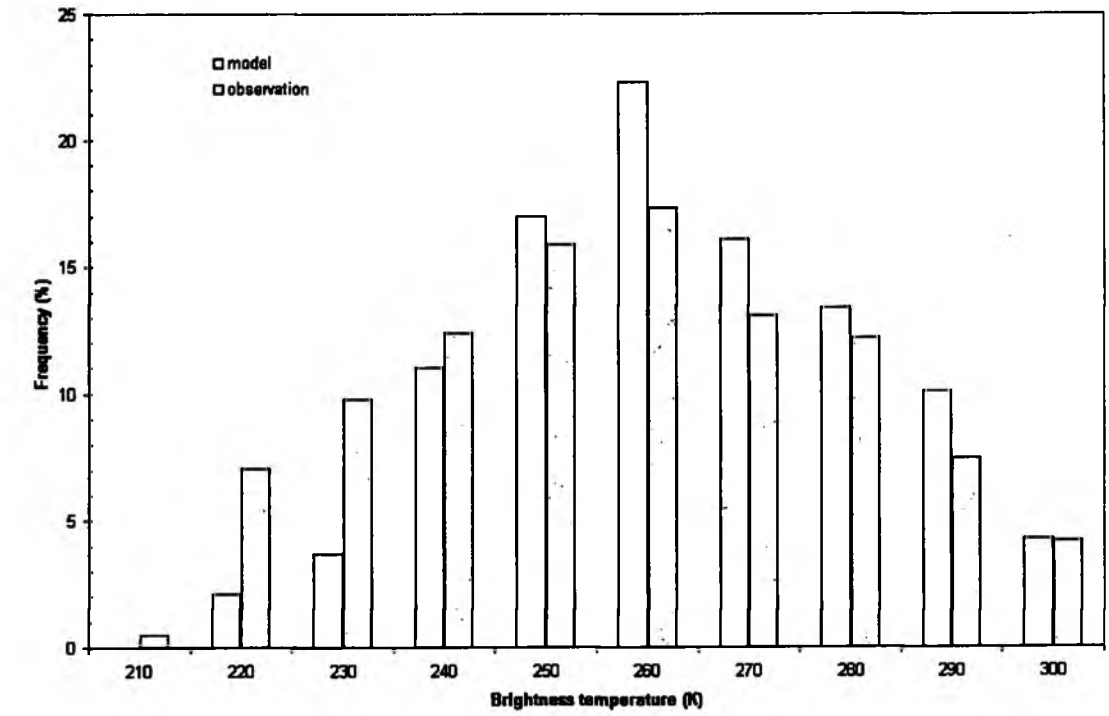

Fig. 20: Histogram of observed and simulated brightness temperatures for IR channel of METEOSAT satellite

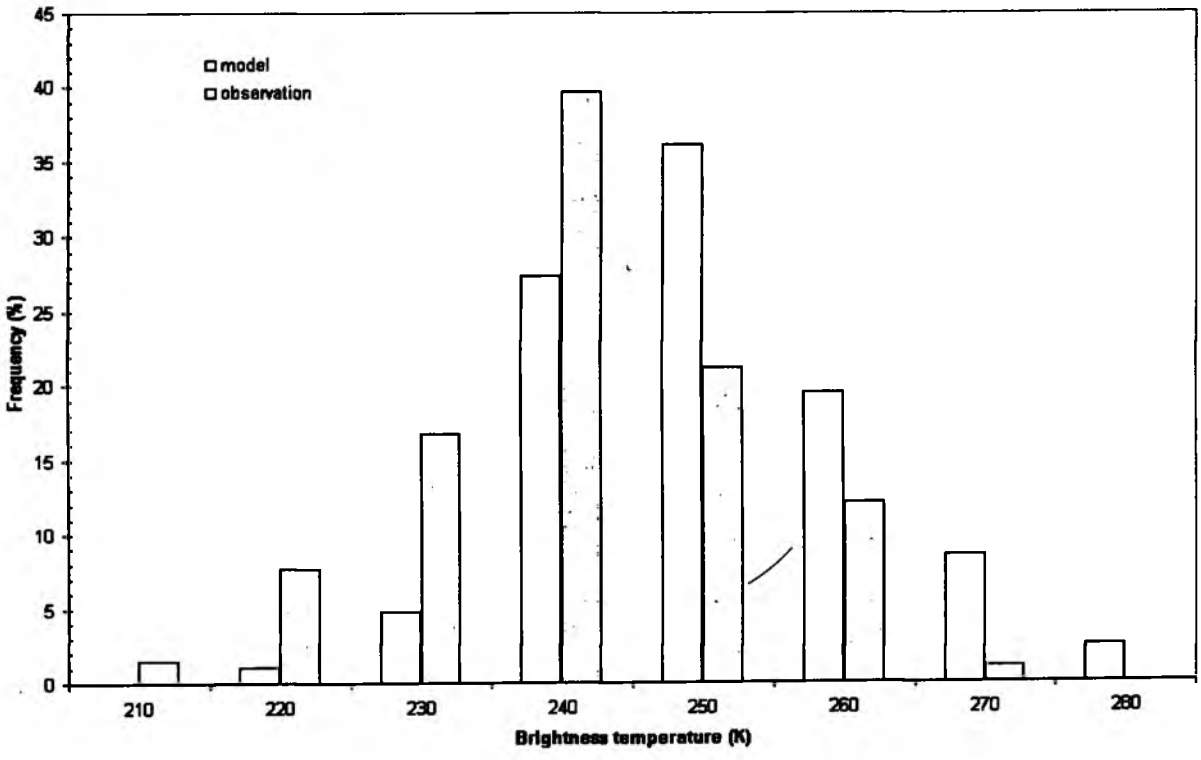

Fig. 21: Histogram of observed and simulated brightness temperatures for WV channel of METEOSAT satellite

4.2 November 2004

Synoptic description

The meteorological and synoptic situation over Europe was very unstable during the second decade of November 2004. High pressure ridge was changed by deep cyclone during one day. The dominating synoptic feature consisted in the regenerating cyclone over northern parts of Europe. The pressure gradient between this cyclone and the Azores anticyclone was quite intensive causing strong winds and quick weather changes in central Europe. The baroclinic zone was situated in the belt from British Islands to western Russia. On periphery of the low pressure field over northern Europe deep cyclone was formed in the region of eastern Atlantic and Northern Sea during November 18th (see Fig. 22 for surface pressure field on November 18th 2004 00 UTC). Next night a frontal wave on cold front of this cyclone was developed (Fig. 23). In this way new cyclone with very rapidly development was created over Germany. The pressure dropped down to 985 hPa during 24 hours (more than 20 hPa) and this new cyclone moved to north-western part of Russia during November 20th (Fig. 24) Pressure in its centre dropped down to 975 hPa during the night to November 21st. Next day this cyclone became to fill up while moving to the north.

Let's focus now on development at middle and upper troposphere and lower stratospheric levels. The situation at 500 hPa level (Fig. 25) can be characterized by strong gradient between very deep trough over north-eastern Europe and anticyclone over south-western Europe on November 19th 00 UTC. The similar features can be identified at 200 hPa level as well (Fig. 26). Interesting dynamical development can be observed on temperature fields at 500 hPa level on Figs. 27-29 (analysis for November 18th, 19th and 20th, always at 00 UTC) and at 200 hPa level on Figs. 30-32 (analysis again for November 18th, 19th and 20th, always at 00 UTC). Comparing temperature fields at these two levels with corresponding fields of geopotential heights, quite strong cold advection at middle troposphere (500 hPa level) and warm advection at upper troposphere/lower stratosphere (200 hPa level) can be identified in the region of this rapidly developing cyclone. This development is in a good agreement with the theory described in chapter 1, part 6. It was found that the deepening low centre is located underneath region with relatively cooler tropospheric and warmer stratospheric air.

Cyclone mentioned above caused on November 19th 2004 a short but extremely damaging violent storm with gusts up to 170 km/h over northern parts of the territory of Slovakia. Several parts of this territory were seriously affected, with the most severe devastation occurring in the High Tatras Mountains where a 60 km long and 10 km wide belt of forest has been completely destroyed. Some houses and extensive infrastructure have also been destroyed or seriously damaged. This storm also caused the first severe shot of winter on this autumn, with intensive snowing at first on early November 19th over eastern Germany, and then over plains of Poland and southern Byelorussia with snow cover creation of about 10 to 25cm. In connection with wind gusts serious problems in traffic were caused.

Comparison model-to-observation

The situation from November 19th 00 UTC in WV channel is presented on Fig. 33 (model simulation of brightness temperatures) and on Fig. 34 (satellite measurement). We can see quite good correlation between the observed and modelled features. The cloud systems are found in corresponding places over central Europe region. The forecast for the next day also shows only small differences between the reality and the model simulation. On Figs. 35 and

36 the potential temperature at 2 PVU level is presented as it has been analyzed by the model for November 19th 00 UTC and for November 20th 00 UTC. We can see sharp gradient of potential temperature in the vicinity of frontal zone stretching from Hungaria to the NW to British Islands. Partly we can also see it just behind the cold front in the region of explosively developing cyclone. As can be recognized on the Fig. 34, this sharp gradient of potential temperature is very well correlated with the dry belt position in the WV channel imagery (the region where the air comes down from the tropopause or from lower stratospheric levels).

Also, the model analysis from the November 19th represents the observed synoptic features with developing wave on the cold front over the Germany quite well. So, not surprisingly, also the forecast from this start point is quite good, getting slowly worse with integration time increasing, of course.

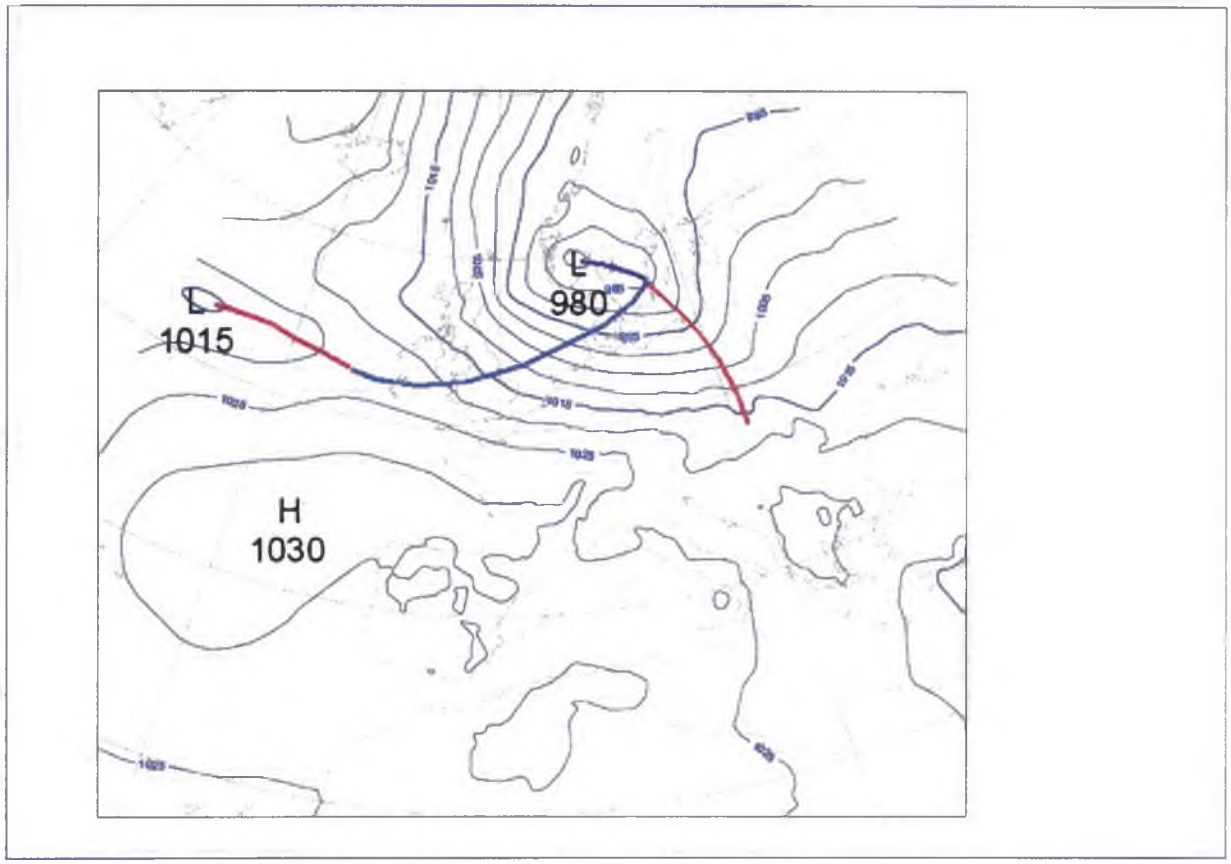

Fig. 22: Surface analysis for November 18th 2004 00 UTC (isobars interval 5 hPa)

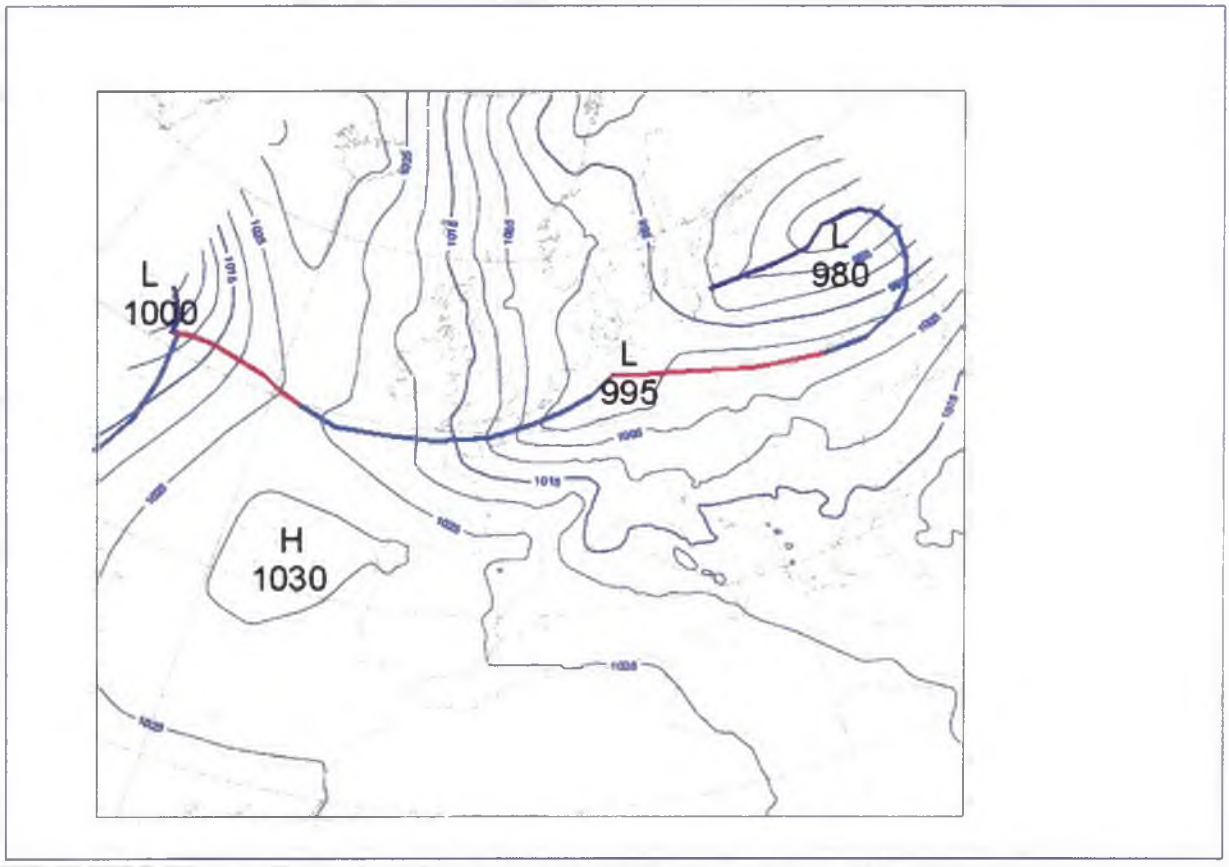

Fig. 23: Surface analysis for November 19th 2004 00 UTC (isobars interval 5 hPa)

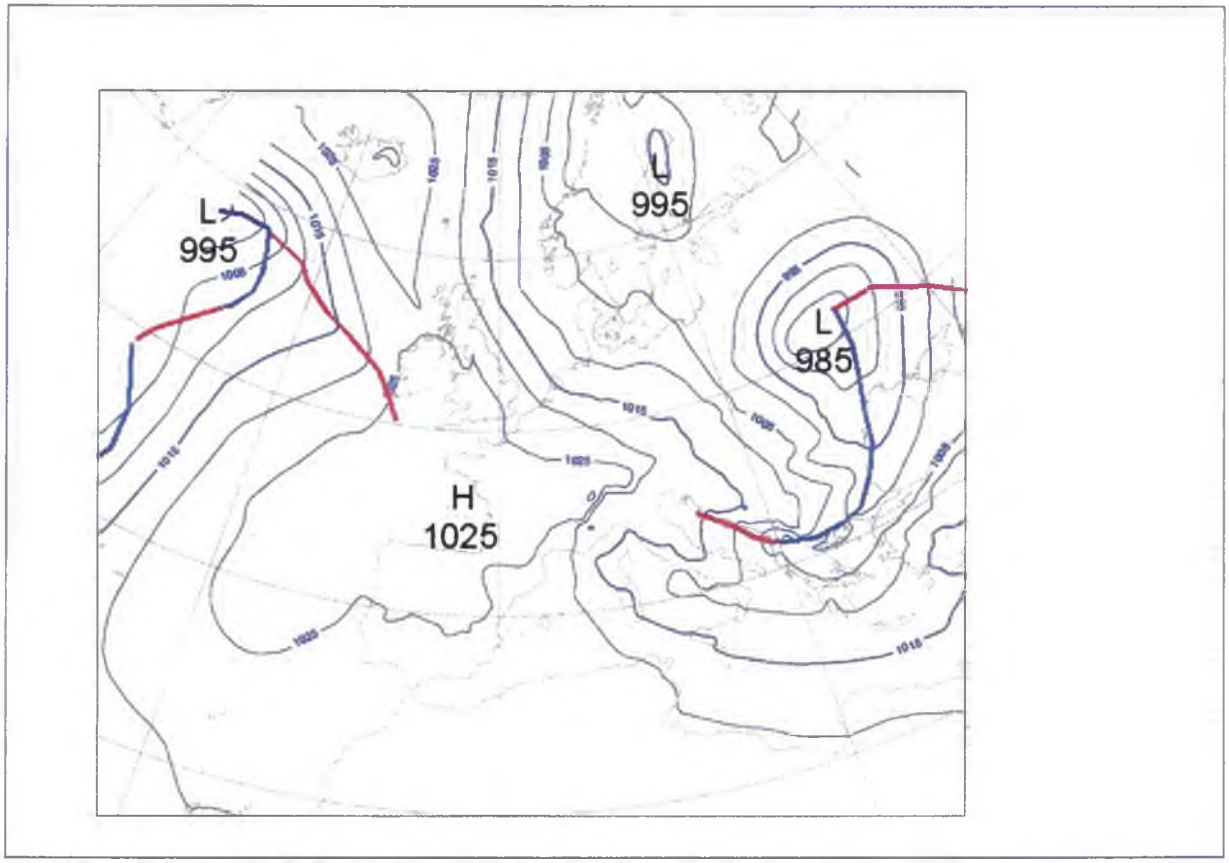

Fig. 24: Surface analysis for November 20th 2004 00 UTC (isobars interval 5 hPa)

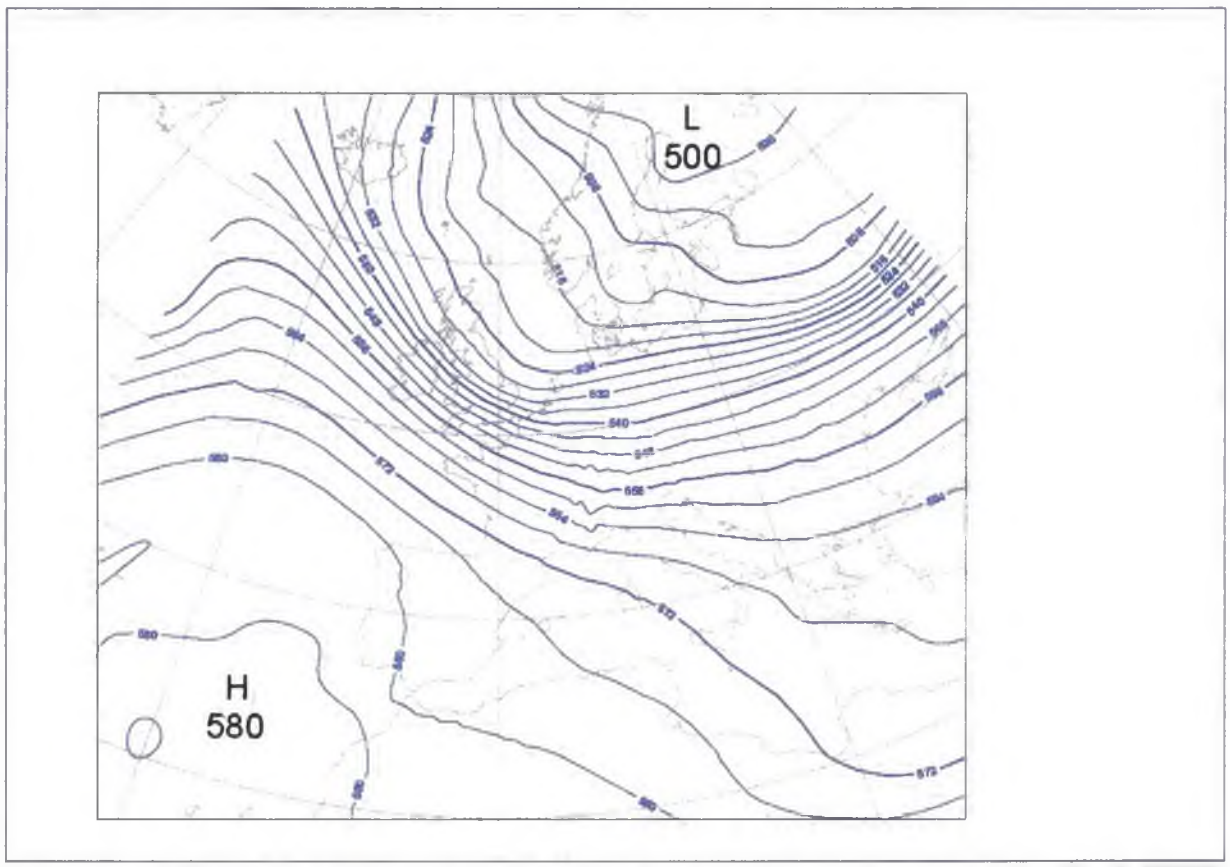

Fig. 25: Geopotential height of 500 hPa level (interval 4 decametres), analysis for November 19th 2002 00 UTC

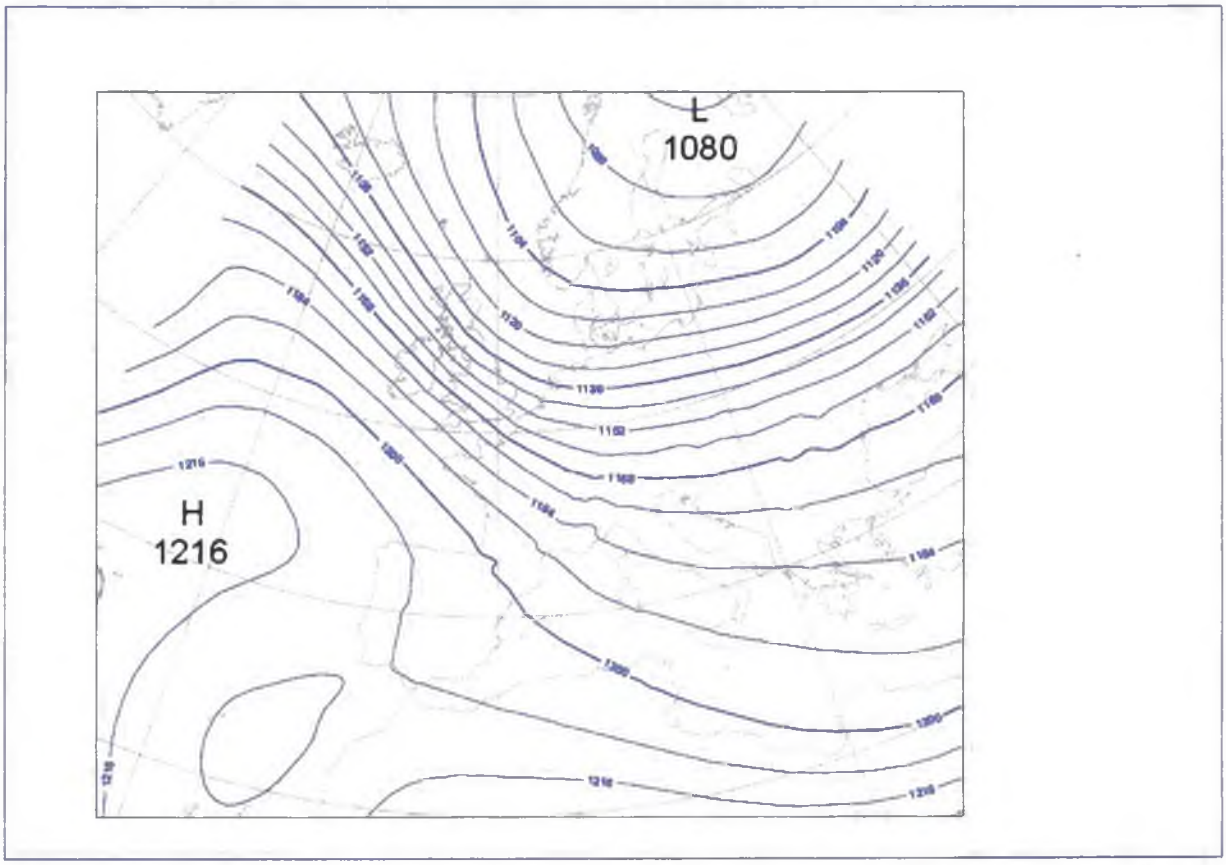

Fig. 26: Geopotential height of 200 hPa level (interval 8 decametres), analysis for November 19th 2002 00 UTC

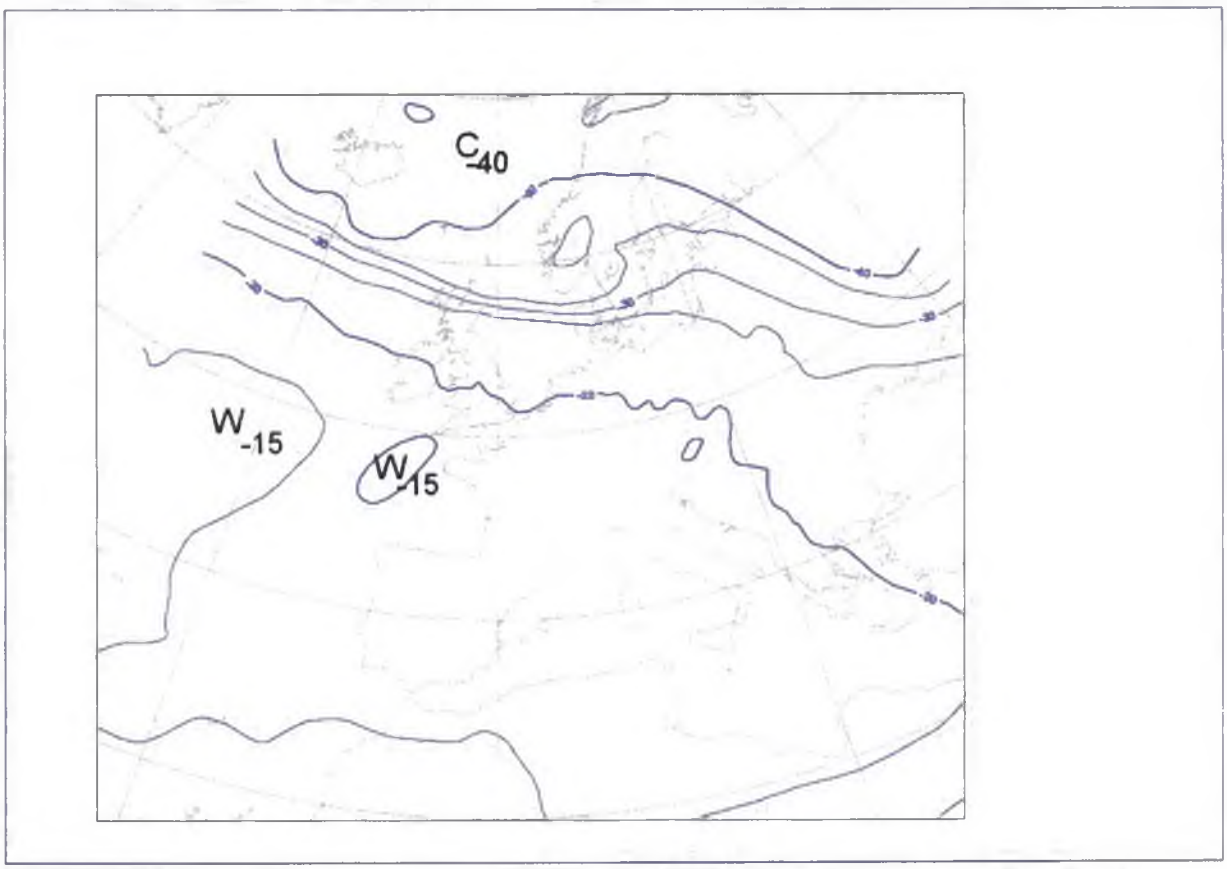

Fig. 27: Temperature in 500 hPa level (interval 5 °C), analysis for November 18th 2002 00 UTC

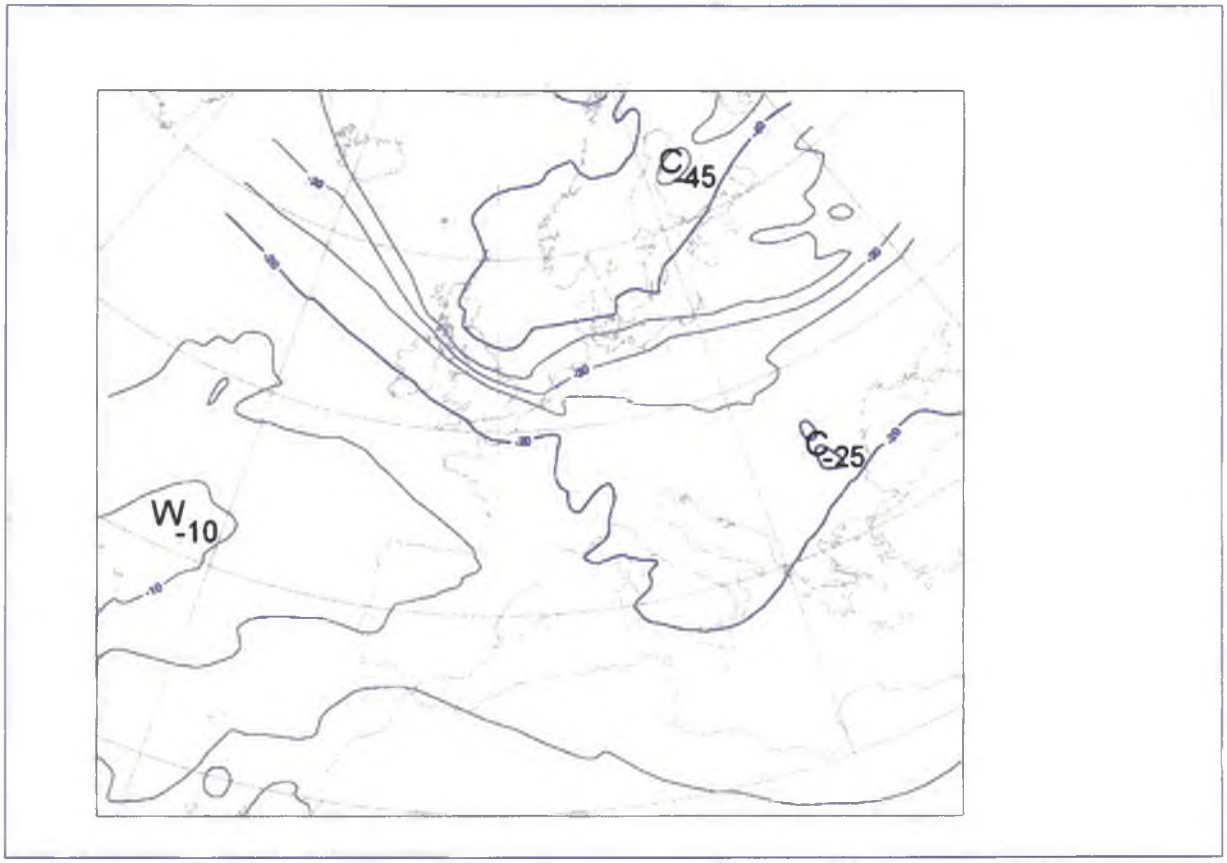

Fig. 28: Temperature in 500 hPa level (interval 5 °C), analysis for November 19th 2002 00 UTC

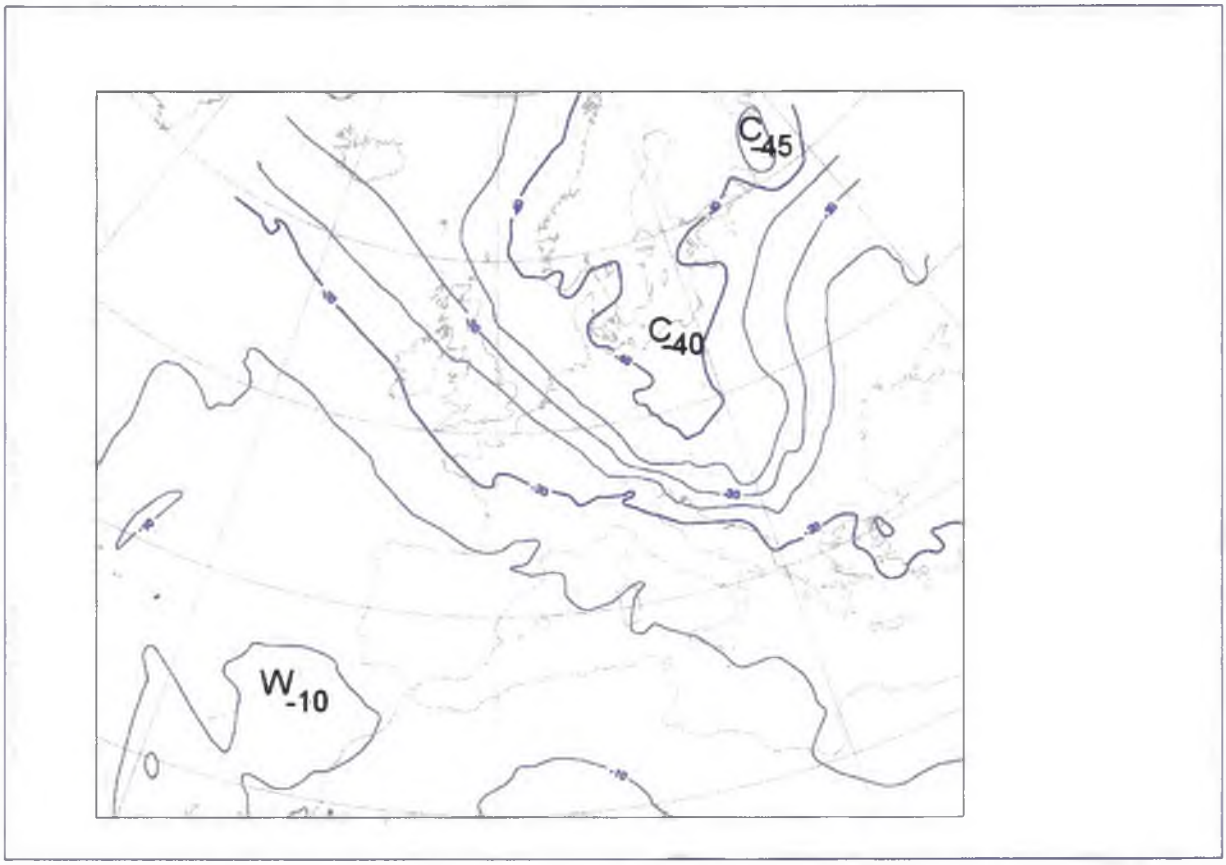

Fig. 29: Temperature in 500 hPa level (interval 5 °C), analysis for November 20th 2002 00 UTC

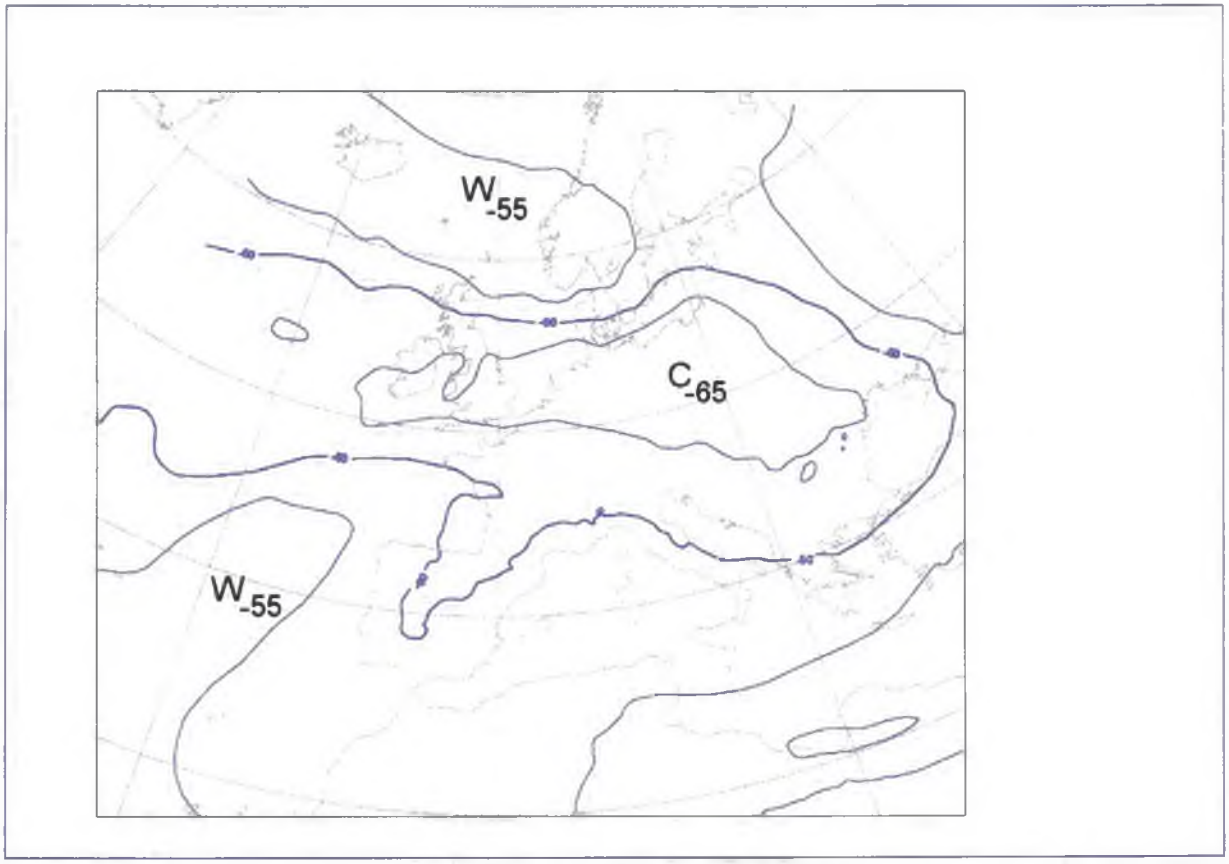

Fig. 30: Temperature in 200 hPa level (interval 5 °C), analysis for November 18th 2002 00 UTC

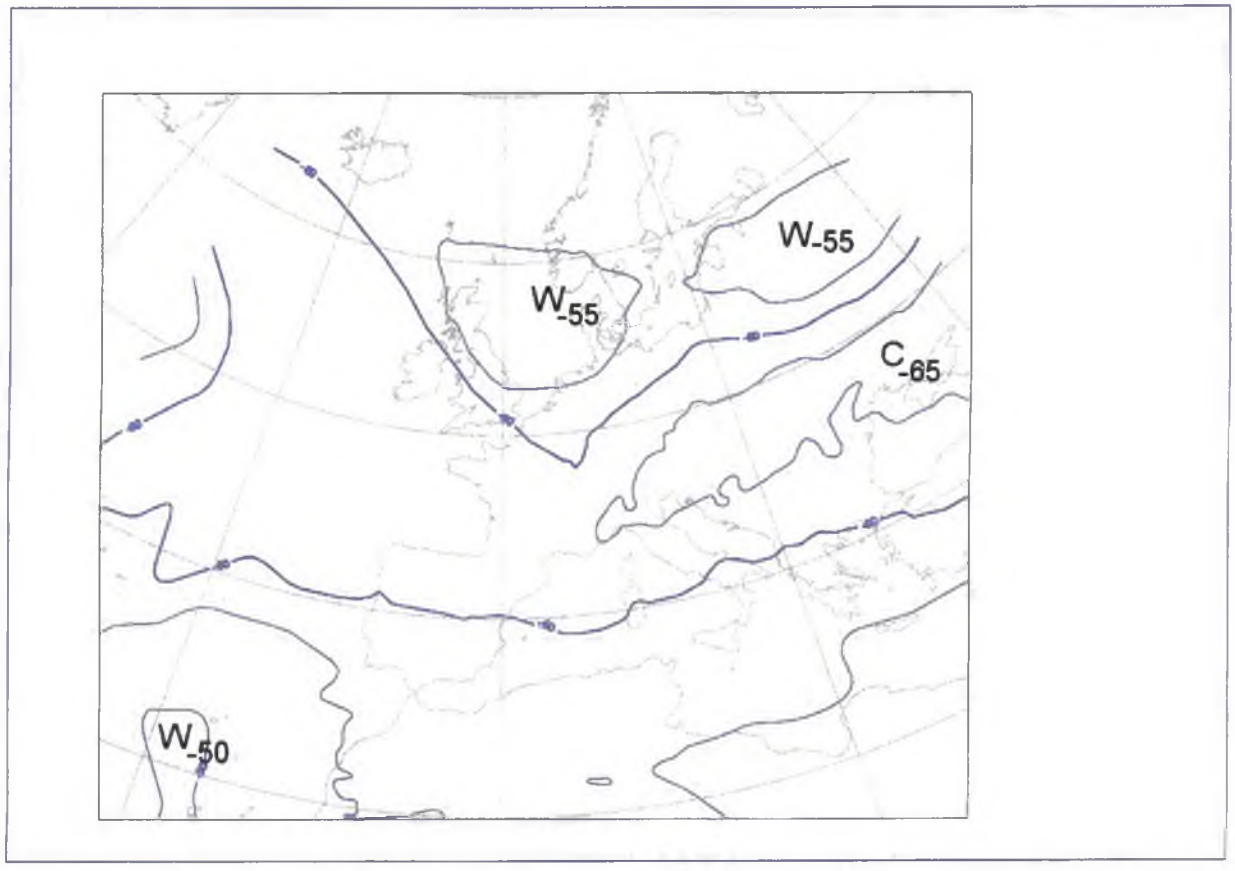

Fig. 31: Temperature in 200 hPa level (interval 5 °C), analysis for November 19th 2002 00 UTC

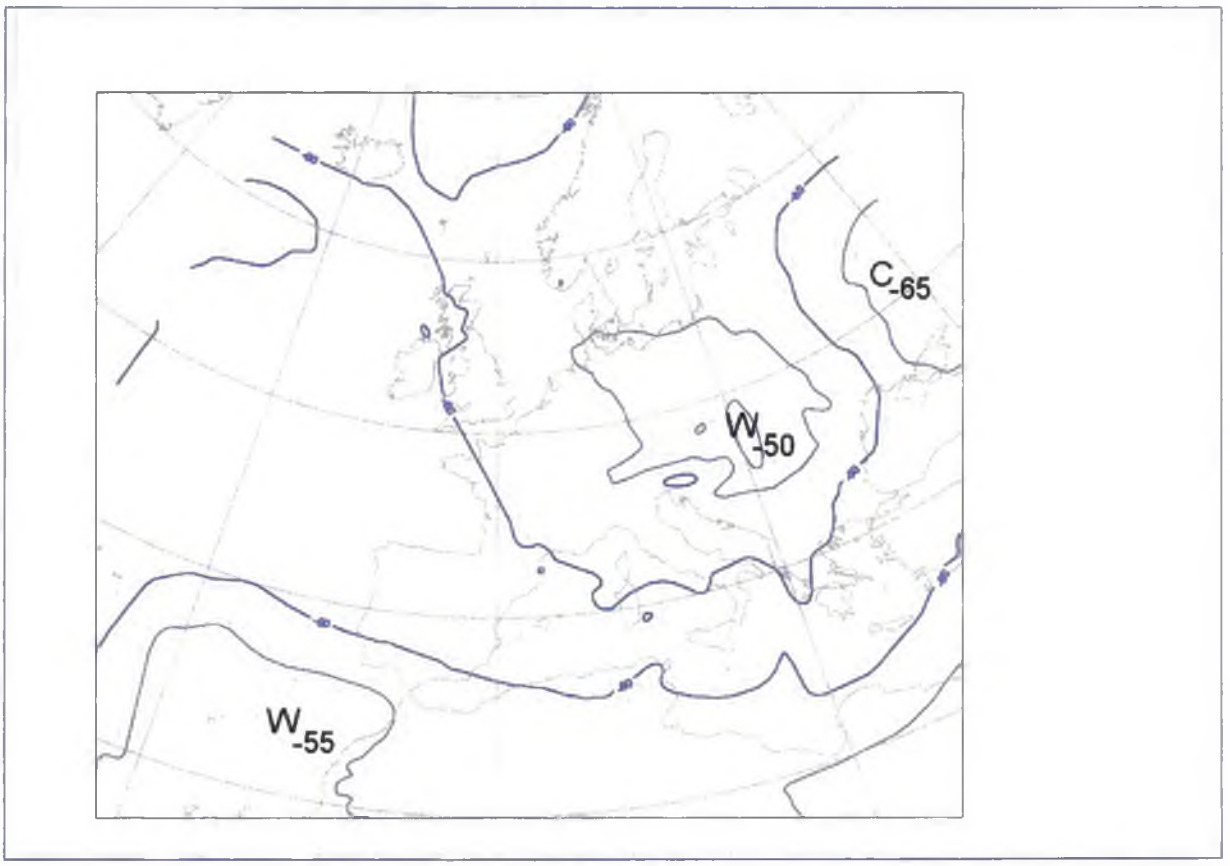

Fig. 32: Temperature in 200 hPa level (interval 5 °C), analysis for November 20th 2002 00 UTC

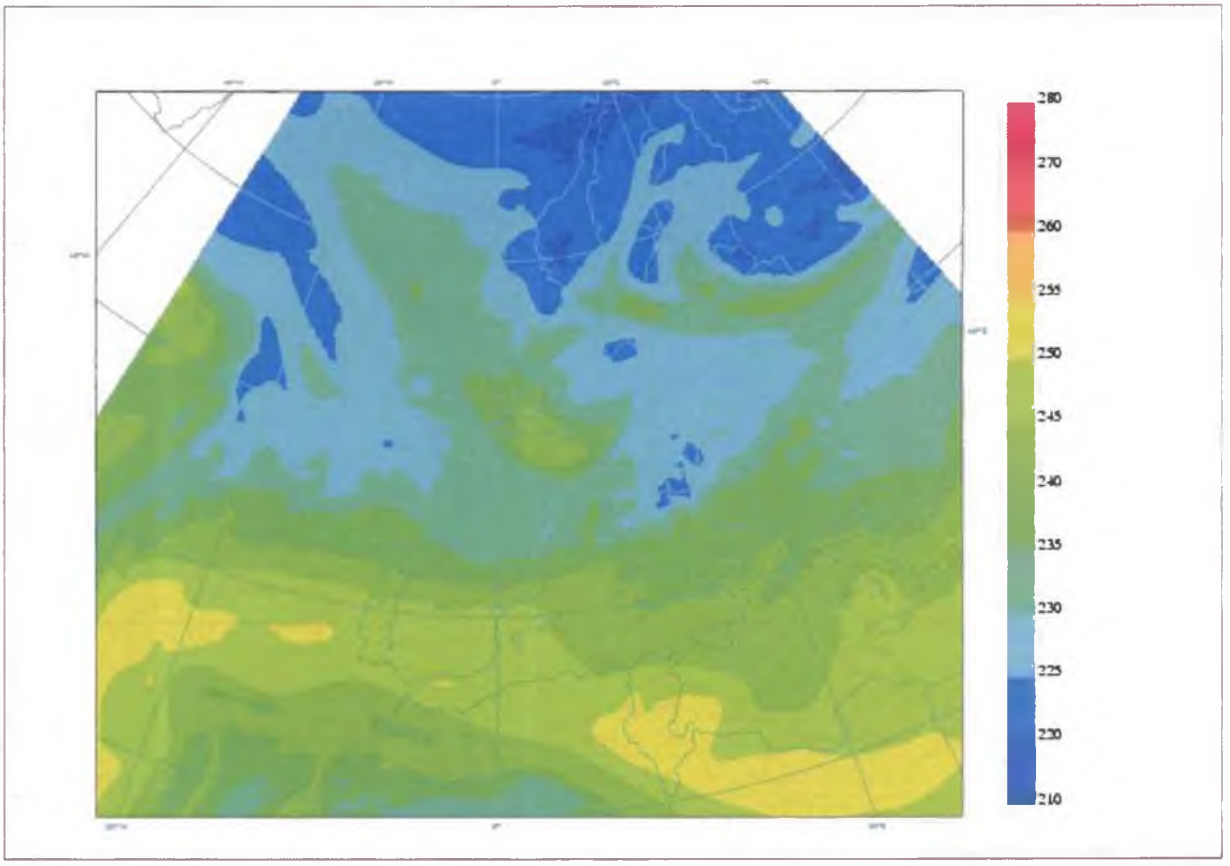

Fig. 33: Model analysis of the brightness temperatures (in K) of WV channel, November 19th 2004 00 UTC

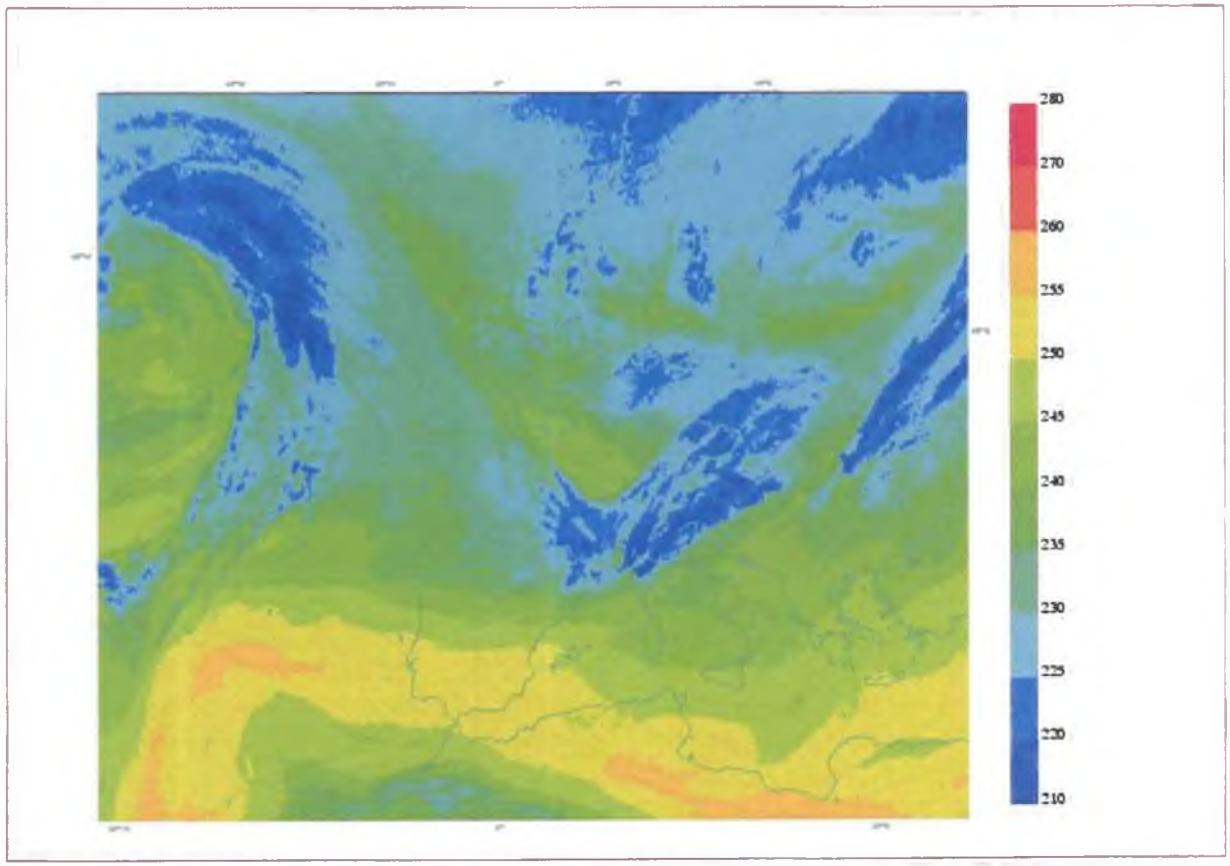

Fig. 34: WV channel image of METEOSAT-7 satellite, November 19th 2004 00 UTC

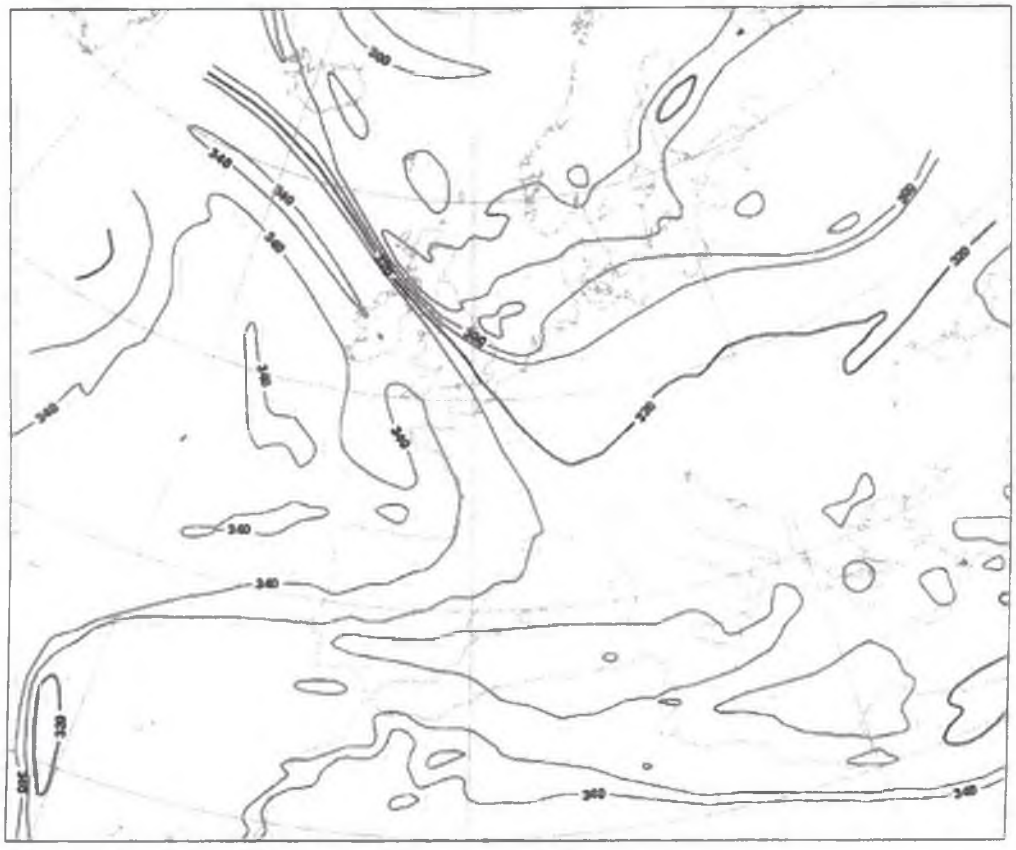

Fig. 35: Potential temperature at 2 PVU level (interval 10 K), analysis from November 19th 2004 00 UTC

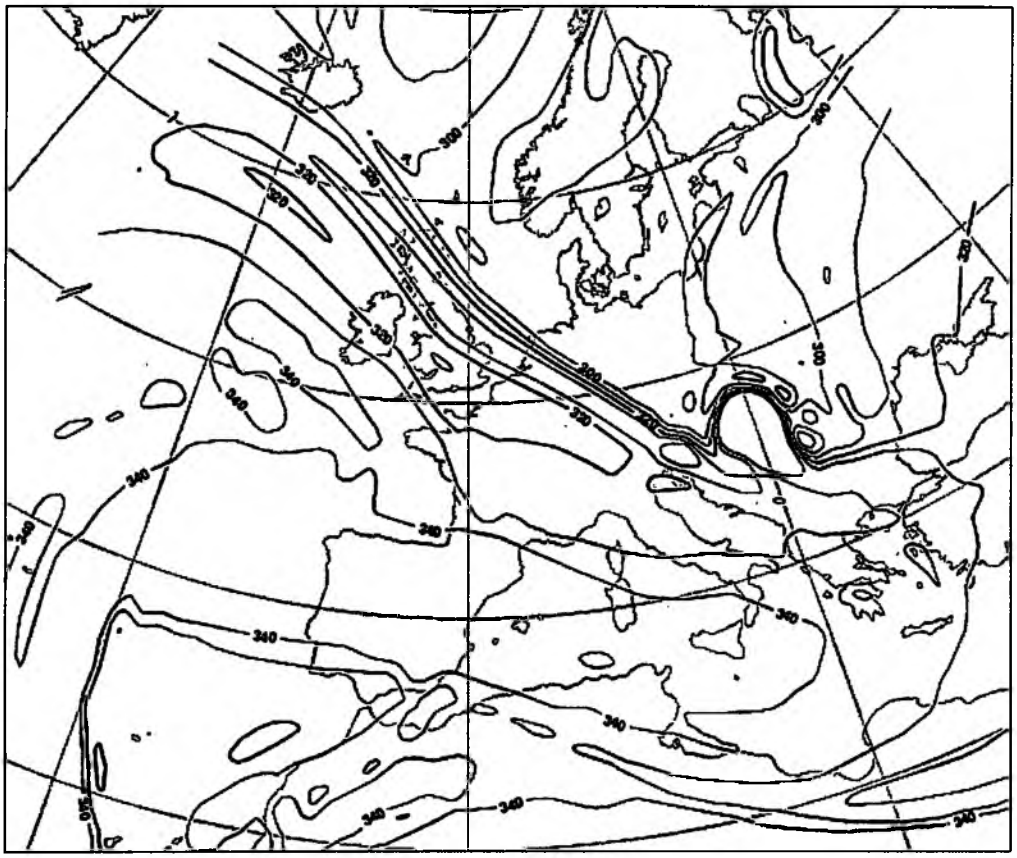

Fig. 36: Potential temperature at 2 PVU level (interval 10 K), analysis from November 20th 2004 00 UTC

4.3 August 2002

Synoptic description

The synoptic situation in the first half of the August 2002 was characterized by high pressure region over northern Europe and as a consequence of pressure field configuration meridional circulation over central Europe was established. The cyclones with frontal systems moved from Atlantic over Mediterranean region to the central Europe and they were connected with strong fruitful precipitation. Very high precipitation rates were recorded in many parts of the Mediterranean region, too.

In the first decade of August, two lows moved over middle Europe during one week. The first low caused heavy precipitation connected with soil saturation and local floods in the southern part of Bohemia. The second low then caused heavy rains and floods in one third of the Czech Republic territory and so that our attention will be paid to this cyclone.

This low moved originally from eastern Atlantic and reached Ireland and British Islands on August 8th (Fig. 37). The temperature difference between warm sector and head part of this low was about 7°C during night to August 9th. At this time, the elongated trough can be detected from stretching from Island to British Islands at 500 hPa level (Fig. 38). During next day the frontal system moved to the western Mediterranean and the clouds grew in bulk over the warm sea with well developed convective clouds over Balearic Islands (see Fig. 48). The low pressure centre was situated over southern part of North Sea at sea level. The temperature contrast on the frontal system became to increase (up to 12°C at 850 hPa level – see Fig. 39). The beginning cut-off process can be seen at the 500 hPa level over Western Europe (Fig. 40). During the night to August 11th the separate cyclone centre formed over Gulf of Genoa and the cut-off cyclone was well developed over the western Mediterranean during August 11th (Fig. 41).

The critical day for floods period in the Czech Republic was August 12th. The centre of the low was situated over southern Bohemia during the midnight to August 12th. At 850 hPa level, the centre of thermally greatly asymmetric and strongly developed cyclone was over Austria (Fig. 42), with temperatures in its warm sector of about 20°C over Balkan Peninsula and in its head part of about 7 to 10°C over Germany (see Fig. 43 for analysis of temperature at 850 hPa level and Fig. 44 for surface analysis from August 12th 00 UTC). At levels 500 hPa and 200 hPa the centre of this cyclone was situated east of the Alps. During August 12th the cyclone moved to the northeast and it became slowly to fill up over Poland during the following day.

Comparison model-to-observation

The situation for August 9th 00 UTC in the IR channel analyzed by the model and observed by satellite can be seen on Figs. 43 and 44. A good agreement between modelled and observed synoptic features can be found. It can be seen a quite well simulated position of the cloud band stretching from British Islands over western France to Gulf of Biscay, clouds over German as well as the band with higher brightness temperatures (it means the region with less or no cloudiness) over North Sea and Benelux. Some underestimation of the tops of clouds is connected with the fact that they have higher brightness temperature in the modelled then in the observed images. It can be observed by detailed investigation. The similar situation can be found on figs. 45 and 46 where the temperatures for WV channel are demonstrated.

The situation for August 10th 00 UTC can be seen on figs. 47 and 48 for IR and 49 and 50 for WV channel. A good agreement between positions of the main features can also be found here, but with more underestimation (over 20°C for some areas) of the convective cloudiness over western Mediterranean.

Let's focus now on the forecast quality for August 12th 00 UTC according to the length of the forecast time. Figs. 51 to 54 demonstrate, in sequence, the forecast of the brightness temperatures in the IR channel from August 8th, 9th, 10th and 11th, it means +96 to +24 hours. For comparison, the observed situation in IR channel can be seen on Fig. 55 for August 12th 00 UTC. Relatively good agreement can be detected for 24 h forecast (Fig. 54) with well simulated cloudiness of the low as well as with quite correctly situated areas of higher brightness temperatures stretching from Hungary to Sicily. But again some underestimation of the convective clouds, mainly over Carpathian Mountains, can be observed.

As for forecast +48 h (Fig. 53), still quite satisfactory representation of the main features forecasted by the model can be seen, with some shift of cloudiness to the east.

Focussing on forecast +72 h (Fig. 52), the situation is qualitatively worse. The cloud system of the low is simulated more southerly with centre over northern Adria. A relatively wide spread area with a lower brightness temperatures can be seen over northern Europe what could bee caused by lower level cloudiness.

Finally, for +96 h (Fig. 51) forecast, the trough reaching from Gulf of Genoa with cold front cloudiness in the front part of it is more pronounced and spread in model forecast then observed by satellite. The main cyclone centre is now simulated over Gulf of Genoa instead of over central Europe. That's probably also the reason why more cloudiness over Balkan Peninsula and Carpathian Mountains is simulated.

The of the 2 PVU level, the so-called dynamical tropopause (see chapter 1 for theory about it) can be thought as a useful and helpful characteristic. This characteristic shows good correlation between the position of the cyclone mentioned above and the region of the driest air (the region with relatively high brightness temperatures). This can be well observed on August 10th 00 UTC, see the model analysis on Fig. 56 and compare it with satellite measurement in WV channel on Fig. 50.

In general, we can conclude that for this case a good agreement between model and reality can be seen for the forecast up to +60 hours. For longer forecast, the discrepancies are significant.

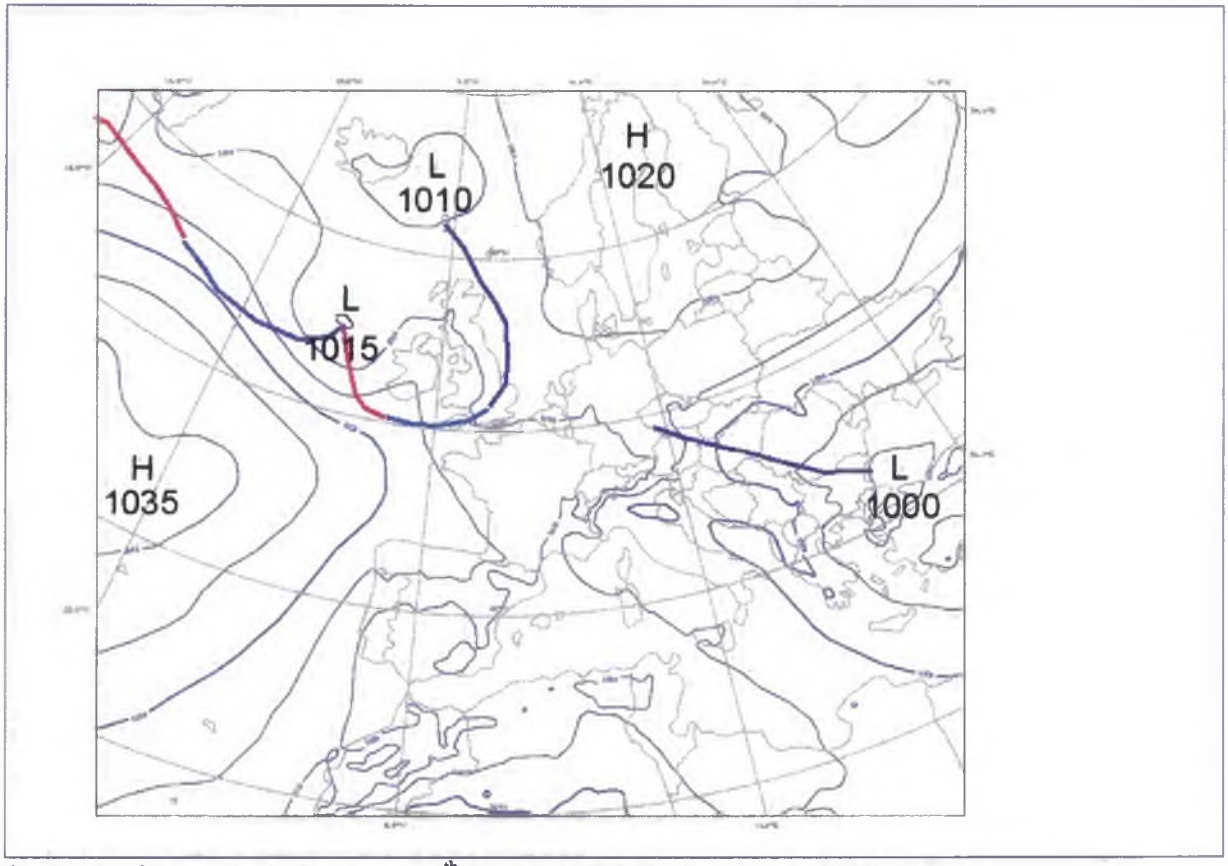

Fig. 37: Surface analysis for August 8th 2002 00 UTC (isobars interval hPa)

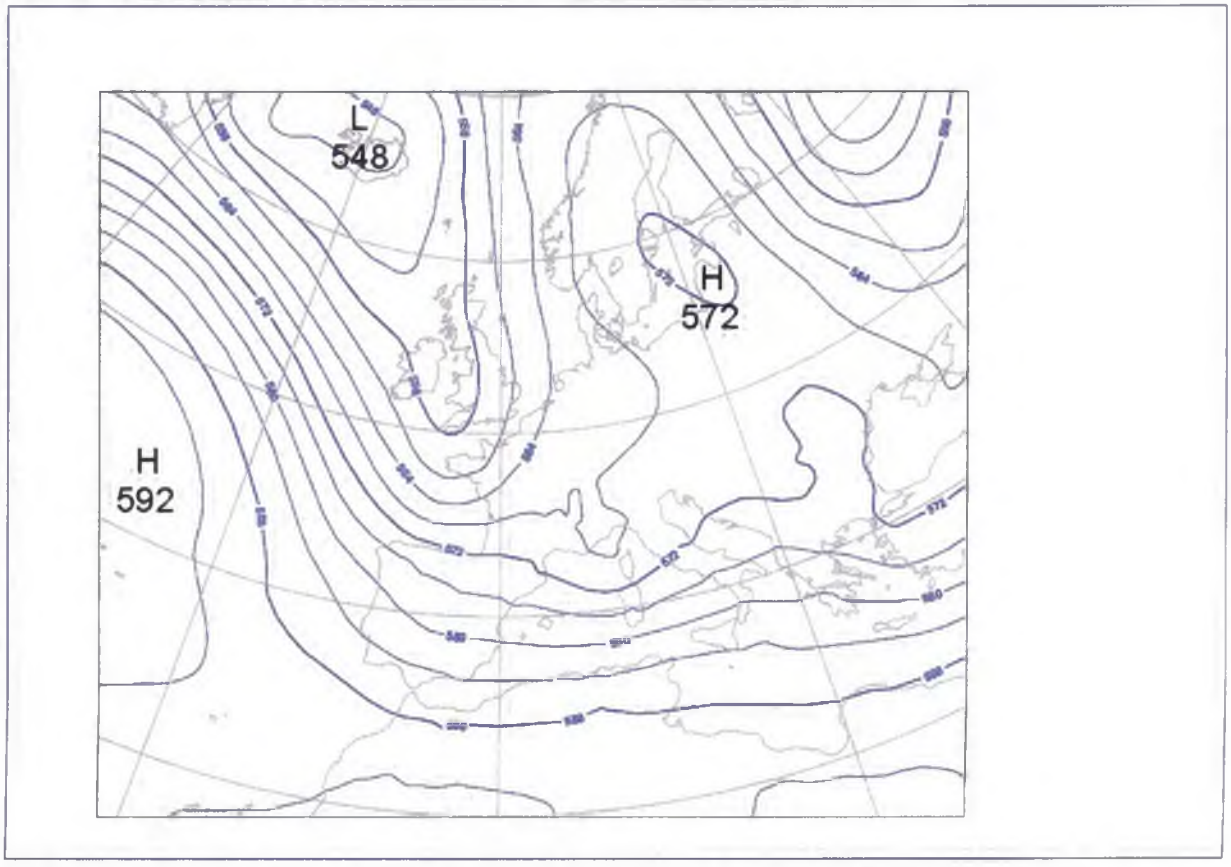

Fig. 38: Geopotential height of 500 hPa level (interval 4 decametres), analysis for August 9th 2002 00 UTC

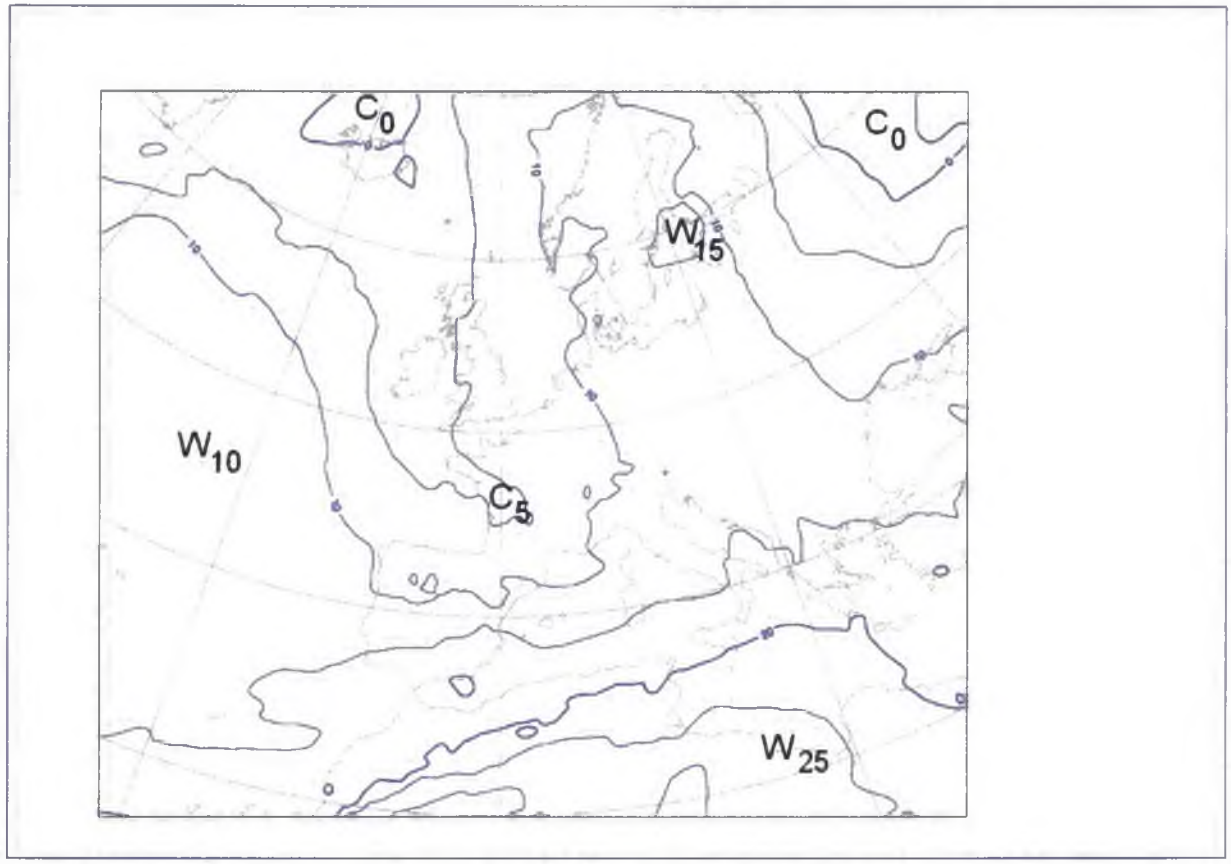

Fig. 39: Temperature in 850 hPa level (interval 5 °C), analysis for August 10th 2002 00 UTC

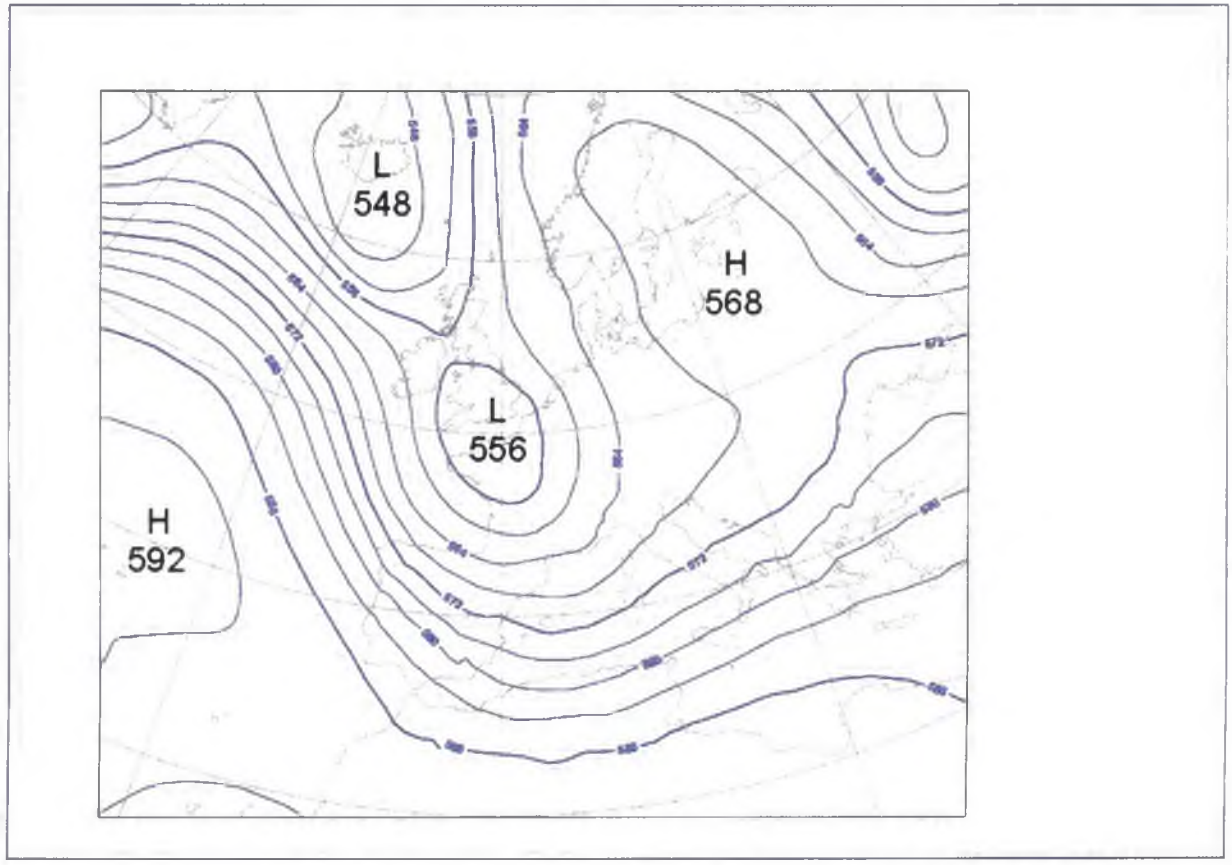

Fig. 40: Geopotential height of 500 hPa level (interval 4 decametres), analysis for August 10th 2002 00 UTC

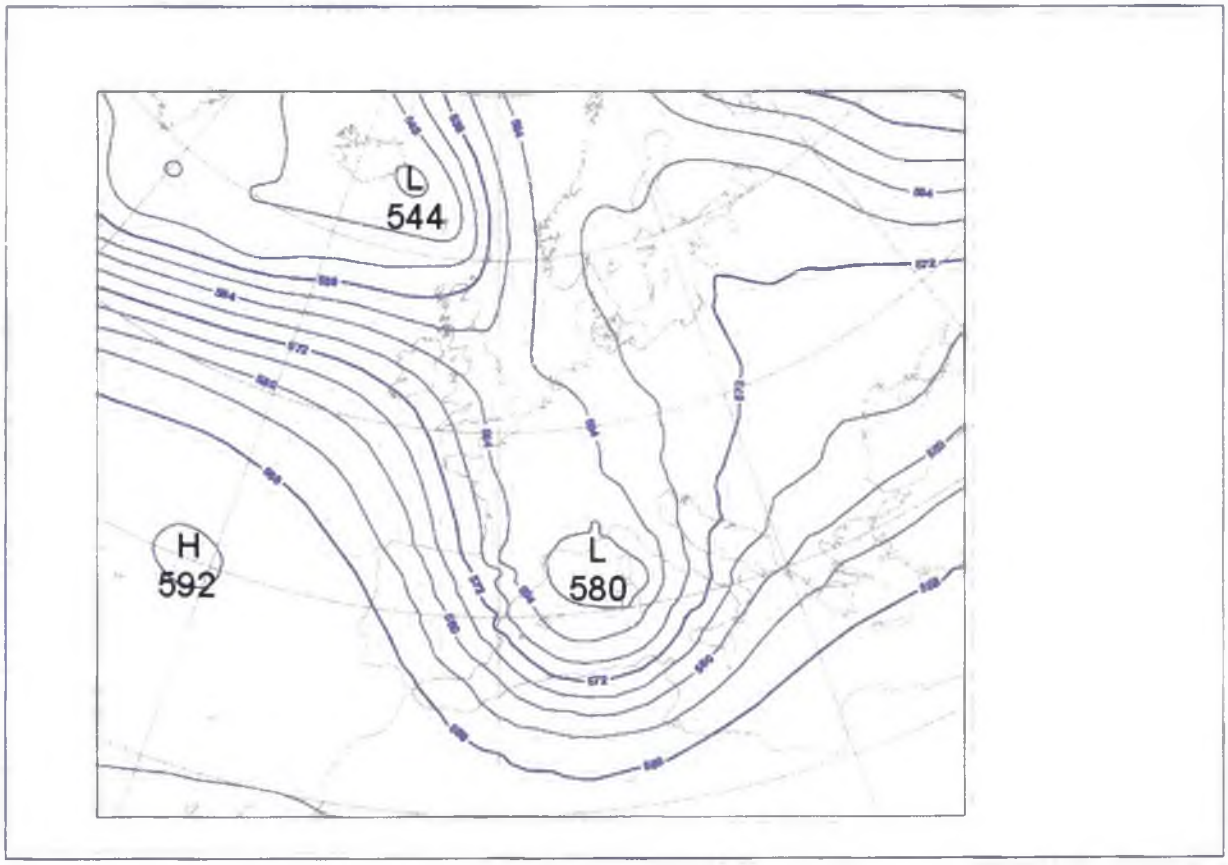

Fig. 41: Geopotential height of 500 hPa level (interval 4 decametres), analysis for August 11th 2002 00 UTC

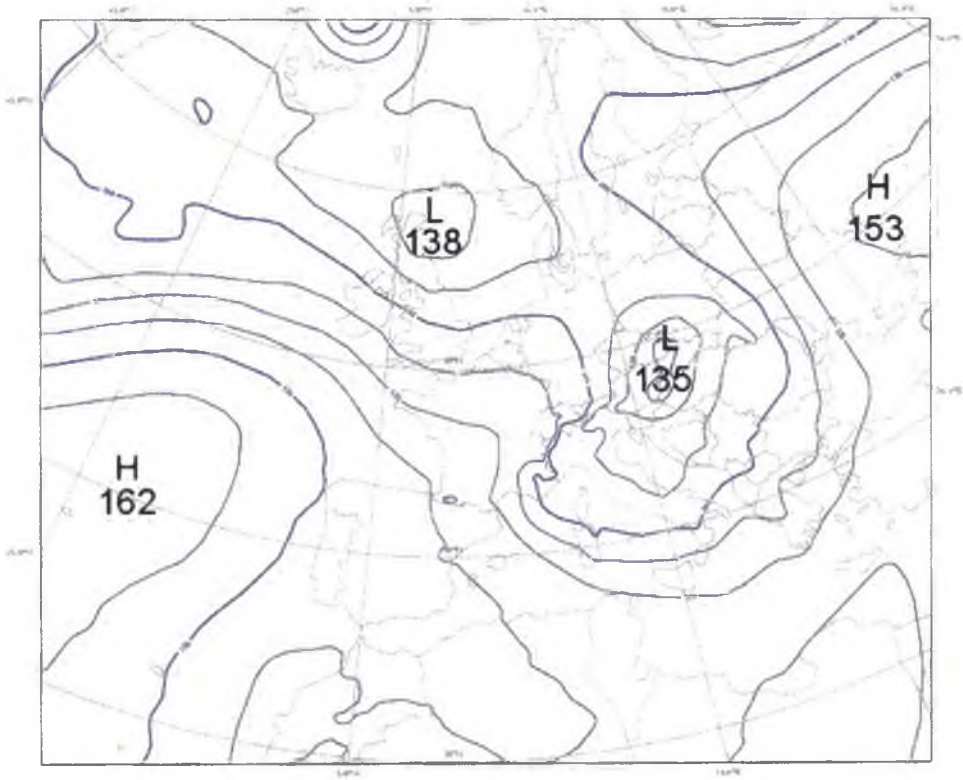

Fig. 42: Geopotential height of 850 hPa level (interval 3 decametres), analysis for August 12th 2002 00 UTC

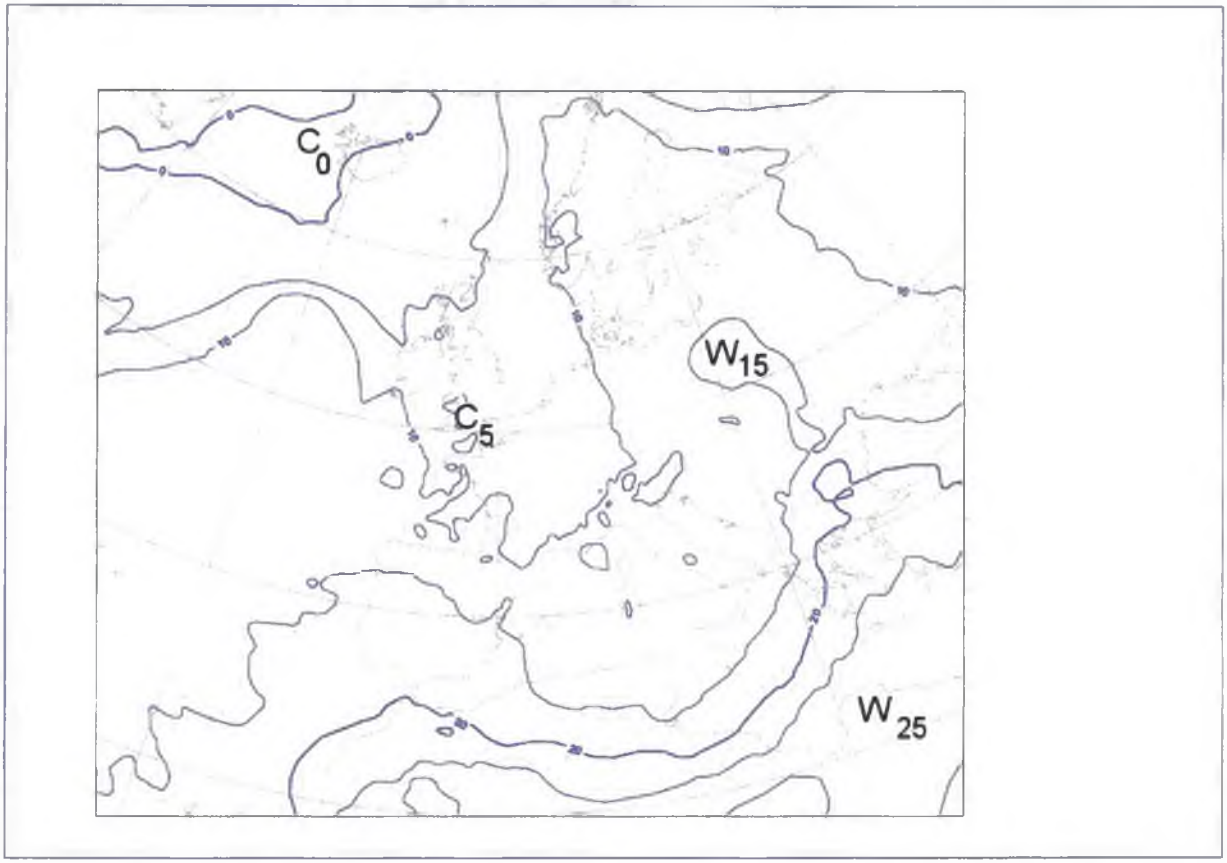

Fig. 43: Temperature at 850 hPa level (interval 5 °C), analysis for August 12th 2002 00 UTC

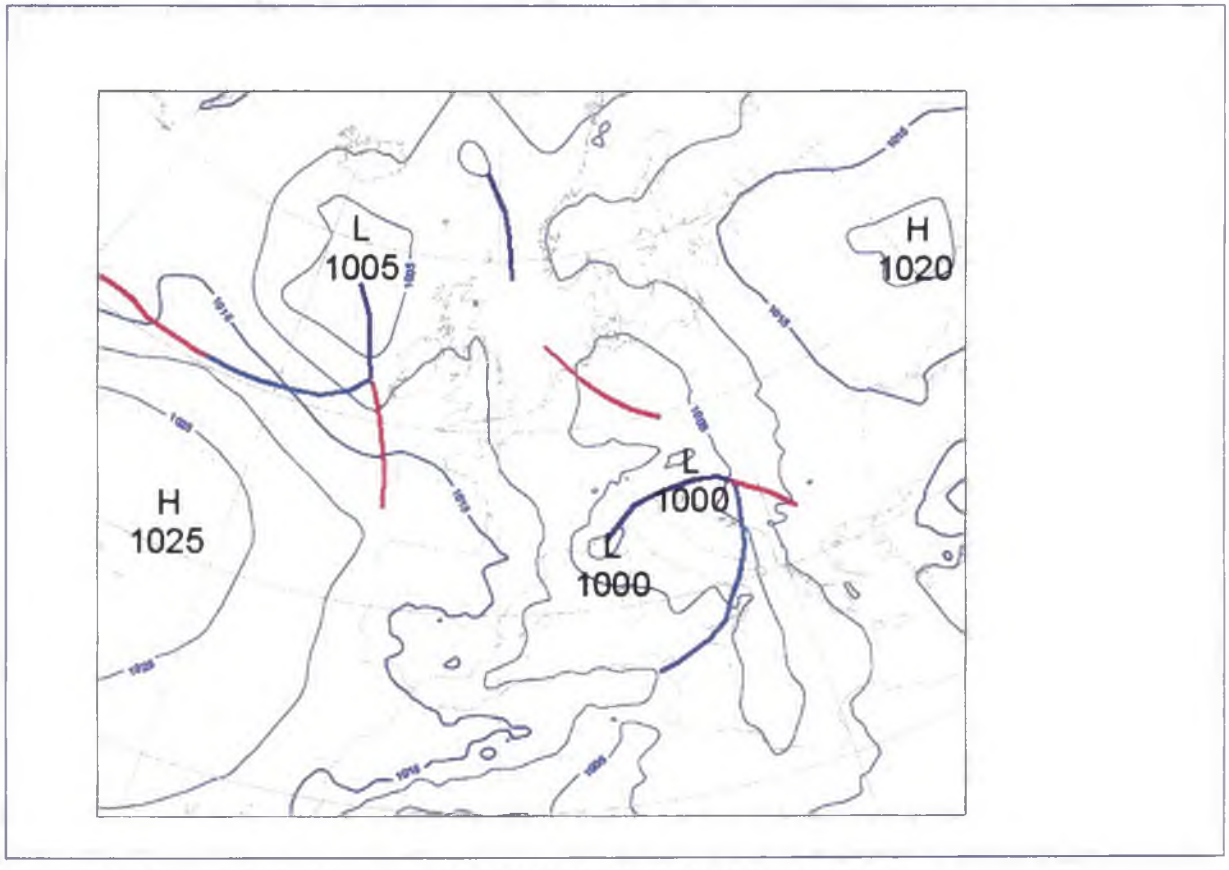

Fig. 44: Surface analysis for August 8th 2002 00 UTC (isobars interval hPa)

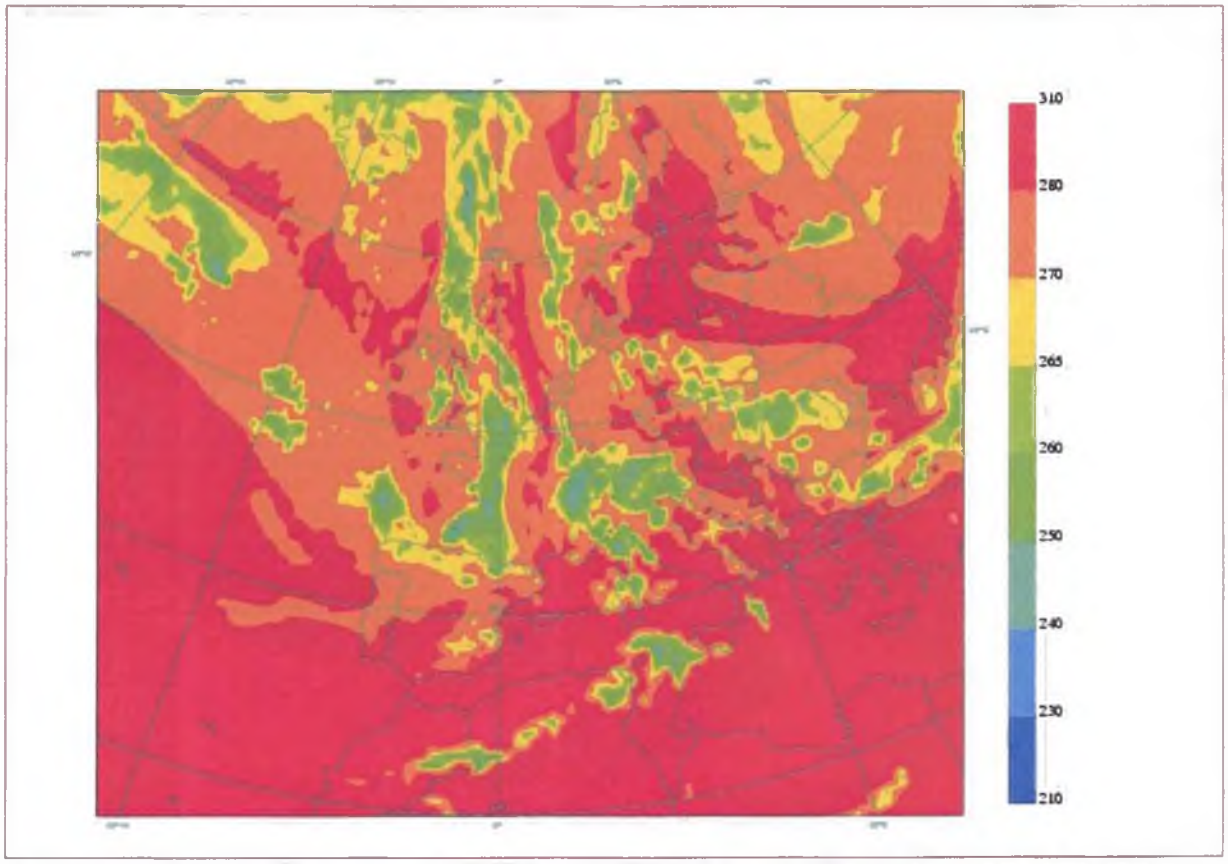

Fig. 43: Model analysis of the brightness temperatures (in K) of IR channel, August 9th 2002 00 UTC

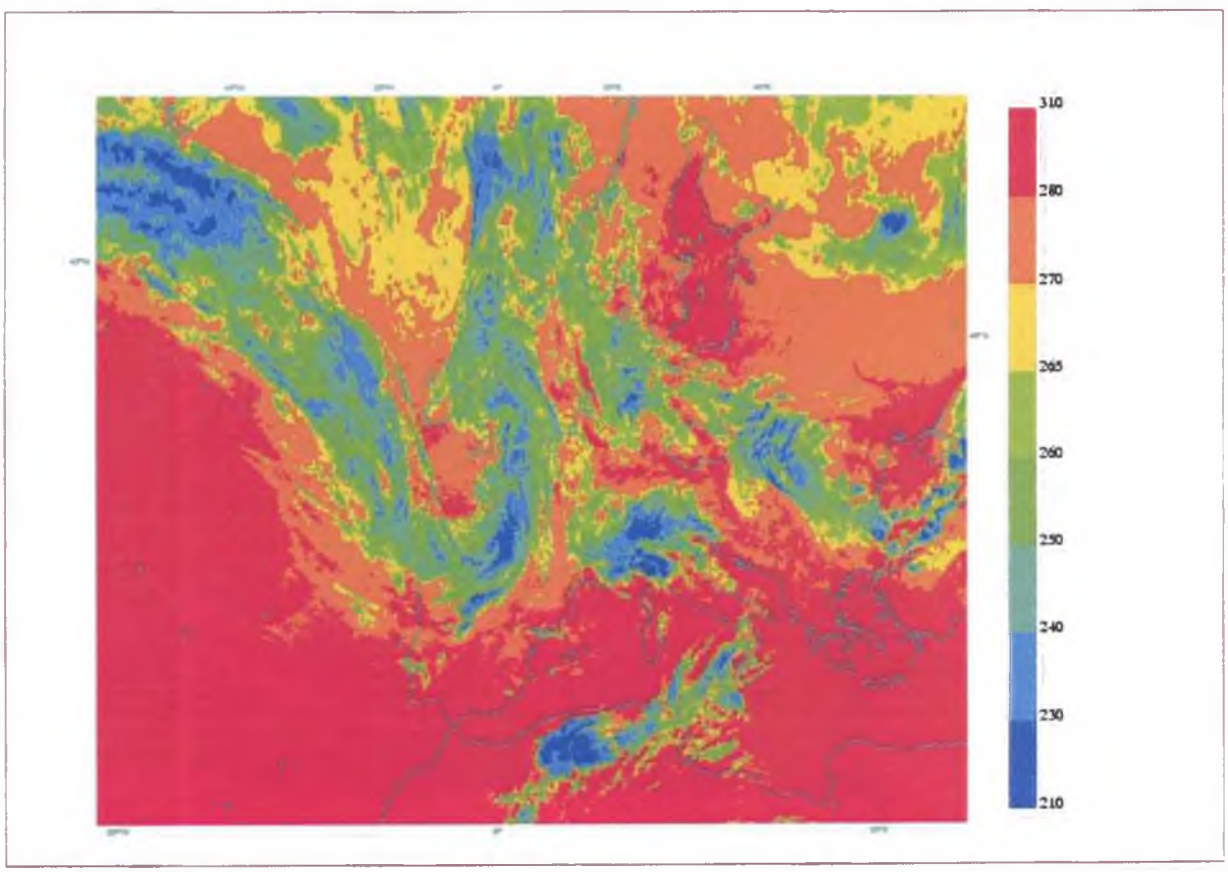

Fig. 44: IR channel image of METEOSAT-7 satellite, August 9th 2002 00 UTC

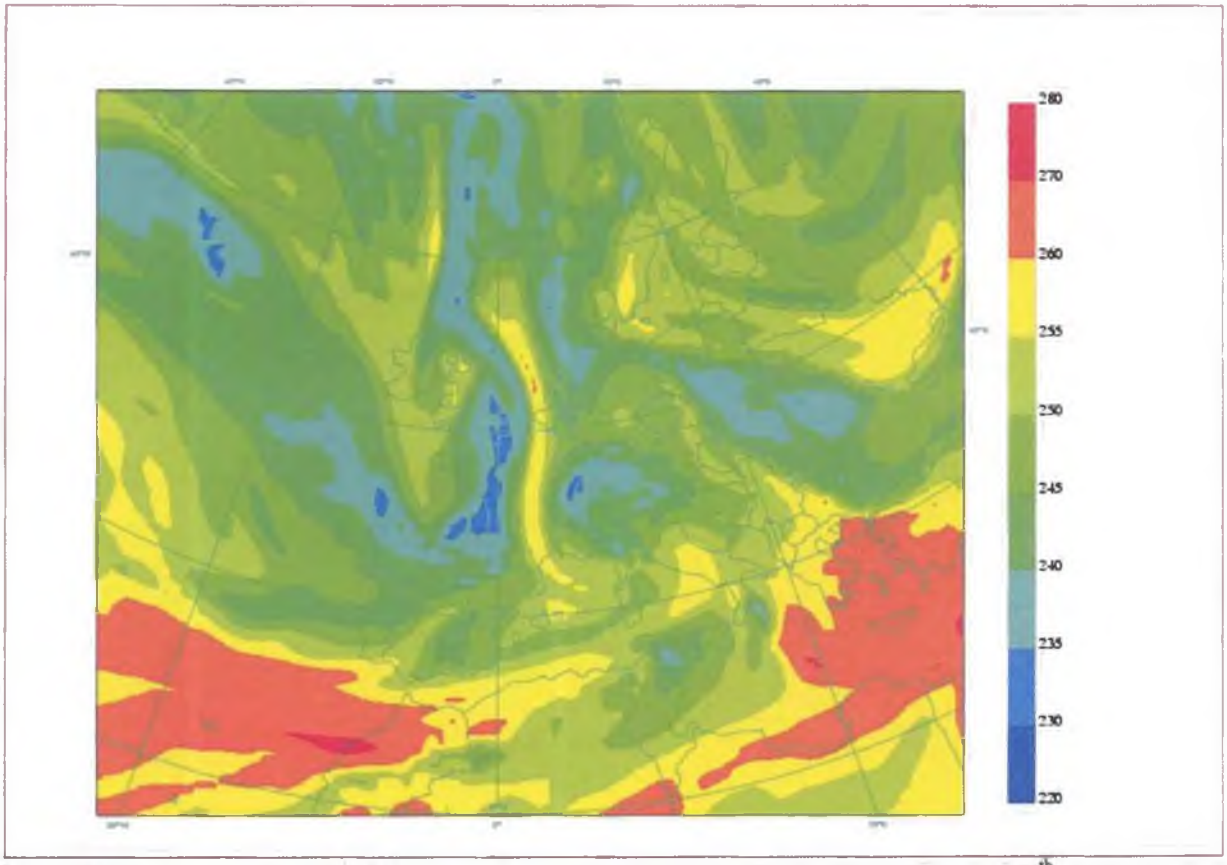

Fig. 45: Model analysis of the brightness temperatures (in K) of WV channel, August 9th 2002 00 UTC

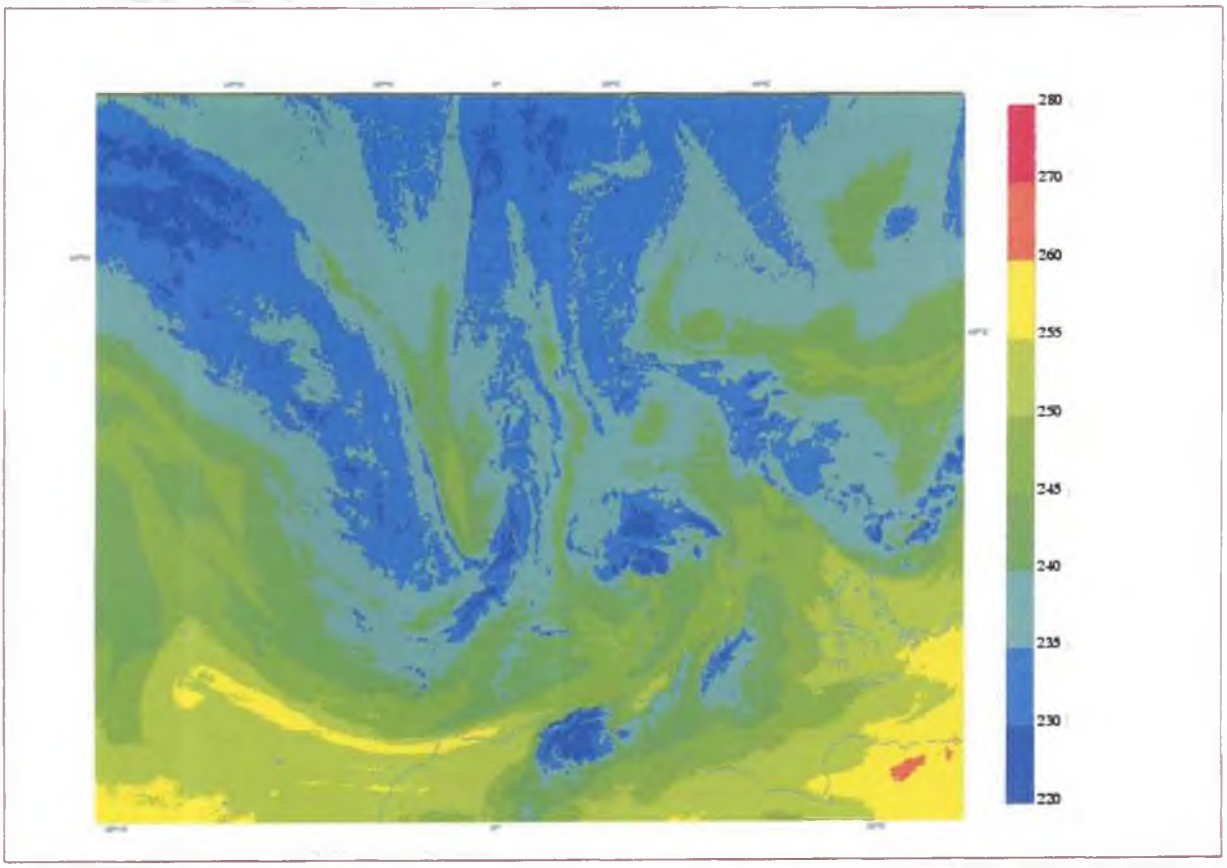

Fig. 46: WV channel image of METEOSAT-7 satellite, August 9th 2002 00 UTC

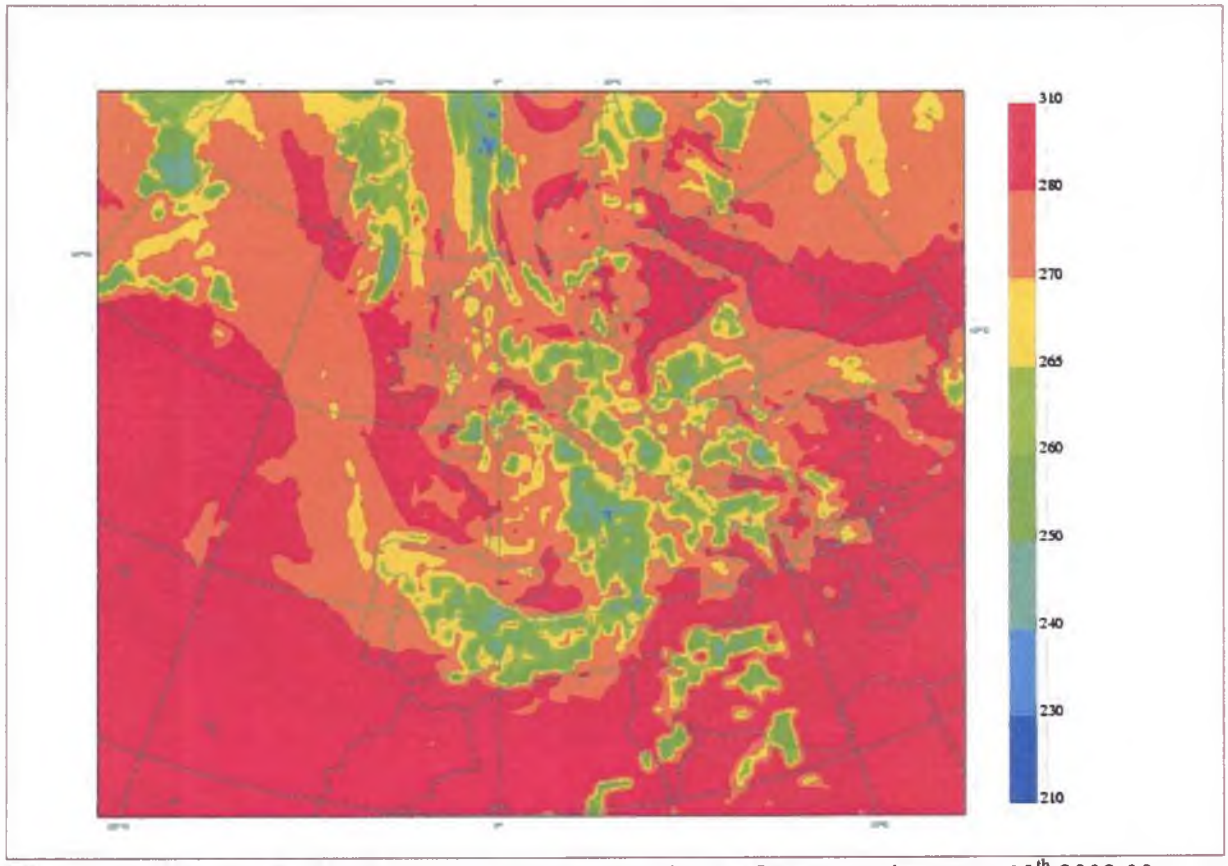

Fig. 47: Model analysis of the brightness temperatures (in K) of IR channel, August 10th 2002 00 UTC

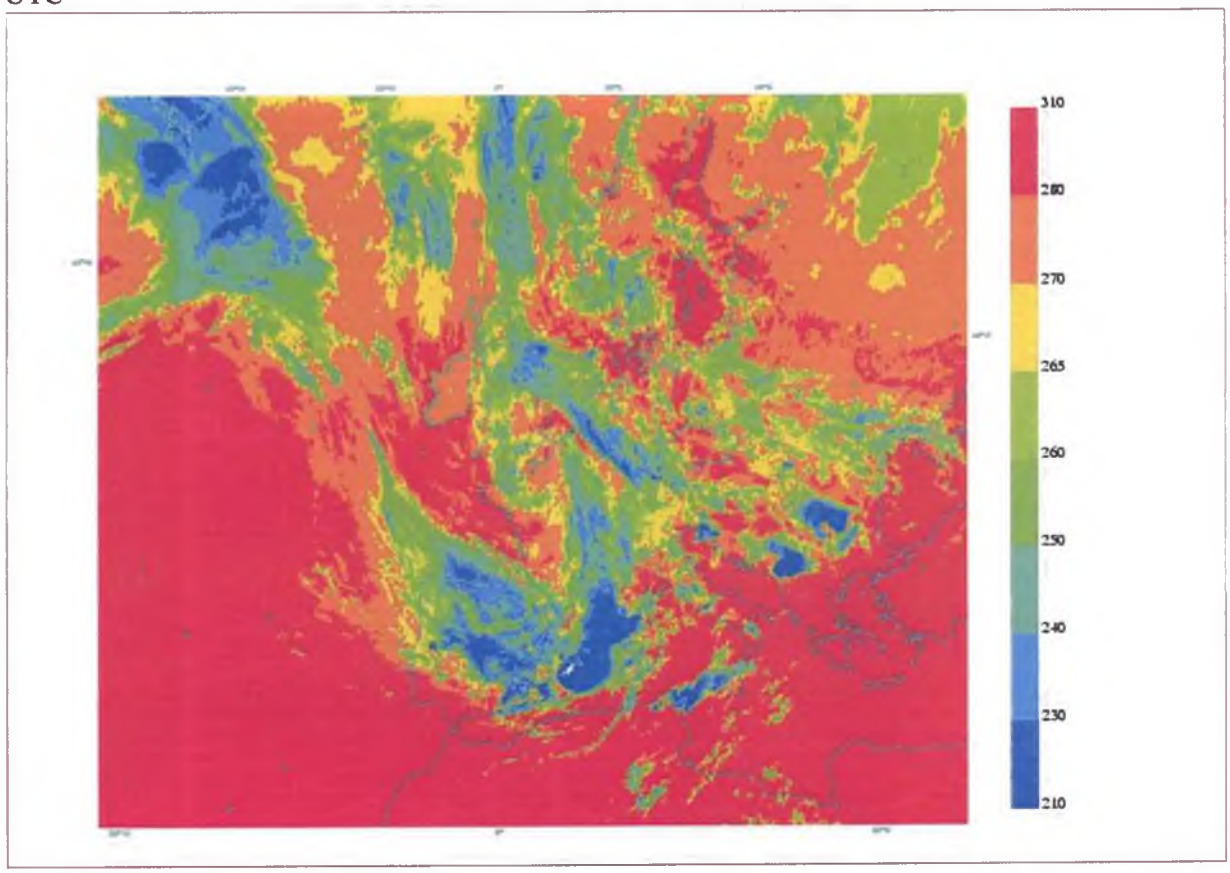

Fig. 48: IR channel image of METEOSAT-7 satellite, August 10th 2002 00 UTC

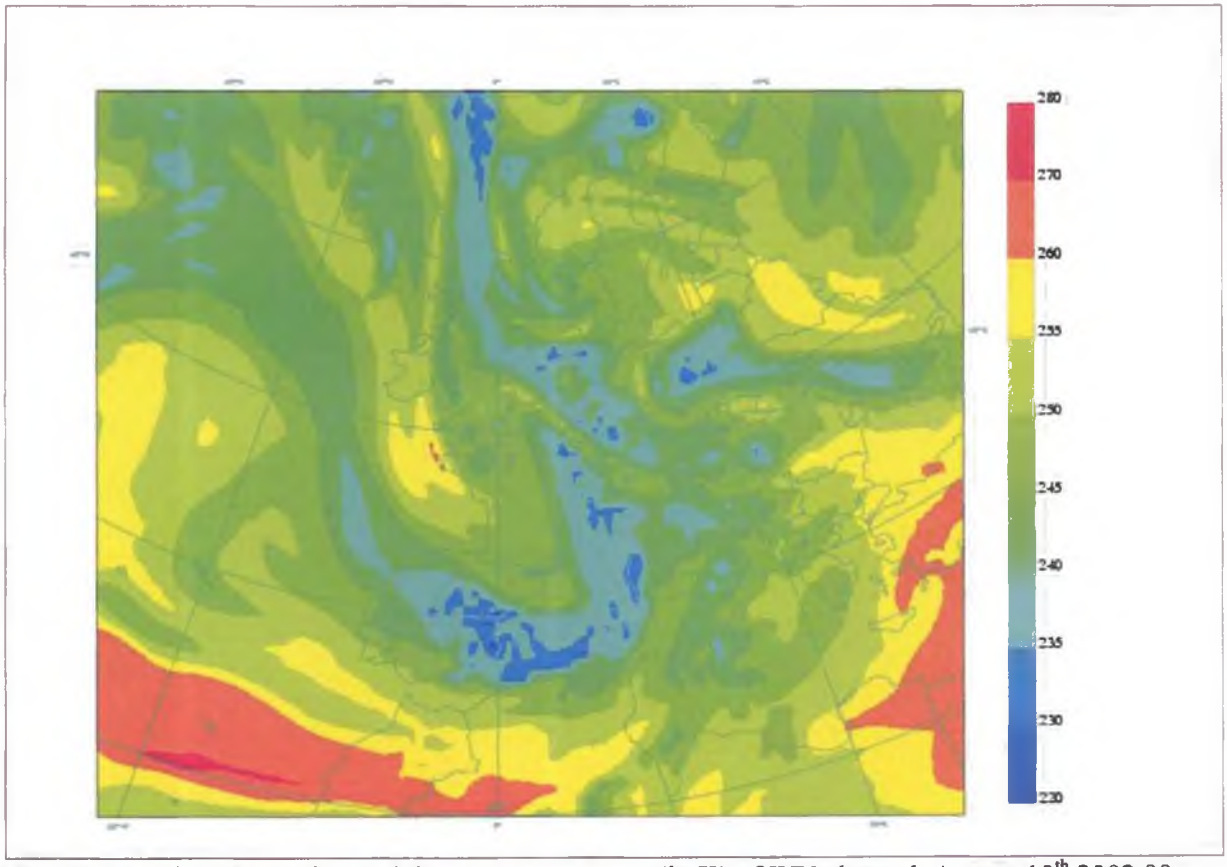

Fig. 49: Model analysis of the brightness temperatures (in K) of WV channel, August 10th 2002 00 UTC

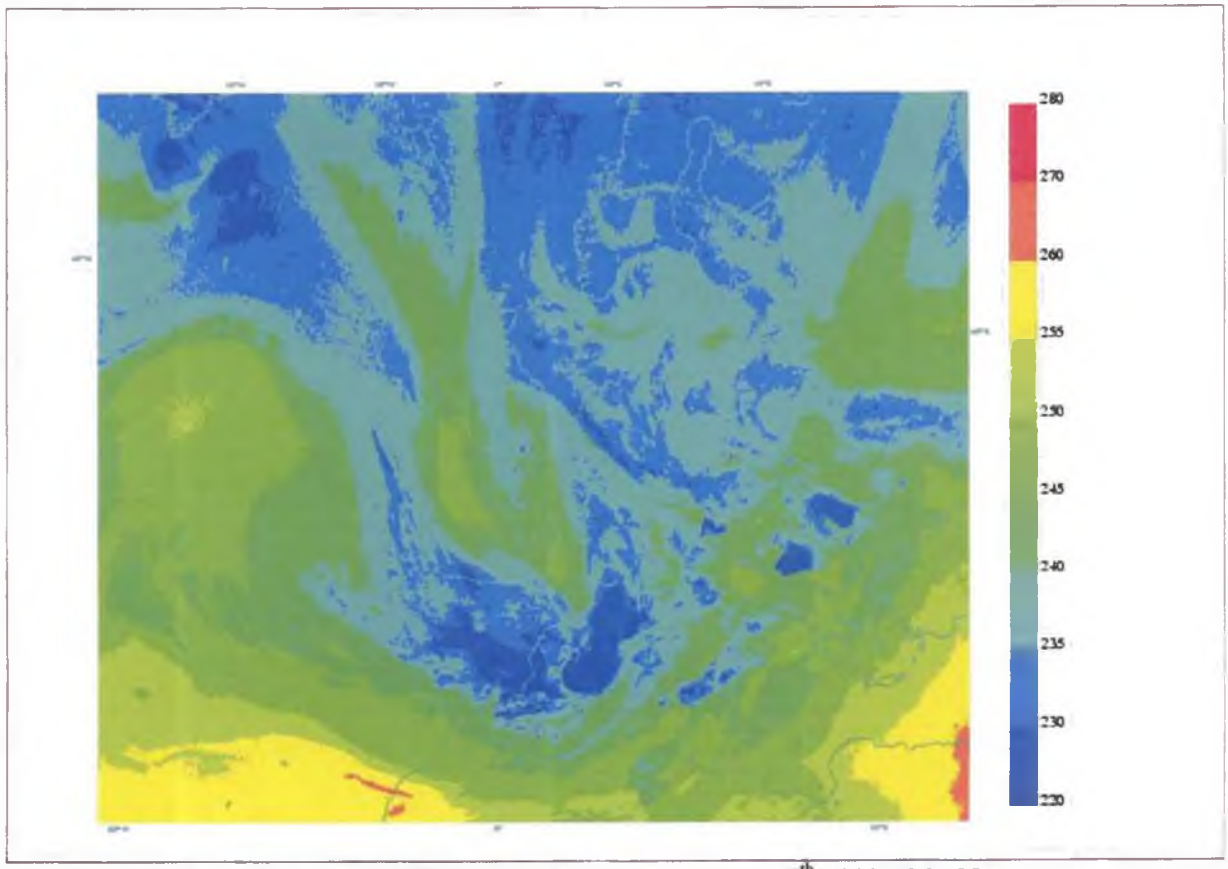

Fig. 50: WV channel image of METEOSAT-7 satellite, August 10th 2002 00 UTC

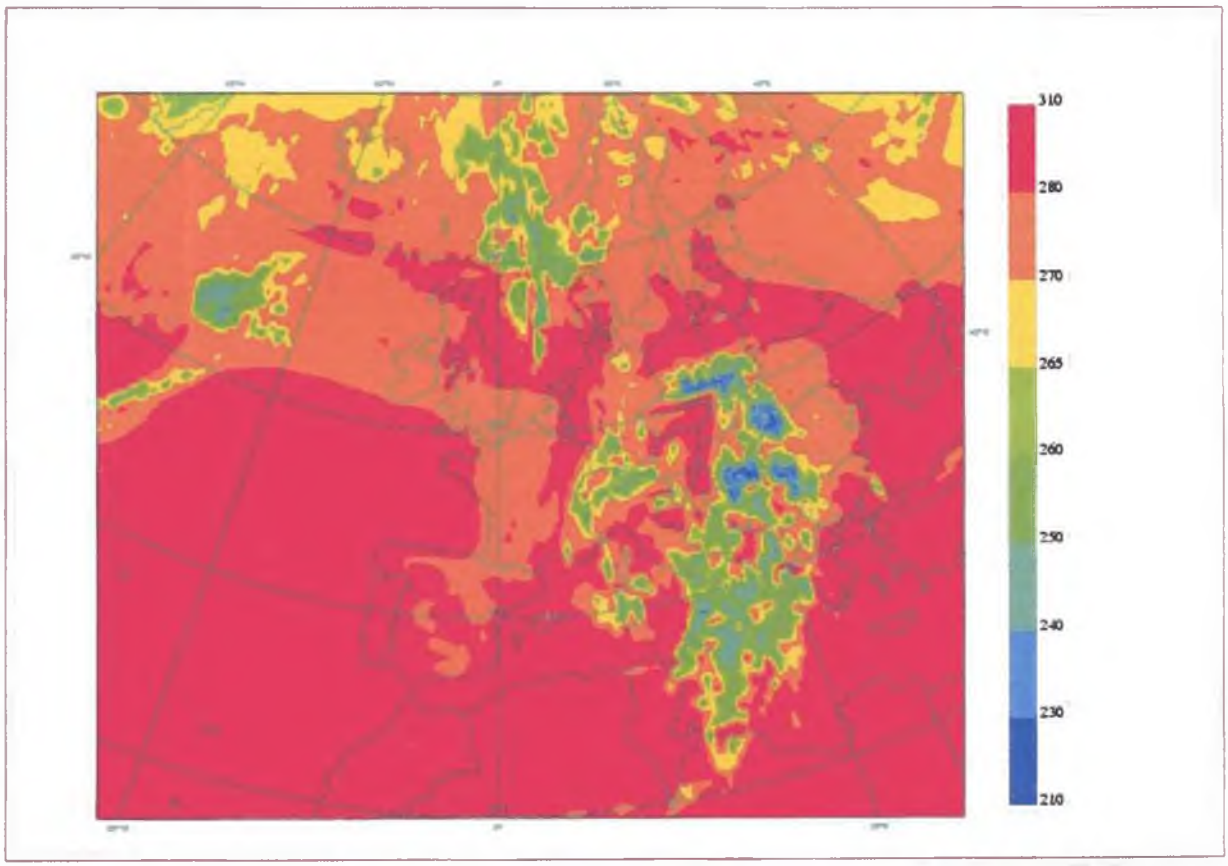

Fig. 51: Model forecast of the brightness temperatures (in K) for IR channel from August 8th 2002 00 UTC for August 12th 2002 00 UTC

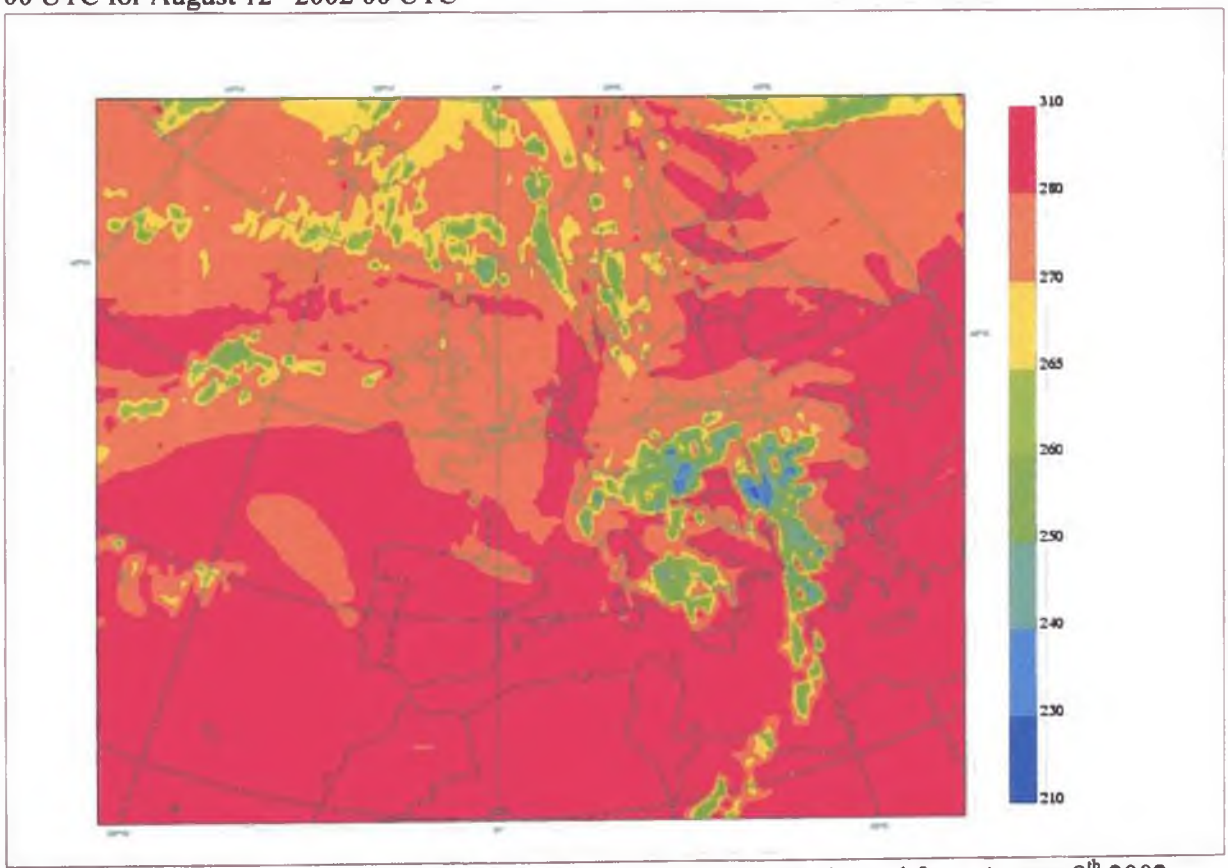

Fig. 52: Model forecast of the brightness temperatures (in K) for IR channel from August 9th 2002 00 UTC for August 12th 2002 00 UTC

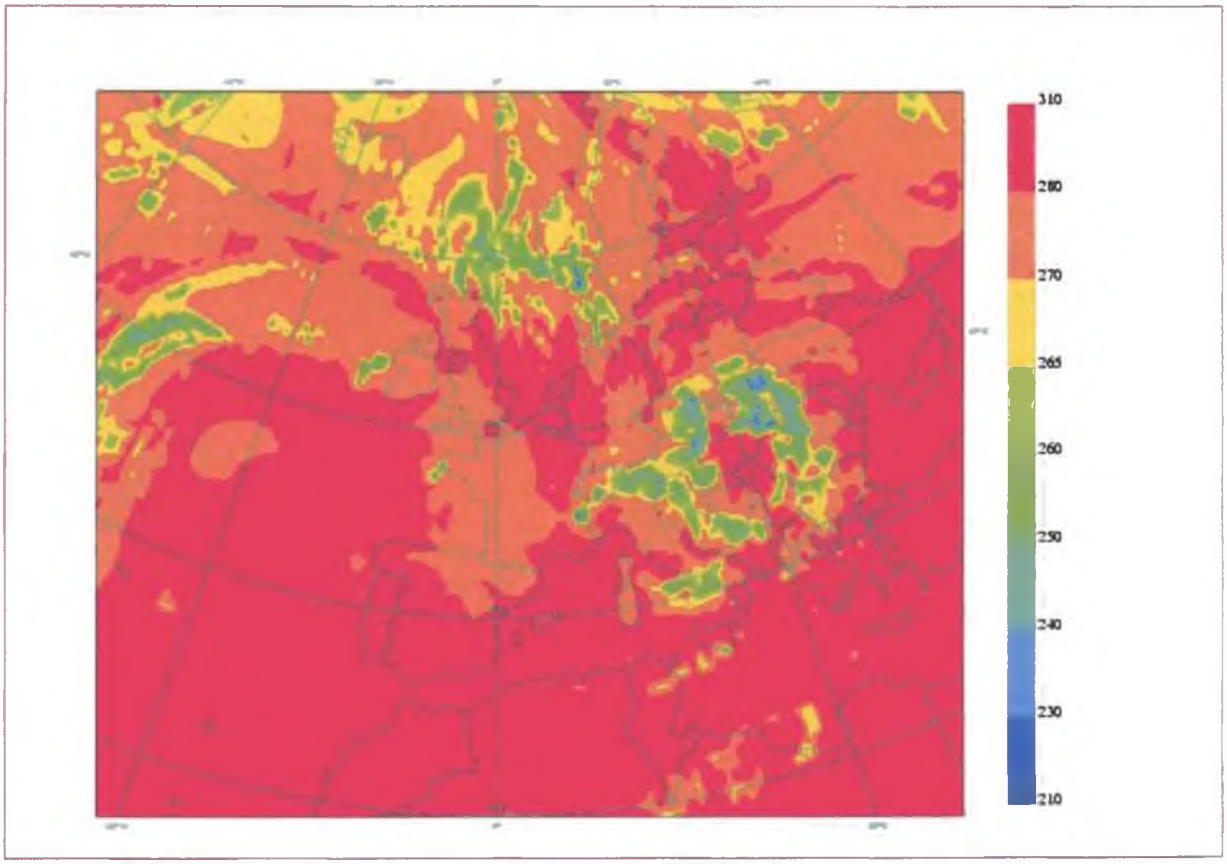

Fig. 53: Model forecast of the brightness temperatures (in K) for IR channel from August 10th 2002 00 UTC for August 12th 2002 00 UTC

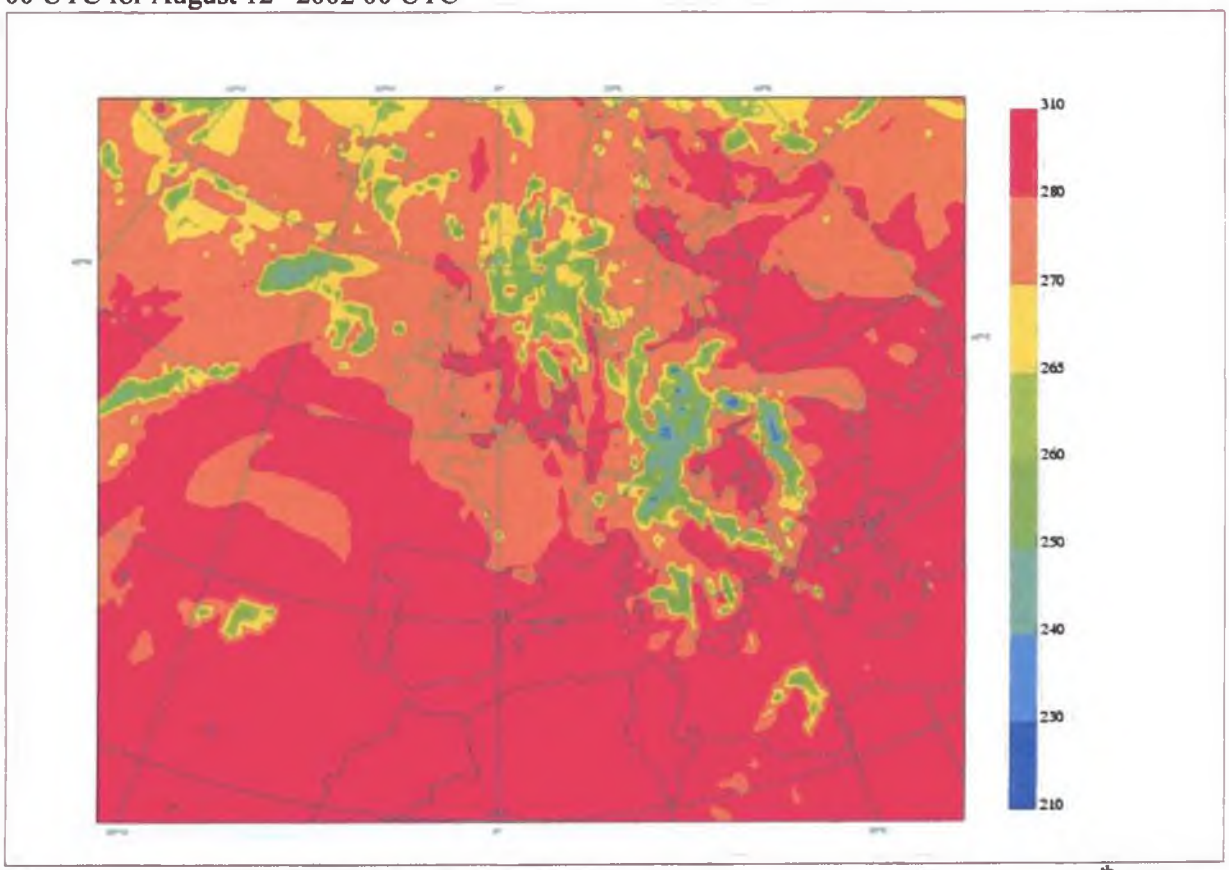

Fig. 54: Model forecast of the brightness temperatures (in K) for IR channel from August 11th 2002 00 UTC for August 12th 2002 00 UTC

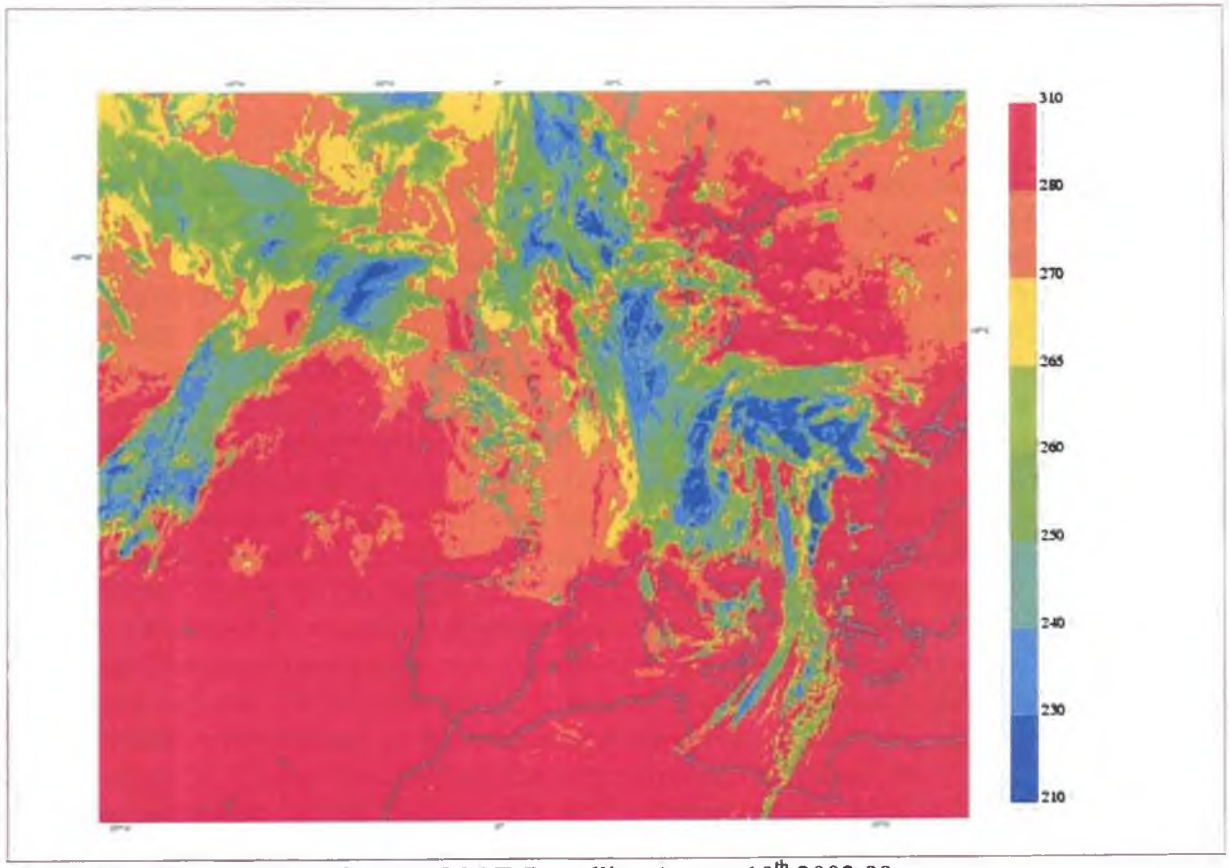

Fig. 55: IR channel image of METEOSAT-7 satellite, August 10th 2002 00 UTC

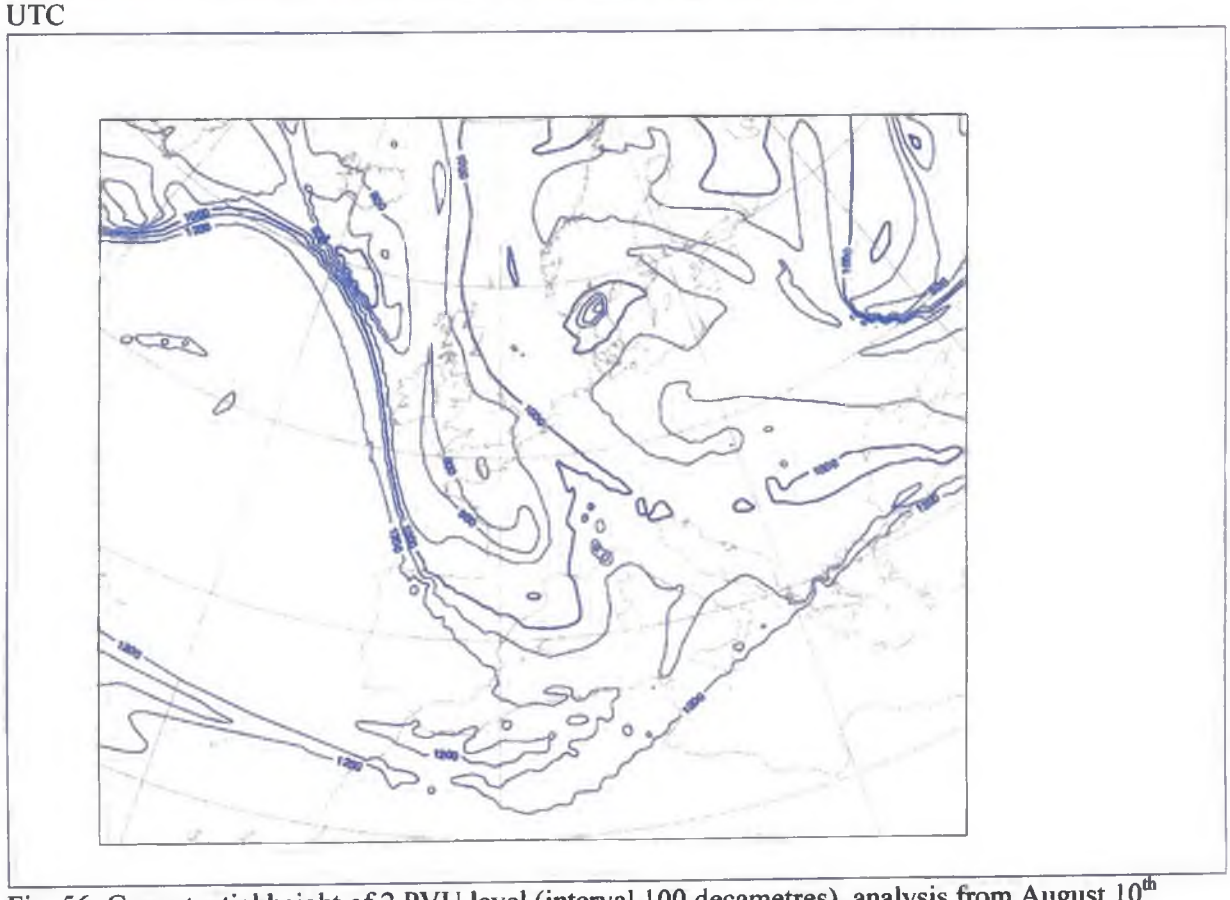

Fig. 56: Geopotential height of 2 PVU level (interval 100 decametres), analysis from August 10th 2004 00 UTC

4.4 December 2004

Synoptic description

The last decade of December 2004 was characterized by frequent weather changes with prevailing west-wind circulation over central Europe. The general situation between December 22nd and 26th can be characterized by primary cyclone positioned over Norwegian Sea with sea level pressure in its centre under 970 hPa. A high pressure ridge reaching from central Atlantic to central Europe could be followed for middle troposphere at 500 hPa level on December 23rd (Fig. 57). This ridge removed during next day and then a trough developed over Western Europe on December 25th at 500 hPa level (see Fig. 58). A cut-off cyclone was then evolved from this trough in the region of south-western Europe. The similar development can be seen at 200 hPa level as well (Fig. 59 for December 25th 00 UTC).

Let's focus now in more details on sea level pressure field. During December 22nd a weakening high pressure ridge could be found in the central Europe. Next day a low moved from northern Atlantic to the Baltic Sea. This low was connected with strong winds, wind gusts and with intensive warming (massive thaw weather, surface temperatures about 10 °C) over central Europe. Another low was formed as a secondary depression in the strong west-wind circulation over British Islands and it moved to east. So called Christmas-Thaw (quite typical weather phenomenon in the central Europe) with surface temperatures over Czech Republic up to 12 °C was the result of these circulation conditions (see Fig. 60 for sea level pressure on December 24th 00 UTC and Fig. 61 for December 25th 00 UTC).

Comparison model-to-observation

The situation for December 23rd expressed by help of brightness temperatures fields can be seen on Figs. 62 and 63 for model analysis and for satellite observation, both for IR channel. Very satisfactory representation of the main synoptic features, such as the cloudiness of occlusion/cold front reaching from the Finland over central Europe region to the southern France can be seen here. Very slight discrepancies (colder cloud tops in model computation in comparison with observed image) can be mentioned only. The forecast from December 23rd 00 UTC is also successful for various integration times. This is documented by Figs. 64 and 65 with forecasted and observed situation for December 26th 00 UTC (+72 hours).

But the different conclusions must be mentioned in connection with forecast simulated from 24th December (see Fig. 66 for model outputs and Fig. 67 for satellite observation, both in IR channel). As it can be seen by comparison between these two images, the cloud system of the developing frontal wave south-westerly of British Islands is analyzed more to the north, approximately to the Ireland region, and cloudiness over France is missing in contradiction with reality. Besides that lower brightness temperatures and more extensive low-level cloudiness in the region of central Europe can be observed in comparison with analyzed situation. For the forecast from December 24th (+12 h) greater differences between model computation (Fig. 68) and satellite observation (Fig. 69) in central Europe, mainly over the Czech Republic, can be identified (much more observed clouds in comparison with forecasted cloudiness). According to expectation forecasts for longer integration times are then getting worse quite quickly. For demonstration see Fig. 70 with model forecast for December 26th 00 UTC (+48 h) and Fig. 65 with satellite observations for the same time. Next conclusions for comparison between the model forecast and reality can be mentioned here: developing cut-off cyclone in the Mediterranean region is forecasted more westward and the cloudiness over central Europe is simulated somewhat to the west.

Finally, if we look on situation for December 25th 00 UTC, we could see an adequate representation of the synoptic features by the model outputs (Fig. 71) in comparison with satellite observations (Fig. 72), in IR channel again. Satisfactory representation of the synoptic features by the model outputs can be seen. A belt of higher temperatures stretching from south-western Germany to southern Poland is worth to notice. This belt separates the cloud whirl of the occlusion front from the other part of the frontal system (e.g. from the cloudiness of the warm and cold front). This corresponds to the occlusion of a cold conveyor type according to *Manual of Synoptic Satellite Meteorology*. Focussing now on the forecasts for next times from December 25th 00 UTC, we could find a good coincidence between forecasts and observations. The situation is demonstrated for example on Figs. 73 (model forecast for +48 h) and 74 (satellite observations). Generally, only small differences between observed and computed values of the brightness temperatures can be found here.

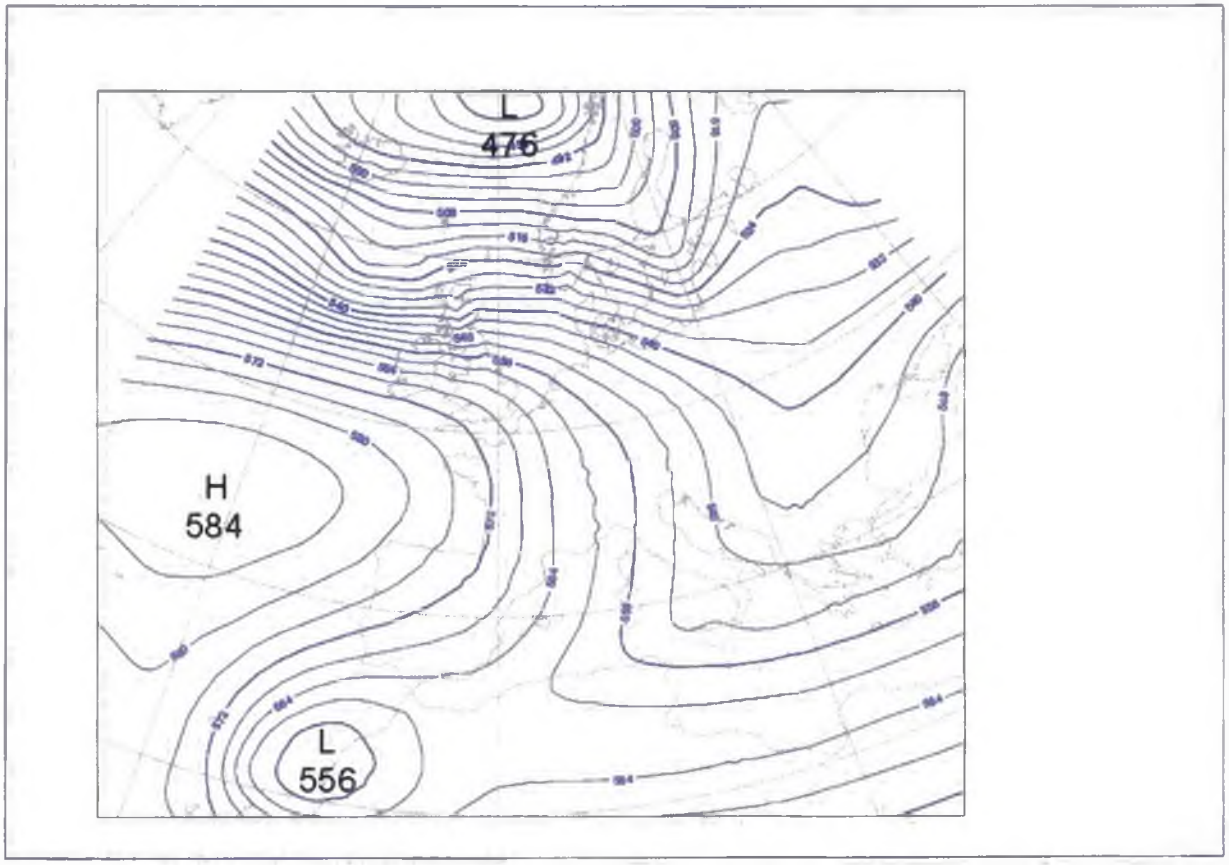

Fig. 57: Geopotential height of 500 hPa level (interval 4 decametres), analysis for December 23rd 2004 00 UTC

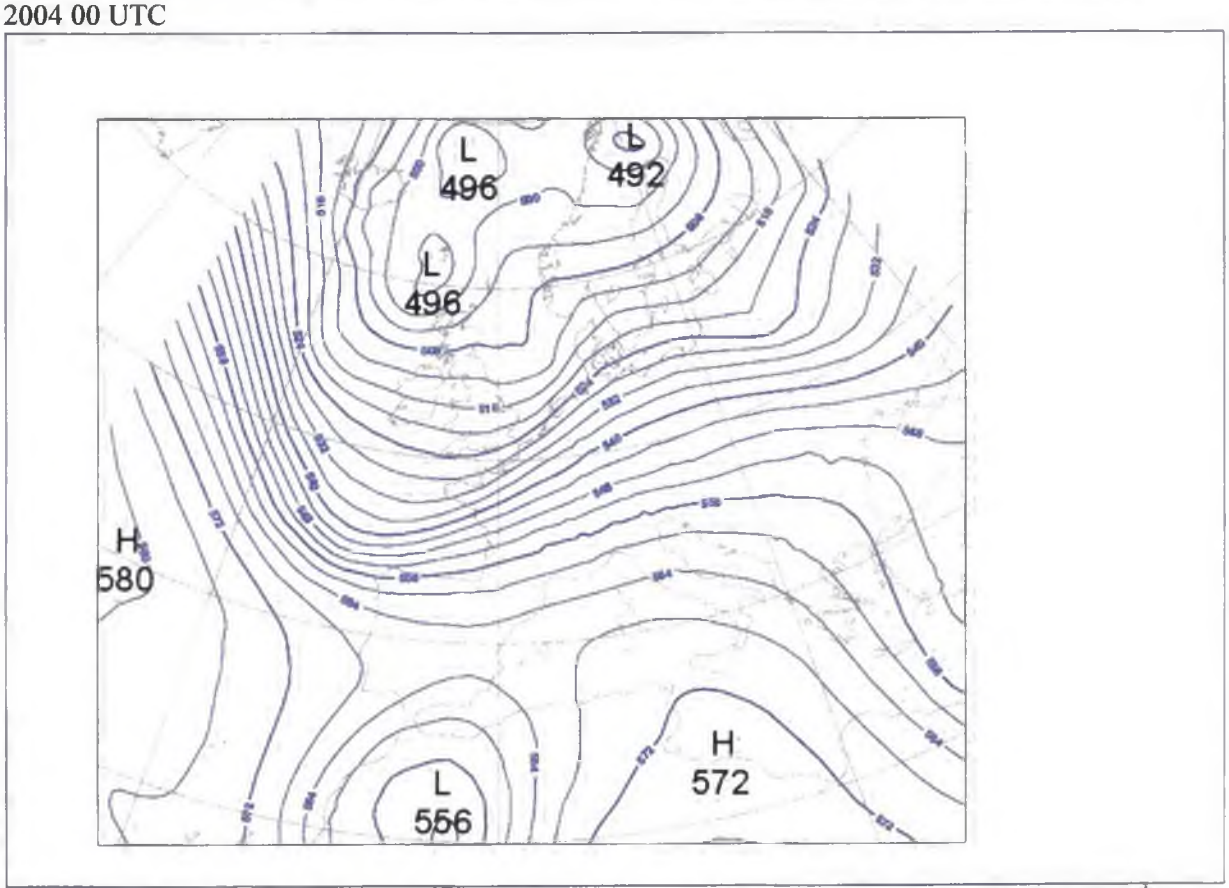

Fig. 58: Geopotential height of 500 hPa level (interval 4 decametres), analysis for December 25th 2004 00 UTC

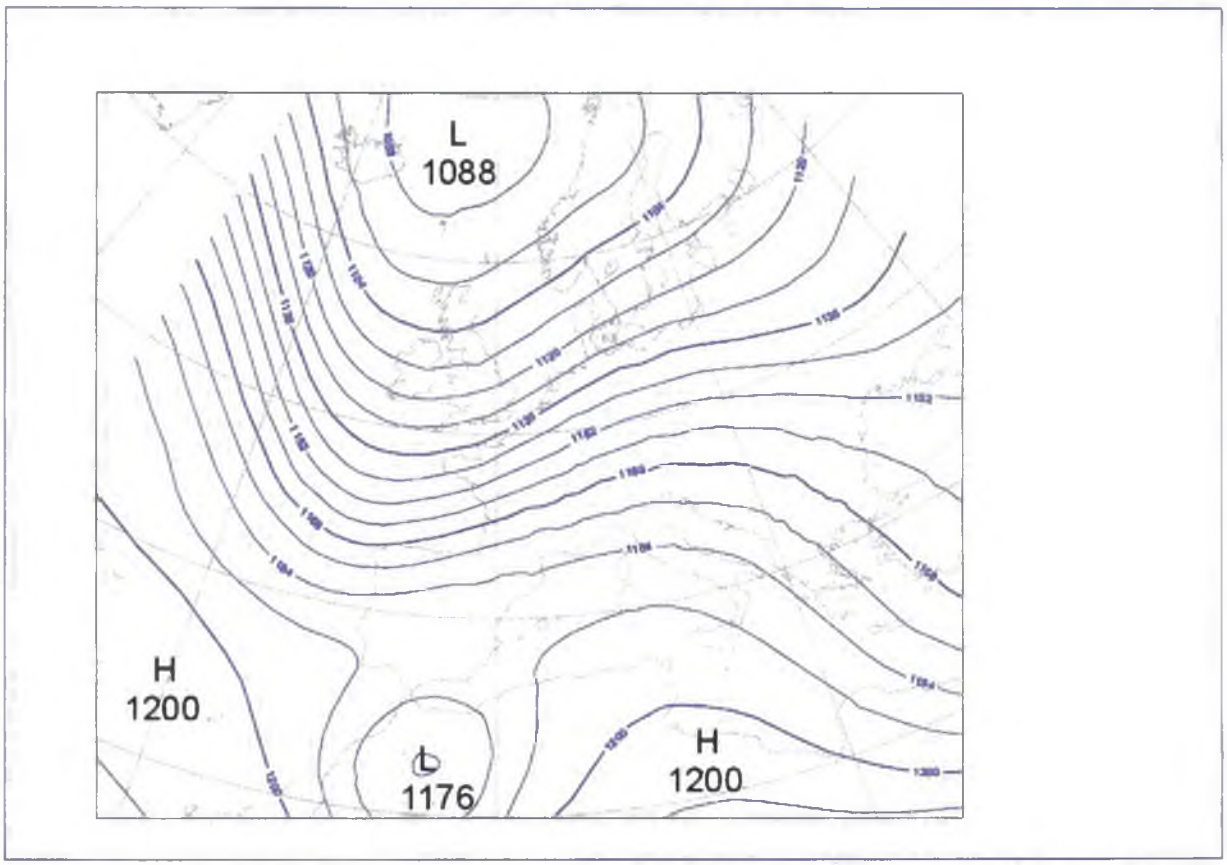

Fig. 59: Geopotential height of 200 hPa level (interval 8 decametres), analysis for December 25th 2004 00 UTC

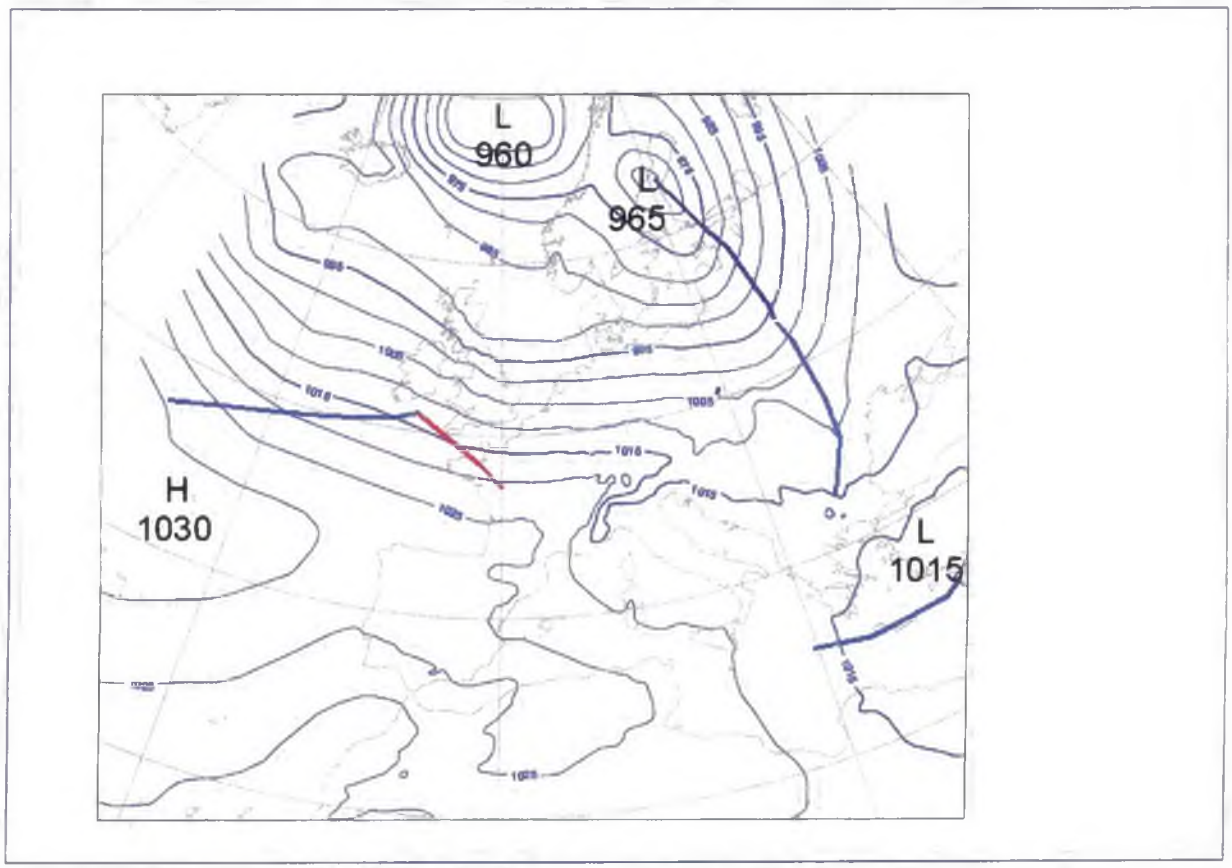

Fig. 60: Surface analysis for December 24th 2004 00 UTC (isobars interval 5 hPa)

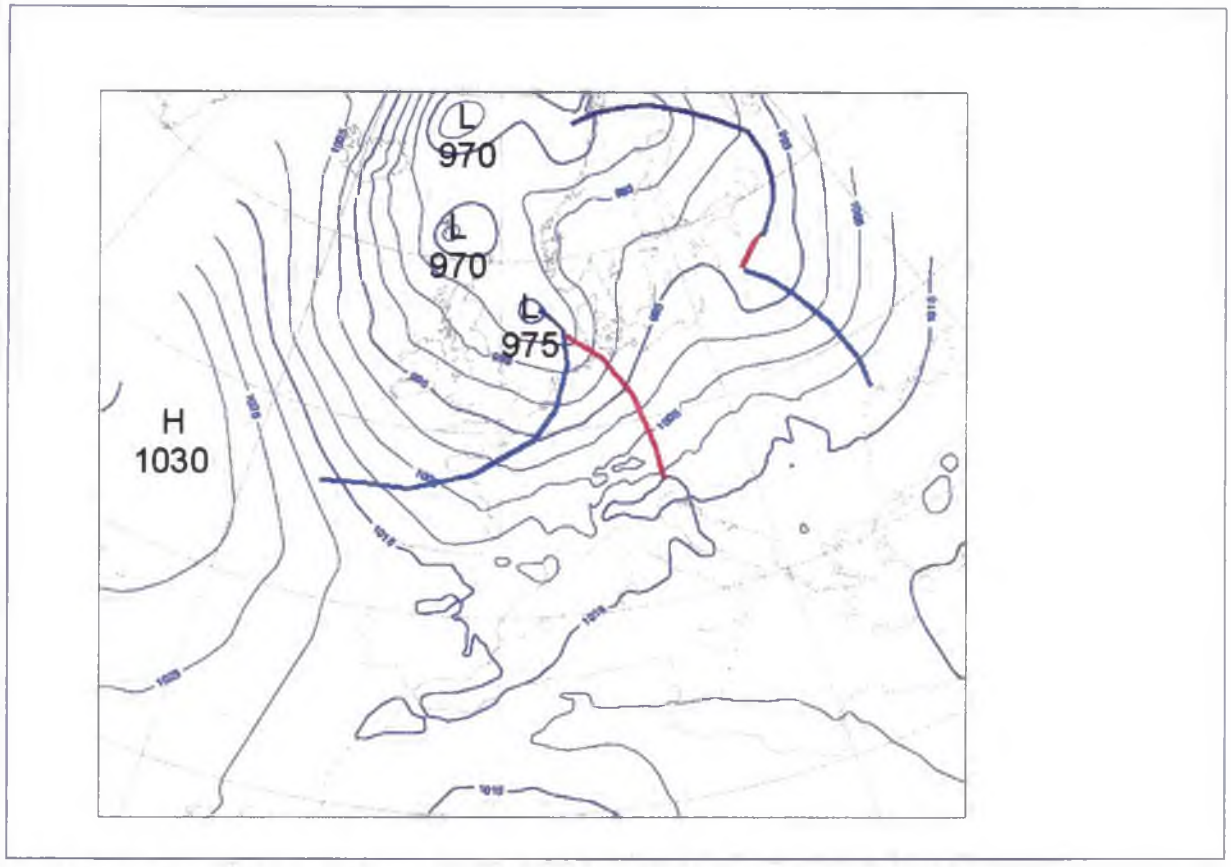

Fig. 61: Surface analysis for December 25th 2004 00 UTC (isobars interval 5 hPa)

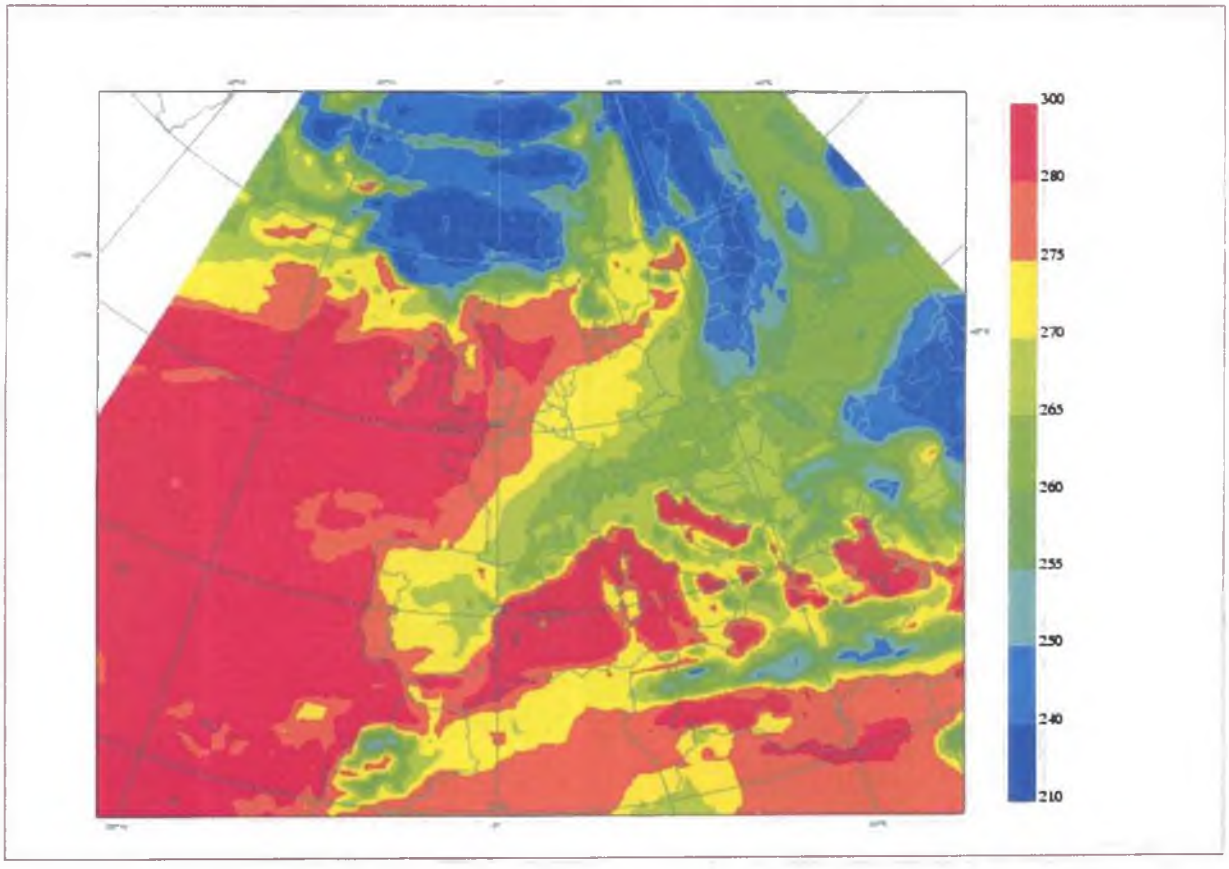

Fig. 62: Model analysis of the brightness temperatures (in K) of IR channel, December 23rd 2004 00 UTC

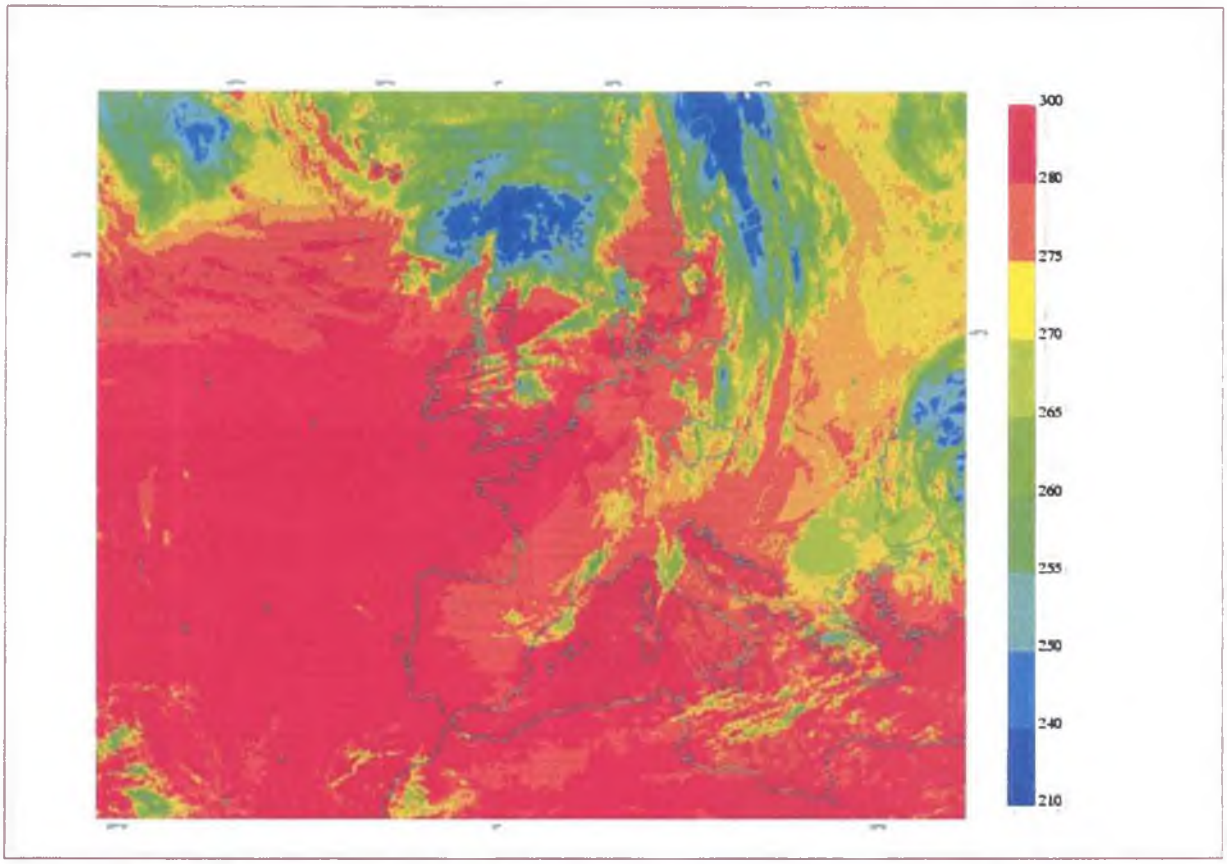

Fig. 63: IR channel image of METEOSAT-7 satellite, December 23rd 2004 00 UTC

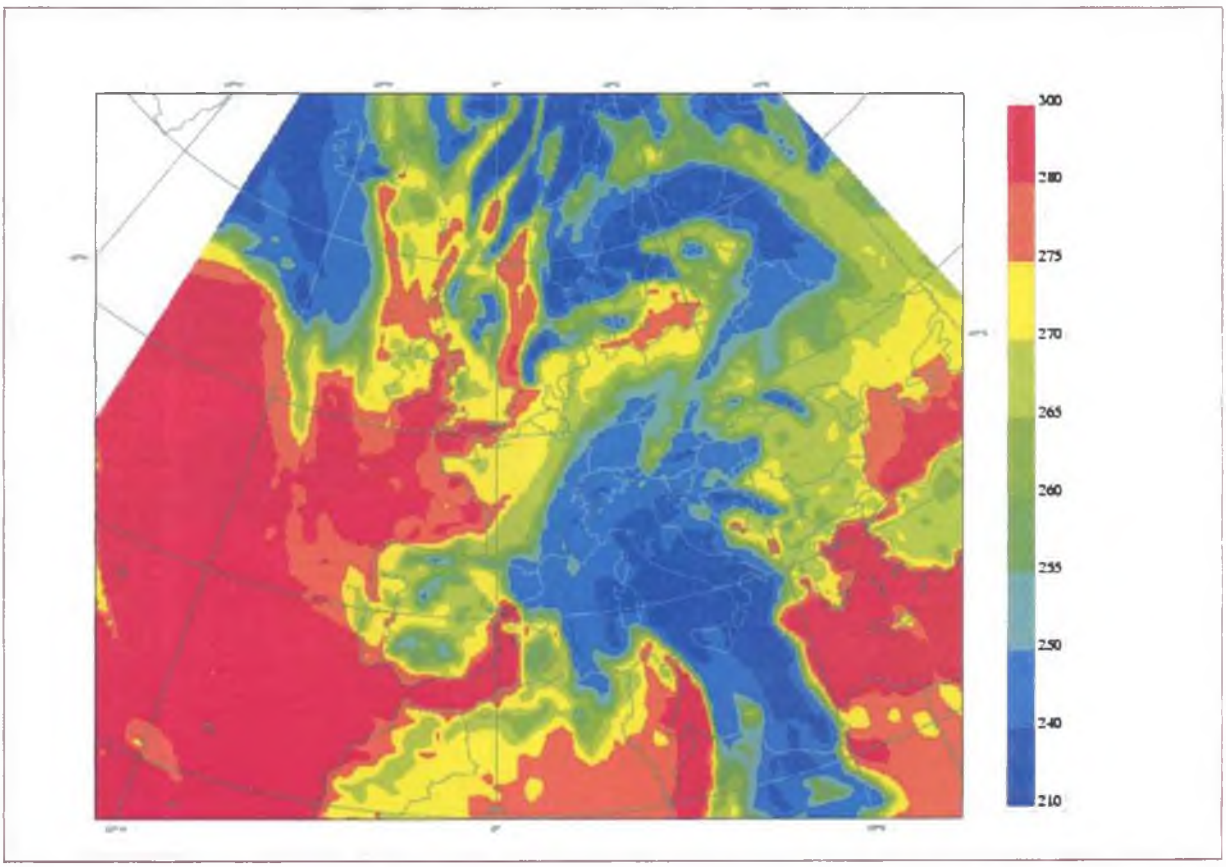

Fig. 64: Model forecast of the brightness temperatures (in K) for IR channel from December 23rd 2004 00 UTC for December 26th 2004 00 UTC

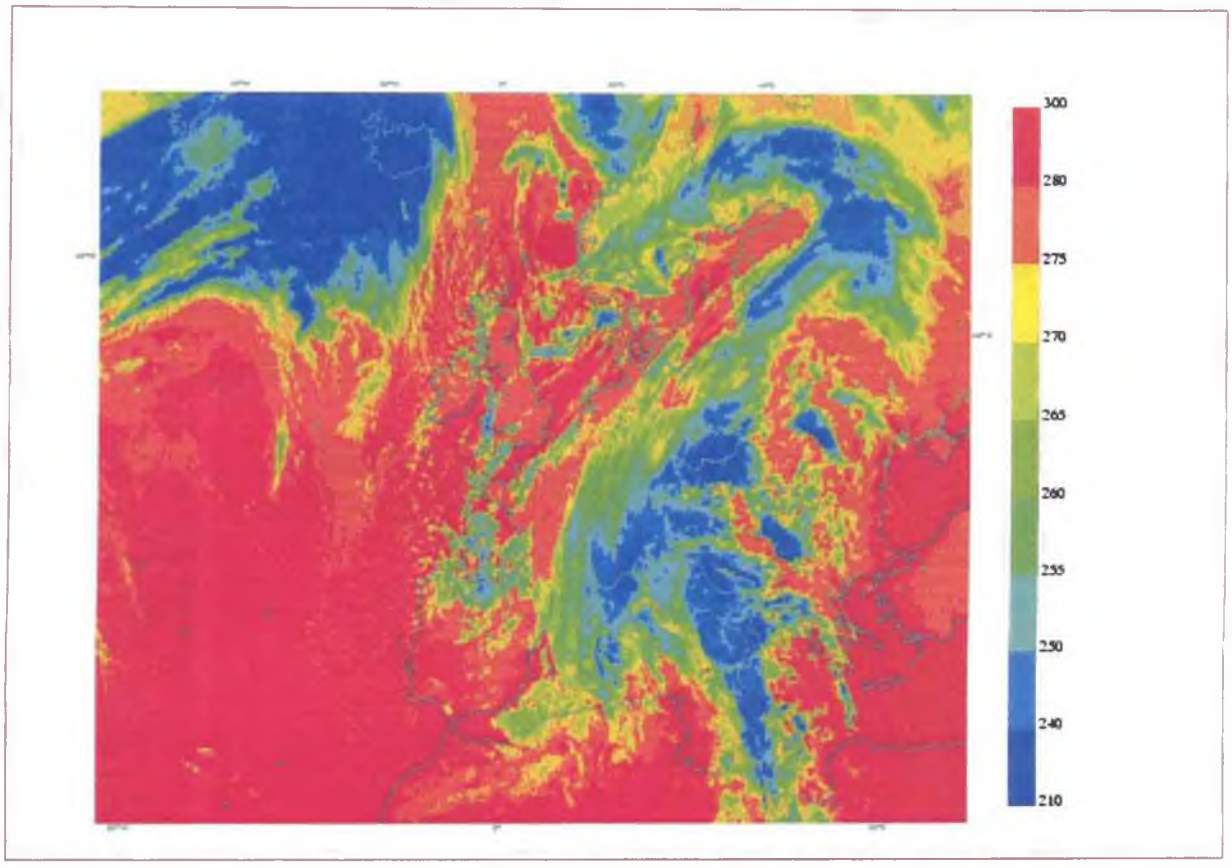

Fig. 65: IR channel image of METEOSAT-7 satellite, December 26th 2004 00 UTC

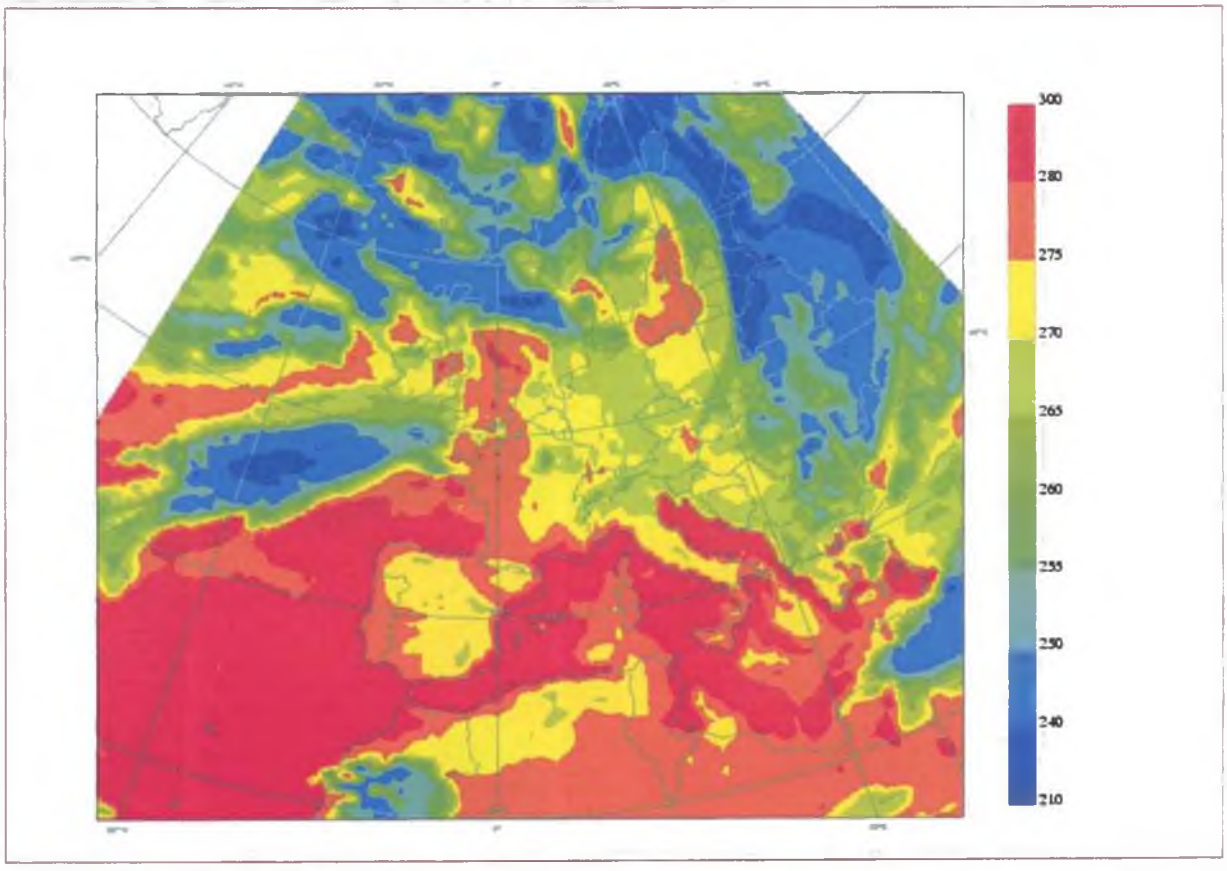

Fig. 66: Model analysis of the brightness temperatures (in K) of IR channel, December 24th 2004 00 UTC

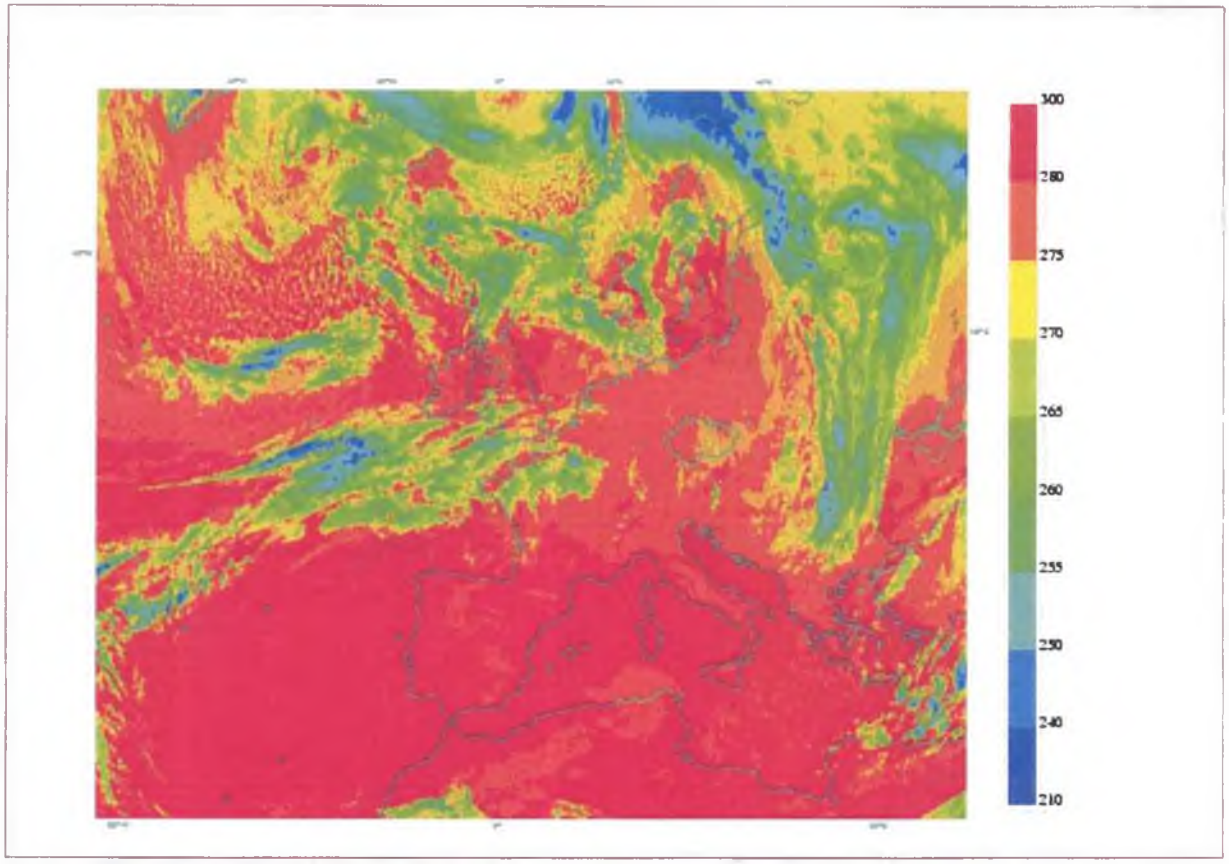

Fig. 67: IR channel image of METEOSAT-7 satellite, December 24th 2004 00 UTC

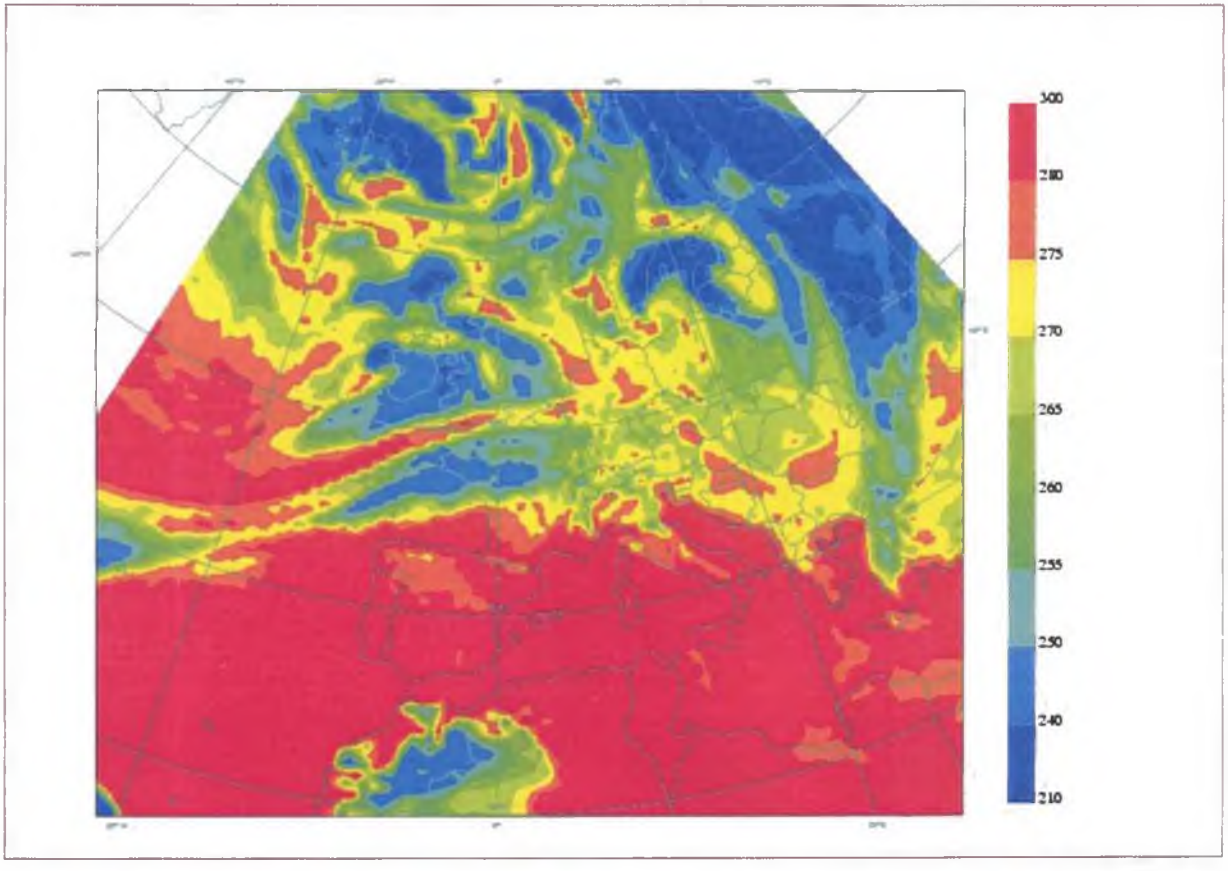

Fig. 68: Model forecast of the brightness temperatures (in K) for IR channel from December 24th 2004 00 UTC for December 24th 2004 12 UTC

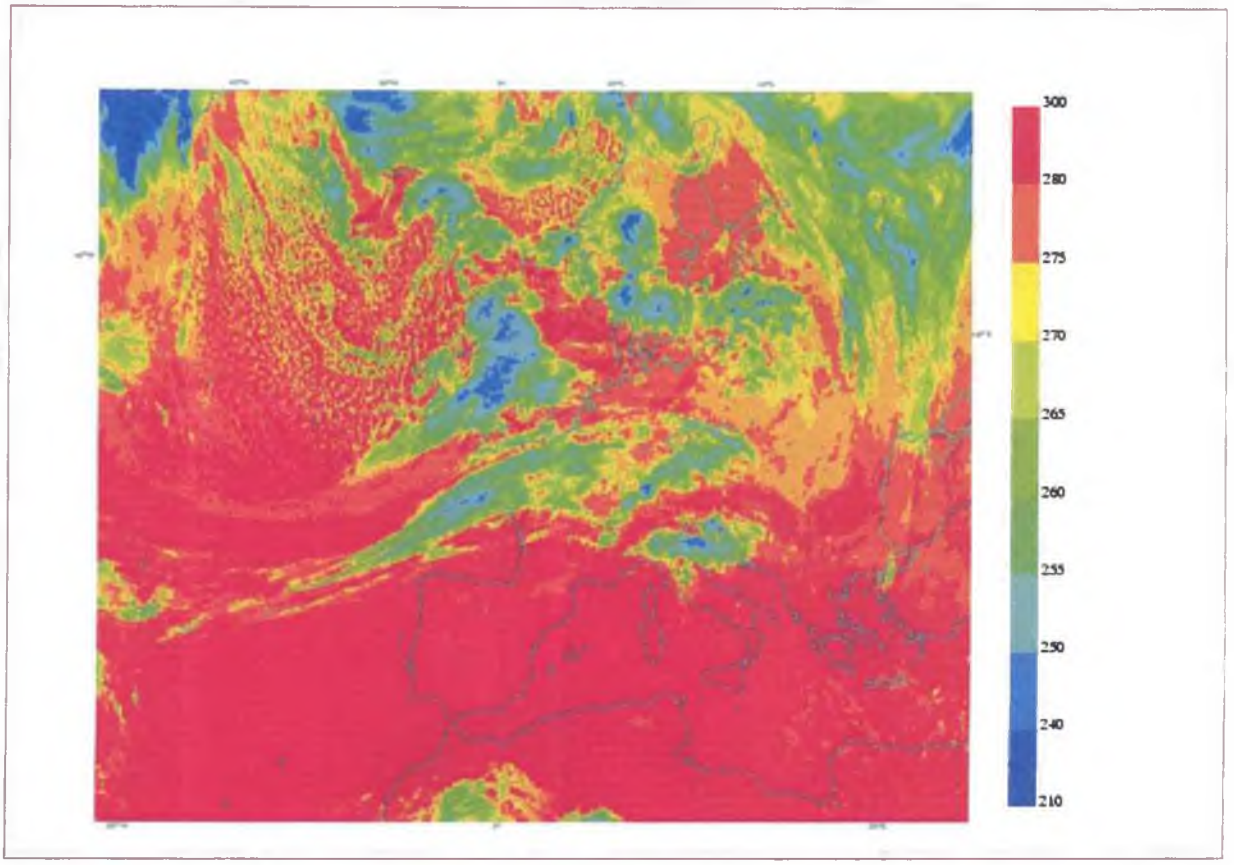

Fig. 69: IR channel image of METEOSAT-7 satellite, December 24th 2004 12 UTC

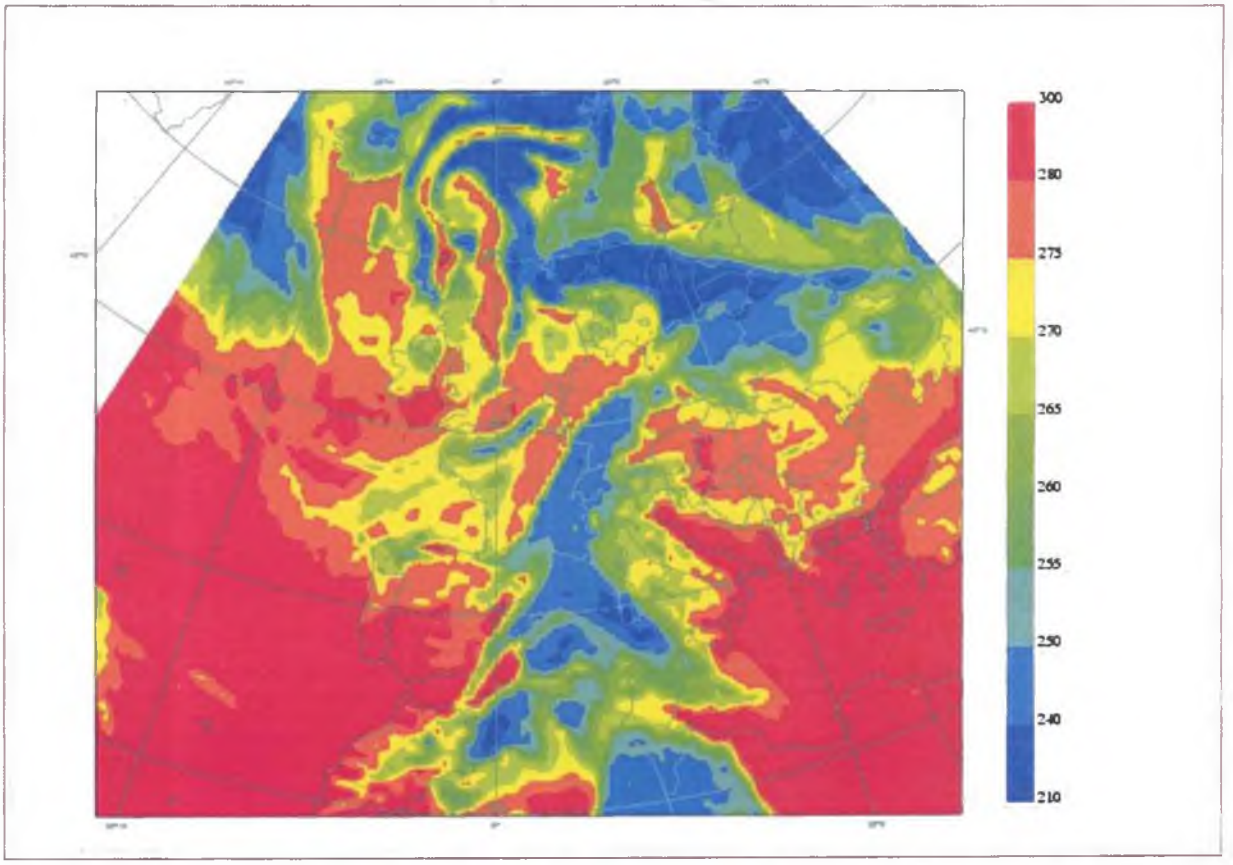

Fig. 70: Model forecast of the brightness temperatures (in K) for IR channel from December 24th 2004 00 UTC for December 26th 2004 00 UTC

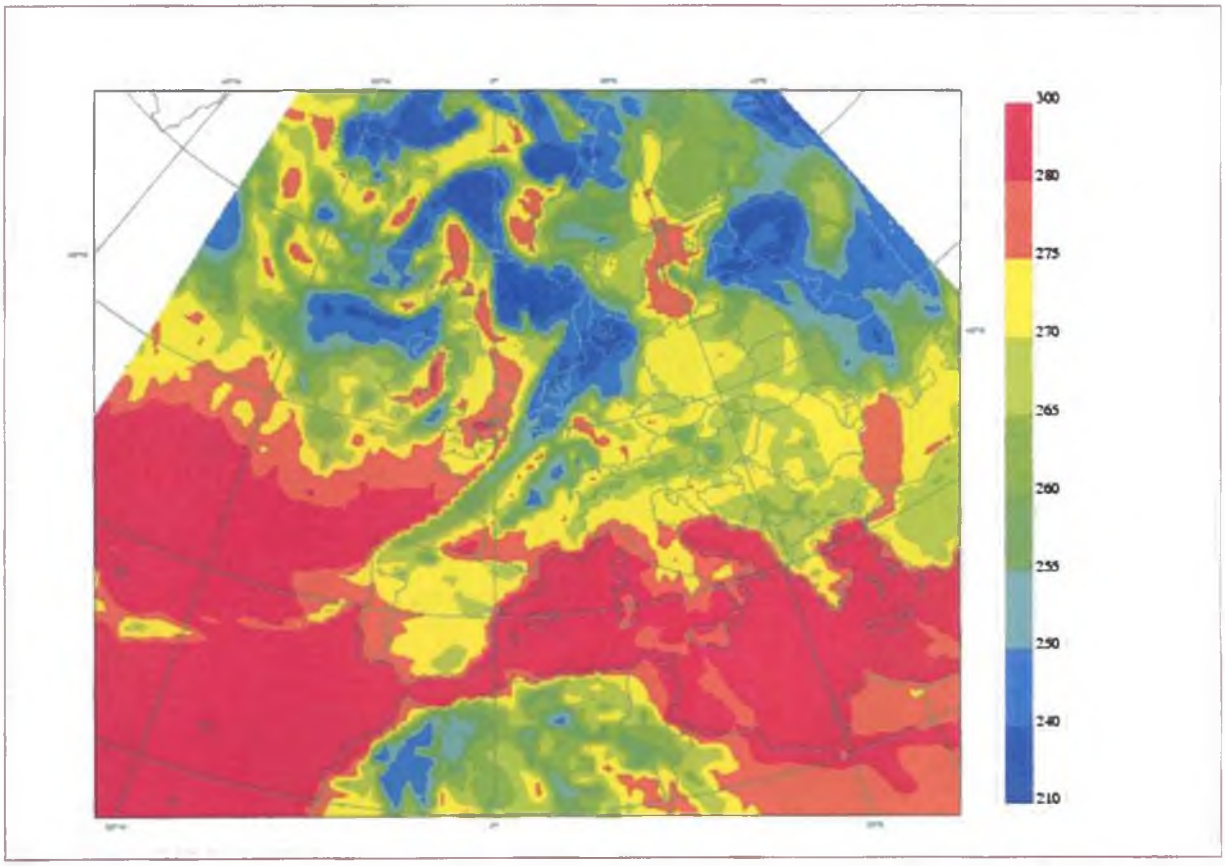

Fig. 71: Model analysis of the brightness temperatures (in K) of IR channel, December 25th 2004 00 UTC

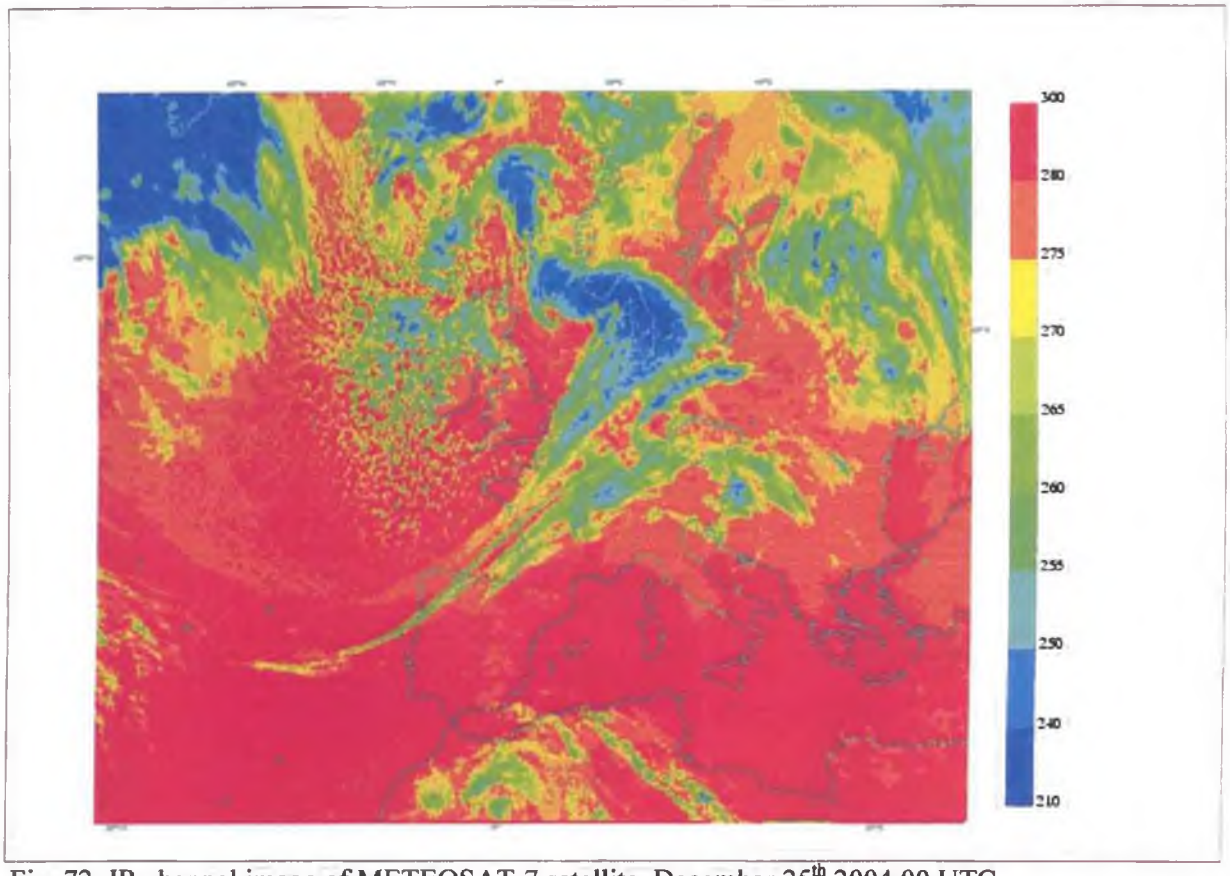

Fig. 72: IR channel image of METEOSAT-7 satellite, December 25th 2004 00 UTC

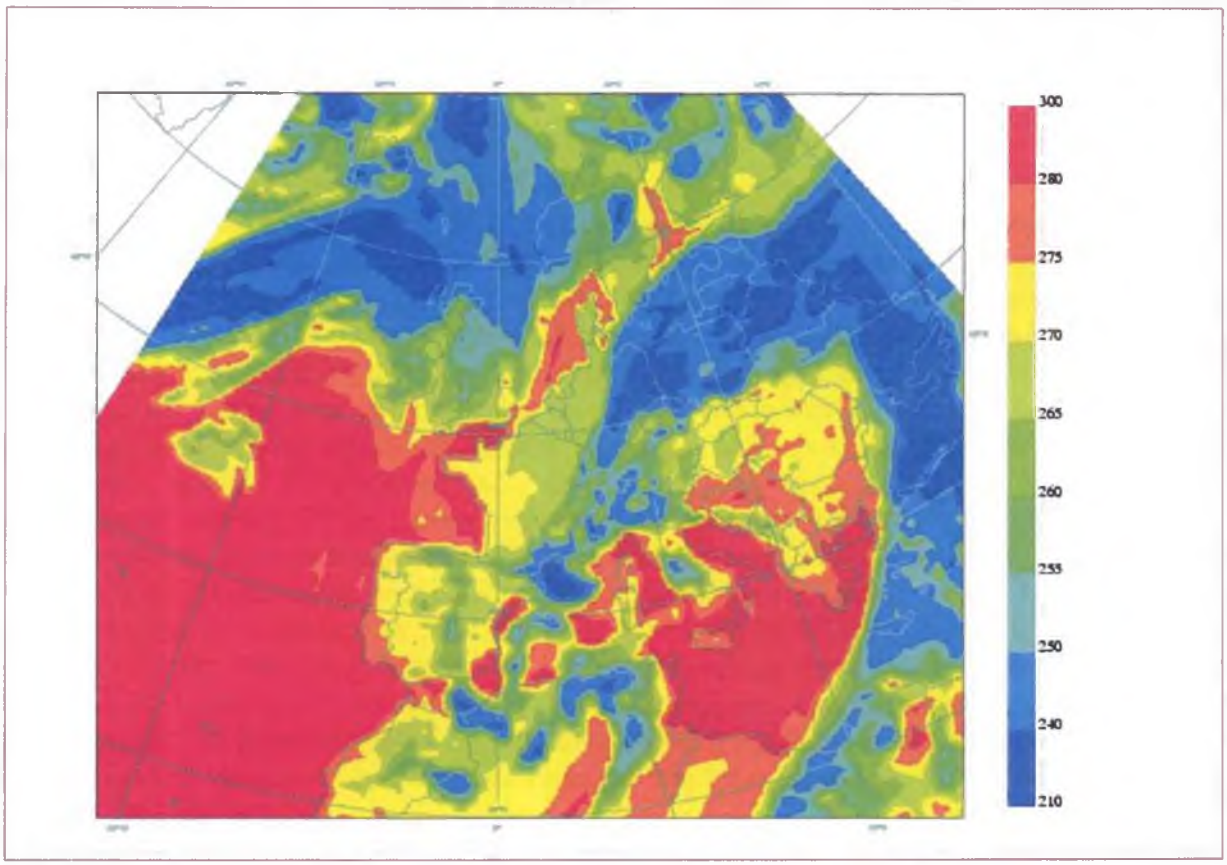

Fig. 73: Model forecast of the brightness temperatures (in K) for IR channel from December 25th 2004 00 UTC for December 27th 2004 00 UTC

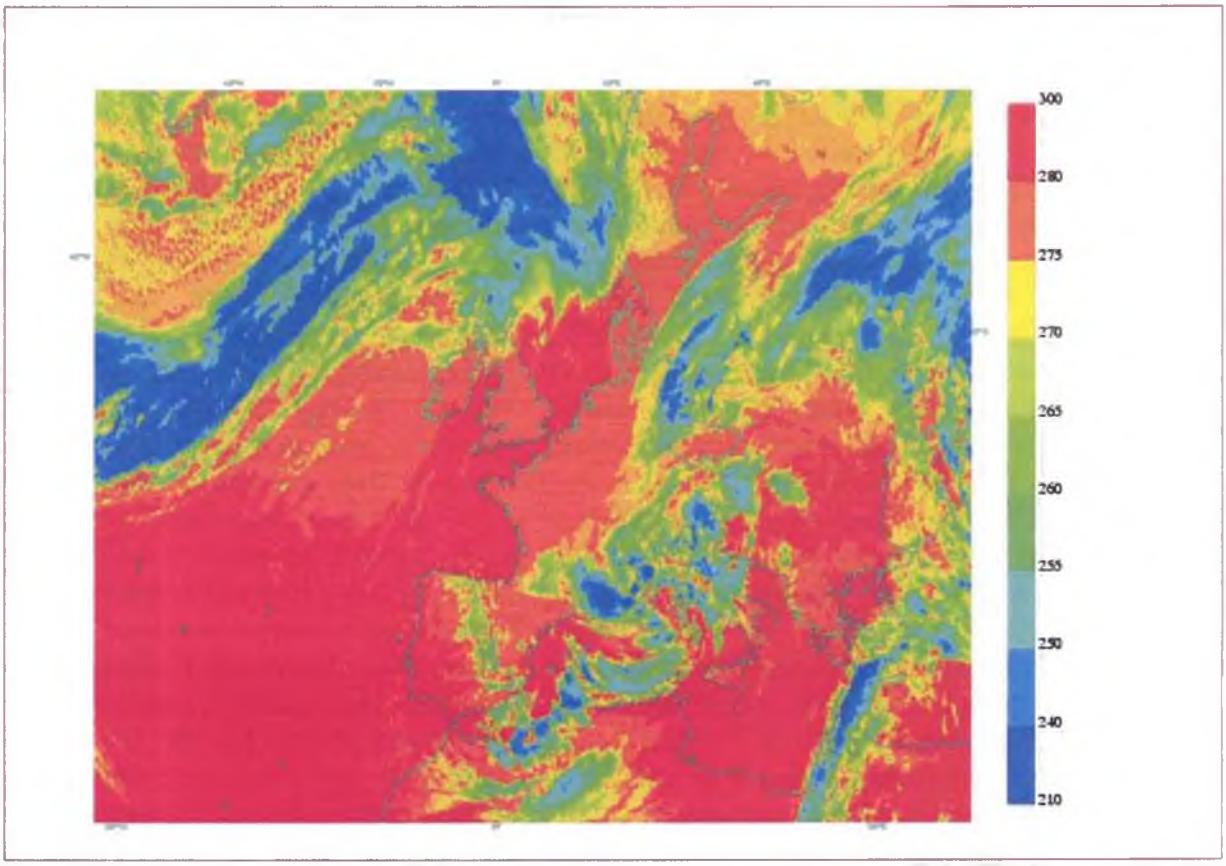

Fig. 74: IR channel image of METEOSAT-7 satellite, December 27th 2004 00 UTC

4.5 April 2005

Synoptic description

Surface pressure field for April 8th 2005 00 UTC can be seen on Fig. 75. The situation over Europe can be characterized by extent cyclone with centre over southern Scandinavia and with elongated trough reaching to Spain. The cold front of the frontal system belonging to this cyclone has several waves and is stretched from southern Finland over central Europe to Spain. In the rear part of this cyclone, cold advection is occurring over British Islands and northern Atlantic, as can be seen e.g. on temperature field at 850 hPa level for April 8th 00 UTC (Fig. 76). During next two days, this cold front with it waves became almost stationary in the region of central and north-eastern Europe. Cold advection in upper parts of the troposphere caused development of new secondary cyclonic centre over central Mediterranean (see Fig. 77 for surface pressure field on April 10th 00 UTC). The temperature on the mentioned front increased up to 15 °C at 850 hPa level on April 10th 00 UTC (Fig. 78). The interesting development can be observed in upper levels, mainly at 500 hPa level. On Figs. 79-81 the development at 500 hPa from April 8th 00 UTC to April 10th 00 UTC is presented. At the beginning, there was a trough reaching from the cyclone centre over northern Norwegian Sea to the northern France. During next two days, this trough deepened and elongated. The separate cut-off cyclone over western Mediterranean formed on April 10th. Only trough can be observed at 200 hPa level, as can be seen on Fig. 82 where situation on April 10th 00 UTC is given.

Comparison model-to-observation

The situation for April 8th 2005 00 UTC in IR channel analyzed by the model is presented on Fig. 83 and the same situation observed by satellite can be seen on Fig. 84. Quite good representation of the cold front cloudiness can be seen, but with one exception. There is observed relatively large, well developed cloud cluster over Slovenia, west Hungary, east Austria and partly also over east of the Czech Republic in the satellite image that can not be recognized in the analyzed image for model outputs. According to its low brightness temperature (in some parts under 230 K), some parts of this cluster could be of convective origin at least. The size of this cluster is about 1000 x 500 km; it means it is somewhat between mesosynoptic and synoptic feature. Following the development in next few hours, it can be seen that this cloud cluster was firstly further developed (for next 12 hours – see Fig. 85 for observation at April 8th 12 UTC) while moving to east-northeast and then it was disappeared over eastern parts of central Europe (see Fig. 86 for observation at April 9th 00 UTC). When comparing 24h forecast from April 8th 00 UTC (Fig. 87) and satellite observation for the same time (Fig. 86), some differences can be found. These differences can be identified over central Europe (region of higher forecasted temperatures reaching from south Polland to Hungary), but larger discrepancies are detected over Italy, Adriatic Sea and over the region of former Yugoslavia. The cloud fields are almost totally missing here by model ouputs while large cloud formations were observed here by satellite measurement. And for longer time of forecast, the discrepancies became larger (compare the model forecast for +72 h on Fig. 88 and observation on Fig. 89 on April 11th 00 UTC). The cloud system of the cyclone with centre over Italy is simulated somewhat westward, especiallyin connection with the cold front of this system (it is forecasted in the region from northern Italy to Tunis while it may be observed over Greek).

Focusing now on the forecast from April 9th 00 UTC and from April 10th 00 UTC, satisfactory correlation can be found not only between model analysis and observation but also between forecasts and observations at the corresponding times. Worse situation can be again found for April 10th 00 UTC. Quite large underestimation of the cloudiness (in vertical as well as horizontal extent) can be detected over central Europe and some underestimation is also detectable over north-eastern Balkan (compare model analysis for April 10th 00 UTC on Fig. 90 with satellite measurement presented on Fig. 91). The consequence is quite worse forecast for +6 hours (see Figs. 92 with observation and 93 with forecast), where only small vertical extent clouds over Czech Republic are forecasted and larger discrepancies can be also found over southern Italy. Similar discrepancies can be found also in the 24h forecast (see Fig. 94 with model forecast and Fig. 89 with satellite observation).

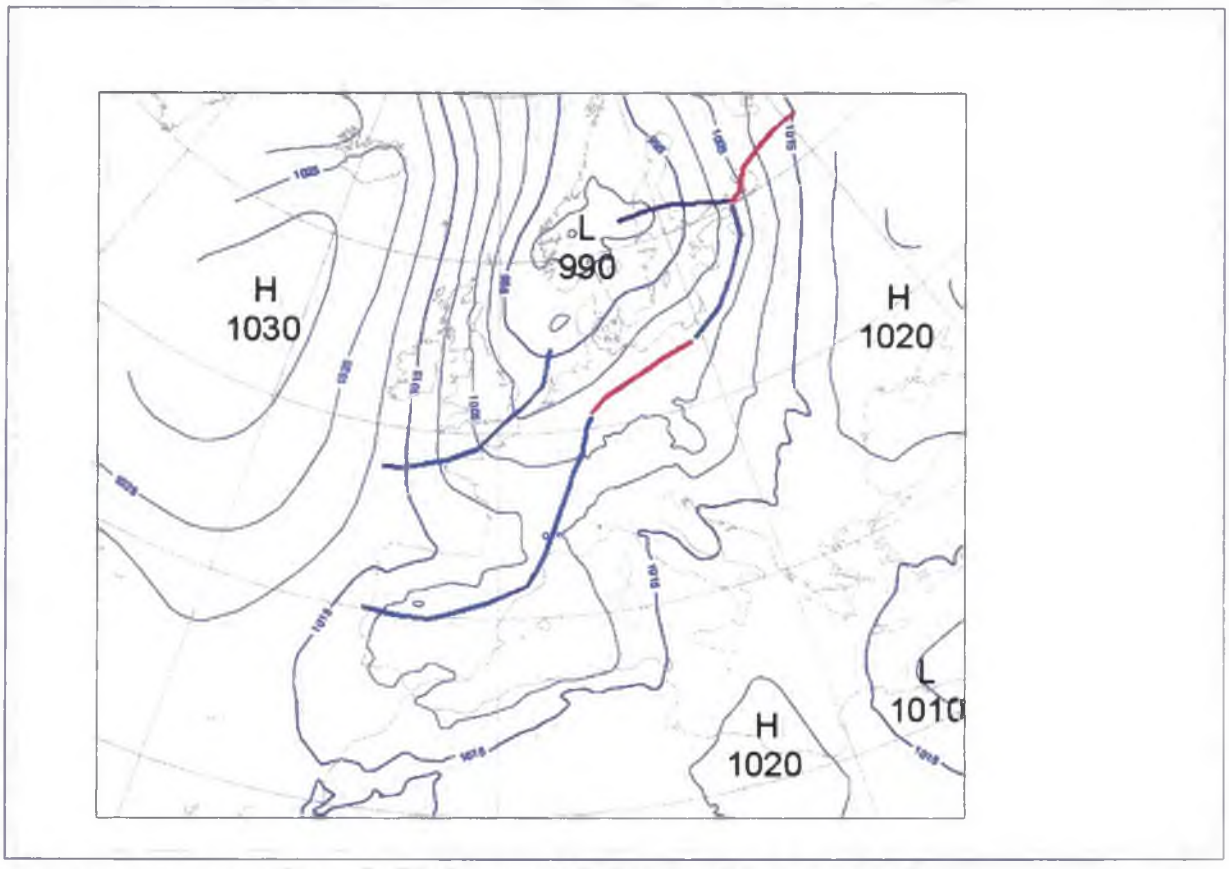

Fig. 75: Surface analysis for April 8th 2005 00 UTC (isobars interval 5 hPa)

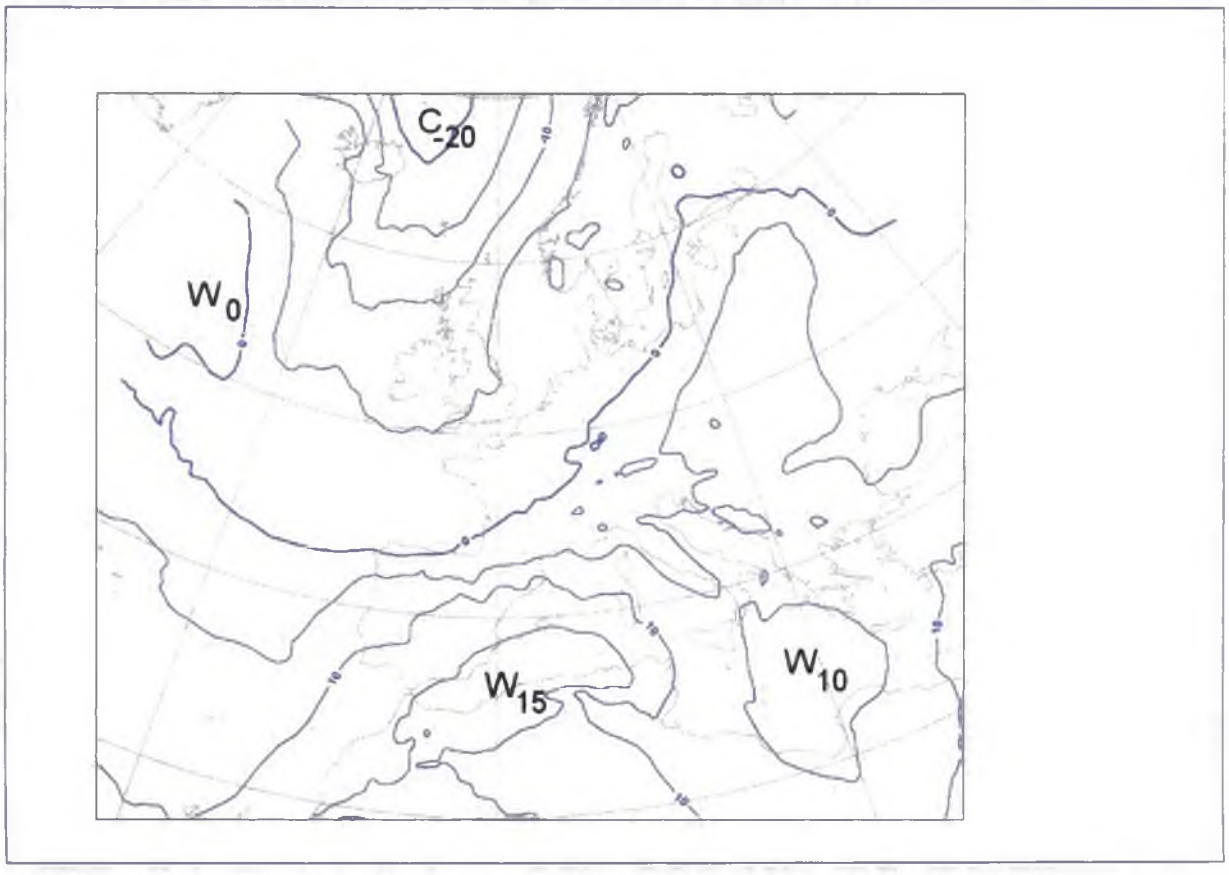

Fig. 76: Temperature at 850 hPa level (interval 5 °C), analysis for April 8th 2005 00 UTC

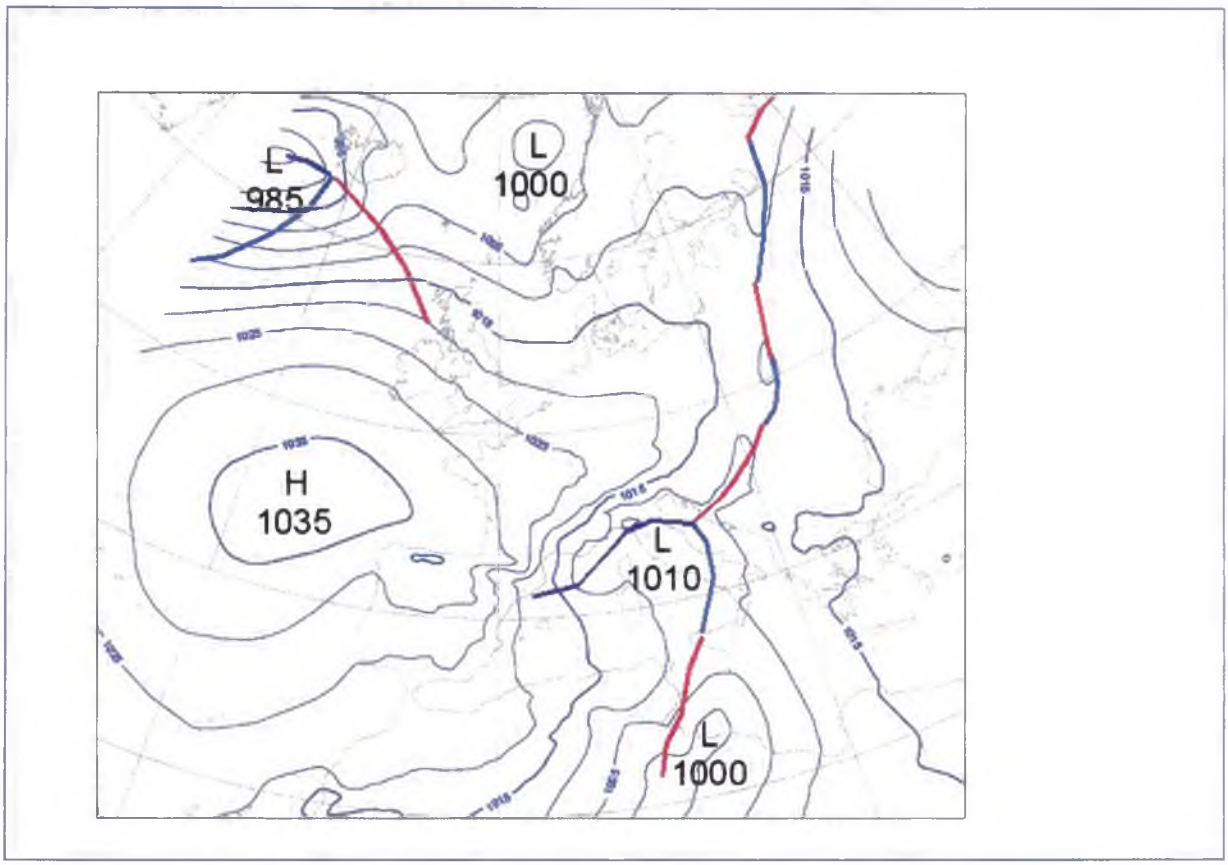

Fig. 77: Surface analysis for April 10th 2005 00 UTC (isobars interval 5 hPa)

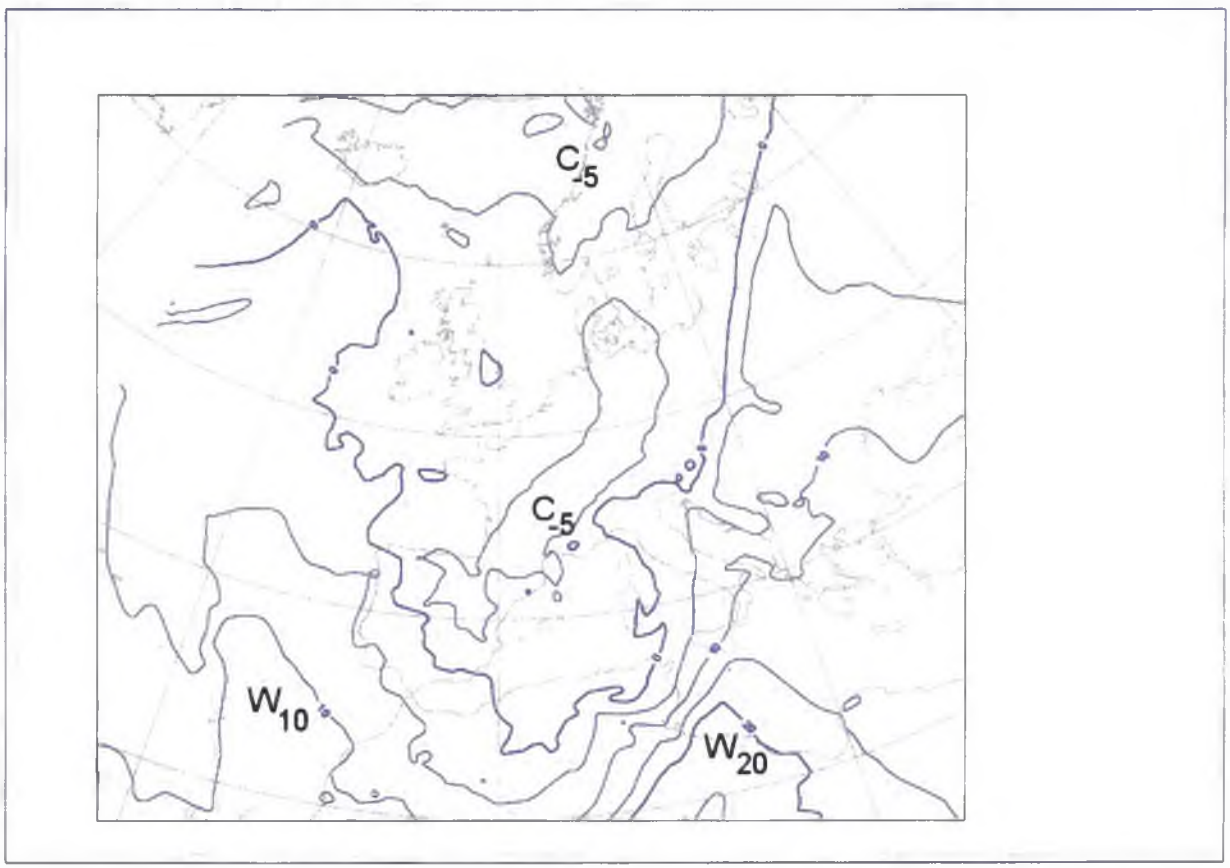

Fig. 78: Temperature at 850 hPa level (interval 5 °C), analysis for April 10th 2005 00 UTC

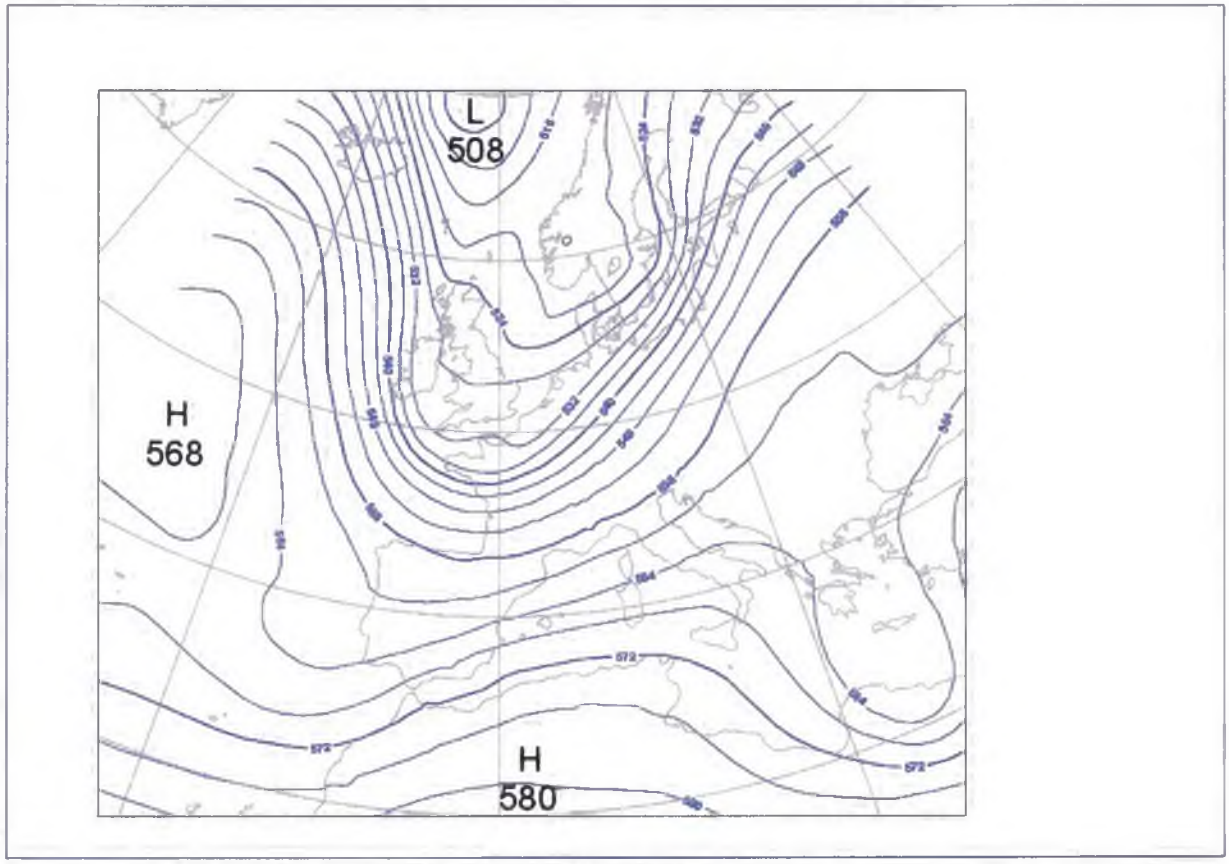

Fig. 79: Geopotential height of 500 hPa level (interval 4 decametres), analysis for April 8th 2005 00 UTC

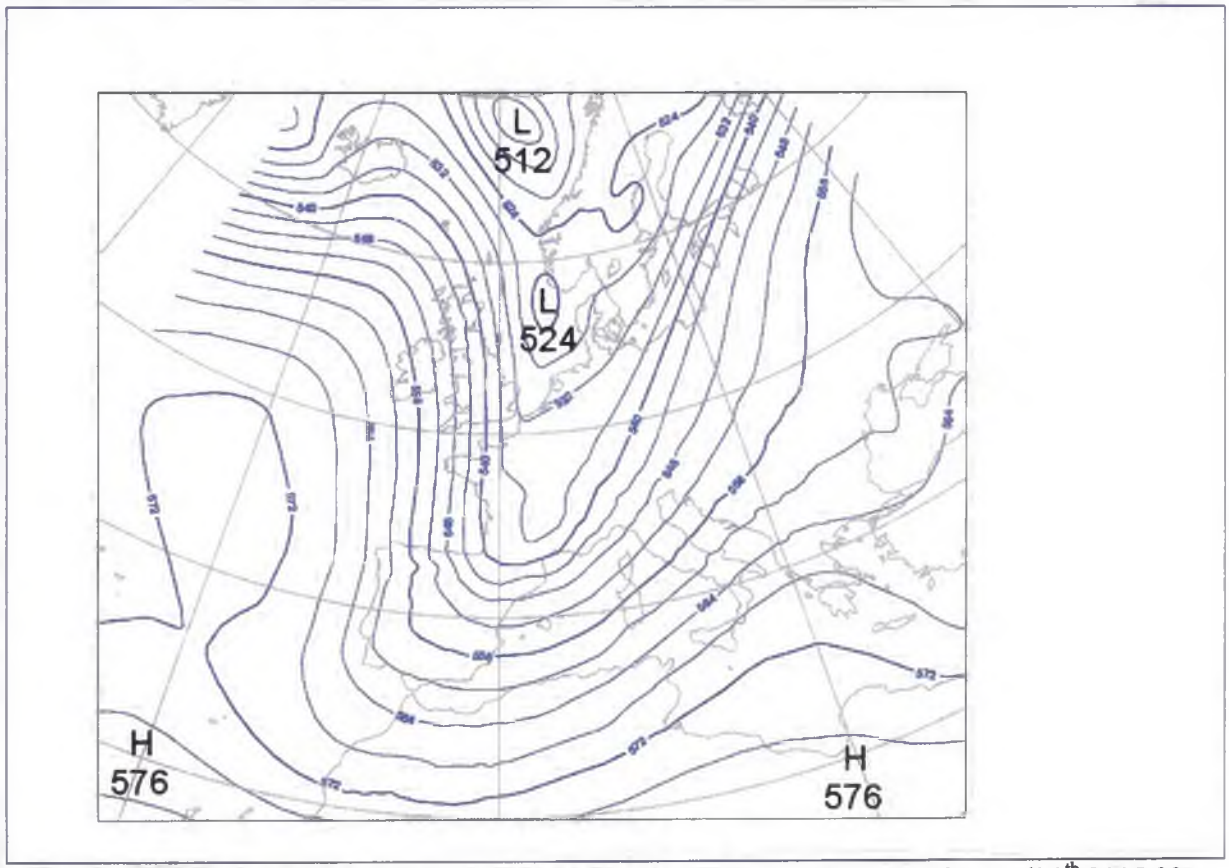

Fig. 80: Geopotential height of 500 hPa level (interval 4 decametres), analysis for April 9th 2005 00 UTC

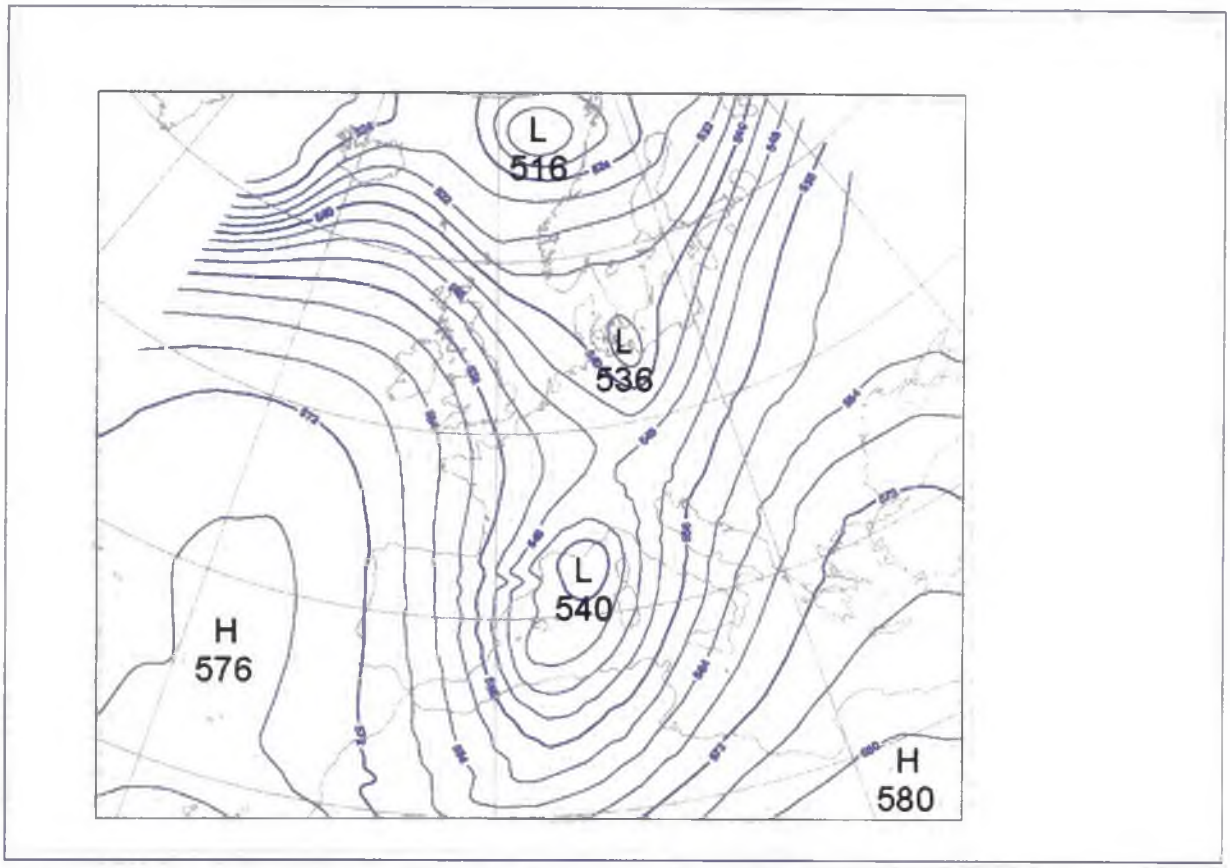

Fig. 81: Geopotential height of 500 hPa level (interval 4 decametres), analysis for April 10th 2005 00 UTC

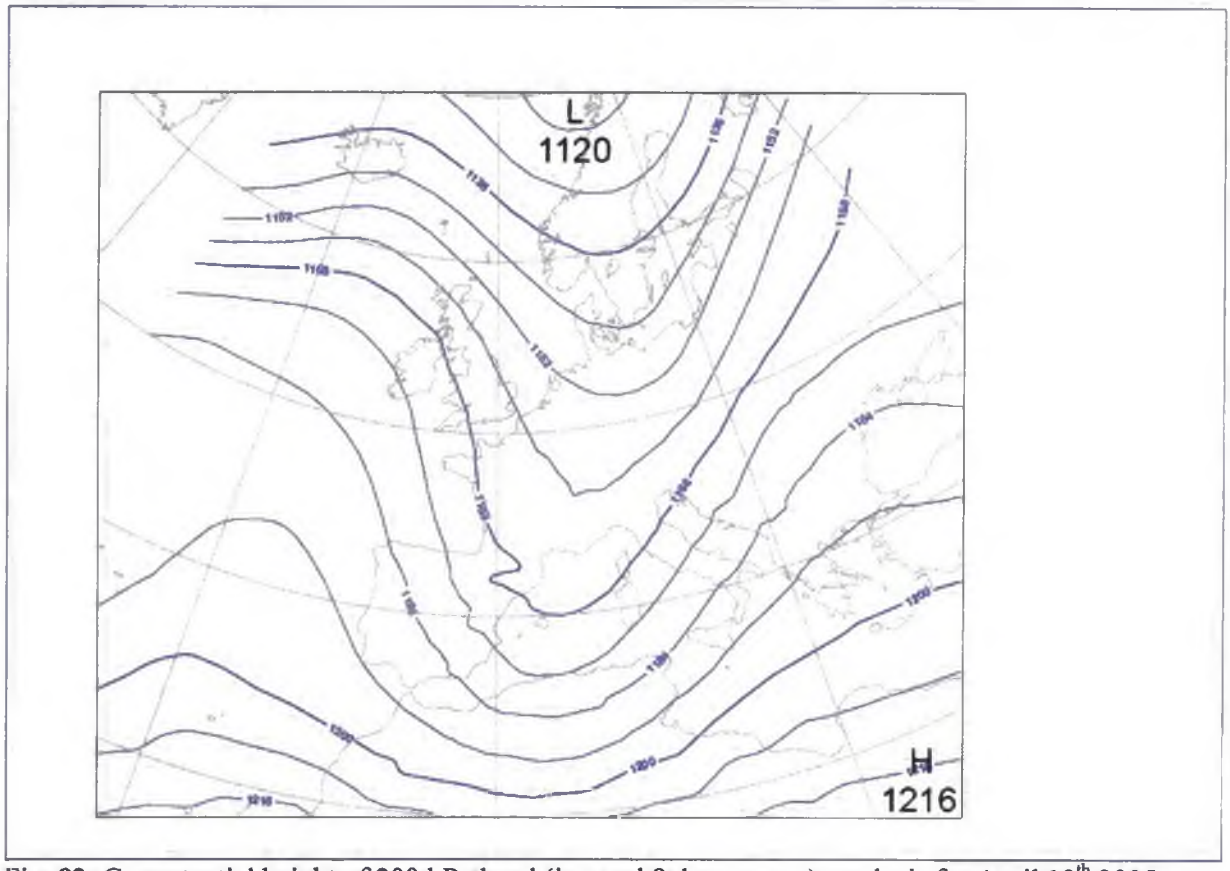

Fig. 82: Geopotential height of 200 hPa level (interval 8 decametres), analysis for April 10th 2005 00 UTC

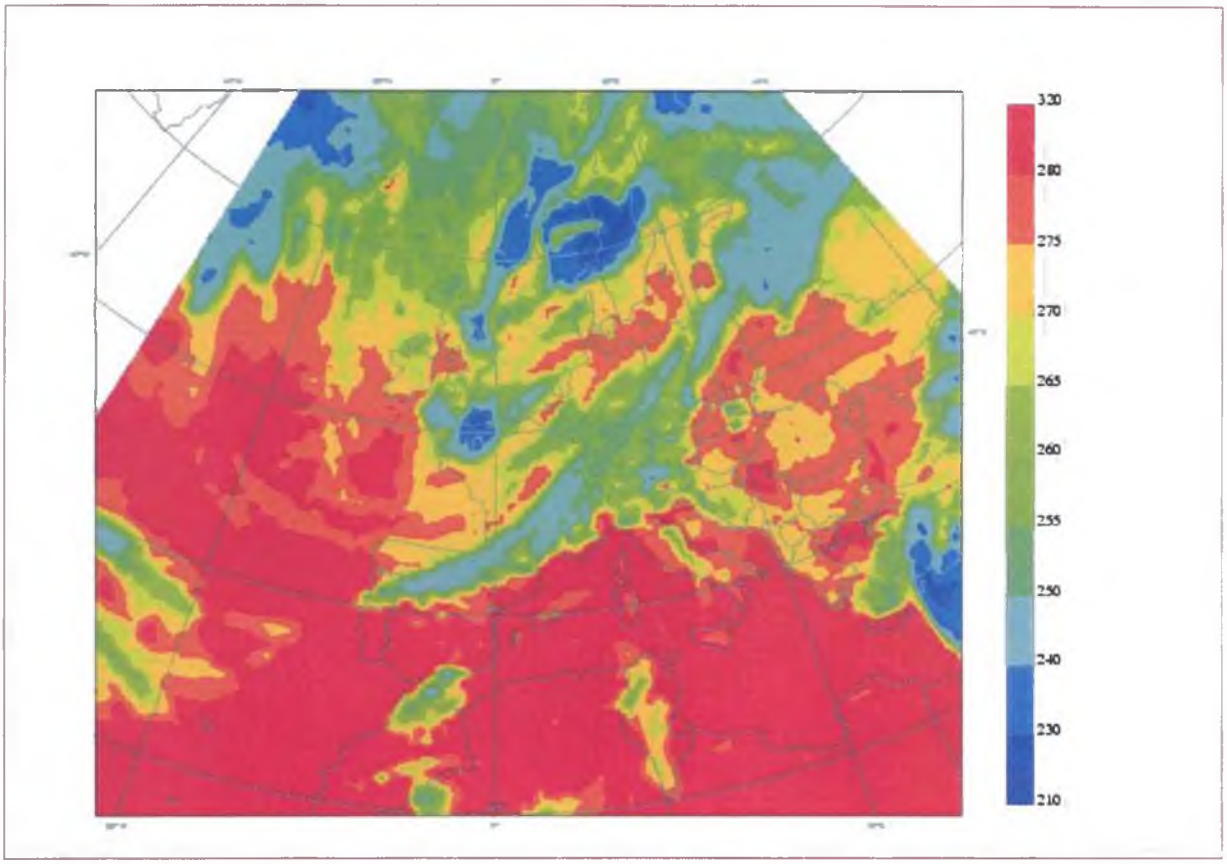

Fig. 83: Model analysis of the brightness temperatures (in K) of IR channel, April 8th 2005 00 UTC

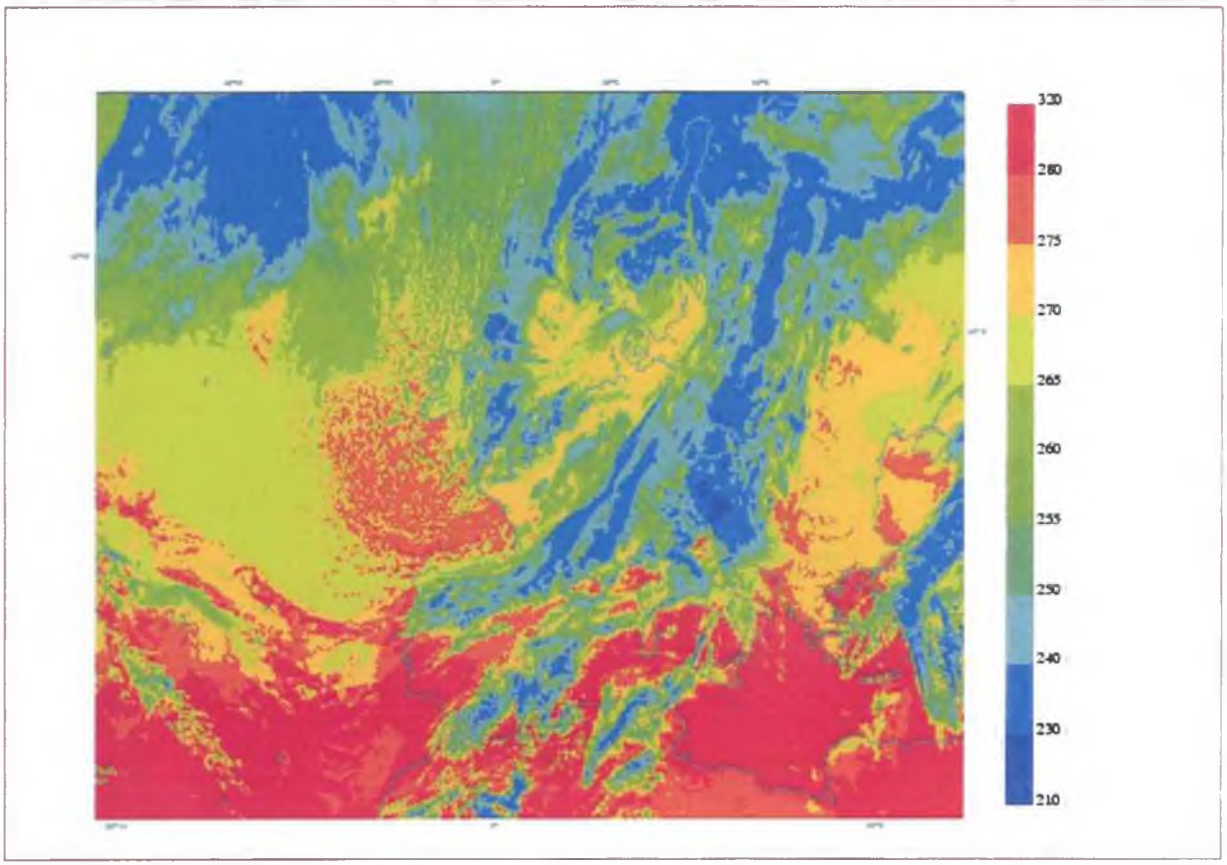

Fig. 84: IR channel image of METEOSAT-7 satellite, April 8th 2005 00 UTC

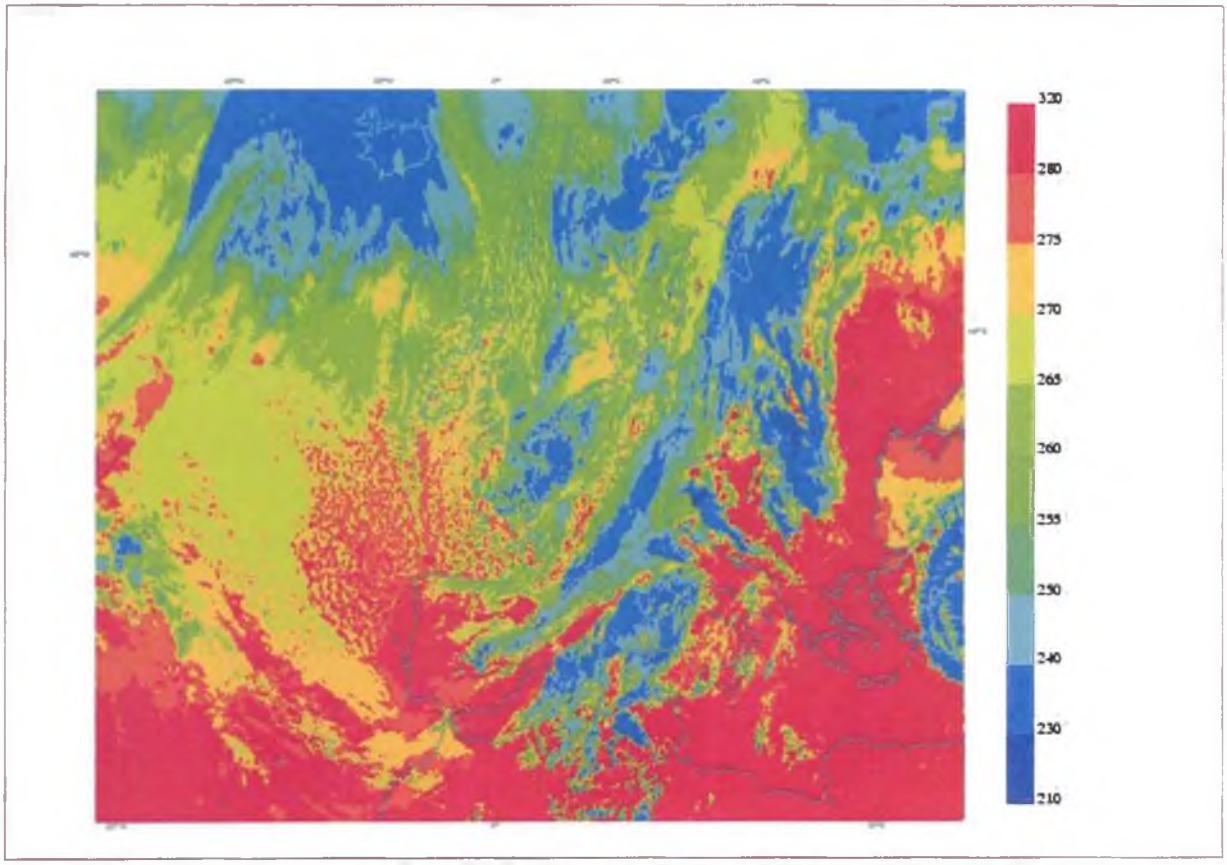

Fig. 85: IR channel image of METEOSAT-7 satellite, April 8th 2005 12 UTC

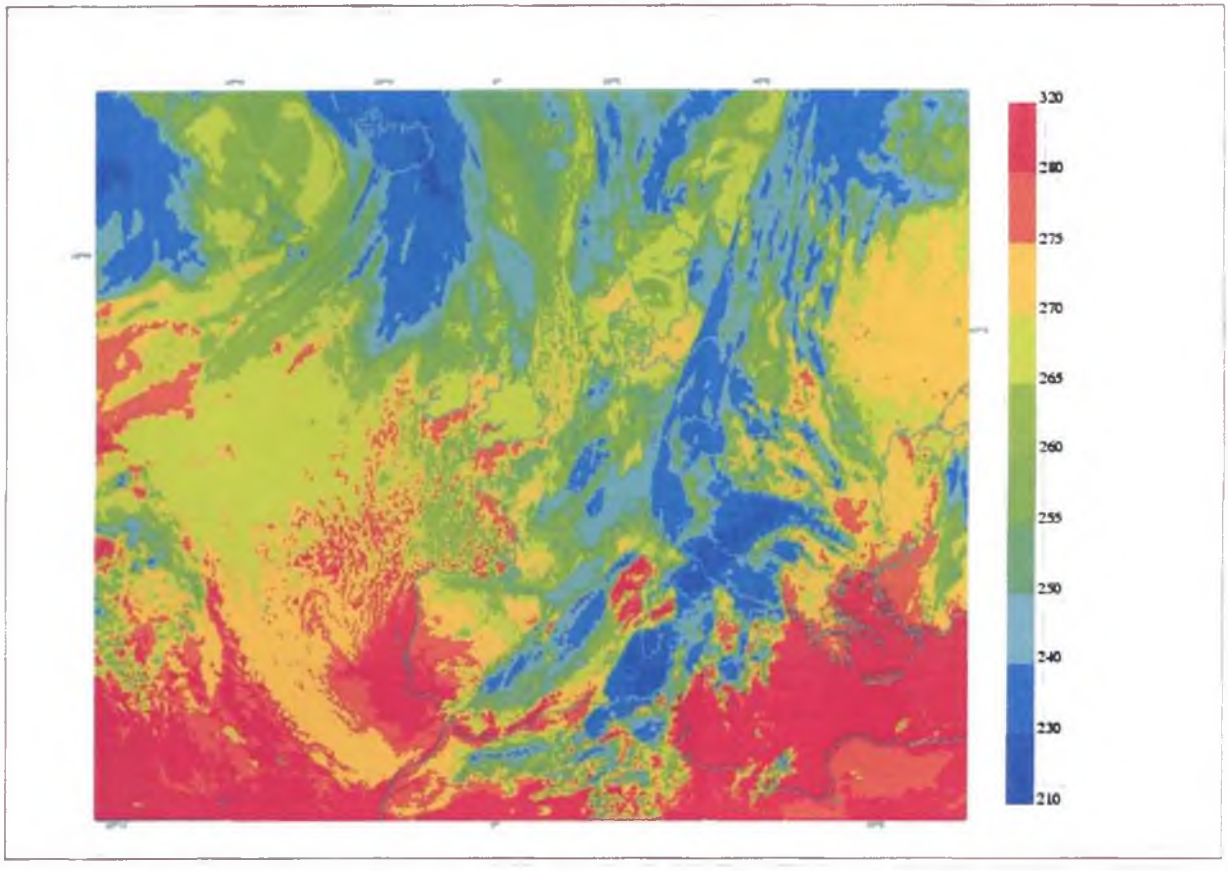

Fig. 86: IR channel image of METEOSAT-7 satellite, April 9th 2005 00 UTC

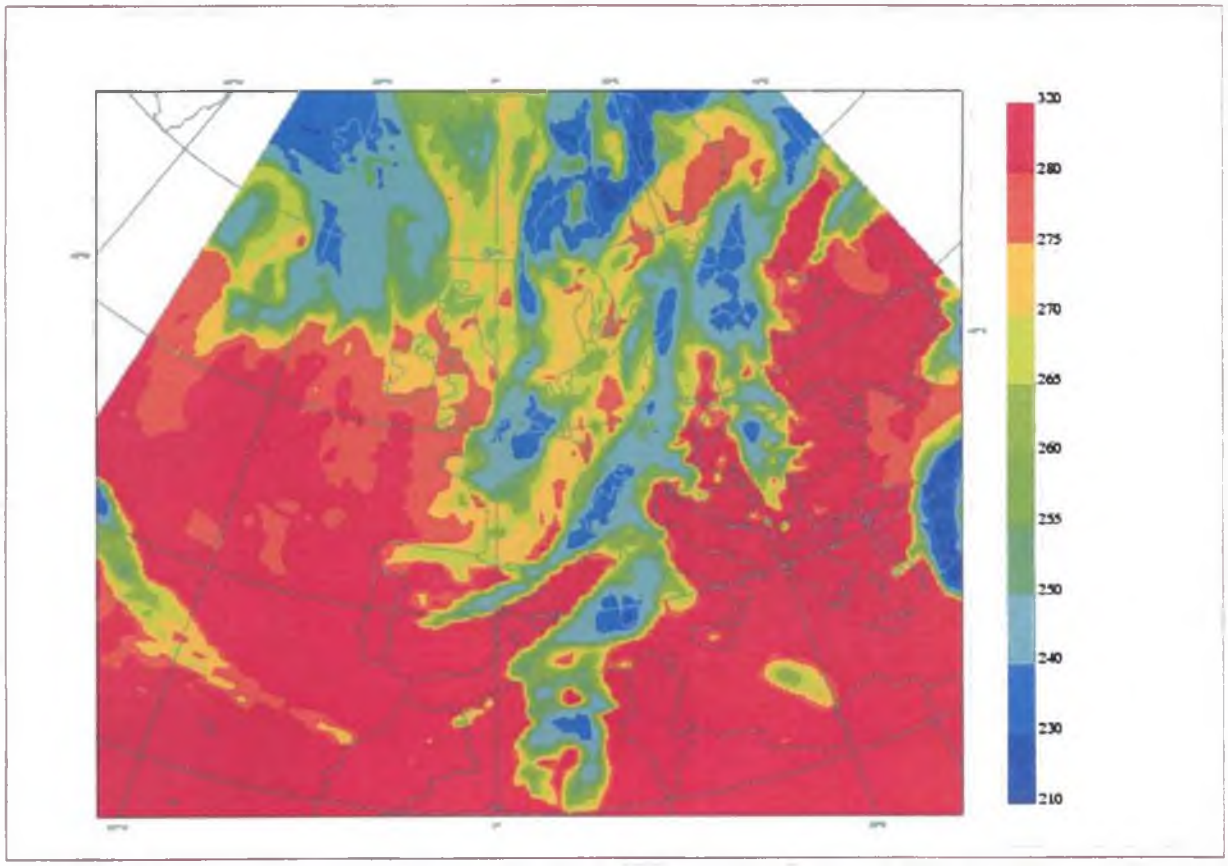

Fig. 87: Model forecast of the brightness temperatures (in K) for IR channel from April 8th 2005 00 UTC for April 9th 2005 00 UTC

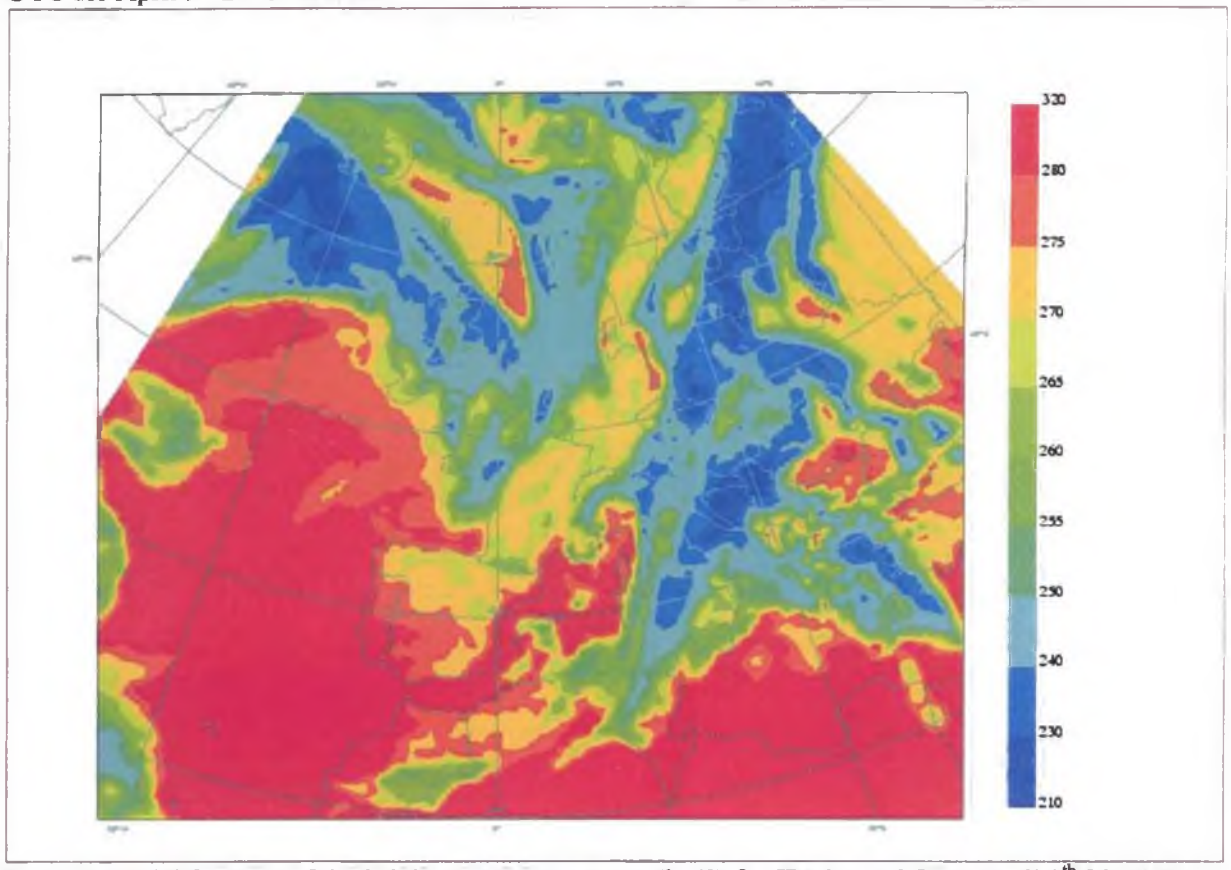

Fig. 88: Model forecast of the brightness temperatures (in K) for IR channel from April 8th 2005 00 UTC for April 11th 2005 00 UTC

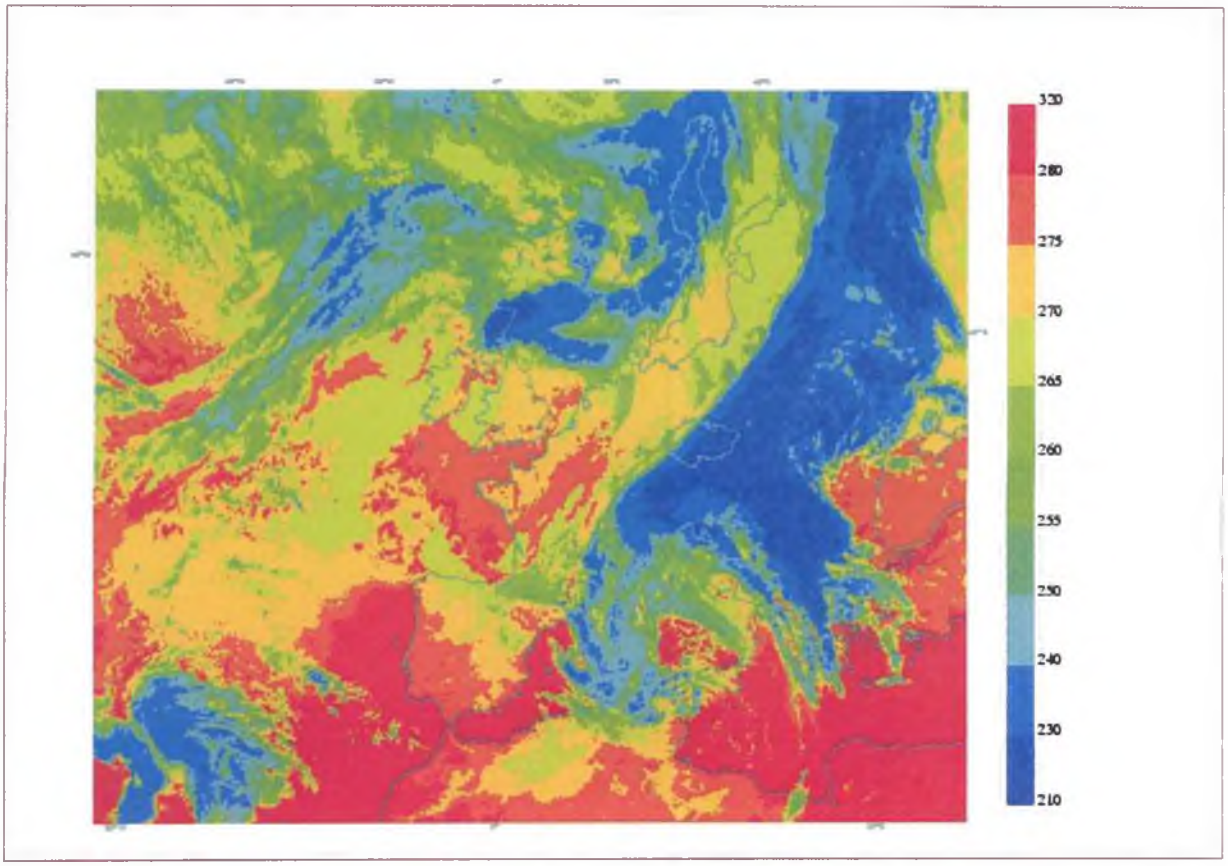

Fig. 89: IR channel image of METEOSAT-7 satellite, April 11th 2005 00 UTC

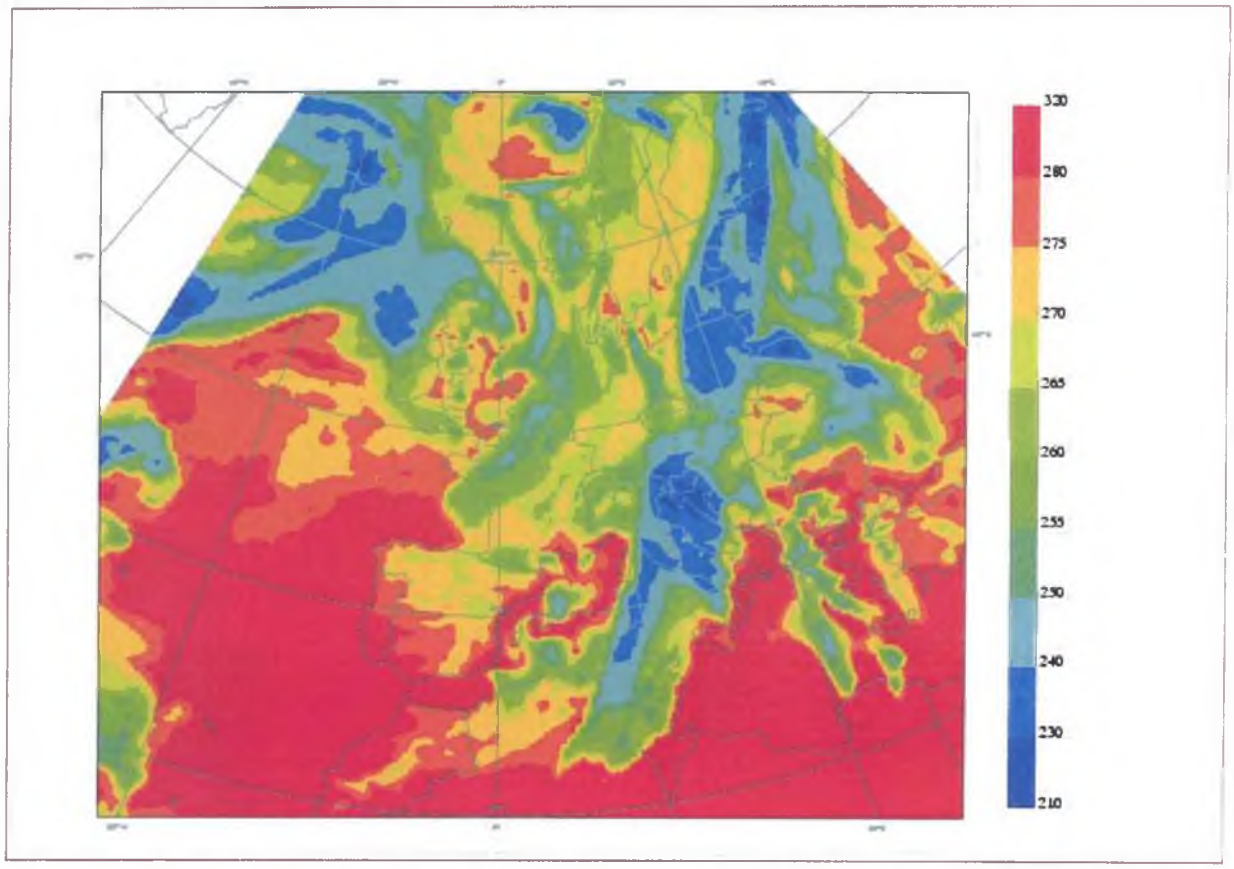

Fig. 90: Model analysis of the brightness temperatures (in K) of IR channel, April 10th 2005 00 UTC

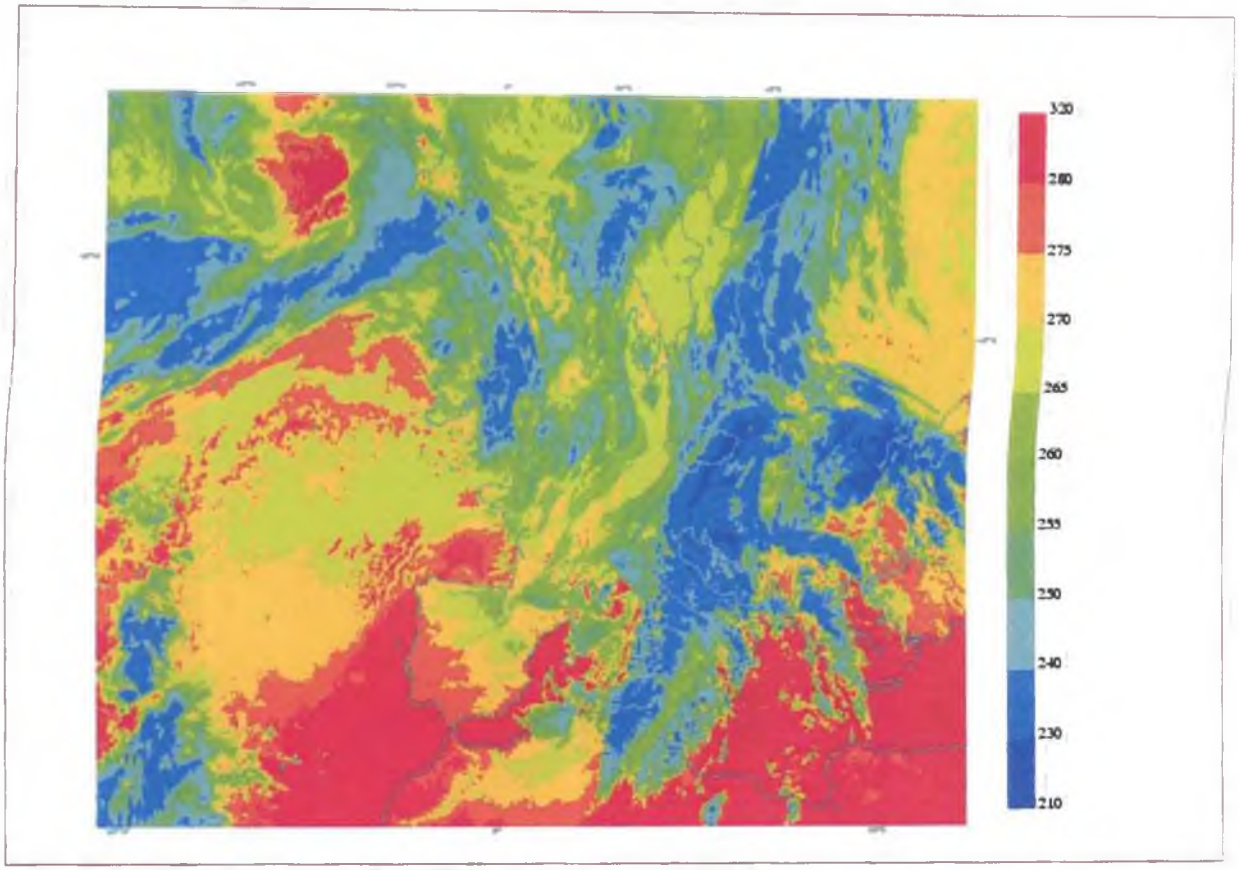

Fig. 91: IR channel image of METEOSAT-7 satellite, April 10th 2005 00 UTC

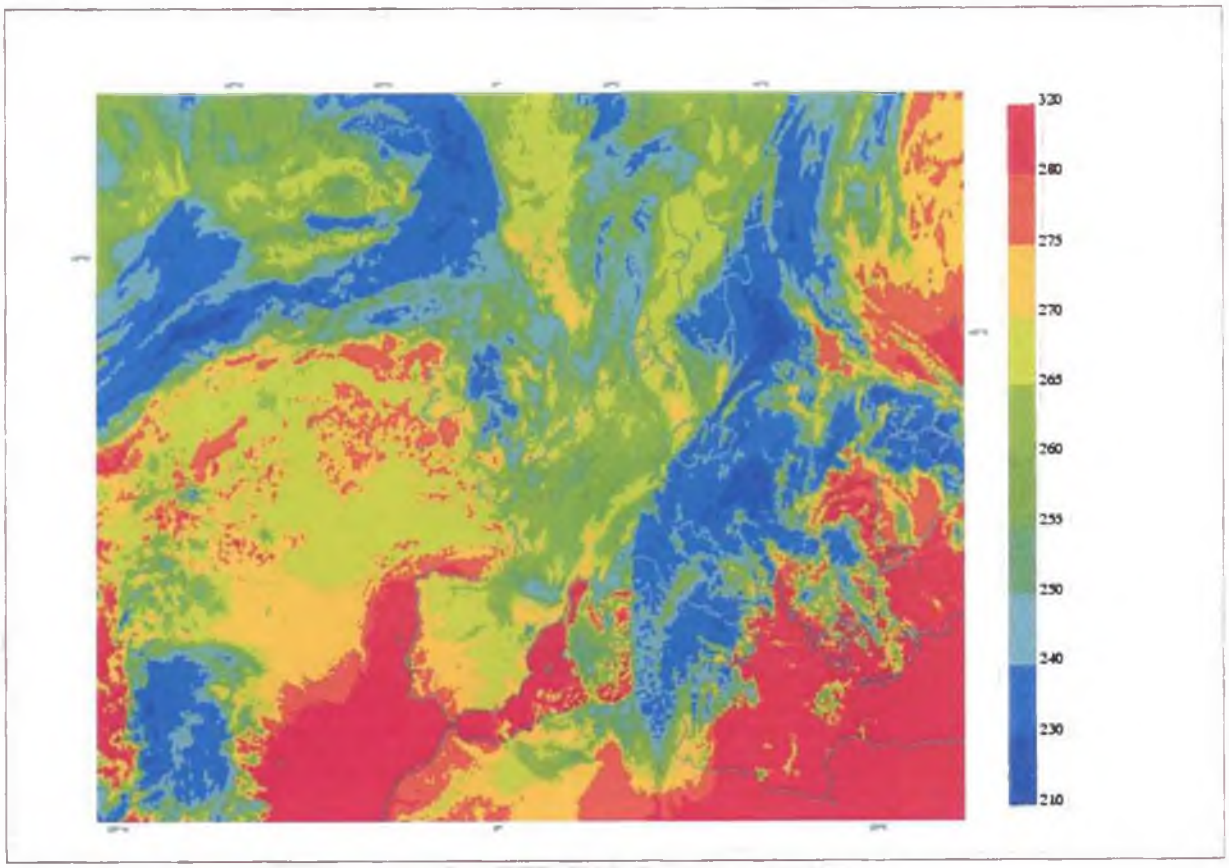

Fig. 92: IR channel image of METEOSAT-7 satellite, April 10th 2005 06 UTC

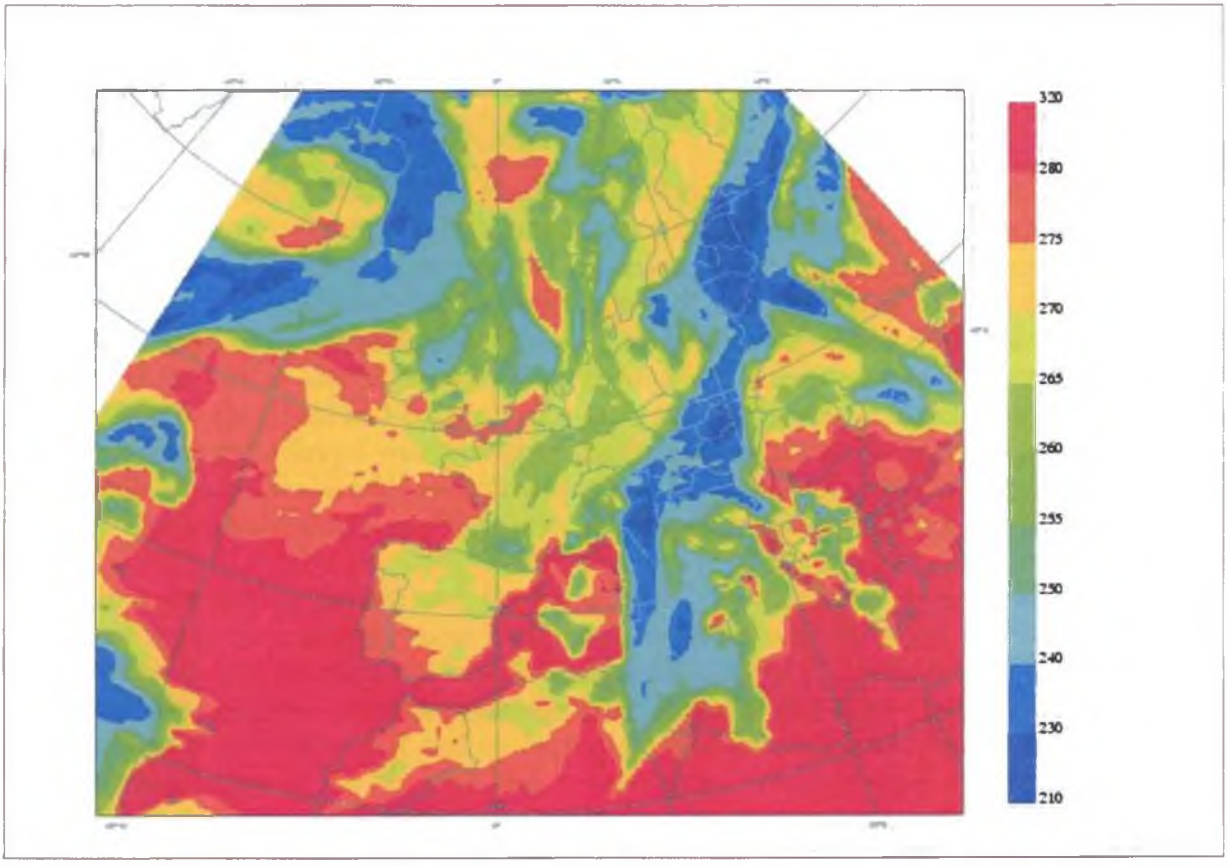

Fig. 93: Model forecast of the brightness temperatures (in K) for IR channel from April 10th 2005 00 UTC for April 10th 2005 06 UTC

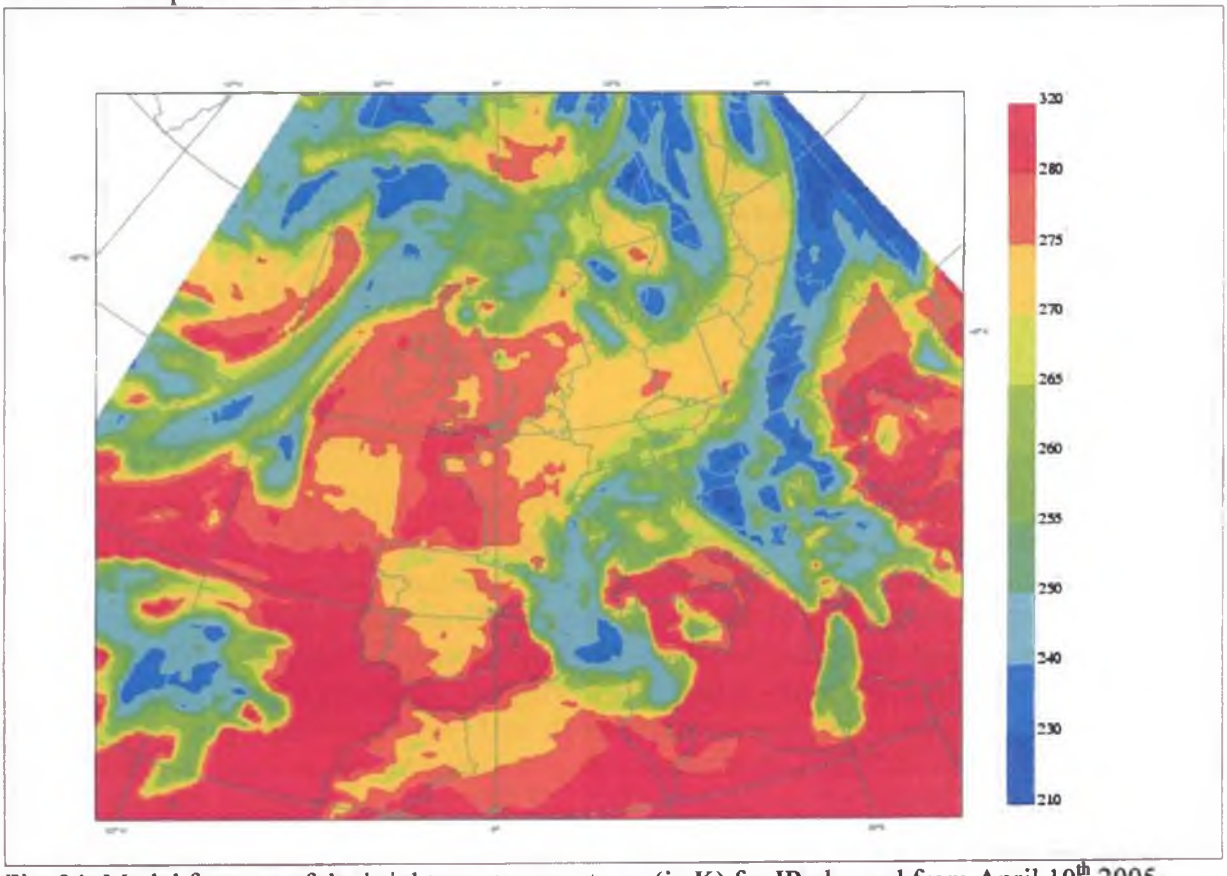

Fig. 94: Model forecast of the brightness temperatures (in K) for IR channel from April 10th 2005 00 UTC for April 11th 2005 00 UTC

4.6 May 2005

Synoptic description

The second half of May 2005 can be characterized by relatively shallow and flat lows in the surface pressure field. This can be observed on development from May 15th 2005 to May 17th 2005 on Figs. 95-97. Two or three separate cyclone centres can be seen on May 15th 2005 00 UTC (Fig. 95), one over the very north of Europe, the second one over central Europe and the third one over Bay of Biscay. The last two cyclones are more important for further development, as can bee seen on Figs. 96 and 97. The mentioned cyclone moved from Bay of Biscay to the Spain and Balearic Islands, although its weakening can be detected. The cyclone from central Europe was moved to the Scandinavia and its intensification occurred concurrently. A cold front with several waves can be analyzed as stretching from southern Finland to the central Europe and further to southwest to southern Spain on 17th May 2005 (Fig. 97).

More interesting picture can be found when focussing on upper levels mainly at middle and upper troposphere where mentioned cyclones were strongly developed. At 500 hPa level three cyclone centres can be also analyzed for May 15th 2005 00 UTC (Fig. 98). Concerning the cyclonic centres over northern Europe and over Bay of Biscay their expressions on the surface level and on high atmospheric levels were horizontally near and these cyclones begun to fill up. The high levels centre corresponding to the cyclone over central Europe was situated over Benelux, indicating that this cyclone could have possibilities of new development. It really occured (see Fig. 99 for situation on May 16th 2005 00 UTC), although this centre merge with the trough over northern Europe during May 17th 2005 (Fig. 100). At 200 hPa the situation is quite similar, although no separate cyclone centre can be detected over central Europe or Benelux, but well developed cyclone can be detected over Bay of Biscay on May 15th 2005 00 UTC (Fig. 101). Very interesting temperature field at 200 hPa level could be observed. Analyses for May 15th - 17th 2005 are presented on Figs. 102-104. Warmer regions (over -50 °C) can be found in the vicinity of the cyclone over Bay of Biscay as well as over Benelux on May 15th 2005 00 UTC (Fig. 102). While the warm region was moved from Bay of Biscay to southeast and it was weakening, the field connected with the cyclone over Benelux and central Europe, was moved to northeast and then was merged with the warmer area in the upper trough region over north-western Europe.

Comparison model-to-observation

The situation for May 15th 2005 00 UTC expressed by help of brightness temperatures fields can be seen on Figs. 105 and 106 for model analysis and for satellite observation, both for IR channel. Relative good correlation between simulated and observed cloud fields can be noticed, inclusive the representation of the whirl cloudiness in the cyclone centre over Bay of Biscay. But some discrepancies occurs already for the 6 h forecast (see and compare Figs. 107 and 108) – mainly over Yugoslavia, Hungary and Slovakia where the forecasted cloudiness is missing or strongly underestimated. This differences become more significant during next hours of forecast time, as can be seen for + 18 h forecast on Figs. 109 (model forecast) and 110 (satellite measurement for May 15th 18 UTC) – mainly in the central Europe region, the cloudiness is forecasted more eastward and only small cloudiness is forecasted over Czech Republic (in comparison with satellite observation).

The similar situation, in the sense that quite quick decrease of forecast quality can be detected, is seen also for the case of May 16th 00 UTC. Again, the model analysis (Fig. 111) and satellite measurement (Fig. 112) are quite well correlated, with satisfactory simulated main synoptic cloud features but the forecast for next day is already quite fault in the region of the south-east central Europe (see Figs. 113 and 114 for situation on May 17th 12 UTC). It can be seen that the cloudiness is partly underestimated and partly even missing in forecast for region stretching from Slovenia/Croatia to Ukraine. This cloudiness is probably partly of convective origin (see cold tops in the satellite measurement on Fig. 114), but in the model forecasts the coldest tops (the lowest brightness temperatures) are located over Italy and Sardinia. The reason of this may be caused by some underestimation of the cloud fields over southern Adria and Italy in the model analysis (compare Fig. 111 and 112).

Finally, focusing on the situation for May 17th 00 UTC, a relatively good correlation between model analysis and satellite observation could be found and also the forecast from this time is better comparing to the previous two cases mentioned and described above, although some underestimation of cloud fields over central Mediterranean can be detected – in analysis as well as in forecast (see and compare model analysis on Fig. 115 with satellite measurement on Fig. 116 for May 17th 00 UTC and model forecast for May 18th 00 UTC on Fig. 117 with satellite observation on Fig. 118 for the same time).

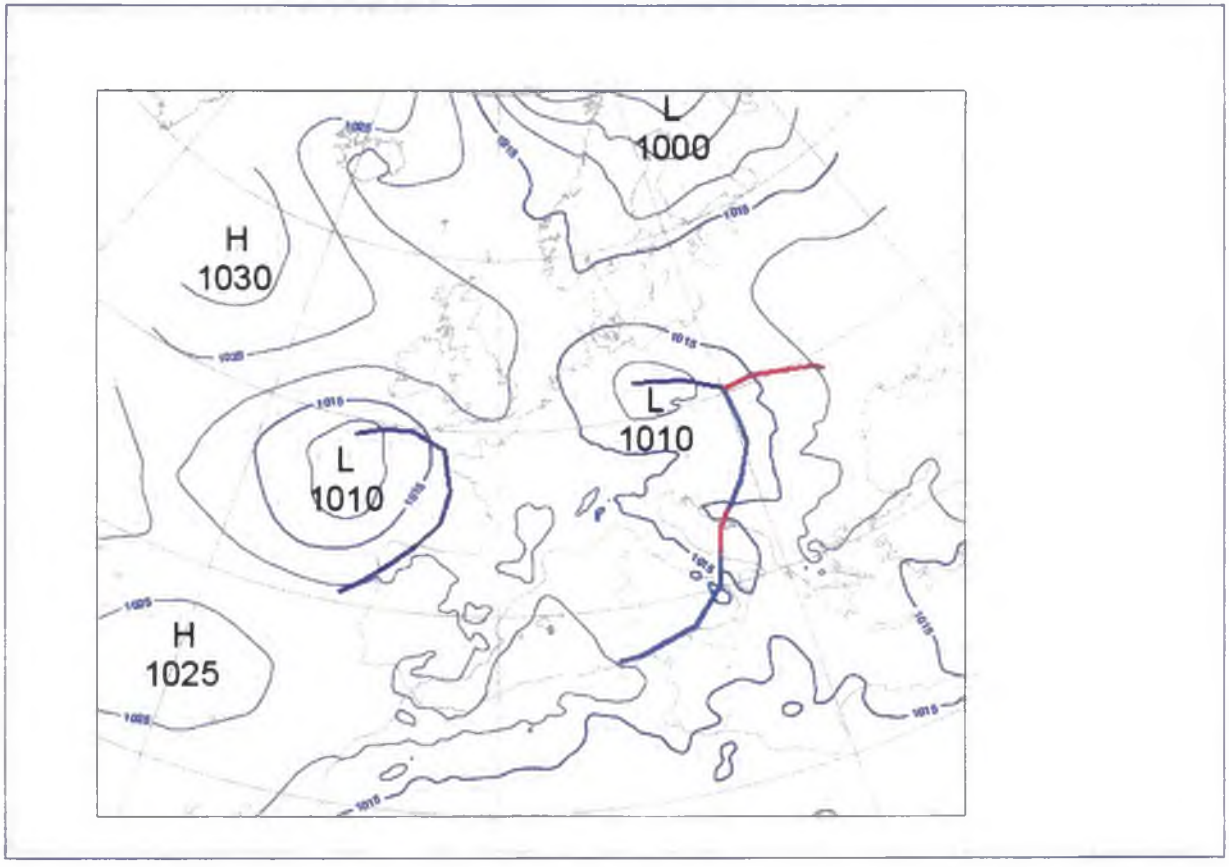

Fig. 95: Surface analysis for May 15th 2005 00 UTC (isobars interval 5 hPa)

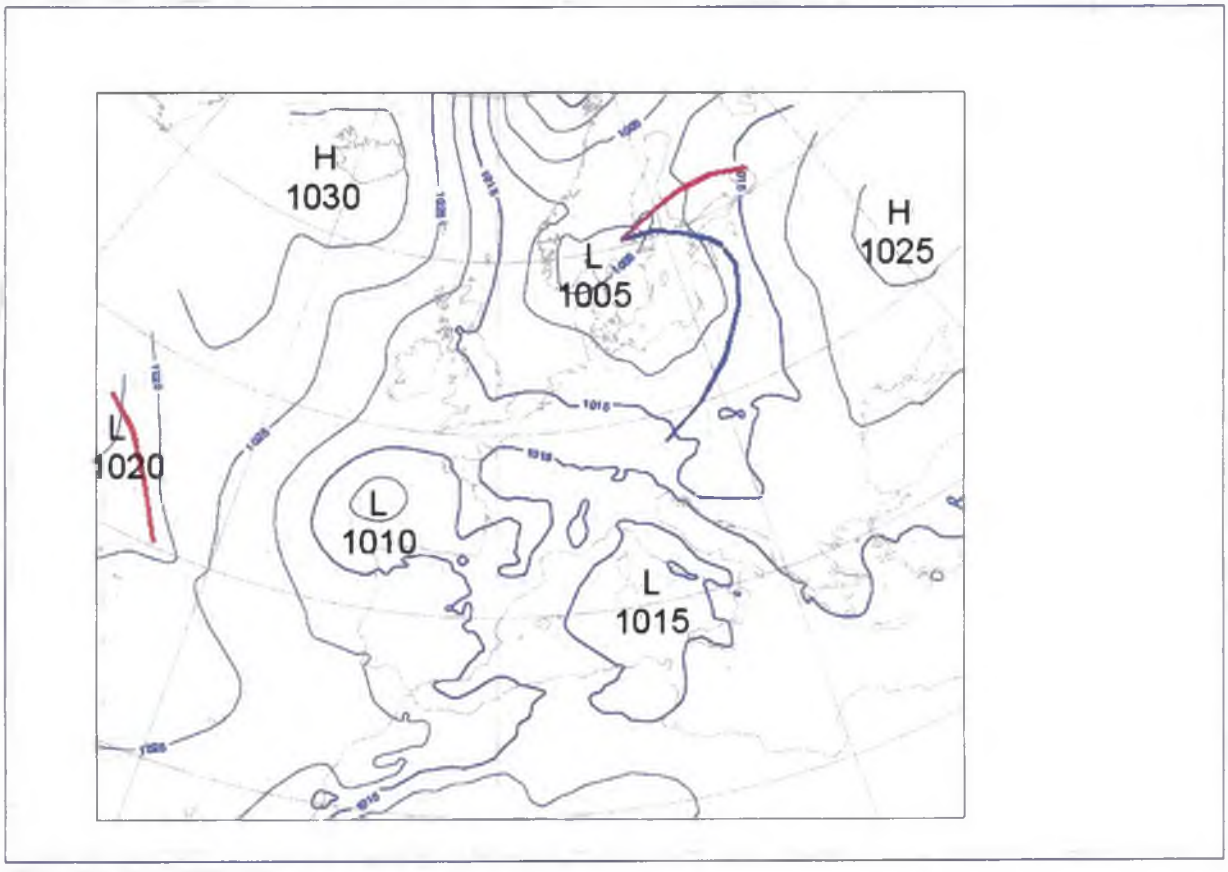

Fig. 96: Surface analysis for May 16th 2005 00 UTC (isobars interval 5 hPa)

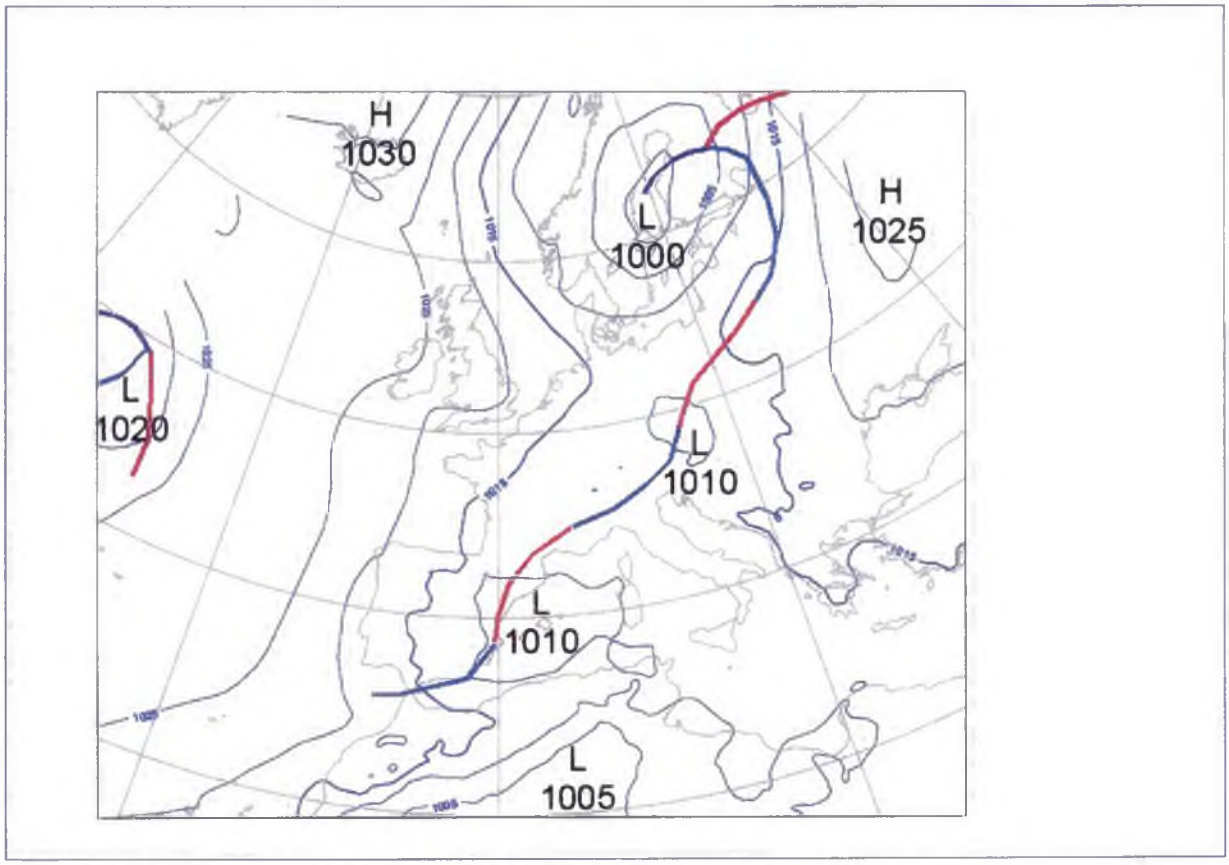

Fig. 97: Surface analysis for May 17th 2005 00 UTC (isobars interval 5 hPa)

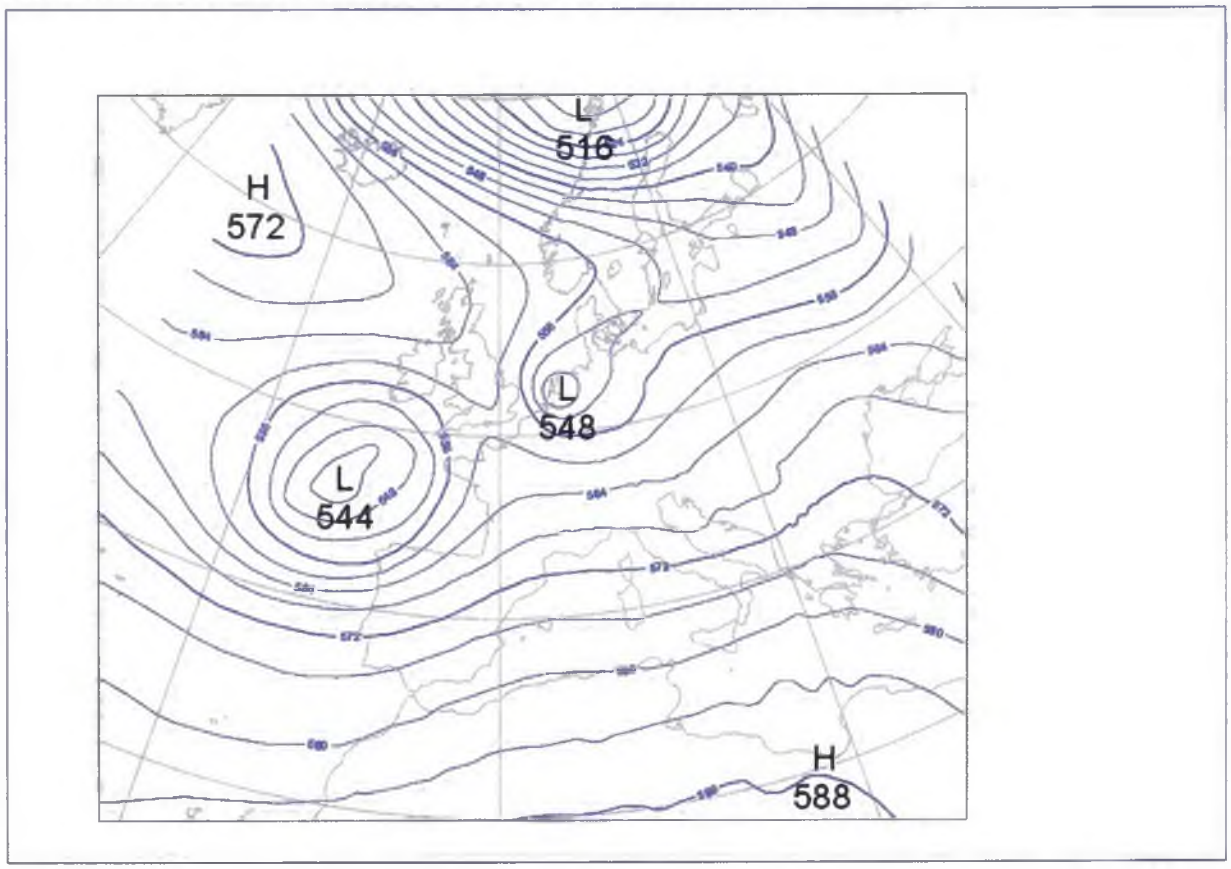

Fig. 98: Geopotential height of 500 hPa level (interval 4 decametres), analysis for May 15th 2005 00 UTC

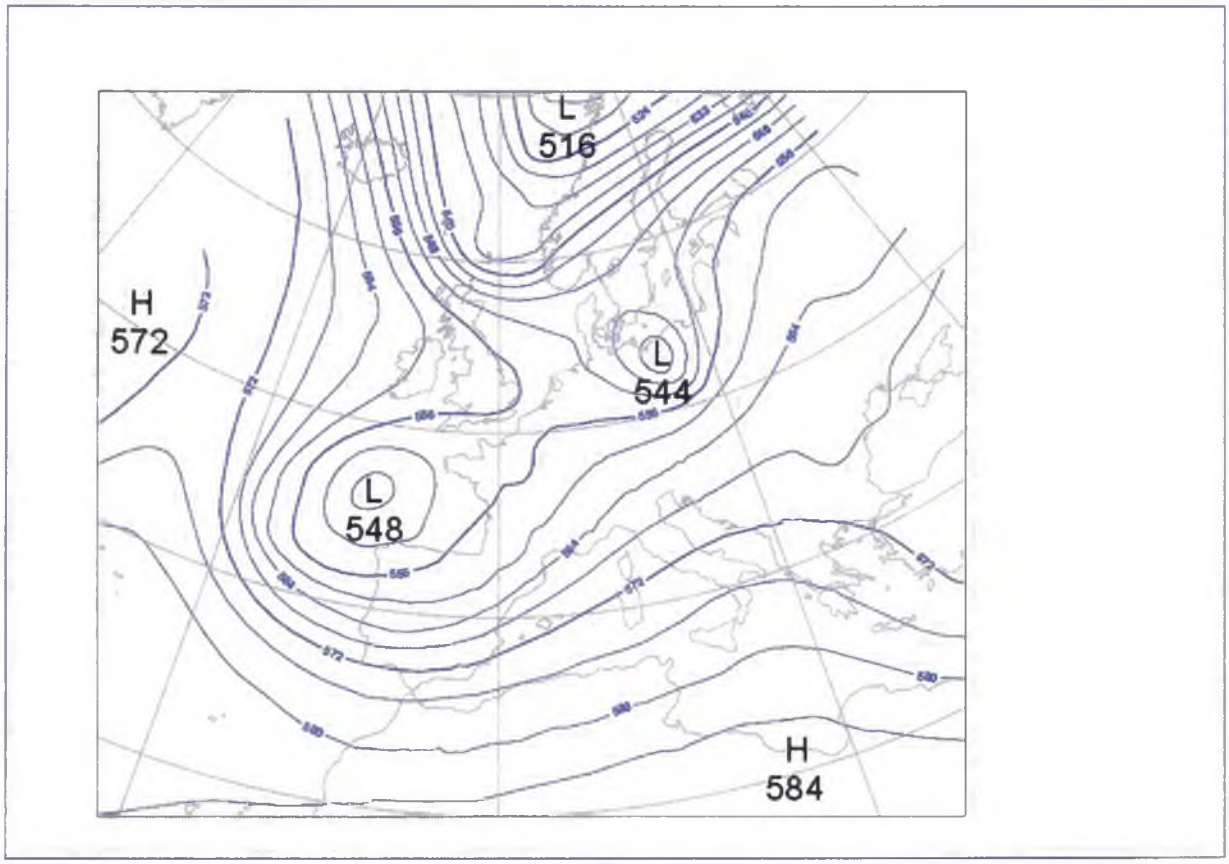

Fig. 99: Geopotential height of 500 hPa level (interval 4 decametres), analysis for May 16th 2005 00 UTC

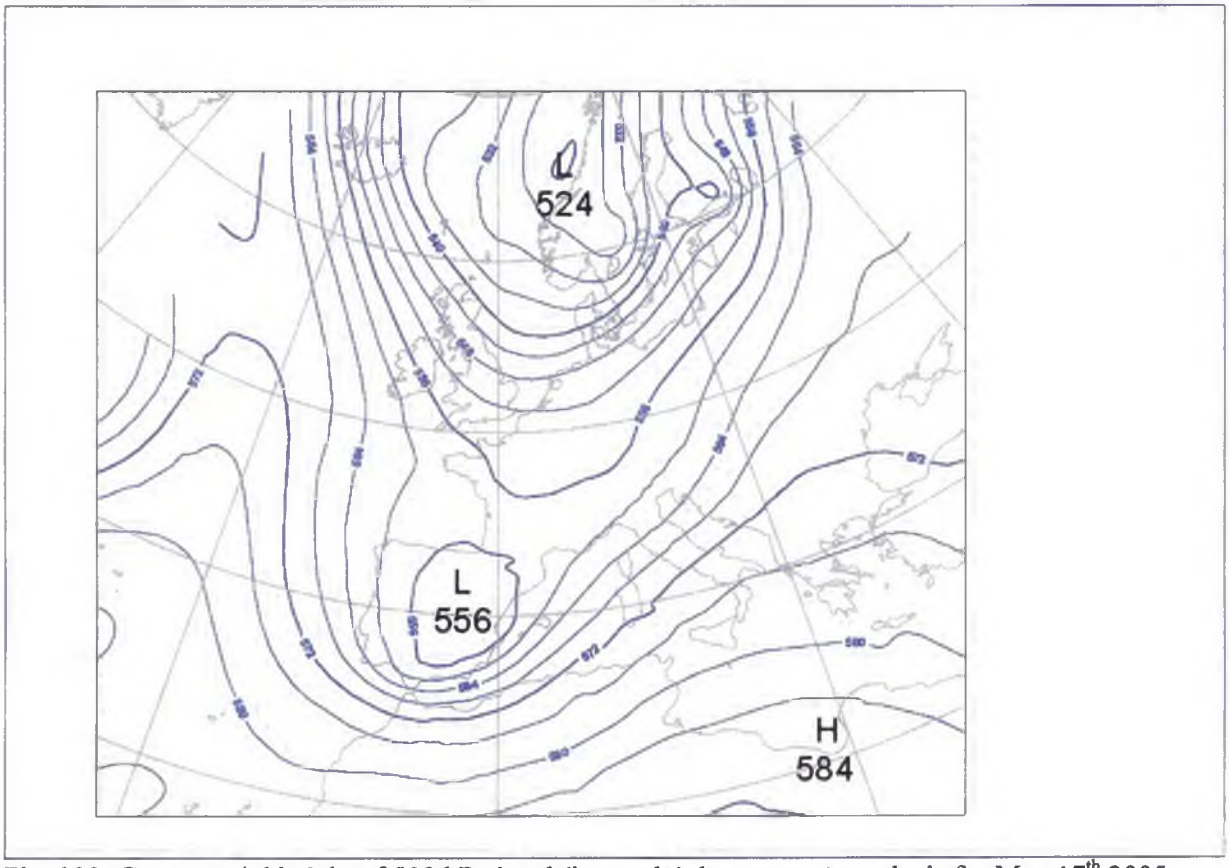

Fig. 100: Geopotential height of 500 hPa level (interval 4 decametres), analysis for May 17th 2005 00 UTC

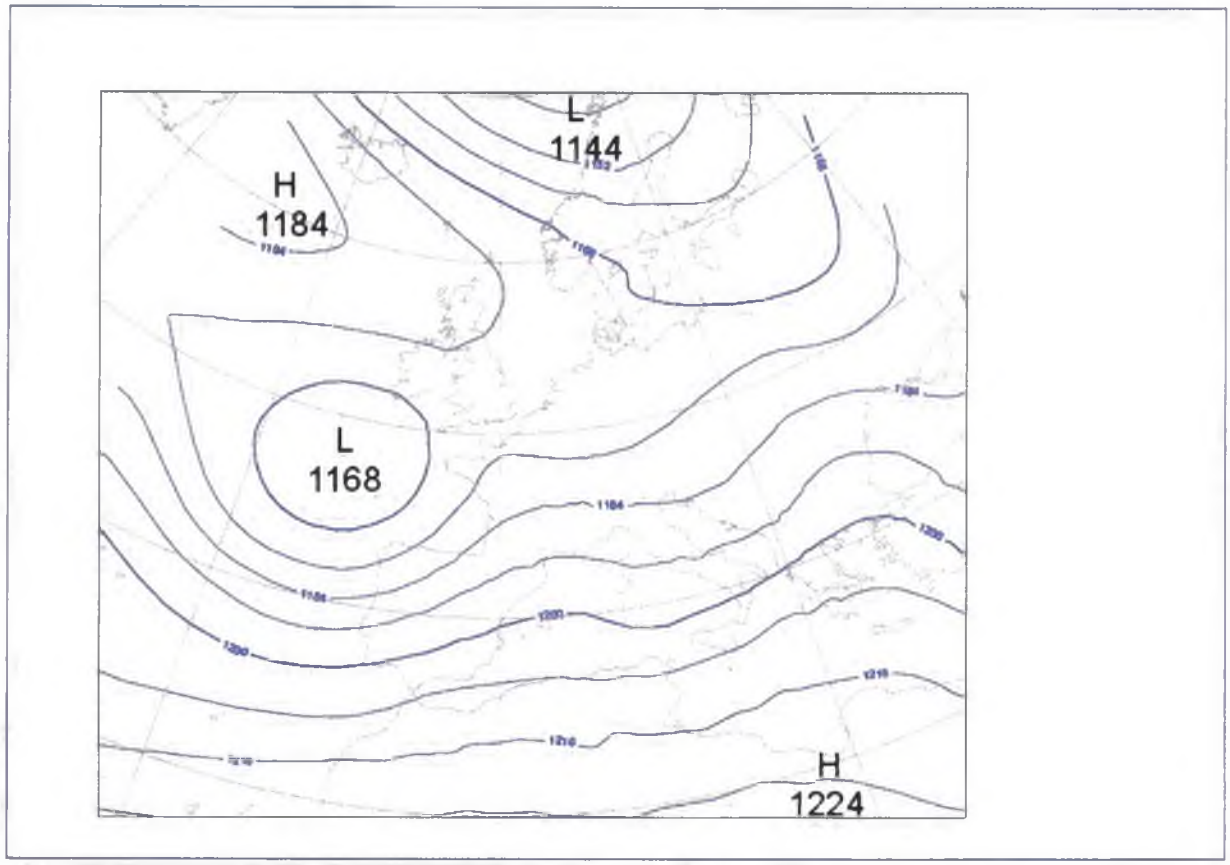

Fig. 101: Geopotential height of 200 hPa level (interval 8 decametres), analysis for May 15th 2005 00 UTC

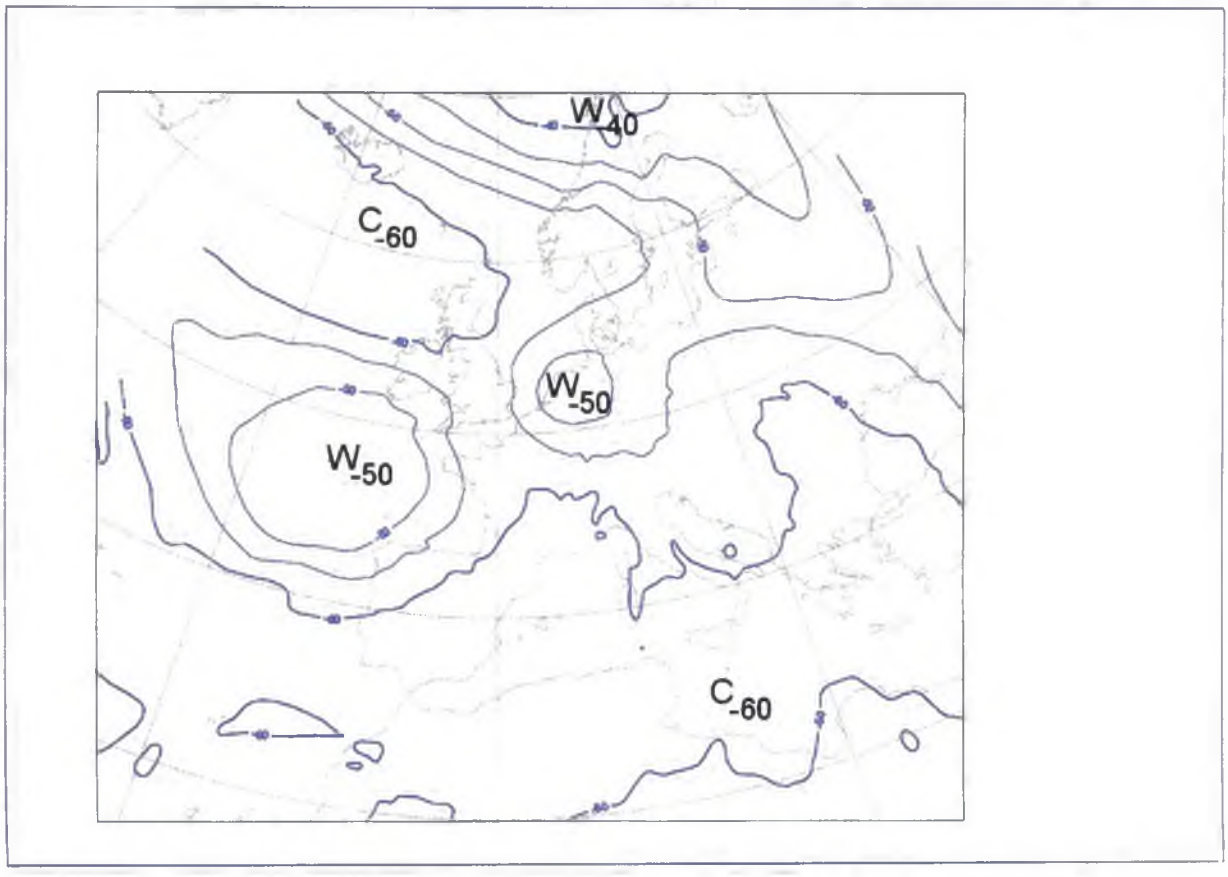

Fig. 102: Temperature at 200 hPa level (interval 5 °C), analysis for May 15th 2005 00 UTC

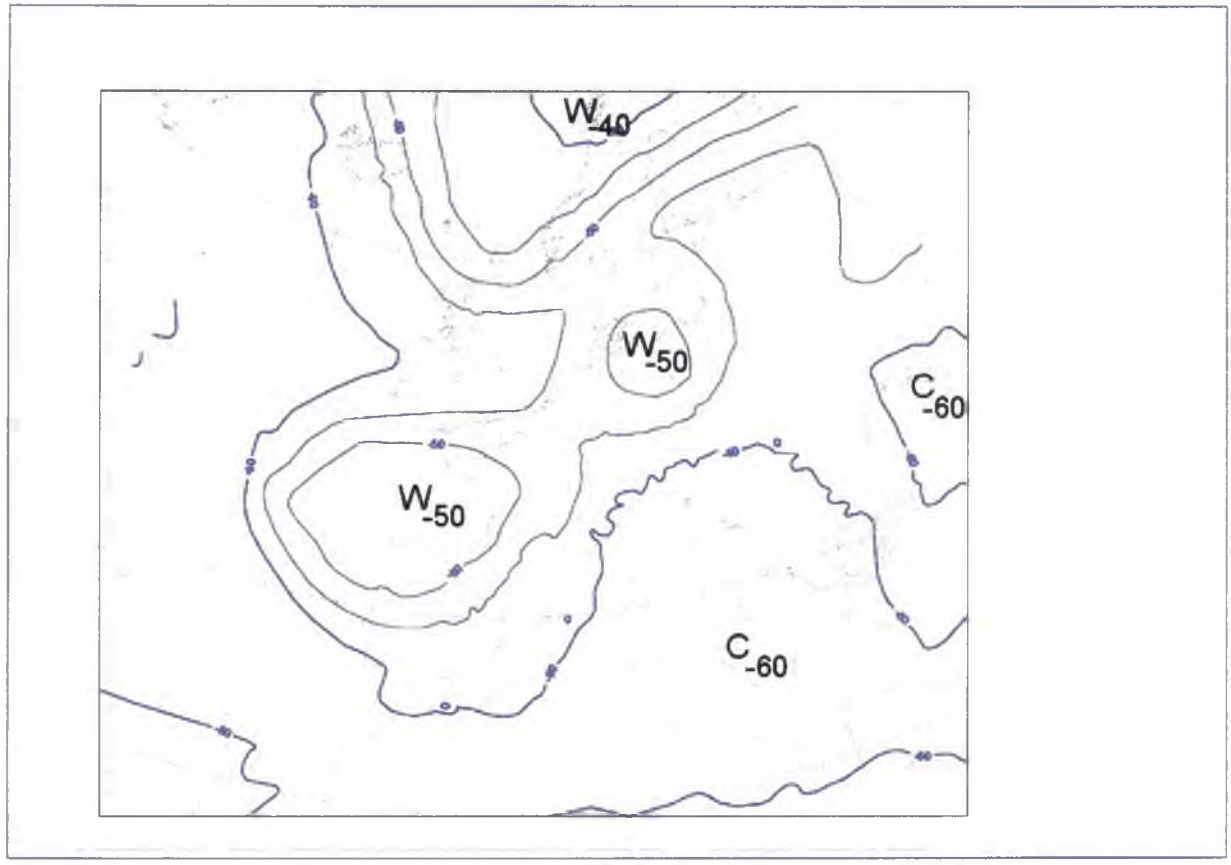

Fig. 103: Temperature at 200 hPa level (interval 5 °C), analysis for May 16th 2005 00 UTC

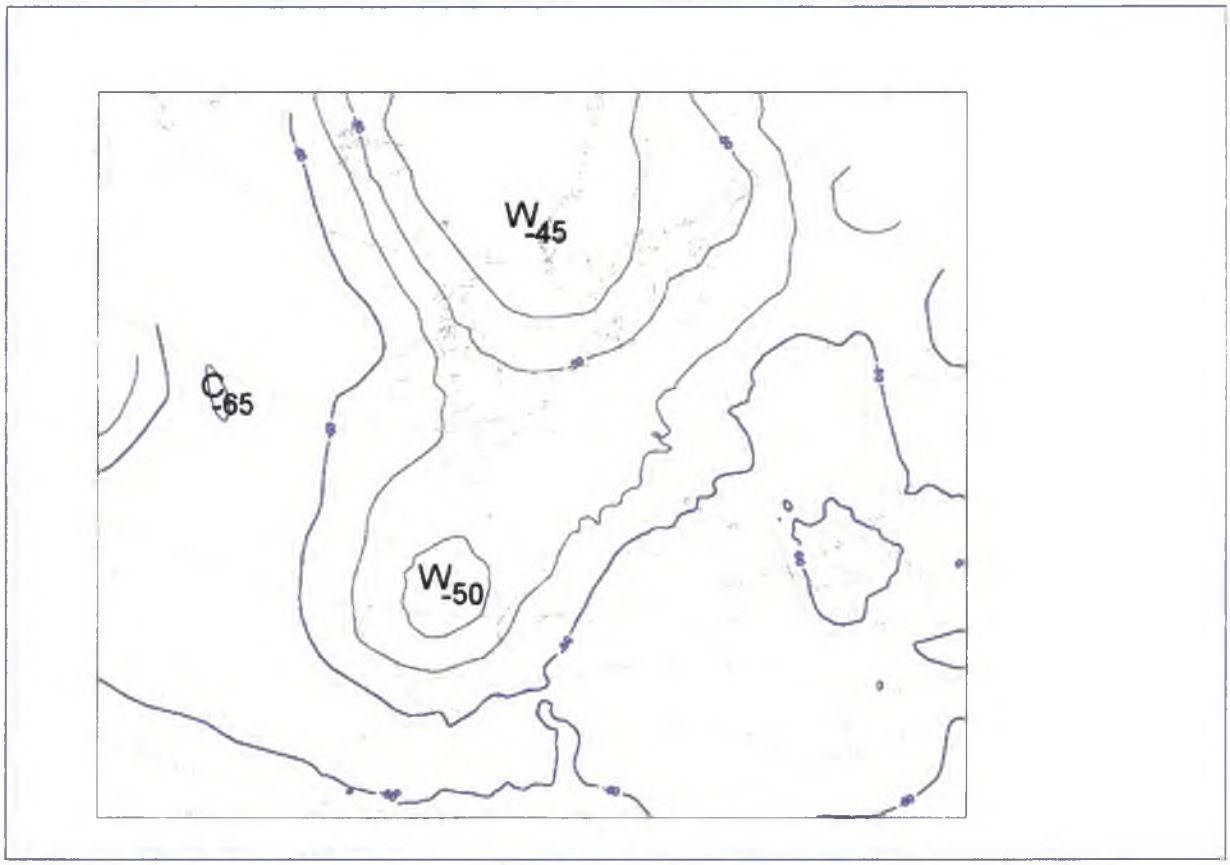

Fig. 104: Temperature at 200 hPa level (interval 5 °C), analysis for May 17th 2005 00 UTC

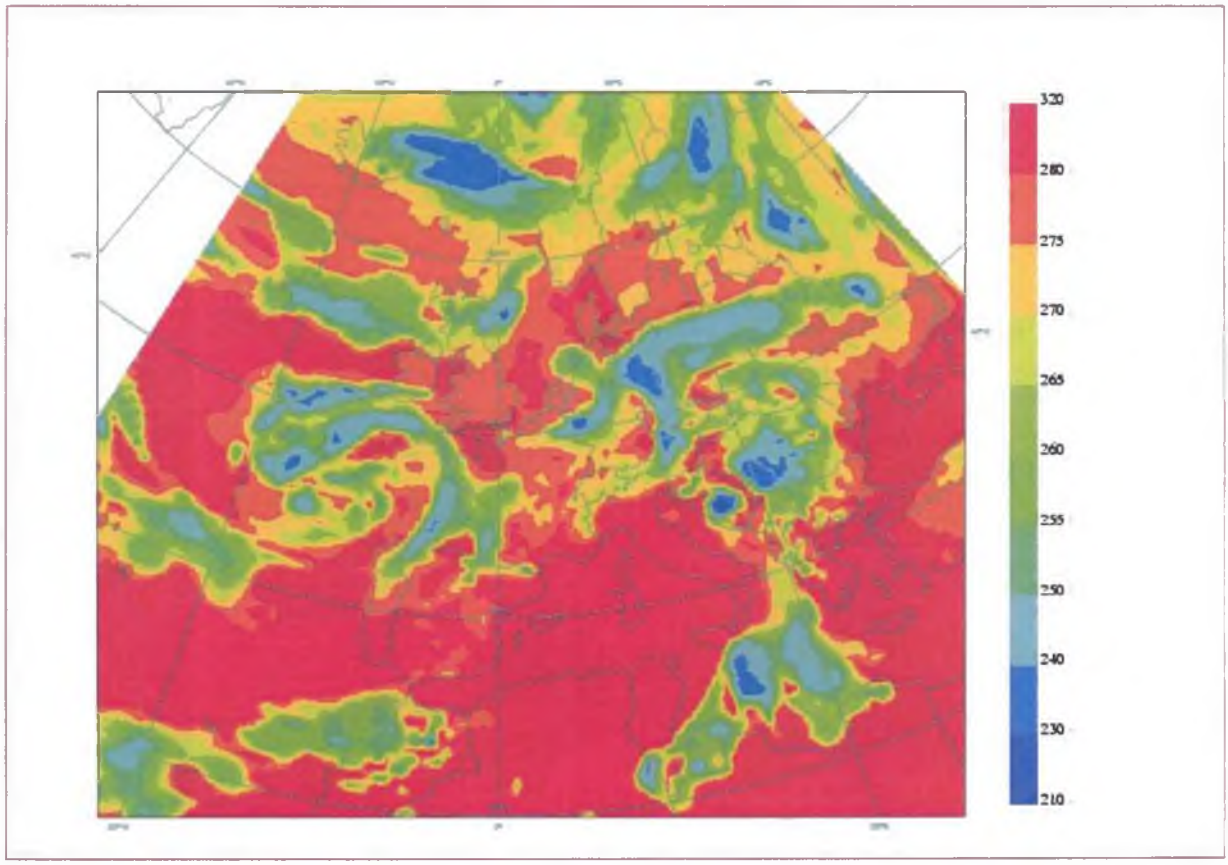

Fig. 105: Model analysis of the brightness temperatures (in K) of IR channel, May 15th 2005 00 UTC

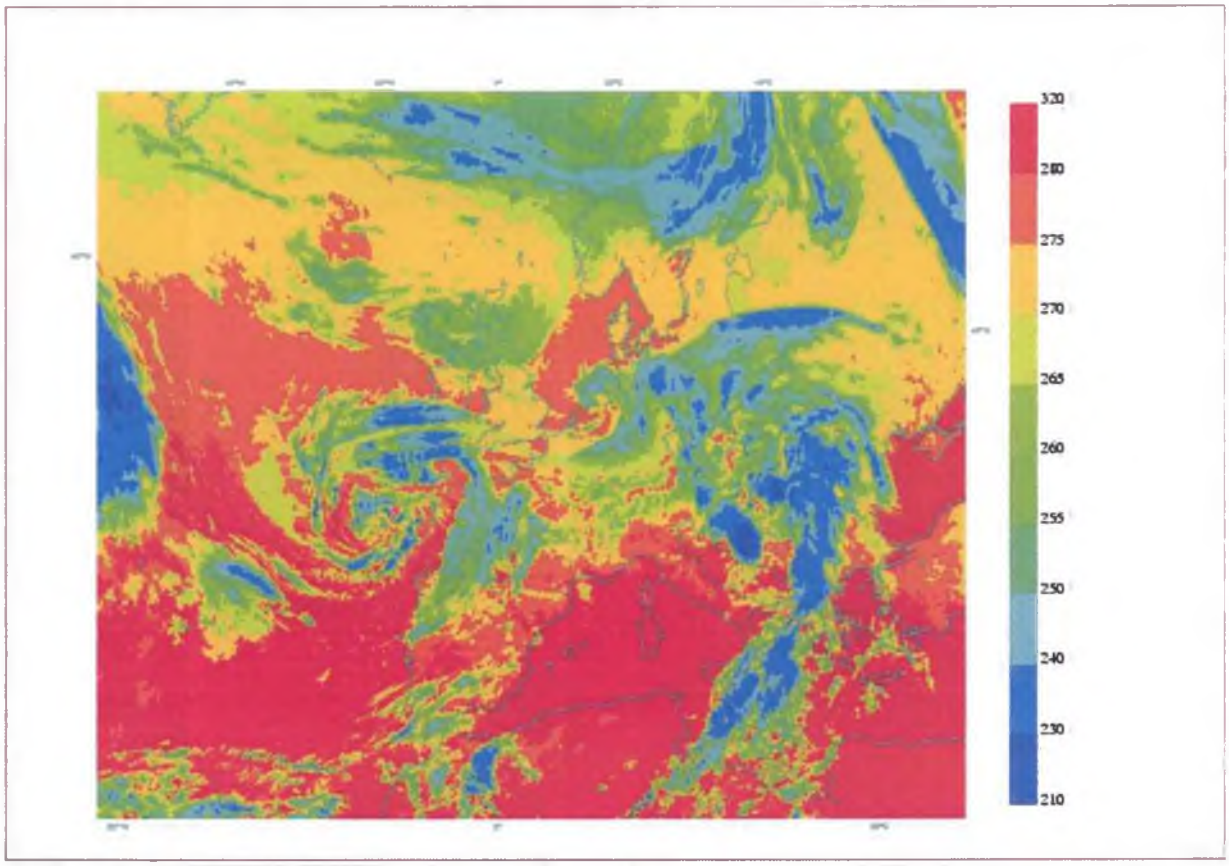

Fig. 106: IR channel image of METEOSAT-7 satellite, May 15th 2005 00 UTC

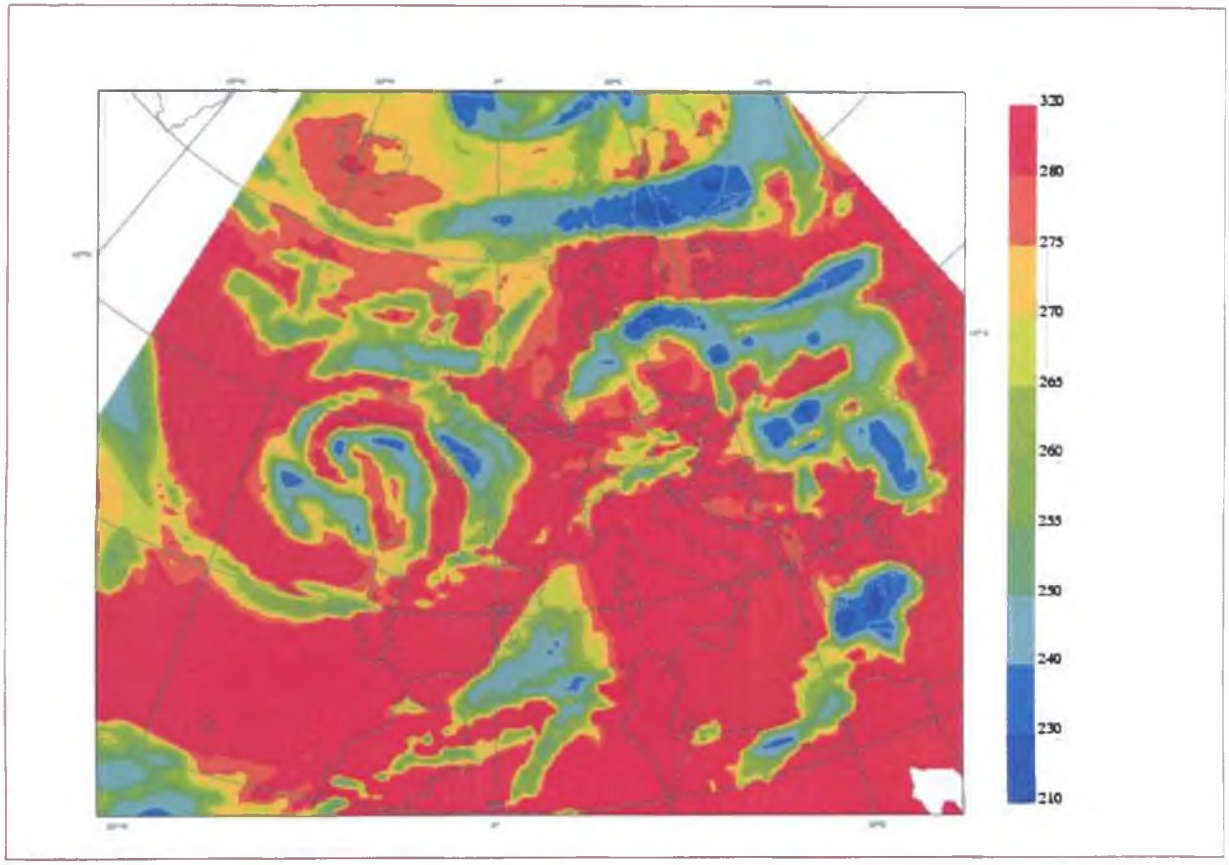

Fig. 107: Model forecast of the brightness temperatures (in K) of IR channel for May 15th 2005 06 UTC from May 15th 2005 00 UTC

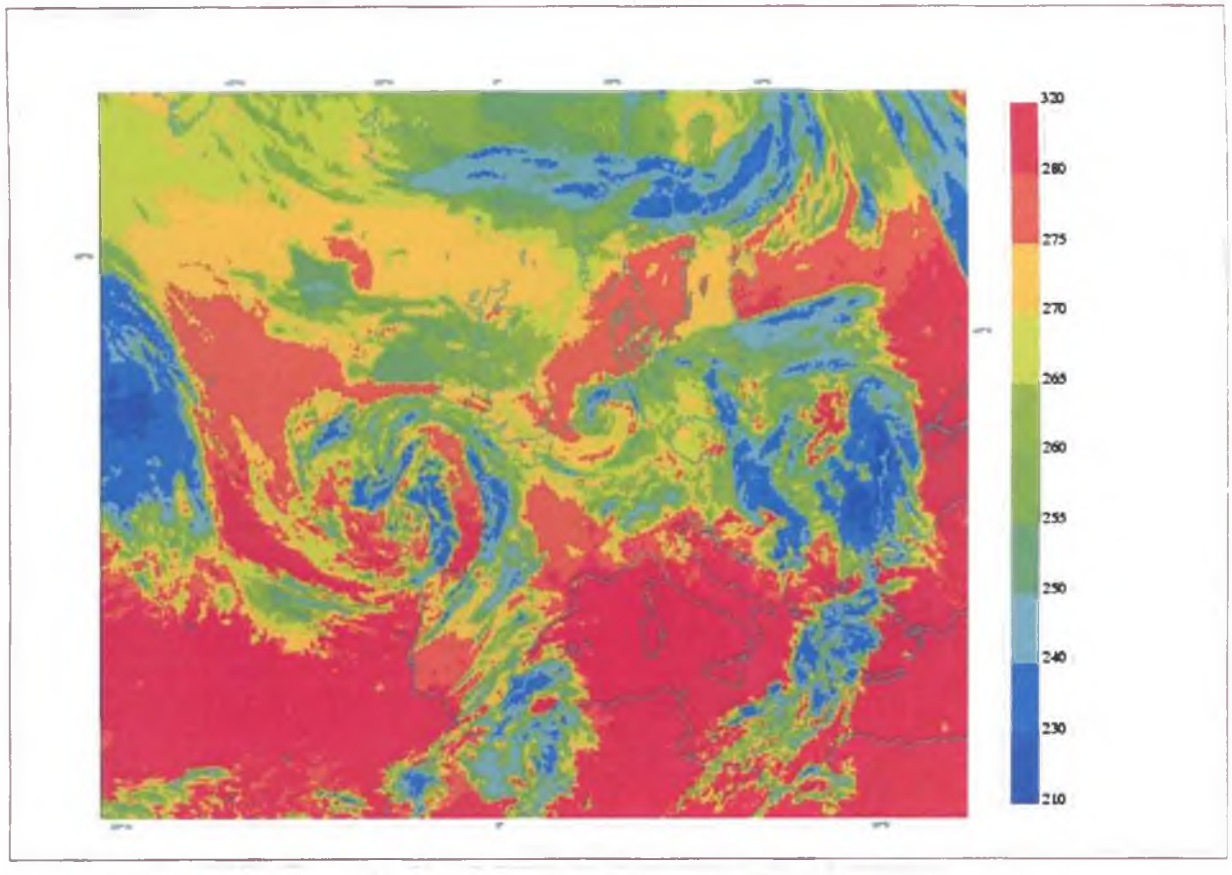

Fig. 108: IR channel image of METEOSAT-7 satellite, May 15th 2005 06 UTC

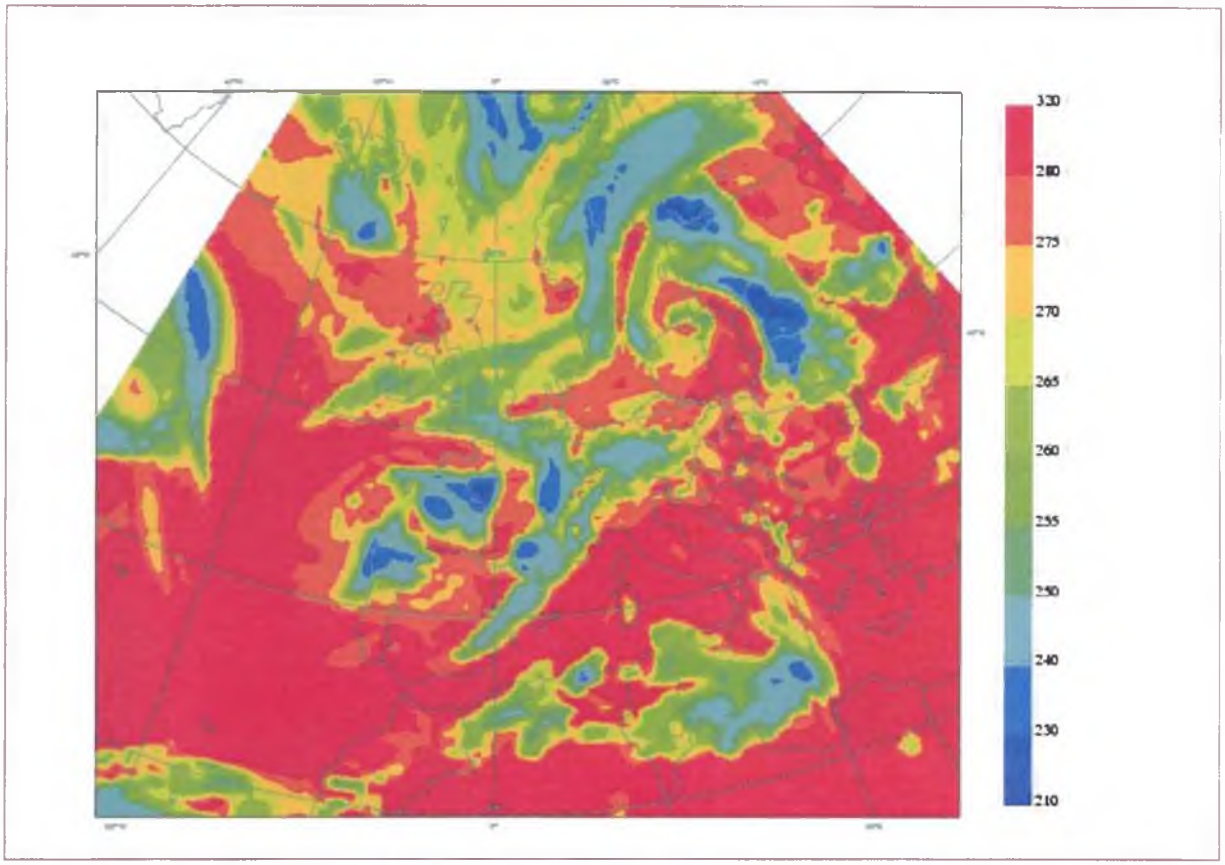

Fig. 109: Model forecast of the brightness temperatures (in K) of IR channel for May 15th 2005 18 UTC from May 15th 2005 00 UTC

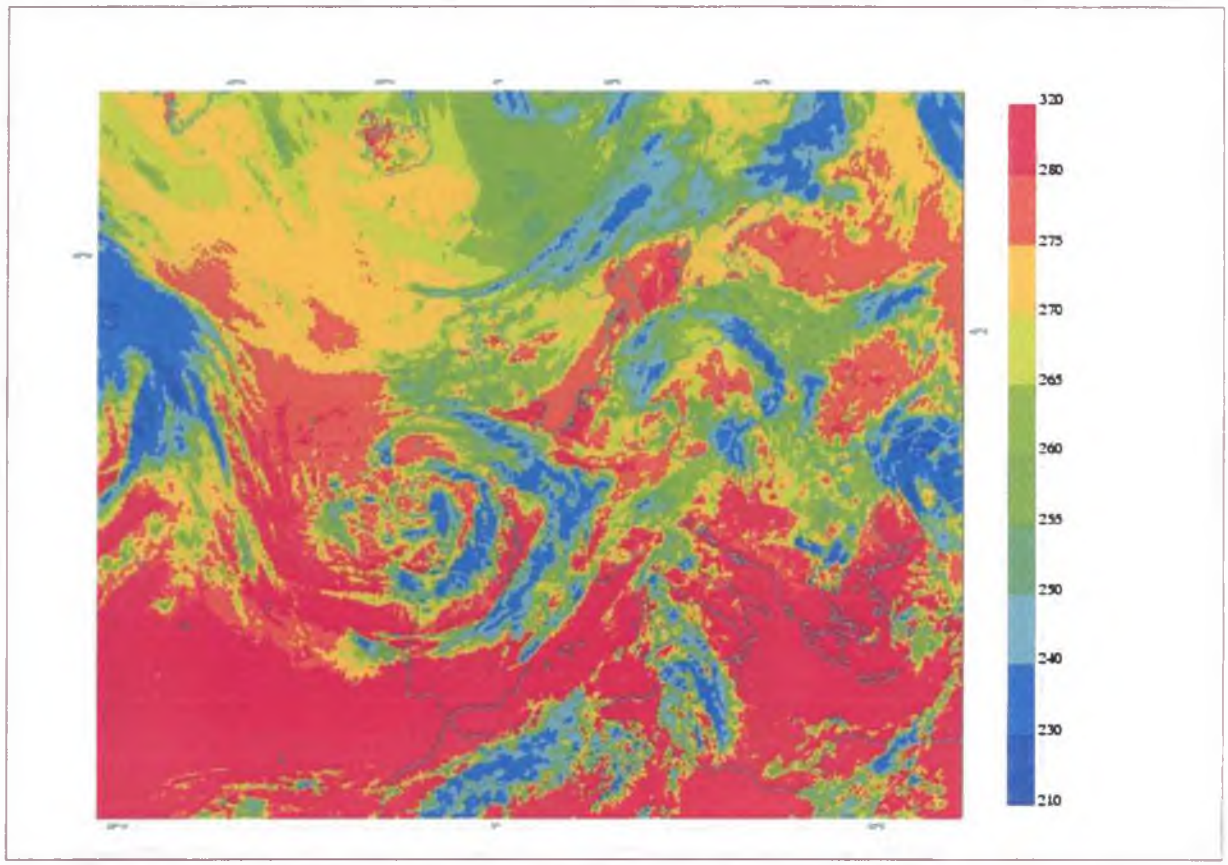

Fig. 110: IR channel image of METEOSAT-7 satellite, May 15th 2005 18 UTC

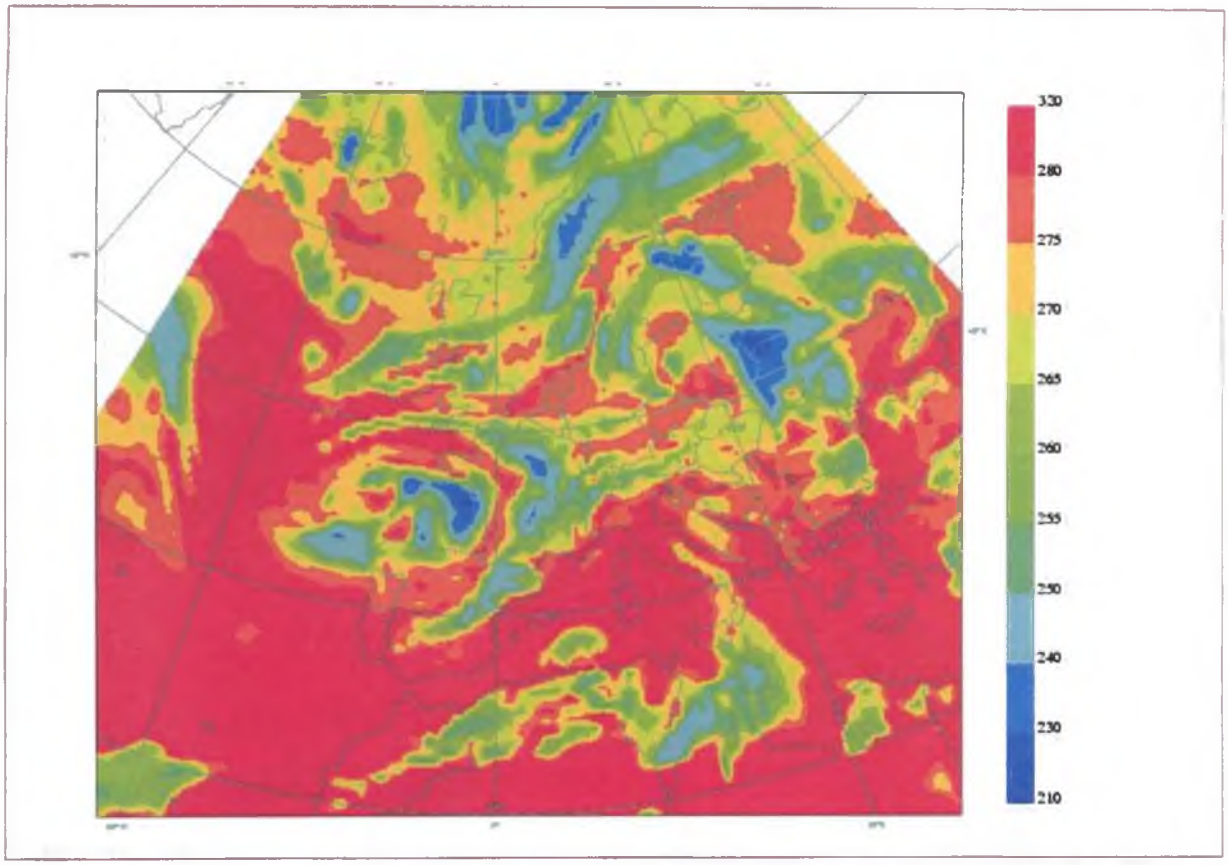

Fig. 111: Model analysis of the brightness temperatures (in K) of IR channel, May 16th 2005 00 UTC

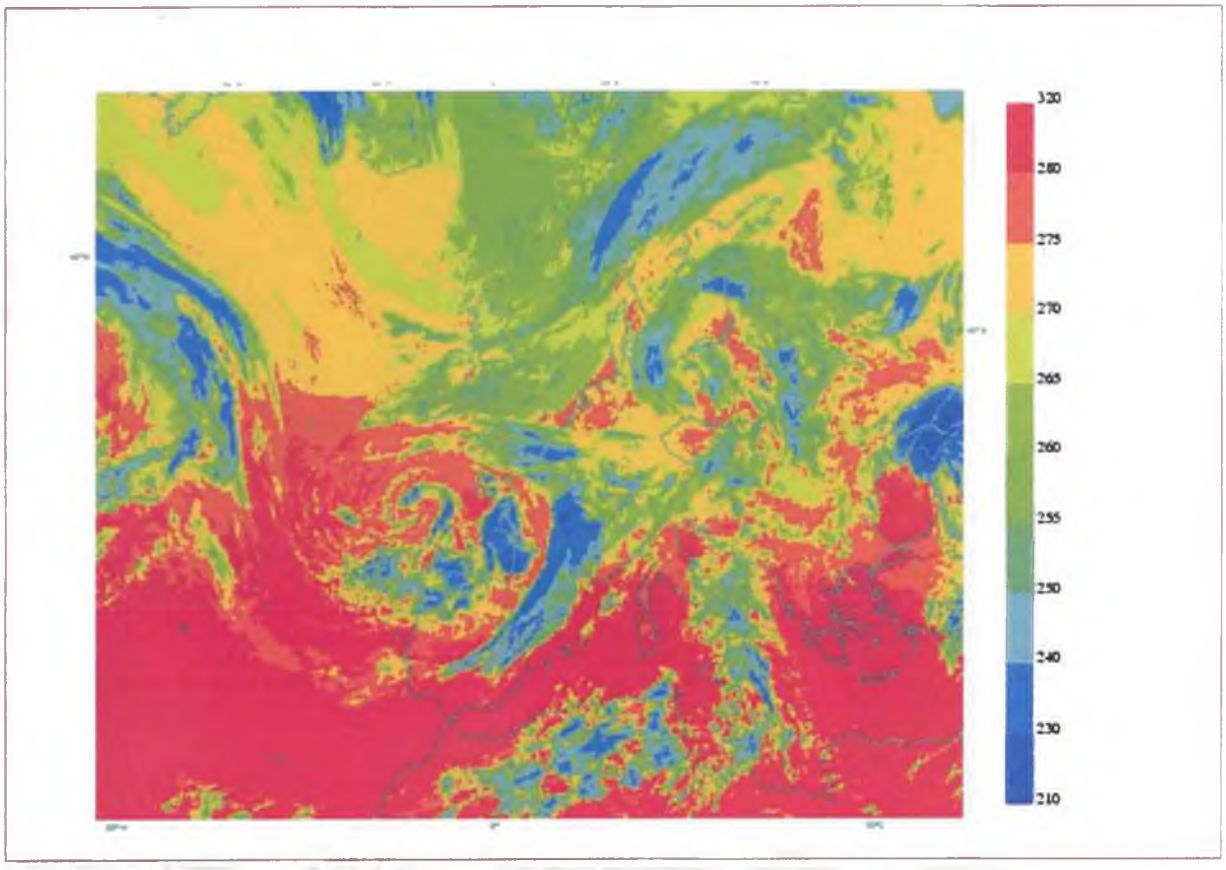

Fig. 112: IR channel image of METEOSAT-7 satellite, May 16th 2005 00 UTC

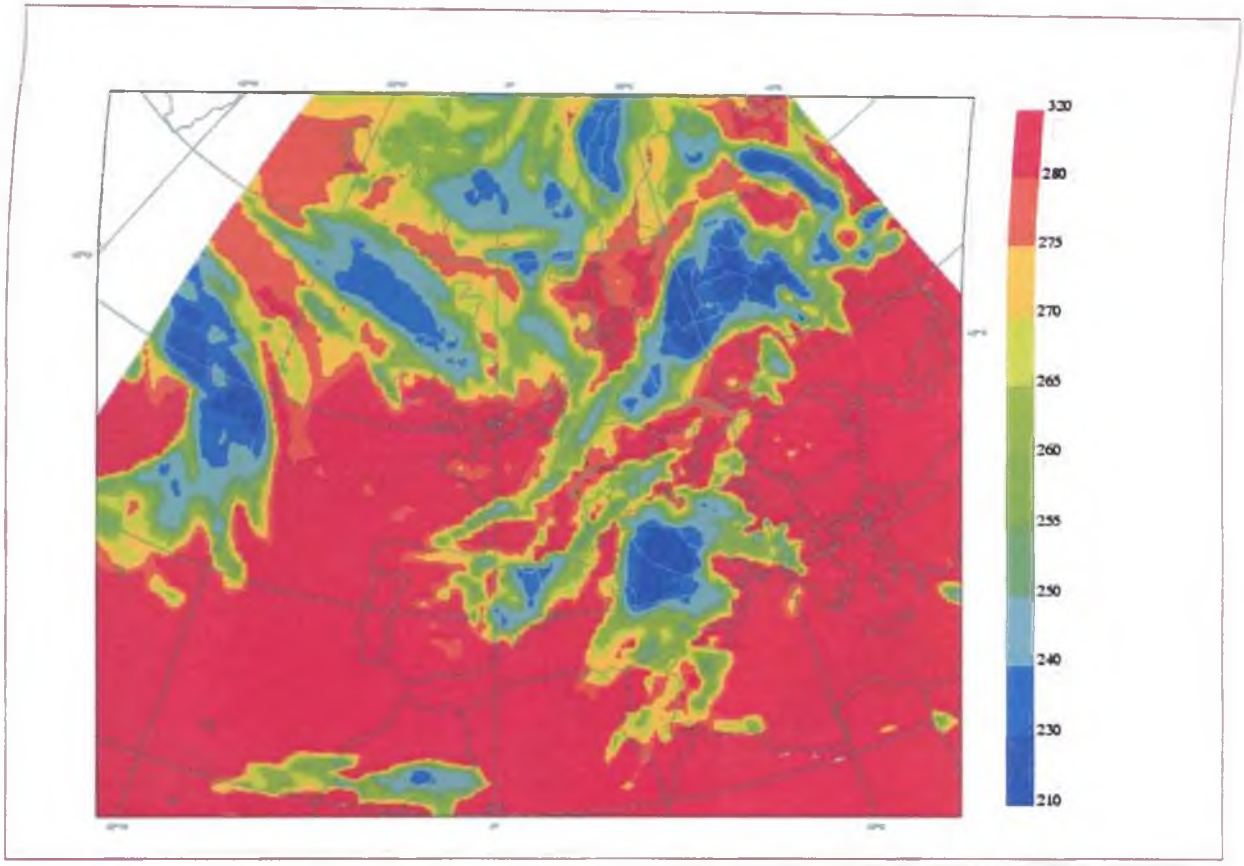

Fig. 113: Model forecast of the brightness temperatures (in K) of IR channel for May 17th 2005 12 UTC from May 16th 2005 00 UTC

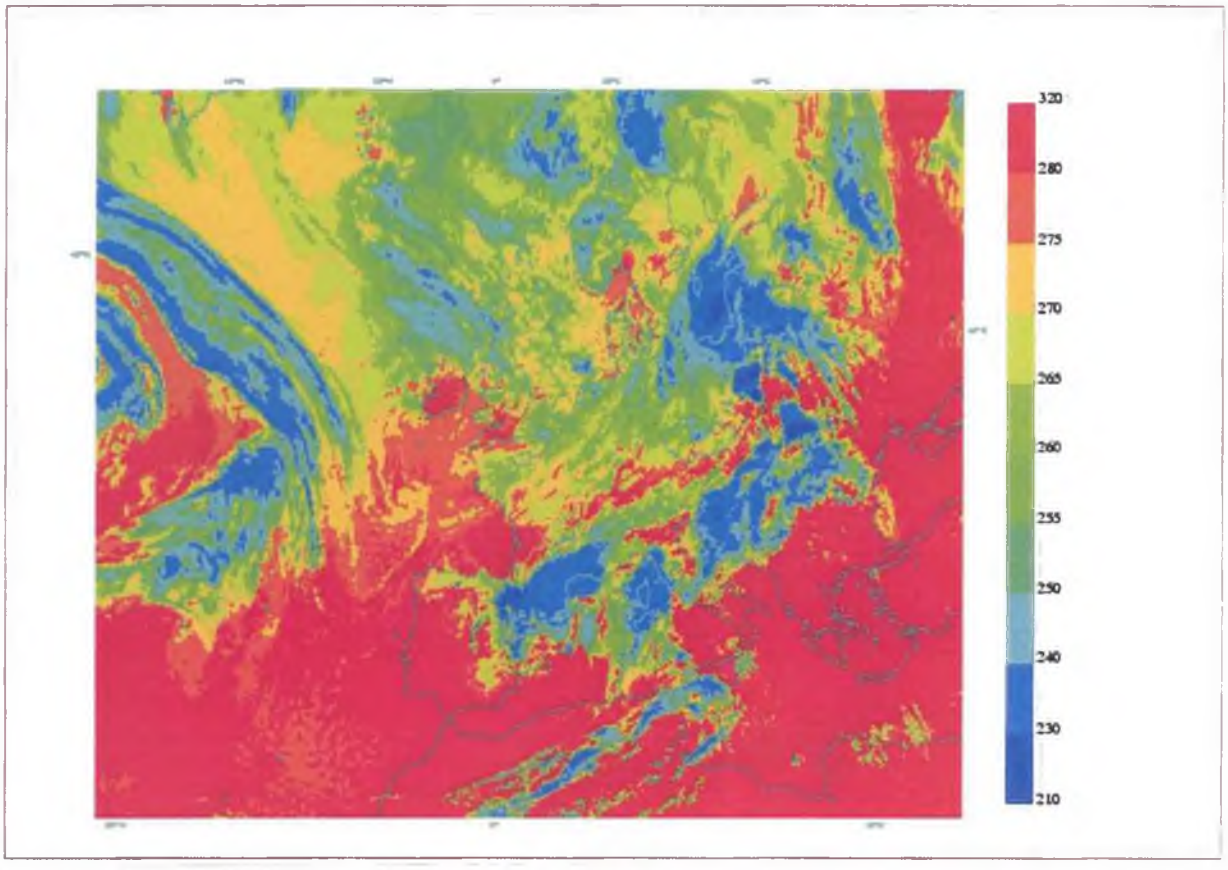

Fig. 114: IR channel image of METEOSAT-7 satellite, May 17th 2005 12 UTC

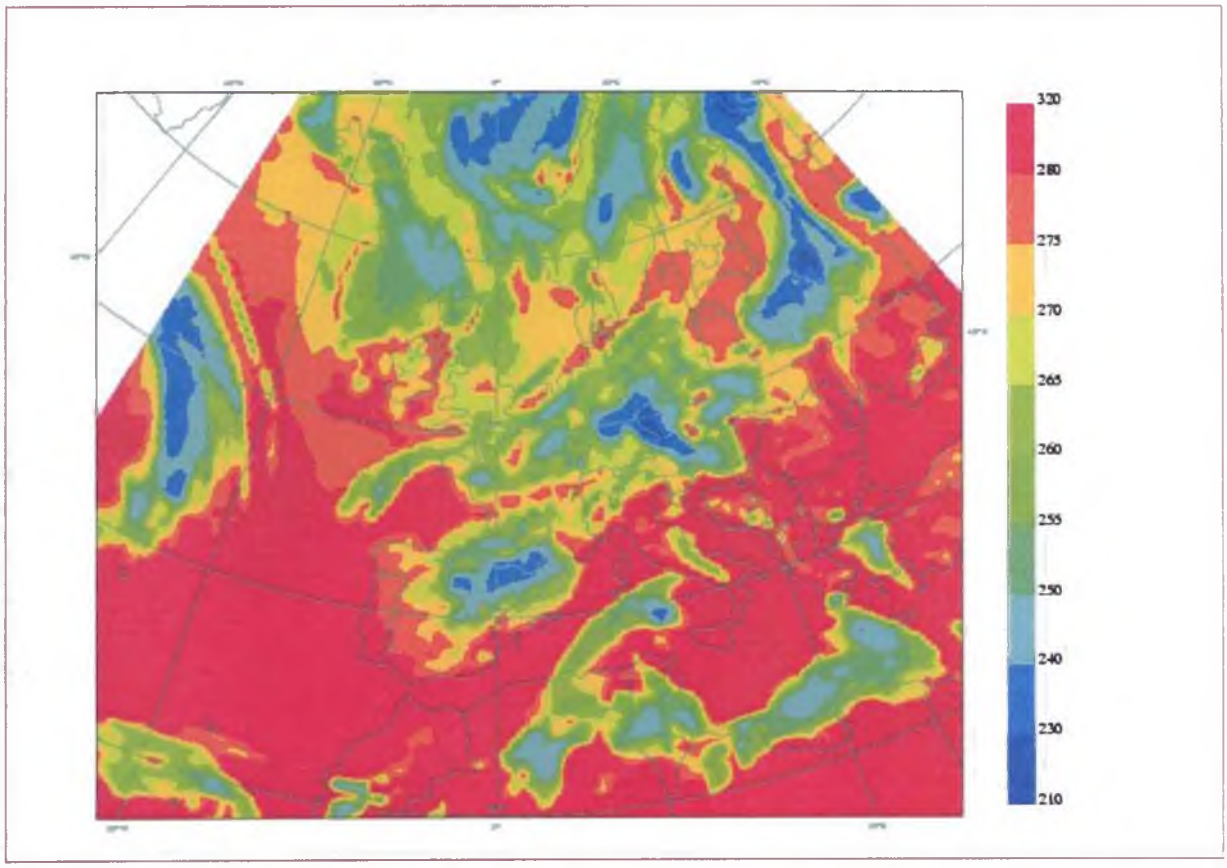

Fig. 115: Model analysis of the brightness temperatures (in K) of IR channel, May 17th 2005 00 UTC

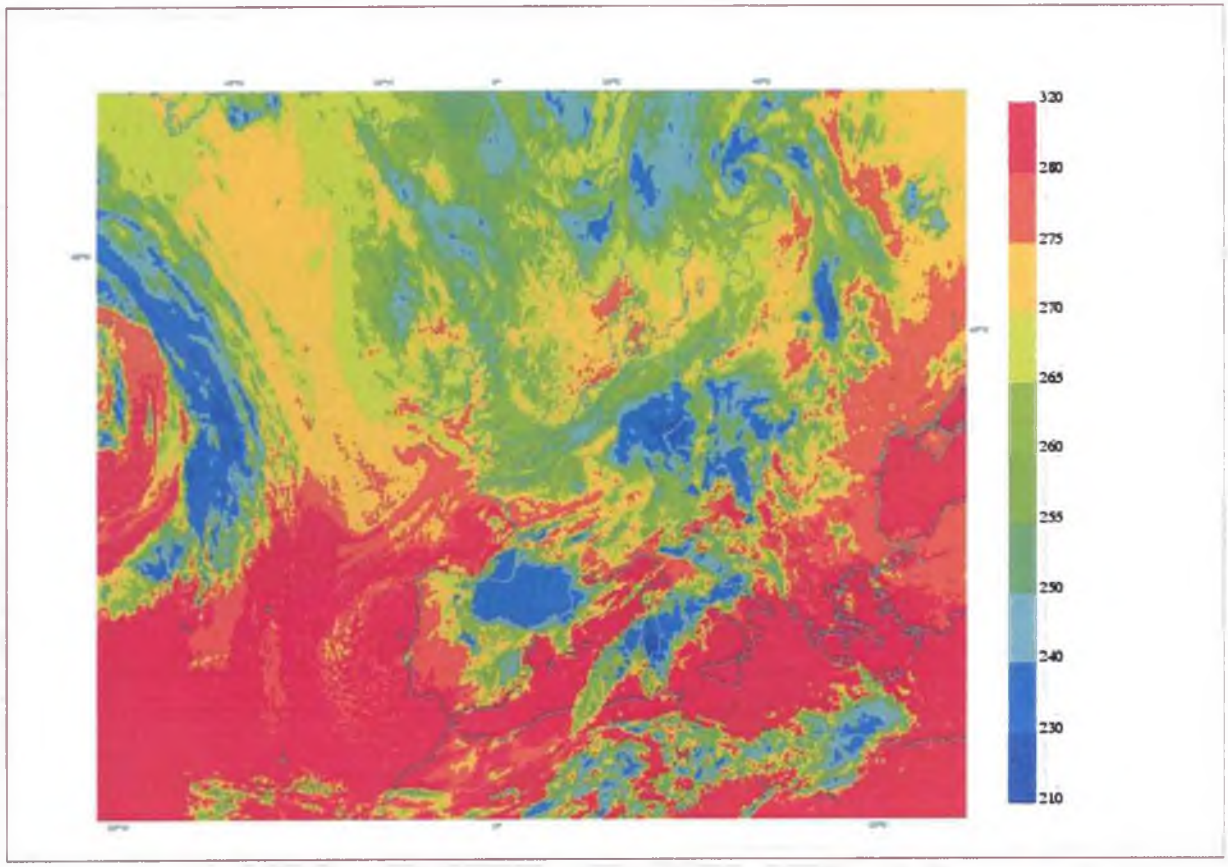

Fig. 116: IR channel image of METEOSAT-7 satellite, May 17th 2005 00 UTC

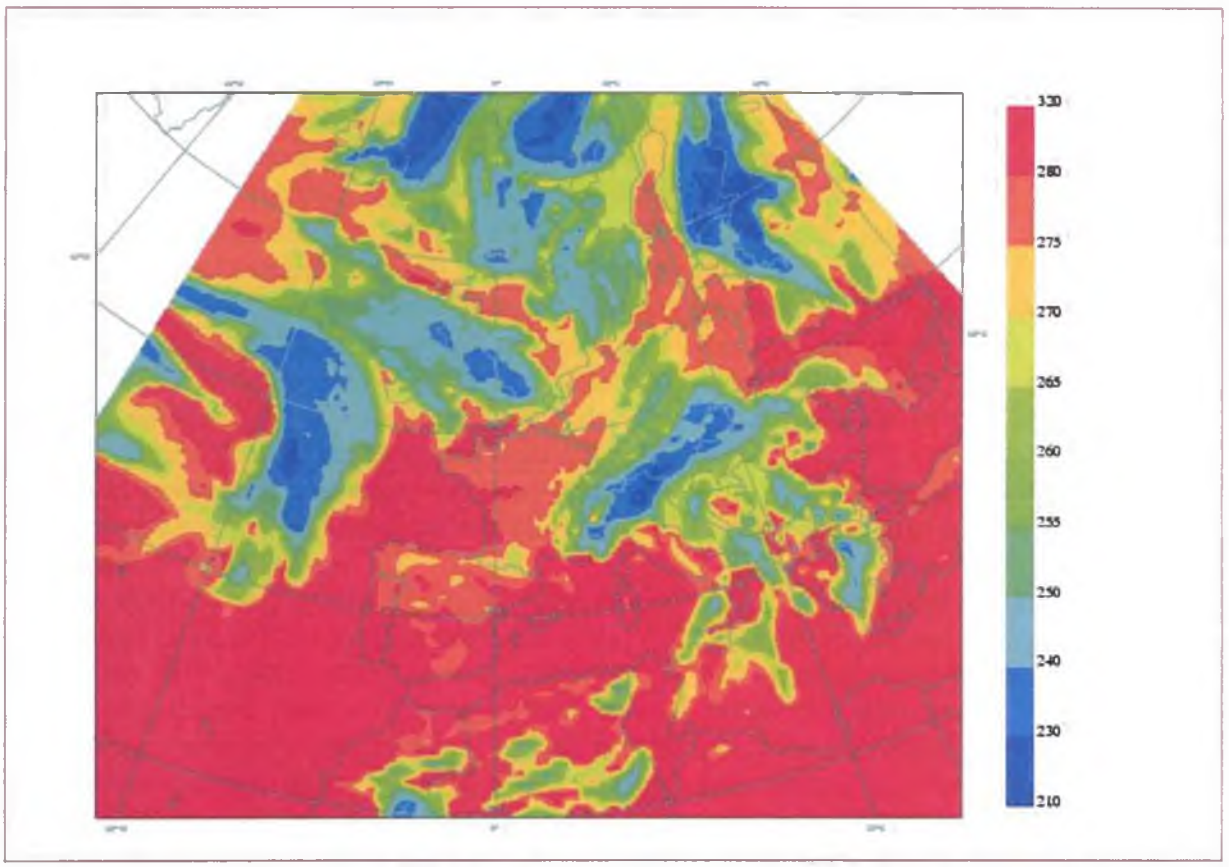

Fig. 117: Model forecast of the brightness temperatures (in K) of IR channel for May 18th 2005 00 UTC from May 17th 2005 00 UTC

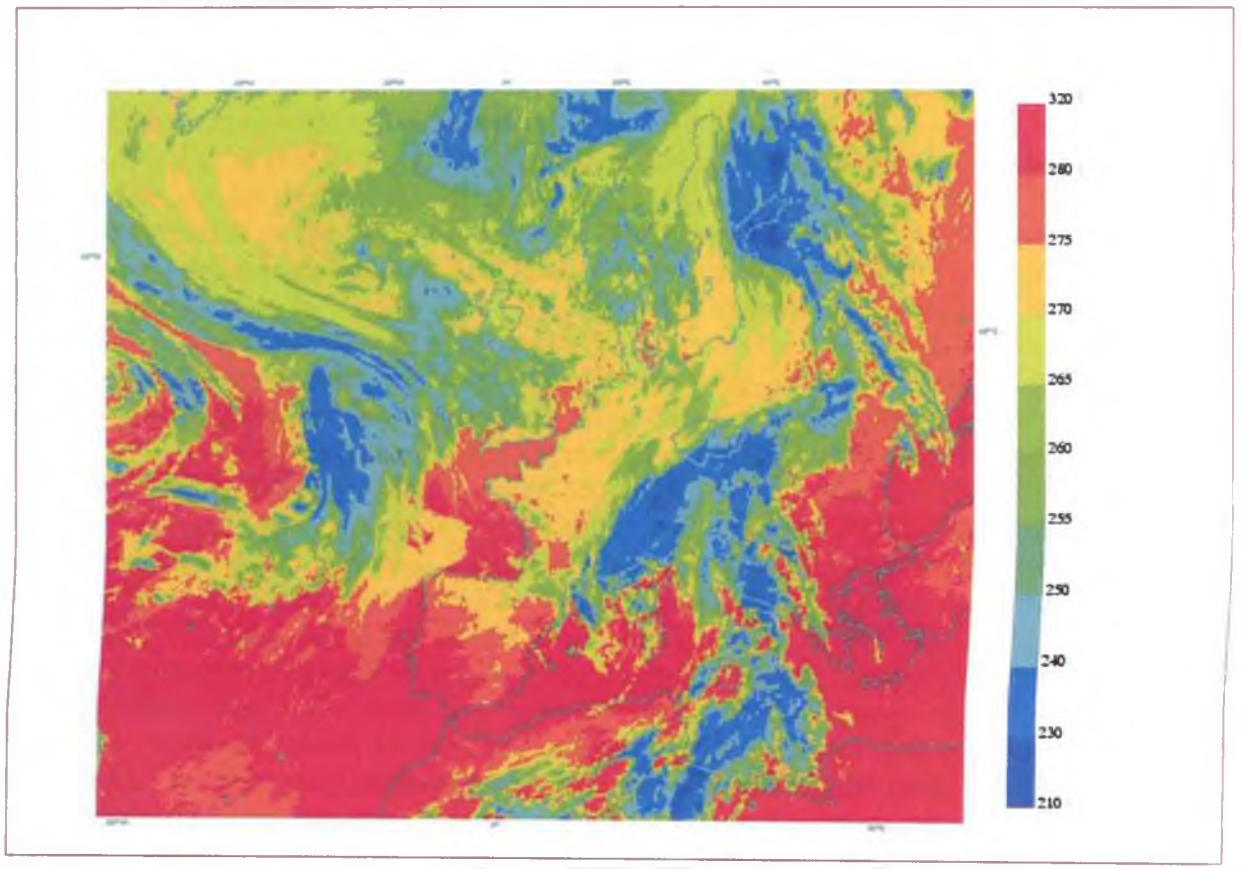

Fig. 118: IR channel image of METEOSAT-7 satellite, May 18th 2005 00 UTC

Chapter 5: Conclusions and discussions

Utilizing of Meteosat satellite data tio „model to satellite" approach for synoptic interpretation of numerical weather prediction model outputs, for studying of upper troposphere and tropopause dynamics and for comparison of these data with results of the numerical weather prediction (NWP) models has been the main ideas of this work. For this purpose the global model ARPEGE has been used as tool.

Simulation of the measured channels (in our case measured by Meteosat satellite) by the NWP model with their predicted variables has been realized in the form of forecasted brightness temperatures fields. These fields have been constructed for comparison between the results of simulated and measured channels. This comparison has been made for various prognostic times of model integrations up to 72 or 96 hours.

The content of this work has been oriented on the synoptic scale structures, such as tropopause anomalies, frontal structures and large cloud clusters/systems and their connection with intensive cyclogenesis.

In the first part of this work, the introduction and some historical review of synoptic meteorology from the Norwegian Meteorological School times to the end of the 20th century is presented with special attention to cyclone life cycles. Quasi-geostrophic theory and self-development theory then shortly described three-dimensional structure of cyclones and anticyclones. Isentropic perspective was also briefly mentioned. Special attention is paid to cyclogenesis studies, where several points having great impact on our knowledge about cyclogenesis process has been mentioned. And last but not least, the potential vorticity perspective has been discussed due to its very close relationship to the satellite images, mainly in connection with measurements in the water-vapour spectral bands.

In chapter 2, the application of modern knowledge about cyclogenesis and cyclones development with utilizing of satellite measurements has been presented. Some applications in this field have been described, too.

In chapter 3, the description of the computation scheme for the computation of brightness temperatures from the model ARPEGE is mentioned.

Several case studies have been described and studied in details in chapter 4. Here, the synoptic features for these case studies are presented, described and discussed with respect to their representation in the fields of brightness temperatures of NWP model outputs. Six case studies have been selected and studied. One of them was connected with catastrophical floods in the central Europe in August 2002. The synoptic situation was characterized by cyclone slowly moving from the central Mediterranean region to the North and Northeast. Next two case studies (October 2002 and November 2004) were associated with intensive cyclone development and caused strong gales and large damage in the various areas of the central Europe region. For both of them, well developed cyclones moved over central Europe from the west to east, but the case of November 2004 was a typical example of intensive secondary cyclone development on a frontal wave. One case (December 2004) was a typical situation when Christmas thaw in central Europe occurs. For this situation we have had relatively intensive west circulation with cyclones moving from Atlantic Ocean eastward over central Europe and bringing warm sea air in their warm sectors. The case of April 2005 was connected with cold front and its waves in the region of central Europe. And the case of May 2005 was interesting in the sense that two cyclones well developed in upper levels, the first one in the region of central Europe, the second one over Bay of Biscay, were quite badly forecasted by the numerical prediction obtained from the model ARPEGE.

From these case studies, it can be concluded that for intensive and fast developing cyclones, the forecast is usually satisfactory (cases of November 2004, partly also August 2002). Some difficulties were connected with forecasting of less explosive/intensive

development (e.g. December 2004), and the most problems were observed for case of April and May 2005. But it must be said, that the correlation between forecast quality and intensity of cyclone development is probably only small and the focus must be done on the quality of the model analysis.

Case studies described above show that this "model-to-satellite" scheme used for simulation of observed spectral bands in the Meteosat satellite measurements seems to be a good tool for model-to-satellite approach and provides possibilities for assessing of the representations of physical processes within the model. The problem consists in some underestimation of number of grids with the lowest brightness temperatures simulated by the NWP model in comparison with satellite observation. This can be caused by lower cloud tops and also by underestimation of total cloud cover. Good common agreement in synoptic features between model forecast and observations up to +48 or +72 h can be found. Some discrepancies are probably caused here rather by the other factors such as problems appearing during the numerical integration process than by unrealistic simulations in computation of brightness temperatures.

By this comparing of model versus satellite, it can be seen that model is reasonably successful in representation of the cloudiness in various levels and this cloudiness really impacts the top of the atmosphere brightness temperatures. Most of the main cloud systems are properly located. But, overall brightness temperature through high clouds is usually overestimated by the model (both in IR as well as in WV channel, see Figs. 20 and 21), with clouds either absent, not high or not optically thick enough. As for time evolution of the simulation and observed brightness temperatures the results are reasonable satisfactory.

Utilization of this method can help to the prognostic in validating and interpretations of the model analysis or the forecast on the base of comparison with the satellite data. This comparison in the so called observation space offers the possibility to make qualitative validation of the signification of synoptic weather structures forming the atmospheric circulation. So if the prognostic or other person responsible for the weather forecast have a possibility to compare model forecasts with this product, he would be able to correct the model forecast if there is a greater shift between model analysis/forecast and real satellite observations (for example, see situation from December 24th 2004 where the differences between the radiances analyzed by model ARPEGE and observed ones by Meteosat satellite could indicate the danger of fault forecast in some parts of the forecasted area) at least.

The disadvantage of the used scheme is connected with high expensivity in terms of computing time. That's why some other external computation schemes have been used, such as RTTOV - Radiative Transfer model based on TOVs (TOVS = TIROS Operational Vertical Sounder, equipment of NOAA's TIROS series of polar orbiting satellites). But generally, the disadvantage of the quite high computation time expensivity remains. That's why RTTOV is not used in operational practice nowadays yet. But hopefully, in the near future new integration cycle of ARPEGE (and for other numerical weather prediction models as well) is going to be used and it will have new version of model-to-satellite scheme, so that no special external procedures will be needed and the results will be available in real time to help the prognostic for the forecast validating.

Finally, one should mention that the using of the brightness temperatures is effective method for numerical weather prediction models validation but we cannot use them instead of other forecasted high level products. Rather we should use them in parallel way so that the validation of the models would be most effective.

REFERENCES

Anthem R.A., 1990. Advances in the understanding and prediction of cyclone development with limited-area fine-mesh models. *Extratropical Cyclones,* Palmén Memorial Volume, C.W. Newton and E.O. Holopainen, Eds. Amer. Meteor. Soc., 221-253.

Appenzeller C. and Davies H.C., 1992. Structure of stratospheric intrusions into the troposphere. *Nature*, **358**, 570-572.

Austin J.M., 1952. Development in the pressure field. *Massachusetts Institute of Technology Department of Meteorology tech. Rep.*, **11**, 1-43.

Ayrault, F. and Joly A., 2000. Une nouvelle typologie des dépressions météorologiques, classification des phases de maturation, *C. R. Acad. Sci. Paris*, **IIa 330**, 167-172.

Berne R.G. and Bates F.C., 1955. A mechanism for assisting in the release of convective instability. *Mon. Wea. Rev.*, **83**, 1-10.

Bell G.D. and Bossart L.F., 1989. A 15 year climatology of Northern Hemisphere 500 mb closed cyclone and anticyclone centre. *Mon. Wea. Rev.*, **117**, 2142-2163.

Bell G.D. and Bossart L.F., 1993. A case study diagnosis of the formation of an upper level closed cyclonic circulation over the eastern United States. *Mon. Wea. Rev.*, **121**, 1635-1655.

Bell G.D. and Bossart L.F., 1994. Midtropopsheric closed cyclone formation over the southwestern United States, the Eastern United States, and the Alps. *Mon. Wea. Rev.*, **122**, 1712-1729.

Bergeron T., 1934. Die dreidimensional verknüpfende Wetteranalyse. II. Teil: Dynamik und termodynamik der Fronten und Frontalstörungen. Übersetzung von W.I. Romanowskaja ans dem deutschen Manuskript, redigierst von S.P. Chromow. Ausgabe der Zentralverwaltung des Hydrometeorologischen Einheitsdienstes, Moskau (Russ.).

Bergeron T., 1937. On the physics of fronts. *Bull. Amer. Meteor. Soc.*, **18**, 265-275.

Bergeron T., 1959. Methods in scientific weather analysis and forecasting. An outline in the history of ideas and hints at a program. *The atmosphere and the Sea in Motion* (Rossby memorial volume), B. Bolin, Ed Rockefeller Institute Press, 440-474.

Bishop C.H., 1993. On the behavior of baroclinic wavesundergoing horizontal deformation. I: The "RT" phase diagram. *Quart. J. Roy. Meteor. Soc.*, **119**, 221-240.

Bishop C.H. and Thorpe A.J., 1994a. Frontal wave stability during moist deformation frontogenesis. Part I: Linear wave dynamics. *J. Atmos. Sci.*, **51**, 852-873.

Bishop C.H. and Thorpe A.J., 1994b. Frontal wave stability during moist deformation frontogenesis. Part II: The suppression of nonlinear wave development. *J. Atmos. Sci.*, **51**, 874-888..

Bjerknes J., 1937. Theorie der aussertropischen Zyklonenbildung. *Meteor. Zeits.*, **54**, 462-466.

Bjerknes J. and Palmén E., 1937. Investigations of selected European cyclones by means of serial ascents. *Geofys. Publ.*, **12**, 1-62.

Bjerknes J. and Solberg H., 1922. Life cycle of cyclones and the polar front theory of atmospheric circulation. *Geofys. Publ.*, **3**, (1), 1-18.

Bjerknes J., 1930. Practical examples of polar-front analysis over the British Isles in 1925-1926. Meteorological Office, *Geophysical Memoirs,* No. **50**, 50 pp.

Blackmon M. L., 1976. A climatological study of the 500 mb geopotential height of the Northern Hemisphere. *J. Atmos. Sci.*, **34**, 1607-1623.

Bleck R., 1990. Depiction of upper/lower vortex interaction associated with extratropical cyclogenesis. *Mon. Wea. Rev.*, 118, 573-585.

Bleck R., and Dole R.M., 1993. The dynamics of large-scale cyclogenesis over the North Pacific Ocean. *J. Atmos. Sci.*, 50, 421-442.

Bosart L.F., 1970. Mid-tropospheric frontogenesis. *Quart. J. Roy. Meteor. Soc.*, **96**, 442-471.

Bosart L.F., 1981. The President's Day snowstorm of 18-19 February 1979: A subsynoptic-scale event. *Mon. Wea. Rev.*, **112**, 2148-2177.

Bosart L.F., 1981. Observed cyclone life cycles. Proceedings, Symposium on "The Life Cycles of Extratropical Cyclones" Bergen, Norway, 27 June – 1 July 1994.

Bosart L.F. and Lin S.C., 1984. A diagnostic analysis of the President's Day storm of February 1979. *Mon. Wea. Rev.*, **112**, 2148-2177.

Bouniol D., Lemaítre Y. and Protat A., 2002. Upper- and lower-troposphere coupling processes involved in the FASTEX IOP16 frontal cyclone. *Quart. J. Roy. Meteor. Soc.*, **128**, 1211-1228.

Boyle J.S. and Bossart L.F., 1986. Cyclone-anticyclone couplets over North America. Art II: Analysis of a major cyclone event over the eastern United States. *Mon. Wea. Rev.*, **114**, 2432-2465.

Briggs J. and Roach W.T., 1963. Aircraft observations near jet streams. *Quart. J. Roy. Meteor. Soc.*, **89**, 225-247.

Browning K.A., 1986. Conceptual models of precipitation systems. *Wea. Forecast.*,1, 23-41.

Browning K.A., 1990. Organization of Clouds and Precipitation in Extratropical Cyclones. *Extratropical Cyclones*, Palmén Memorial Volume, C.W. Newton and E.O. Holopainen, Eds. Amer. Meteor. Soc., 129-153.

Browning K.A. and Harrold T.W., 1969. Air motion and precipitation growth in a wave depression. *Quart. J. Roy. Meteor. Soc.*, **95**, 288-309.

Browning K.A. and Monk G.A., 1982. A simple model for the synoptic analysis of cold fronts. *Quart. J. Roy. Meteor. Soc.*, **108**, 435-452.

Bullock T.A. and Gyakum J.R., 1993. A diagnostic study of cyclogenesis in the western North Pacific Ocean. *Mon. Wea. Rev.*, **121**, 66-75.

Carlson T.N., 1980. Airflow trough midlatitude cyclones and the comma cloud pattern. *Mon. Wea. Rev.*, **108**, 1498-1509.

Carr F.H. and Millard J.P., 1985. A composite study of comma clouds and their association with severe weather over the Great Plains. *Mon. Wea. Rev.*, **113**, 370-387.

Carrol E.B., 1997. A technique for consistent alteration of NWP output fields. *Meteor. Appl.*, **4**, 142-160.

Chaboreau J.P., Cammas J.P., Mascart P., Pinty J.P., Claud C., Roca R. and Morcrette J.J., 2000. Evaluation of a cloud system life-cycle simulated by Meso-NH during FASTEX using METEOSAT radiances and TOVS-3I cloud retrievals. *Quart. J. Roy. Meteor. Soc.*, 126, 1735-1750.

Chang E.K. and M Orlanski I., 1993. On the dynamics of a storm track. *J. Atmos. Sci.*, **50**, 999-1015.

Charney J., 1947. The dynamics of long waves in a baroclinic westerly current. *J. Meteor.*, **4**, 125-162.

Chen S.J. and Dell'Osso L., 1987. A numerical case study of East Asian coastal cyclogenesis. *Mon. Wea. Rev.*, **115**, 477-487.

Chen S. J., Kuo H., Zhang P.Z. and Bai Q.F., 1991. Synoptic climatology of cyclogenesis over East Asia, 1958-1987. *Mon. Wea. Rev.*, **119**, 1407-1418.

Chevalier F., Bauer P., Kelly G., Jakob C. and Mc Nally T., 2001. Model clouds over ocean as seen from space: Comparison with HIRS/2 and MSU radiances. *J. Climate*, 14, 4216-4229.

Chevalier F. and Kelly G., 2002. Model clouds as seen from space: Geostationary imagery in the 11-micrometers Windows channel. *Mon. Wea. Rev.*, 130, 712-722.

Colucci S.J., 1985. Explosive cyclogenesis and large-scale circulation changes: Implications for atmospheric blocking. *J. Atmos. Sci.*, **42**, 2701-2717.

Colucci S.J. and Davenport J.C., 1987. Rapid surface anticyclogenesis: Synoptic climatology and attendant large-scale circulation changes. *Mon. Wea. Rev.*, **115**, 822-836.

Courtier P., Anderson E., Heckley W., Pailleux J., Vasiljevic D., Hamrud M., Hollingsworth A., Rabies F. and Fischer M., 1998. The ECMWF implementation of three dimensional variational assimilation (3D-Var). Part I: Formulation. *Q. J. R. Meteorol. Soc.*, **124**, 1783-1808.

Danard M.B., 1964. On the influence of released latent heat on cyclone development. *J. Appl. Meteor.*, **3**, 27-37.

Danielsen E.F., 1961. Trajectories: Isobaric, isentropic and actual. *J. Meteor.*, **18**, 479-486.

Danielsen E.F., 1964. Project Springfield Report. Defense Atomic Support Agency, Washington D.C. 20301, DASA 1517, 97 pp.

Danielsen E.F., 1966. Research in four-dimensional diagnosis of cyclonic storm cloud systems. The Pennsylvania State University, Scientific Report no. 1, AFRCL 66-30, pp 1-53.

Danielsen E.F. and Bleck R., 1967. Research in four-dimensional diagnosis in cyclonic storm cloud systems. The Pennsylvania State University, Final Scientific Report, AFRCL 67-0617, pp 1-96.

Danielsen E.F., Hipskind R.T., Gaines S.E., Sachse G.W., Gregory G.L. and Hill G.F., 1987. Three-dimensional analysis of potential vorticity associated with tropopause folds and observed variations of ozone and carbon monoxide. *J.Geophys. Res.*, **82**, 5867-5878.

Davis C.A., 1992. A potential-vorticity diagnosis of the importance of initial structure and condensational heating in observed extratropical cyclogenesis. *Mon. Wea. Rev.*, **116**, 2649-2659.

Davis C.A., 1993. Comments on "Decomposing the atmospheric flow using potential vorticity framework". *J. Atmos. Sci.*, **50**, 2065-2067.

Davis C.A. and Emanuel K.A., 1991. Potential vorticity diagnostics of cyclogenesis. *Mon. Wea. Rev.*, **119**, 1929-1953.

Davies H.C., Schär Ch. and Wernli H., 1991. The palette of fronts and cyclones within a baroclinic wave-development. *J. Atmos. Sci.*, **48**, 1666-1689.

DiMego G.J. and Bossart L.F., 1982a. The transformation of tropical storm Agnes into an extratropical cyclone. Part I: The observed fields and vertical motion computations. *Mon. Wea. Rev.*, **110**, 385-411.

DiMego G.J. and Bossart L.F., 1982b. The transformation of tropical storm Agnes into an extratropical cyclone. Part II: Moisture, vorticity and kinetic energy budgets. *Mon. Wea. Rev.*, **110**, 412-433.

Dines W.H., 1911. The vertical temperature distribution on the atmosphere over England, with some remarks on the general and local circulation. *Phil. Trans.*, Ser. A., **211**, 253-278.

Eady E.J., 1949. Long waves and cyclone waves. *Tellus*, **1**, 33-52.

Eliassen A., 1962. On the vertical circulation in frontal zones. *Geofys. Publ.*, **24**, 147-160.

Farrell B.F., 1985. Transient growth of damped baroclinic waves. *J Atmos. Sci.*, **42**, 2718-2727.

Farrell B.F., 1988. Optimal excitation of neutral Rossby waves. *J. Atmos. Sci.*, **45**, 163-172.

Farrell B.F., 1989. Optimal excitation of baroclinic waves. *J. Atmos. Sci.*, **42**, 1193-1206.

Farrell B.F., 1990. Small error dynamics and the predictability of atmospheric flows. *J. Atmos. Sci.*, **47**, 2409-2416.

Fouquart Y. and Bonnel B., 1980. Computation of solar heating of the Earth's atmosphere: A new parameterization. *Beitr. Phys. Atmos.*, **53**, 35-62.

Fourrie N., Claud Ch., Donnadille J., Cammas J.P., Pouponneau B. and Scott N., 2000. The use of TOVS observation for the identification of tropopause-level thermal anomalies. *Quart. J. Roy. Meteor. Soc.*, **126**, 1473-1494.

Fourrie N., Claud Ch. and Chédin A., 2003. Depiction of Upper-Level Precursors of the December 1999 Storms from TOVS Observations. *Wea. Forecasting*, **10**, 417-430.

Ficker H.v., 1920. Beziehung zwischen Änderungen des Luftdruckes und der Temperatur in der unteren Schichten der Troposphäre (Zusammensetzung der Depressionen). *Sitzber. Akad. Wiss. Wien, Math. Naturn. Kl. Abt. IIa*, **129**, 763-810.

Fleagle R.G., 1948. Quantitative analysis of factors influencing pressure change. *J. Meteor.*, **5**, 281-291.

Flobert J.F., Anderson E., Chedin A., Hollingsworth A., Kelly G., Pailleux J. and Sčoty N.A., 1991. Global data assimilation and forecast experiments using the improved initialization inversion method for satellite soundings. *Mon. Wea. Rev.*, **119**, 1881–1914.

Georgiev Ch., 1999. Quantitative relationship between Meteosat WV data and positive potential vorticity anomalies: a case study over the Mediterranean. *Meteor. Appl.*, **6**, 97-109.

Gronas S. and Shapiro M.A., 1997. *The Life Cycles of Extratropical cyclones.* Amer. Meteor. Soc., 300 pp.

Gyakum J.R., Roebber P.J. and Bullock T.A., 1992. The role of antecedent surface vorticity development as a conditioning process in explosive cyclone intensification. *Mon. Wea. Rev.*, **120**, 1465-1489.

Hakim G.J., Keyser D. and Bosart L.F., 1994. Diagnosis of wave-merger cyclogenesis through quasi-geostrophic potential vorticity inversion. Symposium on "The Life Cycles of Extratropical Cyclones" Bergen, Norway, 27 June – 1 July 1994.

Harris B.A. and Kelly G., 2001. A satellite radiance-bias correction scheme for data assimilation. *Quart. J. Roy. Meteor. Soc.*, **127**, 1453-1468.

Hirschberg P.A. and Fritsch J.M., 1991. Tropopause undulations and the development of extratropical cyclones. Part I: Overview and observations from a cyclone event. *Mon. Wea. Rev.*, **119**, 496-517.

Hirschberg P.A., Spencer R.W., Parke M.C., Wash C.H. and Mickelinc, M., 1997. The Usefulness of MSU3 Analyses as a Forecasting Aid: A Statistical Study. *Wea. Forecasting*, **12**, 324-346.

Hobbs P.V., Locatelli J.D. and Martin J.E., 1990. Cold front aloft and the forecasting of precipitation and severe weather east of the Rocky Mountains. *Wea. Forecast.*, **5**, 613-626.

Holopainen E. and Kaurola J., 1991. Decomposing the atmospheric flow using potential vorticity framework. *J. Atmos. Sci.*, **48**, 2614-2625.

Holton J.R., 1992. An Introduction to Dynamic Meteorology, 3rd Edition, Academic Press, 511 pp.

Hoskins B.J., 1990. Theory of extratropical cyclones. Extratropical Cyclones. In: *Palmén Memorial Volume*, Amer. Meteor. Soc., 63-80.

Hoskins B.J. and Heckley W.A.., 1981. Cold and warm fronts in baroclinic waves. *Quart. J. Roy. Meteor. Soc.*, **107**, 79-90.

Hoskins B.J., McIntyre M.E. and Robertson A.W., 1985. On the use and significance of isentropical potential vorticity maps. *Quart. J. Roy. Meteor. Soc.*, **111**, 877-946.

Hoskins B.J. and West N.V., 1979. Baroclinic waves and frontogenesis. Part II: Uniform potential vorticity jet flows-cold and warm fronts. *J. Atmos. Sci.*, **36**, 1663-1680.

Hövmöller E., 1949. The trough-and-ridge diagram. *Tellus*, **1**, 62-66.

Iskenderian H., 1988. Three-dimensional airflow and precipitation structure in a nondeepening cyclone. *Wea. Forecasting*, **3B**, 18-32.

Jakob C. and Klein S.A., 2000. A parameterization of the effects of cloud and precipitation overlap for use in general circulation models. *Quart. J. Roy. Meteor. Soc.*, **126**, 2525-2544.

Joly A., 1995. The stability of steady fronts and the adjoint method: Nonmodal frontal waves. *J. Atmos. Sci.*, **52**, 3082-3108.

Joly A. et all, 1997. The fronts and Atlantic storm-track experiment (FASTEX): Scientific objectives and experimental design. *Bull. Amer. Meteor. Soc.*, **78**, 1917-1940.

Joly A. and Thorpe A.J., 1990. Frontal instability generated by tropospheric potential vorticity anomalies. *Quart. J. Roy. Meteor. Soc.*, **116**, 525-560.

Jurry M. and Laing M., 1990. A case study of marine cyclogenesis near Cape Town. *Tellus*, **42A**, 246-258.

Keishishian L.G., Bosart L.F. and Bracken E.W., 1994. Inverted troughs and cyclogenesis over interior North America: A limited regional climatological and case studies. *Mon. Wea. Rev.*, **122**, 5656-607.

Klein S.A. and Jakob C., 1999. Validation and sensitivities of frontal clouds simulated by the ECMWF model. *Mon. Wea. Rev.*, **127**, 2514-2531.

Klein W.H., 1958. The frequency of cyclones and anticyclones in relation to the mean circulation. *J. Meteor.*, **15**, 98-102.

Kleinschmidt E., 1950a. Über Aufbau und Entstehung von Zyklonen (1. Teil). *Met. Runds.*, **3**, 1-6.

Kleinschmidt E., 1950b. Über Aufbau und Entstehung von Zyklonen (2. Teil). *Met. Runds.*, **3**, 54-61.

Krishnamurti T.N., 1968. A study of developing wave cyclone. *Mon. Wea. Rev.*, **96**, 208-217.

Kuo Y.H., Shapiro M.A. and Donall E.G., 1991a. The interaction between baroclinic and diabatic processes in a numerical simulation of a rapidly intensifying extratropical marine cyclone. *Mon. Wea. Rev.*, **119**, 368-384.

Kuo Y.H., Reed R.J. and Low-Nam S., 1991b. Effects of surface energy fluxes during the early development and rapid intensification stages of seven explosive cyclones in the western Atlantic. *Mon. Wea. Rev.*, **119**, 457-476.

Kuo Y.H and Reed R.J., 1988. Numerical simulation of an explosively deepening cyclone in the eastern Pacific. *Mon. Wea. Rev.*, **116**, 2081-2105.

Lackmann G.M., Keyser D. and Bosart L.F., 1994. On the evolution of mobile upper-tropospheric troughs preceding western North Atlantic cyclogenesis during ERICA. Symposium on "The Life Cycles of Extratropical Cyclones" Bergen, Norway, 27 June – 1 July 1994.

Le Treut H. and Li Z.X., 1989. Comparison of GCM results with data from operational metrological satellites. *Ocean-Air Interact.*, 221 - 237.

Malardel S., Joly A., Courbet F. and Courtier Ph., 1993. Non-linear evolution of ordinary frontal waves induced by low-level potential vorticity anomalies. *Quart. J. Roy. Meteor. Soc.*, **119**, 671-713.

Mannsfield D.A., 1996. The use of potential vorticity as an operational tool. *Met. Apps.*, **3**, 196-210.

Manual of Synoptic Satellite Meteorology, Version 6.0, **http://www.zamg.ac.at/docu/Manual/SatManu/main.htm**, web-page, ZAMG, Austria (2006).

Mass C.F and Schultz D.M., 1993. The structure and evolution of a simulated midlatitude cyclone over land. *Mon. Wea. Rev.*, **121**, 889-917.

Mlawer E.J., Taubman S.J., Brown P.D., Iacono M.C. and Clough S.A., 1997. Radiative transfer for inhomogeneous atmospheres: RRTM, a validated correlated-k model for the longwave. *J. Geophys. Res.*, **102D**, 16663-16682.

Montgomerry R.B., 1937. A suggested method for representing gradient flow in isentropic surfaces. *Bull. Amer. Meteor. Soc.*, **18**, 210-212.

Morcrette J.J., 1991. Evaluation of model-generated cloudiness: Satellite observed and model-generated diurnal variability of brightness temperature. *Mon. Wea. Rev.*, **119**, 1205-1224.

Morcrette J.J., Buriez J.C., Bonnel B., Fouquart Y. and Geleyn J.F., 1988. Comparison of model-generated and satellite-derived cloud cover and radiation budget. *J. Geophys. Res.*, **93**, 3705-3719.

Morcrette J.J., Chevalier F., Buriez J.C. and Hennequart F., 2001. Using Satellite Radiation Measurements for Model Evaluation, *material ECMWF*, 22 pp.

Namias J., 1938. Thunderstorm forecasting with the aid of isentropic charts. *Bull. Amer. Meteor. Soc.*, **19**, 1-14.

Namias J., 1939. The use of isentropic analysis in short term forecasting. *Journal of Aeronautical Sciences.* **6**, 295-298.

Namias J. and Clapp P.F., 1949. Confluence theory of the high tropospheric jet stream. *J. Meteor.*, **6**, 330-336.

Newton C.W., 1954. Frontogenesis and frontolysis as a three-dimensional process. *J. Meteor., 11,* 449-461.

Newton C.W. and Palmén E., 1963. Kinematic and thermal properties of a large-amplitude wave in the westerlies. *Tellus*, **15**, 99-119.

Orlanski I. and Chang E.K.M., 1993. Ageostrophic geopotential fluxes in downstream and upstream development of baroclinic waves. *J. Atmos. Sci.*, **50**, 212-225.

Orlanski I. and Sheldon J., 1993. A case of downstream baroclinic development over western North America. *Mon. Wea. Rev.*, **121**, 2929-2950.

Palmén E., 1949. On the origin and structure of high-level cyclones south of the maximum westerlies. *Tellus*, **1**, 22-31.

Palmén E., 1951. The aerology of extratropical disturbances. *Compendium of Meteorology*, T.F. Malone, Ed. American Meteorological Society, 599-620.

Palmén E., 1958. Vertical circulation and release of kinetic energy during the development of hurricane Hazel into an extratropical cyclone, *Tellus*, **10**, 1-23.

Palmén E., 1959. On the maintenance of kinetic energy in the atmosphere. *The Atmosphere and the Sean Motion* (Rossby Memorial Volume), B. Bolin, Ed. Rockefeller Institute Press, 212-224.

Palmén E., 1961. On conversion between potential and kinetic energy in the atmosphere. *Geofis. Pura e Appl.*, **49**, 167-177.

Palmén E. and Holopainen E.O., 1962. Divergence, vertical velocity and conversion between potential and kinetic energy in an extratropical disturbance. *Geophysica*, **8**, 89-113.

Palmén E. and Newton C.W., 1951. On the three-dimensional motions in an outbreak of polar air. *J. Meteor.*, **8**, 25-39.

Palmén E. and Newton C.W., 1969. Atmospheric Circulation Systems: Their Structure and Physical Interpretation. Academic Press, 603 pp.

Parker S.S., Hawes J.T., Colucci S. J. and Hayden B.P., 1989. Climatology of 500 mb cyclones and anticyclones, 1950-1985. *Mon. Wea. Rev.*, **117**, 558-570.

Petterssen S., 1955. A general survey of factors influencing development at sea level. *J. Meteor.*, **12**, 36-42.

Petterssen S., 1956. *Weather Analysis and Forecasting*, Vol. I, 2nd ed., McGraw Hill, 428 pp.

Petterssen S., Bradbury D.L. and Pedersen K., 1962. The Norwegian cyclone models in relation to heat and cold sources. *Geofys. Publ.*, **24**, 243-280.

Petterssen S. and Smebye J., 1971. On the development of extratropical cyclones, *Quart. J. Roy. Meteor. Soc.*, **97**, 457-482.

Phillips N.A., 1963. Geostrophic motion. *Rev. Geophys.*, **1**, 123-176.

Rabier F., Jarvinen H., Klinker E., Mahfouf J.-F. and Simmons A., 2000. The ECMWF operational implementation of four-dimensional variational assimilation. Part I: Experimental results with simplified physics. *Quart. J. Roy. Meteor. Soc*, **126**, 1143-1170.

Raisanen P., 1998. Effective longwave cloud fraction and maximum-random overlap of clouds: A problem and a solution. *Mon. Wea. Rev.*, **126**, 3336–3340.

Ramanathan V., 1987. Atmospheric General Circulation and Its Low Frequency Variance: Radiative Influences, *Jour. of the Meteor. Soc. of Japan*, **Special Volume**, 1512-1576.

Ramanathan V., Barkstrom B.R. and Harrison E.F., 1989. Climate and the Earth's Radiation Budget. *Physics Today*, **42(5)**, 22-33.

Reed R.J., 1955. A study of a characteristic type of upper-level frontogenesis. *J. Meteor.*, **12**, 542-552.

Reed R.J., Grell G.A. and Kuo Y.H., 1993a. The ERICA IOP5 Storm. Part I: Analysis and simulation. *Mon. Wea. Rev.*, **121**, 1577-1594.

Reed R.J., Grell G.A. and Kuo Y.H., 1993b. The ERICA IOP5 Storm. Part II: Sensitivity tests and further diagnosis based on model output. *Mon. Wea. Rev.*, **121**, 1595-1612.

Reed R.J. and Sanders F., 1953. An investigation of the development of a mid-tropospheric frontal zone and its associated vorticity field. *J. Meteor.*, **10**, 338-349.

Reed R.J., Stoellinga M.T. and Kuo Y.H., 1992. A model-aided study of the origin and evolution of the anomalously high potential vorticity in the inner region of a rapidly deepening marine cyclone. *Mon. Wea. Rev.*, **120**, 893-913.

Ringer M.A., Edwards J.M. and Slingo A., 2002. Simulation of satellite channel radiances in the Met Office Unified Model. *Quart. J. Roy. Meteor. Soc.*, **129**, 1169-1190.

Rizzi R., 1994. Raw HIRS/2 radiances and model simulations in the presence of clouds. *ECMWF Tech. Memo. No.* **73**, 29 pp.

Roca R., Picon L., Desbois M., Le Treut H. Morcrette J.J., 1997. Direct comparison of Meteosat water vapour channel and general circulation model results, *Geophys. Res. Lett.*, **24**, 147-150.

Roebber P.J., 1984. Statistical analysis and updated climatology of explosive cyclones. *Mon. Wea. Rev.*, **112**, 1577-1589.

Roebber P.J., 1989. On the statistical analysis of cyclone deepening rates. *Mon. Wea. Rev.*, **117**, 2293-2298.

Rogers E. and Bosart L.F., 1986. An investigation of explosive deepening oceanic cyclones. *Mon. Wea. Rev.*, **114**, 702-718.

Rogers E. and Bosart L.F., 1991. A diagnostic study of two intense oceanic cyclones. *Mon. Wea. Rev.*, **119**, 967-997.

Rohn M., Kelly G. and Saunders R., 1999. Impact of a new cloud motion wind product from Meteosat on NWP analyses and forecasts. *Mon. Wea. Rev.*, **129**, 2392-2403.

Rossby, C.G. and Collaborators, 1937a. Aerological evidence of large-scale mixing in the atmosphere. Trans. Amer. Geophys. Union, 19th annual meeting.

Rossby, C.G. and Collaborators, 1937b. Isentropic analysis. *Bull Amer. Met. Soc.*, **18**, 201-209.

Rossby, C.G., 1940. Planetary flow patterns in the atmosphere. *Quart. J. Roy. Meteor. Soc.*, **66**, 68-87.

Rossby C.G. and Willett H.C., 1948: The circulation of the upper troposphere and lower stratosphere. *Science,* 108, 643–652.

Rossow W.B., Mosher F., Kinsella E., Arking A., Desbois M., Harrison E., Minnis P., Ruprecht E., Seze G., Sommer C. and Smith E., 1985. ISCCP cloud algorithm intercomparison. *J. Climate Appl. Meteor.*, **24**, 877-903.

Sanders F., 1986. Explosive cyclogenesis over the West-Central North Atlantic Ocean, 1981-1984. Part I: Composite structure and mean behaviour. *Mon. Wea. Rev.*, **114**, 1781-1794.

Sanders F., 1988. Life history of mobile troughs in the upper westerlies. *Mon. Wea. Rev.*, **116**, 2629-2648.

Sanders F., Bosart L.F. and Lai C.C:, 1991. Initiation and evolution of an intense upper-level front. *Mon. Wea. Rev.*, **119**, 1337-1367.

Sanders F., 1987. A study of 500 mb vorticity maxima crossing the East Coast of North American and associated surface cyclogenesis. *Wea. Forecasting*, **2**, 70-83.

Sanders F. and Gyakum J.R., 1980. Synoptic-dynamic climatology of the "bomb". *Mon. Wea. Rev.*, **108**, 1589-1606.

Sawyer J.S., 1956. The vertical circulation at meteorological fronts and its relation to frontogenesis. *Proc. Roy. Soc. London*, **A234**, 346-362.

Santurette P. and Georgiev Ch., 2005. Weather Analysis and Forecasting: Applying Satellite Water Vapor Imagery and Potential Vorticity Analysis, Elsevier Academic Press, 200 p.

Saunders R., Matricardi M. and Brundel P., 1999. An improved fast radiative transfer model for assimilation of satellite radiance observations. *Quart J. Roy. Meteor. Soc.*, **125**, 1407-1425.

Schmetz J. and van de Berg L., 1994. Upper-tropospheric humidity observations from METEOSAT compared with short term forecast fields. *Geophys. Res. Lett.*, **21**, 573-576.

Schmetz Y.J., Holmund K., Hoffman J., Strauss B., Mason B., Gaertner V., Koch A. and van de Berg L., 1993. Operational cloud-motion winds from Meteosat infrared images. *J. Appl. Meteor.*, **32**, 1206-1225.

Schultz D.M. and Mass C.F., 1993. The occlusion process in a midlatitude cyclone over land. *Mon. Wea. Rev.*, **121**, 918-940.

Shapiro M.A., 1974. A multiple structured frontal zone-jet stream system as revealed by meteorologically instrumented aircraft. *Mon. Wea. Rev.*, **102**, 244-253.

Shapiro M.A., 1976. The role of turbulent heat flux in the generation of potential vorticity in the vicinity of upper-level jet stream systems. *Mon. Wea. Rev.*, **104**, 892-906.

Shapiro M.A., 1980. Turbulent mixing within tropopause folds as a mechanism for the exchange of chemical constituents between the stratosphere and troposphere. *J. Atmos. Sci.*, **37**, 994-1004.

Sinclair M.R., 1993. Synoptic-scale diagnosis of the extratropical transition of a southwest Pacific tropical cyclone. *Mon. Wea. Rev.*, **121**, 941-960.

Slingo J., 1987. The development and verification of a cloud prediction scheme for the ECMWF model. *Quart J. Roy. Meteor. Soc.*, **113**, 899-927.

Soden B. J. and Bretherton F.P., 1994. Evaluation of water vapor distribution in general circulation models using satellite observations. *J. Geophys. Res.*, **99**, 1187–1210.

Staley D.O., 1960. Evaluation of potential vorticity changes near the tropopause and the related vertical motions, vertical advection of vorticity and transfer of radioactive debris from stratosphere to troposphere. *J. Meteor.*, **17**, 591-620.

Starr V.P. and Neiburger M., 1940. Potential vorticity as a conservative property. *J. Marine Res.*, **3**, 202-210.

Sutcliffe R.C., 1947. A contribution to the problem of development. *Quart. J. Roy. Meteor. Soc.*, **73**, 370-383.

Sutcliffe R.C. and Forsdyke A.G., 1950. The theory and use of upper air thickness patterns in forecasting. *Quart. J. Roy. Meteor. Soc.*, **76**, 189-217.

Swarbrick S.J., 1999. Use of water vapour imagery and PV inversion to adjust initial conditions in NWP. JCMM Internal Report No.102. 25 pp.

Swarbrick S.J., 2001. Applying the relationship between potential vorticity fields and water vapour imagery to adjust initial conditions in NWP. *Meteor. Appl.*, **8**, 221-228.

Thorncraft C.D. and Hoskins B.J., 1990. Frontal cyclogenesis. *J. Atmos. Sci.*, **47**, 2317-2336.

Tibaldi S., Buzzi A. and Speranza A., 1990. Orographic Cyclogenesis. *Extratropical Cyclones*, Palmén Memorial Volume, C.W. Newton and E. O.Holopainen, Eds., Amer. Meteor. Soc., 107-127.

Tiedtke M., 1993. Representation of clouds in large-scale models. *Mon. Wea. Rev.*, **121**, 3040–3061.

Tracton M.S., 1973. The role of cumulus convection in the development of extratropical cyclones. *Mon. Wea. Rev.*, **101**, 573-593.

Uccellini L.W., Keyser D., Brill K.F. and Wash C.H., 1985. The Presidents'Day cyclone of 18-19 February 1979: Influence of upstream trough amplification and associated tropopause folding on rapid cyclogenesis. *Mon. Wea. Rev.*, **113**, 962-988.

Uccellini L.W., Petterssen R.A., Brill K.F., Kocin P.J. and Tuccillo J.J., 1987. Synergistic interactions between an upper-level jet streak and diabatic processes that influence the development of a low-level jet and a secondary coastal cyclone. *Mon. Wea. Rev.*, **115**, 2227-2261.

Vederman J., 1949. Changes in vertical mass distribution over rapidly deepening lows. *Bull. Am. Meteor. Soc.*, **30**, 303-309.

Velden Ch., 1992. Satellite-based Microwave Observation of Tropopause-Level Thermal Anomalies: Qualitative Applications in Extratropical Cyclone Events, *Wea. Forecasting*, **7**, 669-682.

Velden C.S., 2000. Satellite-based microwave observations of tropopause-level thermal anomalies: Qualitative applications in extratropical cyclone events. *Wea. Forecasting*, **15**, 669-682.

Velden C.S., Niemann S.J., Menzel W.P. and Wanzong S.T., 1997. Upper-tropospheric winds derived from geostationary satellite water vapour observations. *Bull. Amer. Meteor. Soc.*, **78**, 173-195.

Verkley W.T.M., Moene A.R and Vosbeek P.W.C., 2005. Manually adjusting a numerical weather analysis in term of potential vorticity using three-dimensional variational data assimilation, *Quart. J. Roy. Meteor. Soc.*, **131**, 1713-1736.

Wallace J.M., Lin G.H. and Blackmon M.L., 1988. Relationship between cyclone tracks, anticyclone tracks and baroclinic waveguides. *J. Atmos. Sci.*, **45**, 439-462.

Wang W., Kuo Y.H. and Warner T.T., 1993. A diabatically driven mesoscale vortex in the lee of the Tibetan Plateau. *Mon. Wea. Rev.*, **121**, 2542-2561.

Weldon, R.B. and Holmes S.J., 1991. Water vapor imagery: Interpretation and applications to weather analysis and forecasting. *NOAA Tech. Rep. NESDIS*, **67**, 213 pp.

Wexler H. and Namias J., 1938. Mean monthly isentropic charts and their relation to departures of summer rainfall. Transactions American Geophysical Union, 19th Annual Meeting, pp. 164-170.

Whittaker J.S., 1988. A model-based diagnostic study of the rapid development phase of the Presidents' Day cyclone. *Mon. Wea. Rev.*, **116**, 2337-2365.